Regulation of the ATR Pathway in the Replication Stress Response

By

Jessica Whitney Luzwick

Dissertation

Submitted to the Faculty of the

Graduate School of Vanderbilt University

in partial fulfillment of the requirements

for the degree of

DOCTOR OF PHILOSOPHY

in

Biochemistry

August, 2016

Nashville, Tennessee

Approved By

David Cortez, Ph.D.

Scott Hiebert, Ph.D.

William Tansey, Ph.D.

Jennifer Pietenpol, Ph.D.

Stephen Fesik, Ph.D.

To my husband

and

All those I have met along the way

ACKNOWLEDGEMENTS

This thesis is an accumulation of six years of struggle, accomplishments, disappointments, many highs and many lows. Every person I have meet along the way played some role in helping me complete this journey. I would like to thank my mentor, David Cortez for his guidance and wisdom through the years, for setting high standards, and for teaching me what it is to be a scientist. I would like to thank my committee members, Scott Hiebert, Jennifer Pietenpol, Bill Tansey, Steve Fesik, and Ellen Fanning for their advice and for sticking it out with me all these years. I am also appreciative of the funding I received from the Environmental Toxicology training grant.

Throughout graduate school I had the benefit of working with awesome people every day. Even when the science was rough, the days long and stressful, I knew the people surrounding me would provide a reason to smile. The graduate students who came before me, Carol Bansbach, Edward Nam, Bianca Sirbu, and Jami Couch served as excellent mentors and role models. Carol and Eddie helped me to get started in the lab and set the bar high for being a graduate student in the Cortez lab. Bianca was a constant source of positivity and encouragement and Jami, the wise sage, was always so calm and confident. Gloria always keeps the lab stocked with both needed lab supplies and chocolate and who is constantly keeping things organized. Nancy became the CRISPR guru and made all the CRISPR cell lines and mutant ATR cell lines in this thesis.

Clint, Gina, and Akosua all joined the lab around the same time I did. Clint was a constant source of enthusiasm that even though this experiment did not work, surely the next one would. Gina, the most experienced of the four of us, provided valuable wisdom

and friendship. Akosua was my partner in crime as we navigated classes, quals, and committee meetings together. Huzefa, Kami, Lisa, and Kareem all joined the lab within the following couple years. Kareem convinced me to do the whole genome screen with him and while this resulted in a lot of struggle, I greatly benefited from his scientific guidance and friendship. Huzefa and Kami taught us all about India and very unfortunately, introduced the lab to going to Indian food for lunch. Kami and Lisa quickly became my friends and lab companions. We have had many adventures to concerts, movies, and other places creating many great memories from these years in Nashville. We have had a lot of laughs. Thomas was the latest graduate student to join the lab and fit right into our group. Maybe one day the lab will finally go canoeing.

Finally, I would like to thank all the friends I have met in Nashville. My fellow IGPers with whom I started graduate school, Amanda Myer Johnson, Kate Mittendorf, and Liz Ferrick Kiddie. Liz and I interviewed at Vanderbilt the same weekend and was my first friend in Nashville. Amanda can always be counted on to have a smile on her face and to be enthusiastic about life. Kate, we have endured a lot together through these years and I will always treasure our friendship and being able to be truly me around you, no matter how sarcastic or blunt. There were many other friendships throughout the years and each provided a source of great memories. The friendships you have during graduate school are one of the greatest sources of encouragement and strength and without which, I would not have made it through this marathon of obtaining a Ph.D.

I would like to thank my husband Tom. Who met me during my first year of graduate school and decided for whatever reason to stick it out with me. He never complained about the long hours, my moodiness, or silences when I would physically come

home but mentally would still be back in lab. He became my rock and source of calm. I would like to thank my family for being understanding when I was not always pleasant or present and my sisters for having all the babies. During graduate school my four nieces and nephew were all born. Watching them grow provided perspective that whatever challenge I was currently facing was not all that big in the grand scheme of life and that human life, development from a single fertilized egg to a walking, talking 5-year-old with opinions, is truly a miracle.

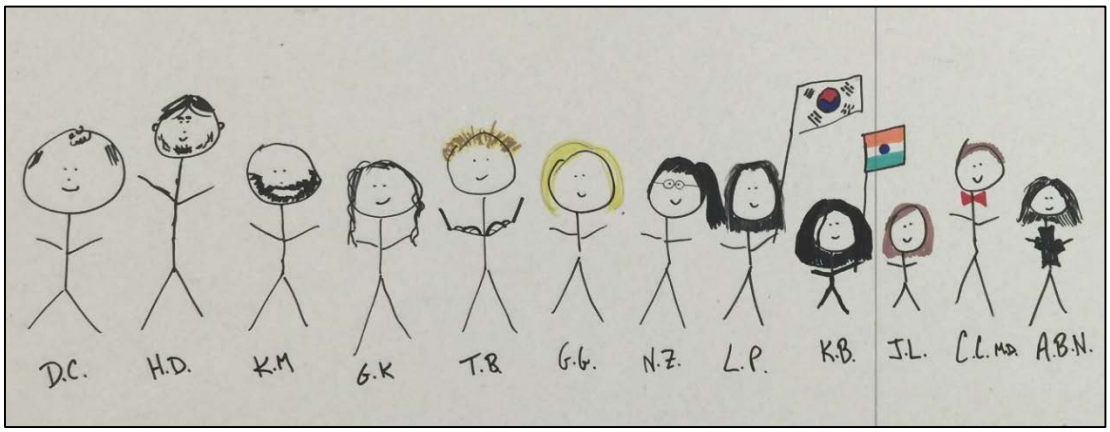

TABLE OF CONTENTS

Page

DEDICATION ii

ACKNOWLEDGEMENTS iii

LIST OF TABLES x

LIST OF FIGURES xi

LIST OF ABBREVIATIONS xiv

CHAPTER

I. INTRODUCTION 1

The Cell Cycle and Checkpoints 2
DNA Replication 4
Origin Licensing 5
Origin Firing 7
Regulation of Origins 7
Regulation Fork Elongation 8
ATR and the Replication Stress Response 8
Activation of ATR: RPA coated ssDNA gaps 9
Activation of ATR: ATR/ATRIP Complex 11
Activation of ATR: 9-1-1 recruitment of TOPBP1 12
Additional Components of the ATR Activation Pathway 13
Alternative Mechanisms of ATR Activation 14
S-phase Checkpoint 17
G2/M Checkpoint 21
Regulation of PIKK Kinases 23
Domain Architecture 23
Regulation by Localization 26
Regulation by Protein Activators 28
Regulation by Post-translational Modifications 29
Targeting the DDR in Cancer 31
Oncogene Induced Replication Stress 31
Inhibition of the DDR 32
ATR Inhibitors 33

II. MATERIALS AND METHODS 36

Site-directed Mutagenesis....36
Cell Lysate for Western Blot....38
Cell Lines....38
Transfection....39
Reagents....40
ATR Kinase Assay....40
Chromatin Fractionation....42
Chromatin Fractionation: Alternative Method....43
DNA Fiber Labeling....43
Flow Cytometry....45
Immunofluorescence....46
Genetic Complementation of ATR Flox/- Cells....47
In Cell Analysis....48
Adenovirus Infection of ATR Flox/- Cells....48
Purification of GST-tagged Protein from bacteria....49
Whole Genome siRNA Screens....51
Secondary Validation Screens....52
Dose Response Assays....53
Clonogenic Assays....53
G2/M Checkpoint....54
Completion of S-phase....54
Generation of CRISPR/Cas Null Cells....54
ATR Purification for Mass Spectrometry....55
FLAG Purification of Screen Hits for Mass Spectrometry....55

III. MUTATION OF ATR S1333 CREATES A HYPERACTIVE KINASE....58

Introduction....58
Results....60
Mutation of Serine 1333 alters ATR kinase activity....60
S1333 is unlikely to be phosphorylated in cultured cells....63
Generation of cells expressing only S1333A or S1333D-ATR....66
S1333A-ATR cell lines have elevated phosphorylation of ATR substrates....68
S1333 mutation to aspartic acid causes modest defects in ATR checkpoint function....71
Discussion....76

IV. WHOLE GENOME SYNTHETIC LETHAL SCREENS IDENTIFY PATHWAYS THAT SENSITIZE CANCER CELLS TO ATR INHIBTION....79

Introduction....79
Results....82
Whole Genome siRNA Synthetic Lethality Screens....82
ATRi, CHKi, and HU Whole Genome Screen Data Analysis....84
ATRi, ATRi/cisplatin Whole Genome Screen Data Analysis....89
Validation of the ATR Pathway and DNA Replication....91

Identification of Cancer Cell Lines with Reduced ATR Pathway Function.....97
There is no clear relationship between ATRIP levels and ATRi IC50.....97
There is no clear relationship between cancer cell lines with ATR signaling defects and ATRi sensitivity. 100
Discussion.....105
Reduction in ATR activity increases the dependence on the remaining kinase activity. 106
The ATR pathway is not frequently mutated in cancer.....106
There is no good biomarker for ATR activity 107
ATRi synergizes with the CHKi.....108
DNA Polymerase D1 and E are mutated in cancer.....109
ATRi synergizes with anti-metabolites.....109
Conclusions.....110

V. siRNA SCREENING IDENTIFIES POTENTIAL NEW ATR PATHWAY OR DNA DAMAGE RESPONSE GENES 111

Introduction.....111
Results.....112
Secondary screens tested selected gene for synthetic lethality with several Inhibitors.....112
Characterization of RNF208, ARID3B, and BRD3.....115
Identification of protein interactors for RNF208, ARID3B/3A, and BRD3.....121
BRD3 does not regulate PCNA levels on chromatin.....126
BRD3 knockdown slows DNA replication.....130
siBRD3 off-target effects creates the sensitivity to the ATRi 132
Discussion.....134
RNF208 could be a novel mitotic regulator.....134
ARID3B could aid in histone remodeling to promote replication processivity...135
BRD3 siRNA is off-target, but BRD3 may still function during DNA replication stress.....136
ATRi screening identifies the major ATR pathway genes as well as other pathways 137
Conclusions.....138

VI. SUMMARY AND FUTURE DIRECTIONS.....139

Summary.....139
Regulation and Activation of ATR.....140
Conflicting evidence of ATR regulation by autophosphorylation.....141
Regulation of ATR by phosphorylation.....142
PIKK kinases undergo conformational changes when activated.....144
Activators of ATR.....148
Utilization of the ATRi to study the ATR pathway.....149
Whole genome siRNA screens aimed to identify new ATR pathway or DNA repair genes 149

ATR, Mitosis, and the Centrosomes 152
ATR Inhibitors in the Cancer Clinic 153
A whole genome siRNA screen identifies synthetic lethal relationships with the ATRi 154
Depletion of ATR pathway proteins sensitizes cells to the ATRi 157
ATRIP gene deletion and ATR and CHK1 frameshift mutations occur in cancer 159
Measuring ATR activity in cells 160
Alternative approaches for identifying a clinically actionable patient population 161
Directed use of the ATRi in the cancer clinic 165

APPENDIX

A. WHOLE GENOME SCREEN DATA AND EXTRA FIGURES 167

B. SECONDARY SCREENS DATA 183

C. ETAA1 IS A NOVEL ATR ACTIVATOR 193

REFERENCES 196

LIST OF TABLES

Table Page

2.1 Site-directed Mutagenesis Primers 36

2.2 Antibodies for Western Blot 37

3.1 Identified ATR phosphorylation sites 78

4.1 Cell lines analyzed for ATRi IC50 98

A.1 Pathways enriched in the ATRi whole genome screen dataset.....171

A.2 Top Genes Synthetic Lethal with the ATRi.....172

B.1 Secondary Validation Screen Data.....184

LIST OF FIGURES

Figure Page

1.1 The Cell Cycle 3

1.2 Origin licensing and firing is divided between two phases of the cell cycle 6

1.3 The canonical ATR activation pathway 10

1.4 Transient inhibition of ATR slows DNA replication and increases origin firing 19

1.5 ATR stabilizes the replication fork during replication stress 20

1.6 The G2/M checkpoint 22

1.7 The common domain architecture of PIKK family kinases 25

1.8 PIKK family kinases share three mechanisms of regulation 27

3.1 Mutation of S1333 to alanine creates a hyperactive ATR kinase 62

3.2 Additional S1333 mutations alter ATR kinase activity 64

3.3 S1333 is a conserved amino acid within HEAT repeat 27 of ATR 65

3.4 The peptide containing unphosphorylated S1333 can be detected by mass spectrometry 67

3.5 S1333A and S1333D-ATR cell lines express ATR at similar levels and maintain a normal cell cycle 69

3.6 S1333A-ATR expressing cell lines contain elevated levels of phosphorylated ATR substrates 70

3.7 S1333A-ATR expressing cell lines maintain elevated levels of phosphorylated substrate at early time points after replication stress induction 72

3.8 S1333A-ATR expressing cell lines maintain elevated levels of phosphorylated substrate at low replication stress levels 73

3.9 Mutation of S1333 to aspartic acid causes modest defects in completing DNA synthesis following UV radiation and in maintenance of the G2 checkpoint 75

4.1 Whole genome siRNA screens identify pathways synthetic lethal with ATR inhibition and cisplatin....83

4.2 Whole genome siRNA screens identify synthetic lethal pathways with ATR inhibition CHK1 inhibition, and hydroxyurea....85

4.3 The ATR pathway and DNA replication when knocked down have synthetic lethal relationships with the ATRi alone and ATRi with cisplatin....86

4.4 DNA replication and the ATR pathway are the top synthetic lethal pathways 90

4.5 The ATR pathway and DNA replication pathways validated using four individual siRNAs....92

4.6 ATR depletion sensitizes triple-negative breast cancer and non-small cell lung cancer cell lines to ATRi....94

4.7 Genetic alteration of the ATRIP or ATR gene sensitizes cells to the ATRi....96

4.8 Identified ATRIP deletion cell lines still express ATRIP and have varied sensitivity to the ATRi....99

4.9 ATR and CHK1 frameshift mutations moderately decrease pCHK1 after HU treatment 101

4.10 The CCLE data of copy number variation and mRNA levels of the ATR pathway genes identifies cell lines with ATR signaling defects 102

4.11 Identified cell lines with ATR defects have varied sensitivities to the ATRi....104

5.1 siRNA synthetic lethality secondary screens included six drug conditions 114

5.2 RNF208 localizes to the nucleus and knockdown induces elevated levels of γH2AX and pCHK1 117

5.3 Knockdown of BRD3 or ARID3A/3B results in no alterations in ATR signaling....119

5.4 ARID3B localizes to the nucleus and knockdown slightly induces γH2AX....120

5.5 BRD3 localizes to small foci in the nucleus 122

5.6 ARID3B interacts with the FACT complex and RNF208 interacts with the RALGAP complex....124

5.7 BRD3 interacts with the ATAD5/RFC2-5 complex....125

5.8 Knockdown of BRD3 sensitizes cells to the ATRi....127

5.9 Knockdown or inhibition of BRD3 does not increase PCNA levels on chromatin...129

5.10 Knockdown but not inhibition of BRD3 slows DNA replication....131

5.11 BRD3 null cell lines are not sensitive to the ATRi....133

6.1 Activation of ATR in vitro increases phosphorylation of the ATR substrate MCM2 but not ATR or ATRIP 145

6.2 Mutation of S1333 induces a partial activating conformational change within ATR....147

6.3 Synthetic Lethality....155

6.4 ATR is essential in S-phase for overcoming replication stress....158

6.5 The lethal event with ATR inhibition occurs within the first cell cycle but the cells need time to continue to cycle in order to die....163

6.6 Directed use of the ATRi in the cancer clinic....166

AA.1 Replicate correlation graphs for the whole genome screens....168

AA.2 The ATR pathway was synthetic lethal with each drug condition....169

AA.3 The robust Z-score average for each gene is graphed by plate and by row....170

AC.1 ETAA1 contains an ATR activating domain within amino acids 75-250....194

AC.2 ETAA1 activates ATR using the same binding surface on ATR as TOPBP1....195

LIST OF ABBREVIATIONS

5' UTR	5' untranslated region
9-1-1	RAD9 RAD1 Hus1
AAD	ATR activating domain
ALT	Alternative lengthening of telomeres
AML	Acute myeloid leukemia
APC/C	Anaphase promoting complex/cyclosome
ARID	AT-rich interactive domain
ATM	Ataxia telangiectasia mutated
ATP	Adenosine triphosphate
ATR	Ataxia telangiectasia and Rad3 related
ATRi	ATR inhibitor
ATRi	ATR inhibitor
ATRIP	ATR interacting protein
BET	Bromodomain and extra terminal domain
BLM	Bloom helicase
BRCA1/2	Breast cancer 1/2, early onset
BRD	Bromodomain
ccRCC	Clear cell renal cell carcinoma
CDK	Cyclin dependent kinase
CHK1	Checkpoint kinase 1
CHK2	Checkpoint kinase 2

CHKi	checkpoint kinase inhibitor
CPT	Camptothecin
DDK	Dbf4-dependent kinase
DDR	DNA damage response
DNA-PKcs	DNA-dependent protein kinase, catalytic subunit
DSB	Double strand break
dsDNA	double stranded DNA
FACT	Facilitates chromatin transcription
FAT domain	FRAP, ATM, and TRRAP domain
G1 phase	Gap 1 phase
G2 phase	Gap 2 phase
HEAT	Huntingtin, elongation factor 3, protein phosphatase 2A and the yeast kinase TOR1
HR	Homologous recombination
HU	Hydroxyurea
IP	Immunoprecipitation
IR	Ionizing irradiation
LC-MS	Liquid chromatography-mass spectrometry
LOH	Loss of heterozygosity
M phase	Mitosis phase
MCM	minichromosome maintenance
MRN	Mre11, RAD50, NBS1
mTOR	Mechanistic target of rapamycin

NHEJ	Non-homologous end joining
NSCLC	Non small cell lung cancer
ORC	Origin recognition complex
PARP	Poly ADP ribose polymerase
PARPi	PARP inhibitor
pCHK1	Phosphorylated CHK1
PCNA	Proliferating cell nuclear antigen
PIKK	Phosphatidylinositol 3-kinase related kinase
PLK1	Polo-like kinase 1
PRD	PIKK regulatory domain
pre-RC	pre Replication Complex
RNF	Ring finger
RPA	Replication protein A
RSR	Replication stress response
S phase	Synthesis phase
S/TQ	Serine/threonine glutamine
siATR	ATR siRNA
siNT	Non-targeting siRNA
SSB	Single strand break
ssDNA	single stranded DNA
TNBC	Triple negative breast cancer
TOPBP1	Topoisomerase binding protein 1
UV	Ultra violet light

V-ATPase	Vacuolar ATPase
WB	Western blot
Wee1i	Wee1 inhibitor

CHAPTER I

INTRODUCTION

Throughout our lifetime, our cells will undergo approximately 10,000 trillion cell divisions, and in every cell division cycle, the cell must accurately and faithfully replicate over 6.8 billion base pairs of DNA. To complicate this process further, DNA is damaged at a rate of 10,000 to 1 million DNA lesions per cell per day. DNA damage occurs from both endogenous and exogenous sources such as exposure to UV light, inhalation of cigarette smoke, or from the byproducts of cellular metabolism. The cell must accurately repair these lesions and faithfully replicate the genome in order to prevent accumulation of DNA mutations and chromosomal aberrations. Failure to do so can lead to disease such as cancer.

However, cells have what is collectively known as the DNA damage response (DDR). The DDR is comprised of a multitude of pathways that promote repair of DNA lesions, regulate the cell cycle, induce changes in transcription, and can signal cells to undergo senescence or apoptosis. These pathways repair a wide variety of DNA lesions such as inter- or intra-strand crosslinks, UV photoproducts, DNA double strand breaks (DSBs), single strand DNA breaks (SSBs), and chemical alterations to DNA bases. The major kinase regulators of the DDR are the phosphoinositide 3-kinase-related protein kinases (PIKKs). These kinases include ataxia-telangiectasia mutated (ATM), ATM and RAD3-related (ATR), and DNA-dependent protein kinase (DNA-PKcs). ATM and DNA-PKcs activate in response to DSBs while ATR activates in response to single-stranded DNA (ssDNA) gaps next to double-stranded DNA (dsDNA). The ATR activating DNA

substrate is generated by a variety of lesions and problems encountered during DNA replication. The versatility of ATR makes it essential in human and mouse replicating cells and during embryonic development [2-4]. My thesis work focuses on understanding the regulation of ATR in response to replication stress.

In this chapter, I will discuss the mechanism and regulation of DNA replication, the activation and regulation of ATR in response to replication stress, and our current understanding of how to use the ATR inhibitors in the cancer clinic.

The Cell Cycle and Checkpoints

Every cell division cycle, a cell must replicate all of its components in order to create two nearly identical daughter cells. To do this, the cell undergoes the cell division cycle, which is comprised of a series of highly regulated events divided into four phases: Gap 1 (G1), DNA synthesis (S), Gap 2 (G2), and mitosis (M) (Figure 1.1). Cell cycle phase transitions occur through regulation of cyclin-dependent kinases (CDKs). During S-phase, DNA replication occurs and one and only one copy of the genome is produced. During G1 and G2, the cell grows and assesses the cells readiness to enter S-phase or mitosis. The G1, S, and G2 phases make up what is known as interphase. During mitosis, the cell physically divides in two and one copy of the genome is segregated into each new daughter cell.

During the cell cycle, there are regulated transitions called checkpoints (Figure 1.1). If conditions are not ideal or if the previous phase of the cell cycle is not complete, the checkpoint will activate and halt the cell cycle until the problem is resolved. The first

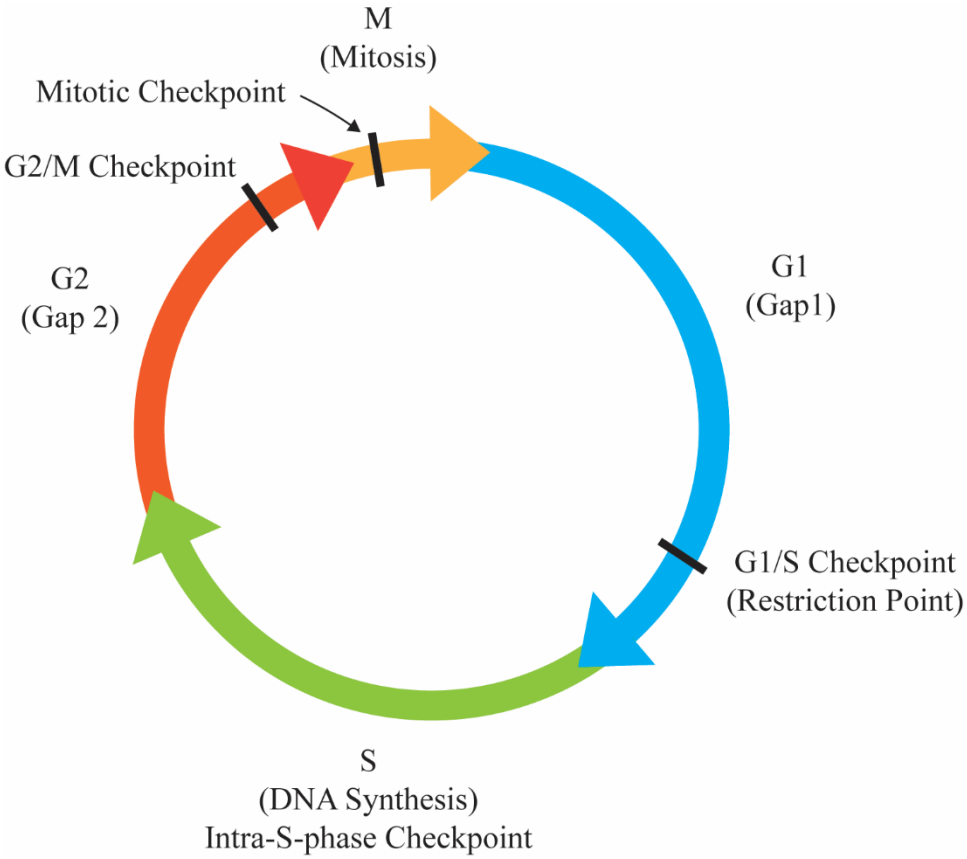

Figure 1.1. The Cell Cycle. The cell cycle is divided into four phases. During S-phase the cell replicates the DNA and during M-phase the cell physically divides in two. G1 and G2-phase the cell grows and assesses the readiness to enter the next phase of the cell cycle. The cell cycle checkpoints ensure the cell does not enter the next phase prematurely.

checkpoint occurs before the cell transitions into S-phase and is called the G1/S checkpoint or restriction point. This checkpoint ensures conditions are ideal for proliferation through sensing of nutrients and external mitogenic signals. This checkpoint also ensures the cell does not enter S-phase with DNA damage. Progression through this checkpoint initiates DNA replication and commits the cell to undergo cell division. During S-phase, if DNA damage or high levels of replication stress occur, the intra-S-phase checkpoint is activated. This checkpoint regulates origin firing, stabilizes stalled replication forks, and promotes DNA repair. Another checkpoint occurs at the G2/M phase transition. Before progressing into mitosis, the cell must have completely and accurately replicated the genome. This checkpoint prevents the cell from entering mitosis if DNA damage is present or if there are under replicated regions of the genome. ATR can activate both the intra-S-phase checkpoint and the G2/M checkpoint. The last checkpoint is within mitosis. Progression through this checkpoint signals the cells readiness to separate the sister chromatids and undergo cytokinesis [5]. These checkpoints ensure the creation of two nearly identical daughter cells each with one complete copy of the genome by the end of the cell cycle.

DNA Replication

The process of replicating the genome predominately occurs during S-phase of the cell cycle. DNA replication is a fast process and the entire human genome is duplicated in approximately 6-8 hours. Replication in bacteria is relatively simple as for the most part they only contain one circular chromosome. However, the human genome is much larger and contains 46 linear chromosomes containing 6.8 billion base pairs. Additionally, each region of the genome must only undergo replication once per cell cycle. To ensure this,

initiation of DNA replication is separated into two tightly regulated steps: origin licensing and origin firing.

Origin Licensing

DNA replication initiates at locations in the genome known as origins. In bacteria and yeast, specific DNA sequences define origins. However, this is not the case in human cells. What defines a human DNA replication origin has remained elusive as thousands of origins are licensed, only a fraction are actually used, and most origins are not consistently used every cell division cycle [6-8]. In human cells, origin use is more determined by transcriptional activity and chromatin structure in that region of the genome rather than specific DNA sequences [9].

The process of duplicating the genome begins in late mitosis and G1-phase of the cell cycle. During the end of mitosis and G1, origins licensing occurs through the formation of the pre-replication complex (pre-RC). First, the origin recognition complex (ORC) binds DNA at specific sites in the genome (Figure 1.2A). The ORC is comprised of six subunits, which bind DNA as a ring-shaped hexamer along with Cdc6 [10,11]. Then Cdt1 binds the ORC and recruits the hexameric core component of the replicative helicase, minichromosome maintenance 2-7 (MCM) complex [9]. The MCM complex is loaded onto dsDNA as an inactive head-to-head double hexamer [12-14]. Upon MCM loading, Cdc6 hydrolyzes ATP to eject from the DNA and promotes the release of Cdt1 [15]. This forms the pre-RC and a licensed origin.

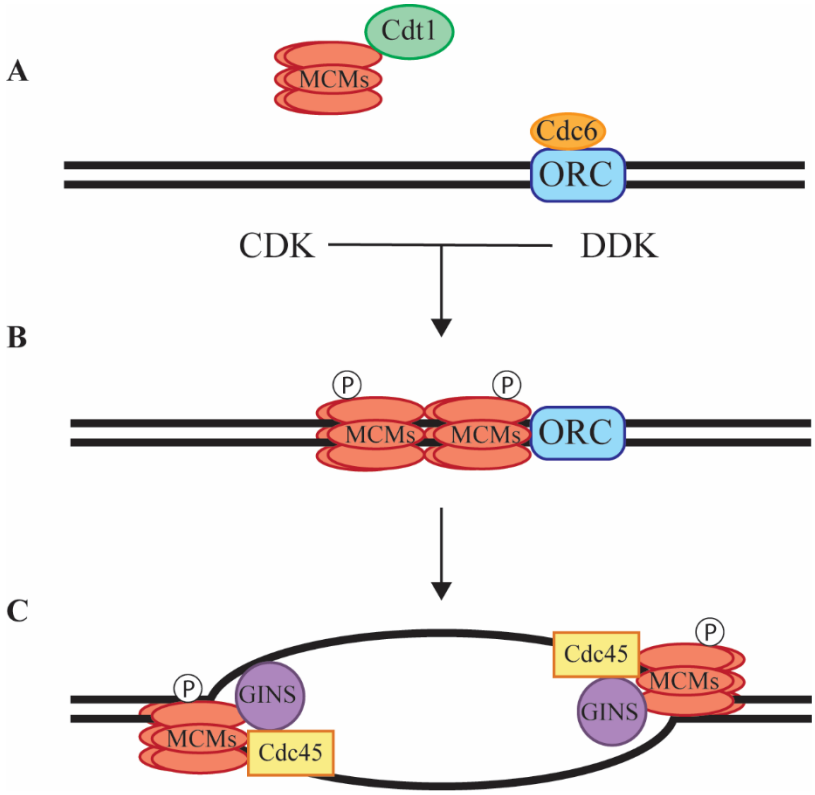

Figure 1.2. Origin licensing and firing is divided between two phases of the cell cycle. During late mitosis and early G1-phase, origins are licensed through ORC binding to the DNA followed by binding of Cdt1 and Cdc6. Cdt1 recruits the MCMs to the origin. MCMs are loaded onto DNA in as an inactive double hexamer. Once the cell progresses into S-phase, CDK and DDK activate, phosphorylating the MCMs, and allowing the recruitment of Cdc45 and GINS to the MCMs. Cdc45, GINS, and MCMs make up the CMG helicase, which once activated, unwinds the DNA initiating DNA replication.

Origin Firing

As the cell cycle progresses into S-phase, the inactive pre-RC converts into an active replication fork. CDK and Dbf4-dependent kinase/Cdc7 (DDK) activate in S-phase and phosphorylate the pre-RC (Figure 1.2B). Phosphorylation of the MCM complex promotes its interaction with Cdc45 and GINS forming the Cdc45-MCM-GINS (CMG) complex [16-18]. Upon activation, the CMG helicase transitions from encircling dsDNA to an active state encircling the leading stand ssDNA [19]. Activation of the CMG helicase initiates DNA replication (Figure 1.2C).

Regulation of Origins

The separation of origin licensing and firing into two different phases of the cell cycle ensures replication of the genome once and only once due to cell cycle regulation of CDK activity. During late M or G1-phase, low CDK activity allows assembly of the pre-RC but prevents origin firing, while S-phase corresponds with high CDK activity, the promotion of origin firing, and inhibition of origin licensing [20]. In human cells, origins are not all fired at the same time, but instead origin-firing follows a predetermined temporal pattern, which is cell type specific [21]. Clusters of origins are fired together to create large replication domains. These clusters are not only located adjacent to each other on the chromosome but spatially adjacent in the nucleus [22]. Origin firing is a complex process regulated on many levels. Additional players in this regulation include ATR and checkpoint kinase-1 (CHK1) and will be discussed below.

Replication Fork Elongation

The replisome synthesizes the nascent DNA and contains multiple proteins. Pol α/primase primes the leading and lagging strand upon replication initiation and continues priming the lagging strand throughout replication. There are two main DNA replication polymerases, Pol ε and Pol δ, which synthesize the leading and lagging strand, respectively [23]. The CMG helicase unwinds the DNA ahead of the DNA polymerases and all ssDNA generated is rapidly coated by replication protein A (RPA). Proliferating cell nuclear antigen (PCNA), a ring shaped clamp, binds the DNA polymerases, and ensures their processivity. PCNA is loaded onto DNA by the pentameric replication factor C (RFC) complex [23,24]. The replisome is a very dynamic machine as translesion synthesis polymerases, also interacting with PCNA, can switch places with Pol ε and Pol δ to aid in bypass of DNA lesions [25]. This machine faithfully replicates all 6.8 billion base pairs of the human genome.

ATR and the Replication Stress Response

Replicating the genome is a complex process. Additional challenges come in the form of replication stress. Replication stress is caused by a variety of sources such as unrepaired DNA lesions, hard to replicate sequences, insufficient nucleotides, collisions with transcriptional machinery, misincorporation of ribonucleotides, and overexpression of oncogenes [26]. Cells must overcome these obstacles and do so through activation of the replication stress response, a complex pathway part of the DDR.

At the apex of the DNA damage response are two major kinase regulators ATM and ATR. ATM activates in response to the presence of DSBs whereas ATR activates in

response to ssDNA gaps next to dsDNA triggering the replication stress response. Once activated, these kinases phosphorylate hundreds of protein substrates preferentially on serine or threonine residues followed by glutamine (S/TQ). Many of these substrates are overlapping [27]. The best characterized substrates are the effector kinases, CHK1 for ATR and checkpoint kinase-2 (CHK2) for ATM [28]. However, only ATR is essential [2-4]. For my thesis work, I studied the mechanisms of ATR regulation and the impacts of transient inhibition.

ATR is a versatile kinase, which activates in response to a wide variety of problems during replication and activates every S-phase. While ATR is essential in replicating cells, rare hypomorphic ATR mutations are linked to Seckel Syndrome. Patients with this syndrome have microcephaly and developmental defects [29]. The essential function of ATR is thought to be during S-phase and less so with activation of the G2/M checkpoint [30]. I will first discuss the canonical ATR activation pathway. Then I will describe more recent advances adding complexity to this pathway as well as other mechanisms leading to activation. Finally, I will discuss ATR activation of the intra-S-phase and G2/M checkpoints.

Activation of ATR: RPA Coated ssDNA Gaps

The DNA substrate, which activates ATR is generated through many mechanisms. One example is when the DNA polymerase encounters a lesion, causing it to stall. The DNA helicase continues to proceed unwinding the DNA, leading to functional uncoupling of the replication fork. This generates stretches of ssDNA next to dsDNA and RPA rapidly coats the ssDNA (Figure 1.3A) [31]. RPA is a heterotrimeric protein

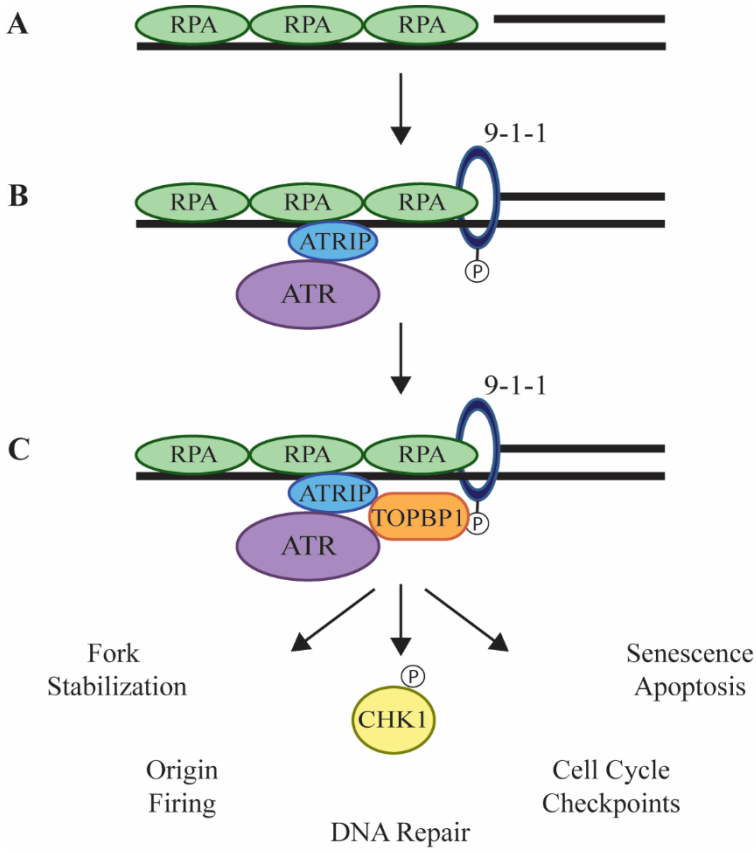

Figure 1.3. The canonical ATR activation pathway. A. Single-stranded DNA is rapidly coated by RPA. **B.** ATRIP, an obligate binding partner of ATR, binds RPA. Additionally, the 9-1-1 complex is loaded onto the 5' overhang at a double-stranded, single-stranded DNA junction. **C.** The 9-1-1 complex recruits TOPBP1. TOPBP1 binds the C-terminal phosphorylated tail of 9-1-1 and can then bind ATR and ATRIP to activate ATR. Once activated, ATR phosphorylates hundreds of downstream targets including the effecter kinase, CHK1. ATR regulates and promotes replication fork stabilization, origin firing, DNA repair, cell cycle checkpoints, and can induce apoptosis or senescence.

comprised of RPA32, RPA70, and RPA14. This DNA structure of RPA coated ssDNA next to dsDNA initiates the recruitment of ATR and its activating proteins.

There are also DNA repair pathways which generate the ATR-activating DNA substrate during repair of DNA lesions. In the elimination of oxidative DNA damage, APE2, an exonuclease, generates ssDNA in a 3' to 5' direction, creating the ATR activating DNA substrate. Additionally, this enzyme has been shown to interact with CHK1 and is essential for CHK1 phosphorylation [32]. ATR is activated in response to DSBs once the DNA is resected in preparation for repair by homologous recombination (HR) [33]. Additionally, during repair of interstrand crosslinks, FANCM/FAAP24 regulate loading of RPA onto the DNA and are critical for the activation of ATR [34,35]. Thus, the ATR activating DNA substrate can be generated through many mechanisms, and activation of ATR occurs before and during repair of DNA lesions.

Activation of ATR: ATR/ATRIP Complex

ATR localizes to RPA coated ssDNA but does not bind RPA itself. Instead, ATR has an obligate binding partner, ATR-interacting protein (ATRIP), which interacts with RPA70 (Figure 1.3B). The association of ATR and ATRIP promotes their stability and is not regulated. Loss of one results in the loss of the other [3]. ATRIP binds to the N-terminal oligonucleotide binding domain of RPA70 (RPA70N) [36]. Additionally, ATRIP contains a coiled-coil domain, which facilitates oligomerization and is required for ATR signaling [37]. While the ATRIP: RPA interaction helps localize the ATR-ATRIP complex to ssDNA gaps, it is not essential for ATR signaling. Mutants of ATRIP which can no longer bind RPA, have no significant ATR signaling defects in response to replication

stress induced by hydroxyurea, ionizing radiation, or UV [38]. Additionally, ATR can directly bind DNA and has an increased affinity for UV damaged DNA [39,40]. The functional significance of ATR being able to bind DNA has not been examined. Important future work should map the ATR DNA binding region and examine if DNA binding is important for ATR activation and signaling.

Activation of ATR: 9-1-1 Recruitment of TOPBP1

Localization of the ATR-ATRIP complex to RPA coated ssDNA is only one of the two steps needed for ATR activation. Activation requires the ATR-independent recruitment of the RAD9-RAD1-HUS1 (9-1-1) complex [41,42]. The 9-1-1 complex is loaded on the ssDNA:dsDNA junction by the RAD17 clamp loader and has a preference for being loaded at a 5' overhang (Figure 1.3B) [43-45]. RAD9 also interacts with RPA70 using the same binding surface as ATRIP [45,46]. Additionally, RAD9 is constitutively phosphorylated on the C-terminal tail which was reported to be important for the recruitment of the ATR activator, topoisomerase-binding protein-1 (TOPBP1) [47]. Alternatively, there is contrasting evidence that TOPBP1 binds RPA-coated ssDNA and TOPBP1 recruits the 9-1-1 complex to the stalled replication fork [48,49]. Further work is needed to elucidate the mechanistic details of this step in the ATR activation pathway. Stalled replication forks may activate ATR using a slightly altered mechanism compared to other type of DNA damage. There is already evidence of alterations in the ATR activation pathway as in response to DSBs, ATM phosphorylates TOPBP1, promoting TOPBP1 interactions with ATR and ATRIP [50].

TOPBP1 contains an ATR activation domain (AAD) and interacts with both ATR and ATRIP to activate the kinase leading to phosphorylation of CHK1 and hundreds of downstream substrates (Figure 1.3C) [51-54]. TOPBP1 has other functions outside of ATR activation such as in origin firing and stabilization of bloom syndrome helicase (BLM) protein during S-phase [55-58]. Furthermore, TOPBP1 function in origin firing and checkpoint activation is regulated through acetylation by p300 and deacetylation by SIRT1 [59].

Additional Components of the ATR Activation Pathway

TOPBP1, the 9-1-1 complex, RPA, and ATRIP are the main components facilitating ATR activation. However, many additional proteins bind these components and also aid in activation of ATR. Loss of these proteins often results in reduction or inhibition of ATR signaling. TOPBP1 binds multiple other proteins which aid in TOPBP1 localization and amplify ATR activation. MDC1 is best known for binding γH2AX and aiding in the retention of NBS1 at sites of DSBs [60-63]. However, it can also bind and recruit TOPBP1 to sites of DNA damage and is required for TOPBP1 foci formation [64]. Phosphorylation of BRIT1 by ATM or ATR allows BRIT1 to bind and recruit TOPBP1 to sites of replication stress, amplifying the ATR signal [65]. TOPBP1 also binds phosphorylated Treslin and Treslin stimulates ATR phosphorylation of CHK1 in a TOPBP1-dependent manner [66]. RHINO bridges the interaction between TOPBP1 and the 9-1-1 complex [67,68]. Finally, TOPBP1 binds phosphorylated BACH1 helicase allowing BACH1 to further unwind the DNA at sights of damage, increasing the amount of ssDNA, which in turn increases the amount of RPA, amplifying ATR activation [69].

There are also additional proteins which bind RPA to facilitate ATR activation. The Timeless/Tipin complex binds RPA32 and the CHK1 interactor, Claspin. This promotes increased phosphorylation of CHK1 by ATR [70]. BID and PRP19 bind RPA and ATR/ATRIP to promote accumulation of ATR [71-73]. PRP19 is in an ubiquitin ligase complex, and ubiquitylates RPA, which facilitates ATRIP recruitment [73]. Cdc5L, a component of the PRP19 complex, directly binds ATR [74]. CINP and CDK9/Cyclin K also bind ATR/ATRIP [75,76]. CINP silencing causes modest ATR signaling defects whereas CDK9 silencing does not and may be involved in stabilizing the replication fork. Identification of all these additional players in the ATR activation pathway demonstrates there is still much to learn about the activation of ATR and signifies there are most likely many more components to this pathway not yet discovered. In my dissertation work, I performed a whole genome siRNA screen to identify new ATR pathway genes, discussed in Chapter V.

Alternative Mechanisms of ATR Activation

The pathway described above is the canonical ATR activation pathway. However, some discrepancies leave the possibility of alternative activation mechanisms. As mentioned above, the ATRIP: RPA interaction is dispensable for ATR activation and signaling [36,38]. Additionally, mutation of the RAD9 and TOPBP1 binding sites within RPA70 does not fully suppress ATR activation [46]. This suggests there are mechanisms by which ATR activates independent of RPA. Additionally, in *S. cerevisiae*, the ATR orthologue, MEC1, has three identified activators while in human cells, TOPBP1 is the

only identified activator of ATR [77-80]. Several groups have proposed alternative mechanisms of ATR activation, which diverge from the canonical pathway.

MRE11-RAD50-NBS1 (MRN) complex is hypothesized to activate ATR through two different mechanisms. Which mechanism is used depends on the dose of DNA damaging reagent used and the type of DNA damage generated. When DSBs are generated by CPT or IR, MRN indirectly activates ATR [81]. The formation of DSBs activates ATM and DNA-PKcs, which promote repair by HR or non-homologous end joining (NHEJ), respectively. Processing of the DSB during HR by the MRN complex generates ssDNA next to dsDNA, which allows activation of ATR [81,82]. This mechanism is widely accepted and ATR activates through the canonical pathway.

There is evidence in the literature the MRN complex may also aid in the activation of ATR at stalled replication forks. Depletion of the xMRN complex in *Xenopus* egg extracts results in decreased recruitment of TOPBP1 to the chromatin and decreased pCHK1 after treatment with aphidicolin [83,84]. Additionally, NBS1 also binds RPA70 and the nuclease activity of MRE11 is required for ATR activation [83,85]. The model of how the MRN complex activates ATR at stalled replication forks involves MRN recruiting TOPBP1. The MRN complex processes stalled replication forks, binds the RPA coating the ssDNA, and recruits TOPBP1. Because ATRIP also binds to RPA70 to localize ATR, the MRN recruited TOPBP1 can now activate ATR away from the ssDNA:dsDNA junction independently of the 9-1-1 complex [83-85]. While these initial studies are intriguing, further work is warranted to fully understand if ATR activation is occurring away from the ssDNA:dsDNA junction. It is becoming increasingly clear from work in our lab and

others that TOPBP1 recruitment is not fully understood and may be occurring through different mechanisms at different DNA lesions.

Repair of DNA mismatches may also use a different mechanism of ATR activation that is independent of RAD17 and the 9-1-1 complex. N-methyl-N'-nitro-N-nitrosoguanidine (MNNG) is a DNA alkylating agent commonly used to create DNA mismatches through generation of O(6)-methyl guanine. Treatment of cells with MNNG induces the G2/M checkpoint and arrest of the cell cycle [86]. The activation of the checkpoint is DNA replication and ATR-dependent [87]. General processing of DNA mismatches can result in the generation of the ATR activating DNA substrate. However, several groups have shown ATR activates in a unique manner in response to these lesions. MUTSα and MUTLα interact with ATR and facilitate ATR recruitment to MNNG induced DNA damage sites. MUTSα and MUTLα also interact with Claspin, CHK1, and TOPBP1 but not RAD17 or the 9-1-1 complex. However, there is no enrichment of RPA, RAD17 or the 9-1-1 complex on chromatin after the treatment of cells with MNNG [88,89]. MUTSα and MUTLα may recruit ATR and TOPBP1 to sites of DNA lesions allowing activation of the checkpoint independent of the rest of the components of the ATR pathway.

There is also evidence of alternative mechanisms of ATR activation in response to DNA crosslinks. After treatment of cells with cisplatin, a DNA crosslinking agent, ATR recruitment is also MUTSα-dependent. Additionally, the Fanconi Anemia (FA) core complex promotes localization of ATR to sites of DNA crosslinks and ATR activates the FA pathway through phosphorylation of FANCI in a RAD17 and TOPBP1-independent manner [89,90]. All of these studies evaluated ATR activation in response to specific DNA lesions but follow up work is lacking. Future work needs to keep all of these findings

under consideration when studying mechanisms of ATR activation. Drug dose, drug type, timing, and which ATR substrate is being examined all present variables potentially altering the mechanism of ATR activation or the appearance of kinase activation.

S-phase Checkpoint

The S-phase checkpoint is different from the other cell cycle checkpoints as it does not prevent a cell cycle transition. Instead this checkpoint acts as a DNA surveillance mechanism, activating in response to DNA damage and replication perturbations. Once activated, ATR stabilizes stalled replication forks, regulates origin firing, slows DNA replication, and promotes DNA repair through phosphorylation of hundreds of downstream substrates (Figure 1.3C). The best-characterized substrate is the effector kinase CHK1, which ATR activates by phosphorylating on S317 and S345. Once activated, CHK1 spreads the DNA damage signal to the rest of the nucleus [28].

During the S-phase checkpoint, ATR activation of CHK1 inhibits global origin firing. CHK1 phosphorylates Cdc25, leading to its degradation. Normally, Cdc25 removes the inhibitory phosphate present on CDK, thereby activating CDK, and promoting origin firing. When Cdc25 is phosphorylated and degraded, CDK is left inactivated and global origin firing is inhibited [91]. A second mechanism by which CHK1 inhibits origin firing is through inhibition of Treslin loading of Cdc45, preventing the formation of the CMG helicase [92].

ATR activation inhibits global origin firing, but conversely, it also promotes local origin firing. ATR phosphorylates many components of the replisome including RFCs, RPA32, RPA70, MCM2-7, MCM10, and the DNA polymerases. The consequences of

most of these phosphorylation events remain to be determined. It is known that phosphorylation of MCM2 creates a binding site for Polo-like kinase-1 (PLK1). PLK1 aids in recovery from replication stress by increasing loading of CDC45, thereby increasing nearby origin firing [93]. The ability of ATR to promote local origin firing but inhibit global firing aids in the recovery of stalled or collapsed forks within active replication domains while preventing the creation of new replication domains. Inhibition of global origin firing under conditions of replication stress also prevents exhaustion of the RPA pools thereby preventing replication catastrophe [94]. ATR regulation of origin firing promotes genomic stability in the presence of replication stress.

ATR and CHK1 regulation of origin firing is also important during unperturbed DNA replication. Transient inhibition of either ATR (Figure 1.4) or CHK1 results in increased origin firing and slowed DNA replication in the absence of DNA damage [95-98]. There is no evidence of DNA polymerase speed regulation, but rather alteration of DNA synthesis speed seems to occur indirectly through regulation of origin firing. Inhibition of new origin firing through knockdown of Cdc7 or inhibition of CDK rescues the reduced replication rates observed during CHK1 inhibition [95].

Aside from regulating origin firing, ATR also regulates replication fork stability and promotes DNA repair through regulation of replication fork processing enzymes. If ATR is inhibited during an HU treatment, active replication forks have difficulty recovering from HU and have higher rates of fork collapse (Figure 1.5). Initially, ATR was thought to promote replication fork stability by stabilizing the replisome components at a stalled replication fork [99-101]. This work was done mainly in *S. cerevisiae* and a more recent study, also done in *S. cerevisiae*, found MEC1 does not stabilize the replisome

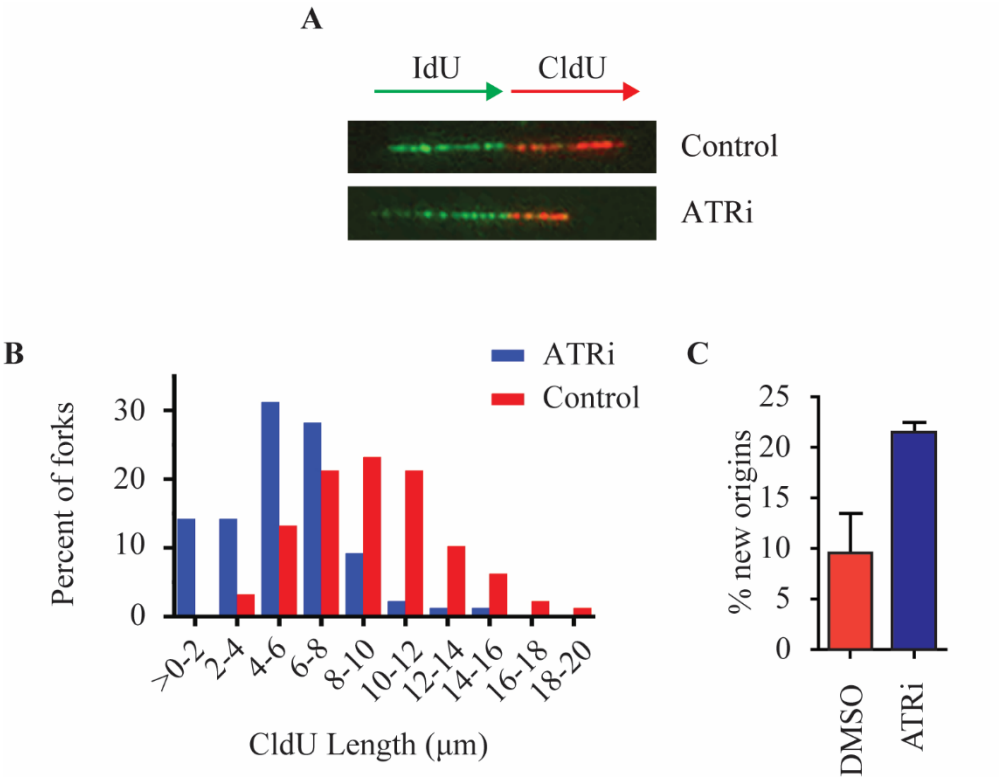

Figure 1.4. Transient inhibition of ATR slows DNA replication and increases origin firing. A-C. RPE-hTERT cells were incubated with 20 μM IdU for 20 minutes followed by a 20 minute incubation with 100 μM CldU in the presence of DMSO or 5μM ATRi (VE-821). **A.** A representative image is shown. **B.** The CldU track length was quantified in dual-labeled tracks and graphed. Blue bars are from cells treated with ATRi and red bars represent cells treated with DMSO. **C.** New origin firing was measured by the percentage of CldU labeled only tracts compared to CldU and IdU labeled tracks. Error bars are SEM. n=100

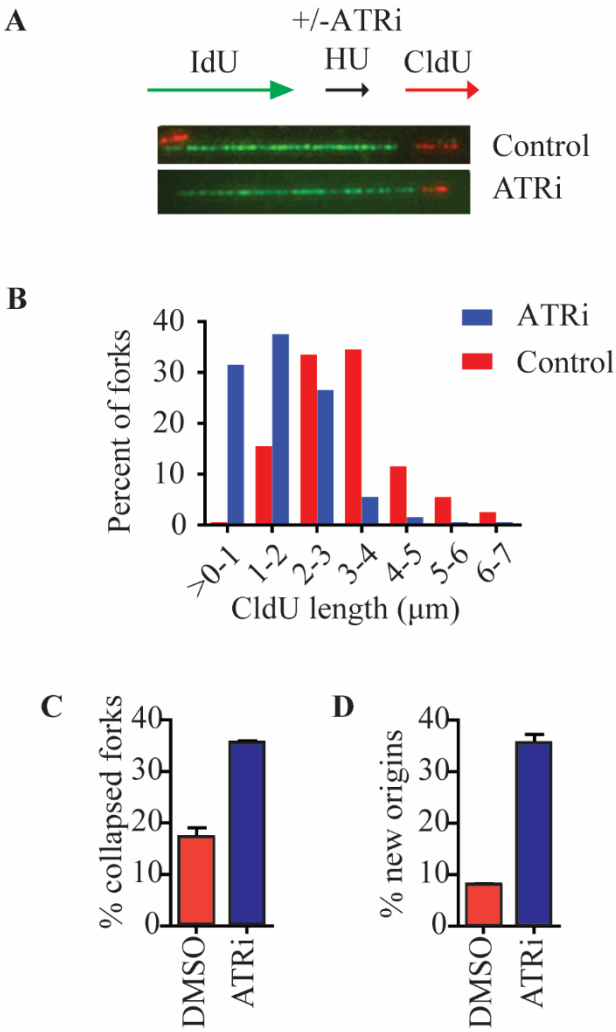

Figure 1.5. ATR stabilizes the replication fork during replication stress. A-D. RPE-hTERT cells were labeled with 20μM IdU for 20 minutes, then incubated with 2mM HU for 2 hours in the presence of DMSO or 5μM ATRi (VE-821), and finally with 100μM CldU for 20 minutes. **A.** A representative image is shown. **B.** The CldU track length was measured and graphed. Blue bars represent cells treated with the ATRi and red bars represent cells treated with DMSO. **C.** The percentage of collapsed forks (IdU only tracks) was calculated. **D.** The percentage of new origins fired (CldU only tracks) was calculated. Error bars represent the SEM. n=100

but rather controls replisome function [102]. In agreement with this work, a recent proteomic analysis done in the lab using human cells found ATR inhibition did not increase displacement of replisome components upon replication fork stalling [103]. However, ATR does regulate fork-remodeling enzymes such as SMARCAL1 at the replication fork. SMARCAL1 promotes stalled replication fork restart and repair when properly regulated [104,105]. However, when ATR is inactivated, SMARCAL1 contributes to replication fork collapse [96]. Recombination can also be used to restart the replication fork and ATR phosphorylates and regulates enzymes involved in recombination such as Bloom syndrome protein, Werner syndrome helicase, and BRCA1 [28]. Werner helicase, similar to SMARCAL1 is phosphorylated by ATR and lose of this phosphorylation leads to an increase in replication fork collapse into DSBs [106]. ATR regulation of fork processing and repair enzymes is a key function of ATR in maintaining genomic integrity.

G2/M Checkpoint

The G2/M checkpoint prevents entry into mitosis in the presence of DNA damage. Both ATM and ATR can activate this checkpoint and do so by similar mechanisms (Figure 1.6). ATM activation leads to CHK2 phosphorylation and active ATR phosphorylates CHK1. CHK1 and CHK2 phosphorylate Cdc25 and in both cases, cause proteasome-mediated Cdc25 degradation. Cdc25 activation of CDK not only promotes new origin firing, as described above, but also allows progression of the cell cycle into mitosis. Activation of CHK1 or CHK2 leads to inhibition of CDK and thereby, prevents entry into mitosis [107,108]. Additionally, inhibition of ATR in the presence of replication stress can cause lethal premature condensation of chromosomes due to loss of the checkpoint.

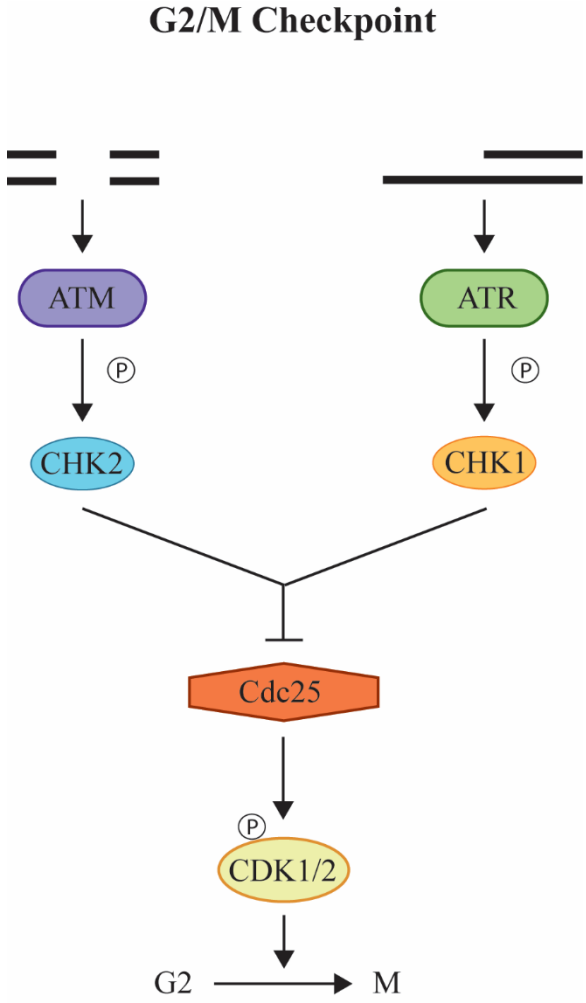

Figure 1.6. The G2/M checkpoint. When activated by the presence of double strand breaks (ATM) or single stranded DNA next to double stranded DNA (ATR), both kinases phosphorylate and activate their respective effector kinases, CHK2 and CHK1. The effector kinases phosphorylate and inhibit Cdc25 phosphatase. The inhibition of Cdc25 prevents cell cycle progression into mitosis.

However, the lethal event seems to be due to S-phase not being prolonged and the cell not having enough time to recover from the stress and finish replicating the genome [109]. As such, the essential function of ATR is in S-phase and not the G2/M checkpoint [30,109,110].

Regulation of PIKK Kinases

ATR is a member of the PIKK family. Other kinase members of this family include DNA-PKcs, ATM, mammalian target of rapamycin (mTOR), and suppressor with morphological effect on genitalia family member (SMG1). ATM, DNA-PKcs, and ATR are DNA damage response kinases while mTOR is a nutrient sensing kinase regulating cell growth and SMG1 regulates nonsense-mediated decay of mRNA. There is evidence in the literature SMG1 can also activate in response to DNA damage and regulates the G1/S phase checkpoint through phosphorylation of p53 and Cdc25 [111-113]. The mechanism of SMG1 activation in response to DNA damage remains unknown. All of these kinases share a common domain architecture (Figure 1.7) and three mechanisms of regulation: localization, protein activators, and post-translational modifications (Figure 1.8). Due to these strong similarities, additional mechanisms of ATR regulation can be elucidated by understanding regulation of the rest of the kinase family.

Domain Architecture

All the PIKK kinases are very large enzymes ranging between ~2500-4000 amino acids and share similar domain architecture (Figure 1.7). On the amino-terminus, are the huntington, elongation factor3, A subunit of protein phosphatase 2A and TOR1 (HEAT)

repeats. HEAT repeats are comprised of two anti-parallel alpha helices linked by a flexible "intraunit" loop [114]. In DNA-PKcs, the HEAT repeats form a half solenoid structure [115]. HEAT repeats facilitate protein-protein interactions and can bind DNA [114,116]. Further work is need to fully understand the function of the HEAT repeats within the PIKK kinases. Work so far in the field has shown these repeats are involved in protein dimerization and as well as facilitating other protein:protein interactions [38,117,118]. The overall significance of kinase dimerization and how the HEAT repeats participate in kinase activation remains unknown. My work, discussed in Chapter III, demonstrates small changes to the HEAT repeats can dramatically alter ATR kinase activity. If the HEAT repeats within PIKK kinases facilitate DNA binding remains unexplored.

Contained within the C-terminal end of the HEAT repeats is the FRAP, ATM, TRRAP (FAT) domain. This domain acts as a potential kinase regulatory domain. In ATM, the FAT domain is auto-phosphorylated on S1981 upon activation [119]. On the far C-terminus of the PIKK kinases is the FAT C-terminus (FATC) domain. The FATC domain is very small and is required for kinase activity. The FAT and FATC domains are only found in PIKK kinases and only occur in combination. It is predicted these two domains interact to facilitate proper folding of the kinase domain [120].

In between the FAT and FATC domains is the kinase domain and the PIKK regulatory domain (PRD). TOPBP1 binds ATR within the PRD to activate the kinase and this domain in the other PIKK family members serves to regulate kinase activation. Tip60 acetylates ATM within the PRD and this acetylation is required for activation of the kinase [121,122]. Additionally, DNA-PKcs activator, KU70/80, binds DNA-PKcs in the region

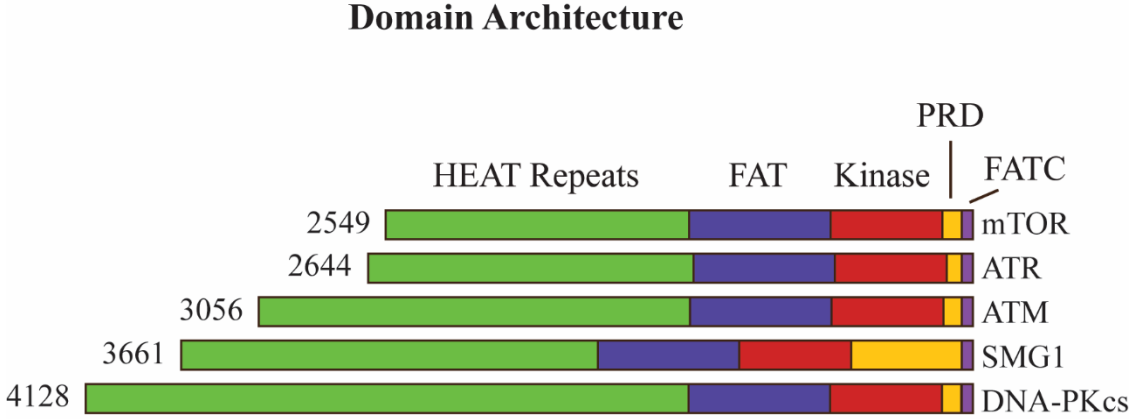

Figure 1.7. The common domain architecture of PIKK family kinases. The N-terminus of PIKK family kinases is comprised of HEAT repeats. The C-terminus of the HEAT repeats contains the FAT domain. The kinase domain is C-terminal to the FAT domain followed by the PRD and FATC domains.

of the PRD [123]. Point mutations of the PRD within DNA-PKcs also prohibits activation of the kinase [51]. The activator of mTOR binds the PRD and deletion of the mTOR PRD creates a constitutively active kinase [124,125]. Thus, the PRD within the PIKK kinases is important for regulating activation of these kinases.

Regulation by Localization

In the activation of the PIKK family, each member localizes to specific subcellular locations, in part to concentrate them with their activators (Figure 1.8A). ATM and DNA-PKcs activate in response to DSBs. When a DSB occurs, the KU70/80 complex binds to the DNA ends. DNA-PKcs is recruited to the DNA breaks through interaction with KU70/80 and DNA-PKcs activation is dependent on DNA and KU70/80 [126,127]. ATM activation also occurs through a similar mechanism. The MRN complex binds to the DNA ends and recruits ATM [128]. However, there is a debate if MRN localizes an already active ATM or an inactive ATM. Changes in chromatin structure, even in the absence of DSBs, can activate ATM [119]. In this case, MRN localizes an already active kinase and is acting as a signal amplification mechanism. Additionally, ATM activates in response to oxidative stress independent of the formation of DSBs or interaction with MRN. Reactive oxygen species activate ATM through formation of a disulfide crosslinked ATM dimer [129]. As described above, ATR activates in response to ssDNA gaps and localizes to these sites through ATRIP binding of RPA. ATR activation has a second step of regulation as the 9-1-1 complex must also localize to these DNA lesions.

To activate mTOR and SMG1, both of these kinases also undergo changes in cellular localization. mTOR complex 1 (mTORC1) activates in response to nutrients and

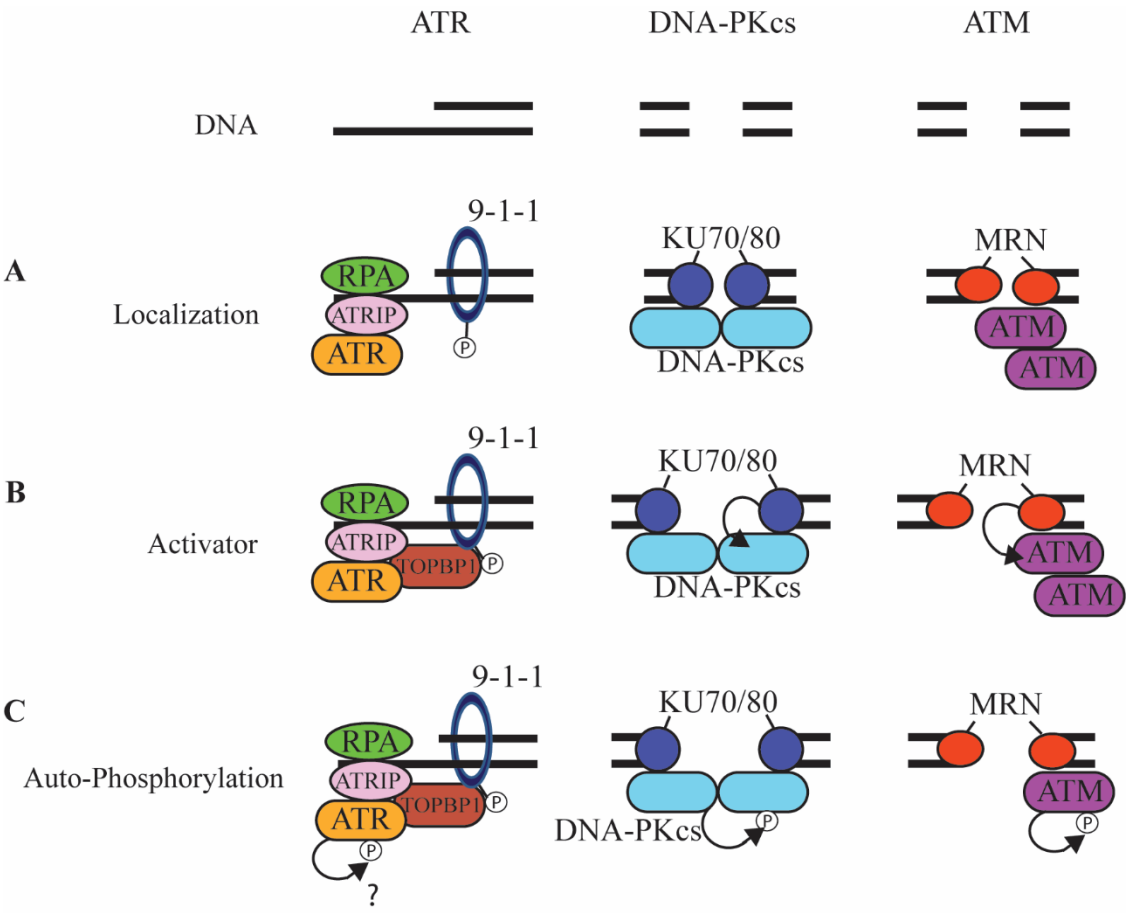

Figure 1.8. PIKK family kinases share three mechanisms of regulation. A. PIKK family kinases are localized to specific subcellular regions. **B.** The PIKK family kinases are activated by specific protein activators. **C.** PIKK family kinases autophosphorylate upon activation, regulating their kinase activity. It is unknown if ATR also undergoes autophosphorylation.

amino acids and contains the binding partner RAPTOR [130,131]. Additionally, mTOR can partner with RICTOR to form mTOR complex 2 [132]. Upon nutrient sensing, RAPTOR localizes mTOR to lysosomes and late endosomes, which co-localizes the complex with its activator, RHEB [133,134]. SMG1 is an mRNA surveyor and ensures cellular mRNA quality. If a premature termination codon is present in an mRNA, SMG1 in complex with Upf1, eRF1, and eRF3 binds protein complexes at the exon-junction and premature stop codon of the mRNA and promotes degradation of the mRNA [135]. Localization is a recurring theme in PIKK kinase activation and occurs commonly through binding partners as ATRIP, KU70/80, RAPTOR, and the MRN complex.

Regulation by Protein Activators

Localization of the PIKK kinases to specific cellular compartments concentrates the kinase in an area with its activator. The PIKK family members activate through binding of a specific activator, which induce a conformational change of the kinase (Figure 1.8B). As previously mentioned, ATR is activated by TOPBP1 [40,51,53]. TOPBP1 binds both ATR and ATRIP and is predicted to induce a conformational change within ATR and increase ATR substrate affinity [136]. In the presence of a DSB, ATM is activated by Mre11/RAD50 and DNA-PKcs is activated by KU70/80 [126,137]. A small GTPase RHEB binds and activates mTOR and displaces the mTOR inhibitor PRAS40 [138-140]. Once properly localized, specific protein binders activate the kinases.

Regulation by Post-Translational Modifications

Post-translational modifications such as phosphorylation, acetylation, and SUMOylation, regulate PIKK family members (Figure 1.8C). mTORC1 undergoes phosphorylation and auto-phosphorylation. Activation of the pathway leads to phosphorylation of S1261 on mTOR. This phosphorylation site increases the kinase activity and is needed for mTOR autophosphorylation on S2481 [141]. mTOR autophosphorylation does not alter kinase activity but instead acts as a marker of an active kinase [142]. Additionally, mTOR phosphorylation on S2448 also corresponds with kinase activity [143].

ATM undergoes auto-phosphorylation, phosphorylation, and acetylation during activation of the kinase. DNA damage activates Tip60, which acetylates ATM and recruits it to sites of DNA damage [121,122]. This initial acetylation partially activates ATM but full activation may require the MRN complex. Four auto-phosphorylation sites on ATM have been identified, S367, S1893, S1981, and S2996 [119,144,145]. Phosphorylation of these sites occurs as ATM transitions from an inactive dimer to an active monomer, and mutation of these sites impairs ATM activation in human cell culture models [119,145]. However, mice expressing ATM with the autophosphorylation sites mutated have normal ATM activation and signaling in response to DNA damage [146,147]. Additionally, activation of ATM by MRN *in vitro* does not require ATM auto-phosphorylation [137]. Differences between murine and human studies remain unresolved.

DNA-PKcs has over 40 identified phosphorylation and autophosphorylation sites [148]. There are two phosphorylation clusters within DNA-PKcs. The first cluster, around S2609, was originally identified as sites of autophosphorylation [149-152]. However,

more recent studies implicate ATM and ATR as phosphorylating these sites in response to DSBs and replication stress, respectively [152,153]. These sites are important for kinase function as mutation to alanine causes radiosensitivity and diminished DNA end joining *in vitro* [149,151,154,155]. In mice, mutation of these sites results in early lethality and congenital bone marrow failure [156]. Structural studies have shown phosphorylation of these sites results in a large structural change resulting in DNA-PKcs release from DNA [157,158]. The second phosphorylation cluster occurs around S2056. S2056 is a bona fide auto-phosphorylation site [150,159]. Mutation of this cluster results in radiosensitivity and less efficient DSB repair. Phosphorylation of these two clusters have opposing roles as S2056 phosphorylation limits DNA end processing while phosphorylation of S2609 cluster promotes end processing [159,160].

Both ATR and ATRIP are subjected to post-translational modifications. ATRIP is phosphorylated in a cell cycle dependent manner by CDK2 and this phosphorylation is important for maintenance of the G2/M checkpoint [161]. ATRIP is also SUMOylated, which promotes localization and binding to ATR, RPA, TOPBP1, and the MRN complex, and elimination of the SUMOylation results in reduced pCHK1 signaling [162]. We and others identified multiple ATR phosphorylation and auto-phosphorylation sites. Protein kinase A can phosphorylate ATR on S435 to enhance ATR binding to XPA, which in turn promotes localization of ATR to DNA lesions [163]. ATR is also phosphorylated on S428, S436, S437, and T1989. Of these only T1989 is characterized and may potentially be an auto-phosphorylation site [164,165]. T1989 is a DNA damage inducible, ATR kinase activity-dependent phosphorylation site. However, phosphorylation of this site does not alter kinase activity but instead marks an active kinase. Mutation of T1989 to alanine does

not confer sensitivity to DNA damaging agents but does result in a modest reduction in cell viability. It remains unknown if ATR contains phosphorylation or autophosphorylation sites which alter kinase activity or confer conformational changes such as seen with ATM and DNA-PKcs. My work towards identifying a potential new ATR autophosphorylation site is discussed in Chapter III.

Targeting the DDR in Cancer

Oncogene Induced Replication Stress

In the early stages of cancer development, most precancerous lesions have high levels of replication stress and an activated DDR [166,167]. The overexpression of oncogenes such as RAS, MYC, Cyclin E, MOS, or Cdc25A induce replication stress through deregulation of the cell cycle and DNA replication resulting in high levels of DSBs [168]. The overexpression of oncogenes, such as Cyclin E, promote increased origin firing, which depletes nucleotide pools, impairs replication fork progression, increases torsional stress in the DNA, and increases collisions between DNA replication and transcription machinery [169-171]. Activation of the DDR in response to these stresses guards against genomic instability and acts as an early anti-cancer barrier [166,167]. In order for tumorigenesis to proceed, cancer cells commonly downregulate DDR checkpoint genes such as p53 or ATM as well as DNA repair pathways [166].

The deregulation of DNA repair and checkpoint genes aids in tumor progression but also presents exploitable defects. Loss of one or more DDR pathways increases genomic instability and creates a higher dependency on the remaining repair pathways. Additionally, deregulation of DNA repair can modulate a cancer cells response to the

traditional DNA damaging chemotherapies. Use of a chemotherapy which induces a type of DNA damage the cancer cell is defective at repairing can induce cell death. However, deregulation of DNA repair may also promote resistance or another repair pathway can compensate for the lost pathway. The cancer cells increased dependence on the remaining repair pathways as well as the potential to sensitize cancer cells to traditional chemotherapies makes development of inhibitors to DNA repair or DDR checkpoint genes a promising anti-cancer therapeutic strategy [172].

Inhibition of the DDR

Inhibitors to the DDR have two therapeutic avenues. First, they are used in combination with traditional chemotherapies to prevent or reverse resistance. This strategy is effective with WEE1 inhibitors (WEE1i) in the clinic. Patients with p53 mutated ovarian cancer already resistant to standard first line therapy (carboplatin and paclitaxel) were treated with the WEE1i in combination with carboplatin. 27% of the patients had a partial response and 41% had no disease progression and response to the drugs was sustained for an average of 10 months [173]. In preclinical data, the PARP inhibitor (PARPi), in combination with temozolomide, a DNA alkylating agent, can resensitize temozolomide resistant cancers [174-176]. One major obstacle in the clinic has been in identifying the correct dose and dosing schedule for these drugs. However, use of DDR inhibitors in combination with DNA damaging chemotherapies remains a promising therapeutic strategy.

DDR pathways when mutated or down regulated can be partially compensated for by other repair pathways. This reliance on remaining intact repair pathways provides an

exploitable therapeutic window through synthetic lethality. Synthetic lethality is when a combination of mutations in two or more genes or pathways leads to cell death whereas the single gene or pathway mutation cells maintain viability [177]. A great success in combining a DDR inhibitor with synthetic lethality is with the PARPi and BRCA mutations. PARP binds ssDNA breaks and signals for repair. PARPi traps the enzyme on the DNA and prevents signaling for DNA repair. This protein:DNA complex is thought to collapse into a DSB when a replication fork encounters this lesion [178]. Normal cells are able to repair the DSB using homologous recombination (HR). However, treatment of cells deficient in HR, primarily through genetic mutation of BRCA1 or 2, with the PARPi induces cell death [179,180]. Identifying clinically exploitable synthetic lethal relationships remains a challenge. Additionally, the tumor cells will eventually acquire resistance and the cancer will progress.

ATR Inhibitors

ATR is the primary kinase that responds to replication stresses and is essential in replicating cells. Cancer cells appear to be even more reliant on the ATR pathway to maintain viability due to high levels of replication stress. Additionally, many traditional chemotherapeutics induce DNA damage and activate ATR. Inhibition of ATR may modulate a cancer cells response to these chemotherapies. Astra Zeneca and Vertex Pharmaceuticals developed ATR-specific inhibitors, AZD6738 and VX-970, respectively. These compounds are currently entering Phase II clinical trials (clinicaltrials.gov [181,182]).

With the development of the ATRi, questions remained of who should receive these inhibitors in the cancer clinic and which chemotherapies should be used in combination with the ATRi. Our work and others shows the ATRi synergizes with many commonly used chemotherapies such as platinums, PARPi, topoisomerase inhibitors, gemcitabine, and ionizing radiation [183-188]. Additionally, we and others observed the ATRi resensitizes cisplatin resistant cells to cisplatin and that maximum cell killing is observed if cells are treated with cisplatin first and then the ATRi (Vertex unpublished data [183,189]). Bromodomain and extra-terminal (BET) protein inhibitors were also shown to synergize with the ATRi due to transcriptional changes but in our hands this effect was only ever additive (Chapter V and [190]). The observed synergy between the ATRi and a wide array of chemotherapies and the ATRi facilitating resensitization of resistant cancer cells to chemotherapies are promising preclinical results.

One remaining question is whether there are pathways when lost that are synthetic lethal with ATR inhibition. We and others have worked extensively to identify these pathways. We conducted a smaller scale siRNA screen identifying loss of ERCC1 and REV3 as synthetic lethal with the ATRi [183,191]. The Helleday lab, in agreement with our findings discussed in Chapter IV, found the CHK inhibitors (CHKi) and ATRi synergize [192]. However, previous CHK inhibitors did poorly in the clinic and many of the studies were terminated due to patient toxicity or funding problems. However, there are new CHK inhibitors currently in phase I and II clinical trials, but it remains questionable if these drugs will gain FDA approval.

Many other groups published findings identifying specific genetic losses that are synthetic lethal with the ATRi. Loss of ATM will moderately sensitize cells to the ATRi,

and in the phase II clinical trials, ATM deficiency is one patient selection strategy being used [193-195]. Loss of XRCC1, overexpression of Cyclin E, and loss of PolD1 also sensitize cells to the ATRi [196-198]. Loss or mutation of p53 was initially found to sensitize cells to the ATRi but this finding has not held true in preclinical studies [194,197]. There are studies showing deficiencies in HR will sensitize cells but we and others failed to replicate this finding [183,187,193,199]. Lastly, cells using the alternative lengthening of telomeres (ALT) pathway to maintain their telomere lengths are more sensitive to the ATRi [200]. Aside from ATM deficiency, none of these findings have yet been translated into the clinic. It remains to be determined which patients will most benefit from these inhibitors. To answer this question, I, in collaboration with a Post-doctoral fellow in the lab Kareem Mohni, conducted a whole genome siRNA screen with the ATRi and ATRi/cisplatin to identify synthetic lethal pathways, discussed in Chapter IV.

Current ongoing clinical trials are combining a wide array of chemotherapies with the ATRi in a wide variety of cancers. As of yet, no clinically actionable patient population has been identified. However, with the completion of Phase II, patient samples will be available with clinical records identifying responders and non-responders. These samples can be used to identify potential genetic backgrounds which confer sensitivity or resistance to the ATRi.

CHAPTER II

MATERIALS AND METHODS

Table 2.1: Site-directed Mutagenesis Primers

The listed primers were used to create the indicated amino acid mutation within ATR. All primers introduce an MfeI restriction enzyme site.

Primer #	Mutation	RE Check	Sequence
JL16	ATR S1333D	Mfe1	GACAGTGAAACAGTAGAACCTATTAT
JL36	ATR S1333K	Mfe1	CAGTGAAACAGTAGAACCTATTATCAAA
JL38	ATR Q1334E	Mfe1	GAAACAGTAGAACCTATTATCTCAGAGCT
JL40	ATR V1338L	Mfe1	GTGAAACAGTAGAACCTATTATCTCACAA
JL42	ATR S1333G	Mfe1	GTGAAACAGTAGAACCTATTATCGGACA
JL44	ATR S1333R	Mfe1	GTGAAACAGTAGAACCTATTATCCGACA

Site-directed Mutagenesis

A fragment of the ATR cDNA was subcloned into pBSKII(-) using the restriction enzymes BstXI and AgeI. The ATR fragment was mutagenized using the QuikChange Site-directed Mutagenesis method (Agilent Technologies) with the primers in Table 1. The mutagenized fragment was subcloned back into the full-length ATR cDNA in a plasmid with a FLAG-HA, just FLAG, or MYC tags. Mutagenesis was confirmed by restriction enzyme checks and sequencing.

Table 2.2: Antibodies for Western Blot

The antibodies listed below were used for western blotting at the indicated concentrations diluted in 1% milk-TBST.

Antibody	Species	Dilution	Company	Catalogue #
ATAD5	Rb	1:2000	Custom	Myung Lab
ATM	Rb	1:3000	Novus	NB100-104
ATR N19	Gt	1:1000	Santa Cruz	SC-1887
ATRIP 403	Rb	1:3000	Bethyl Custom	Cortez
ATRIP N	Rb	1:3000	Custom	Cortez
BRD2	Rb	1:3000	Abcam	ab139690
BRD3	Ms	1:500	Abcam	ab50818
BRD4	Rb	1:1000	Abcam	ab128874
CHK1	Ms	1:1000	Santa Cruz	sc-8408
CHK2	Rb	1:2000	Custom	Cortez
Cleaved PARP	Rb	1:1000	Cell Signaling	9541
Cyclin D1	Ms	1:500	Santa Cruz	sc246
FLAG M2	Ms	1:3000	Sigma	
GAPDH	Ms	1:10000	Millipore	MAB374
GST	Gt	1:1000	Amersham	27457701
Histone H4	Ms	1:10000	Abcam	ab31830
H4K5 Acetyl	Rb	1:10000	Abcam	ab51997
HA	Ms	1:1000	Covance	MMS-101P
KU70	Ms	1:1000	Abcam	ab3114
MCM2	Ms	1:10000	BD Transduction Labs	39289
Myc 9E10	Ms	1:1000	Covance	MMS-150P
NBS1	Rb	1:1000	Novus	NB 100-143B
p1589(1989) ATR	Rb	1:100	Custom	Cortez
p1989 ATR	Rb	1:1000	Epitomics Custom	Cortez
PCNA	Ms	1:200	Santa Cruz	SC-056
PRKAR2A	Ms	1:2000	Abcam	ab124400
pS108 MCM2	Ms	1:5000	Bethyl Custom	Cortez
pS240/244 S6	Rb	1:1000	Cell Signaling	2215
pS317 CHK1	Rb	1:1000	Bethyl	2344S
pS345 CHK1	Rb	1:3000	Cell signaling	2341S
pS4/8 RPA	Rb	1:1000	Bethyl	A300-245A
pS645 Rad17	Rb	1:1000	Bethyl Custom	Cortez
pS966 SMC1	Rb	1:1000	Bethyl	A300-050A
pT68 CHK2	Rb	1:1000	Cell Signaling	2661S
RAD17	Gt	1:5000	Bethyl	A300-151A

RAD9	Rb	1:2000	Bethyl	A300-890A
RFC1	Rb	1:1000	Abcam	ab3853
RFC4	Rb	1:1000	Abcam	ab192021
RPA32 9H8	Ms	1:1000	Cell signaling	ab2175
RPA70	Rb	1:1000	Bethyl	A300-244A
S6	Rb	1:1000	Cell Signaling	2217
SetD2	Rb	1:750	Abcam	ab69836
SMARCAL1 909	Rb	1:5000	Custom	Cortez
TOPBP1	Rb	1:2000	Bethyl	A300-111A-1
WDR82	Rb	1:500	Abcam	ab175071

Cell Lysate for Western Blot

Cells were harvested by trypsinization and washed 2x with PBS. Cells were resuspended in lysis buffer (1% NP-40, 50mM Tris pH 7.5, 200mM NaCl, and protease and phosphatase inhibitors: 1mM PMSF, 1mM Na Vanadate, 1mM DTT, 1mM NaF, 20mM β-glycerolphosphate, 1µg/mL aprotinin, and 1µg/mL leupeptin) and incubated on ice for 30 minutes. Lysates were centrifuged in the cold room at maximum speed for 15 minutes. The supernatant was then transferred to a new tube and protein concentration was measured using the Bradford assay. 2x sample buffer was added and samples were boiled for 5 minutes. Majority of the time, 40µg of protein was loaded into the gel and separated by SDS-PAGE. Proteins were transferred onto nitrocellulose overnight in the cold room (0.2 constant Amps, 8 hours).

Cell Lines

The following cell lines were obtained from ATCC and grown according to their recommendations: A673, MDA-MB-415, H810, H2126, HCC1187, MDA-MB-436, HCC1806, BT549, MDA-MB-231, BT20, Hec-1-a, HCT116, and HCC2218. MDA-MB-

415 cells were transitioned to DMEM but still grown with all the supplements as recommended by ATCC. We obtained the following cell lines from Dr. Pierre Massion: A549, H157, HCC827, H441, H1869, H2172, DMS53, and H520. All cell lines were grown in RPMI except DMS53. DMS53 were grown in Waymouth media. We obtained A704 cells from Dr. Peter Clark and they are grown in EMEM. We received two cell lines from Dr. Jennifer Pietenpol: HDQP1 and CAL51. Both lines are grown in DMEM. We obtained LN319 from AddexBio and GP2D from Sigma. Hec59 cells are from Dr. Tom Kunkel and grown in DMEM/F12. We received IGROV-1 from Dr. Dineo Khabele and TE5 from Dr. Claudia Andl. Both lines are grown in DMEM. All cell lines were grown in 10% FBS unless otherwise indicated by the supplier. Information of cell doubling times, and cell numbers to plate in a 96-well plate are found in Chapter IV.

Transfection

Transfections were completed as stated by the manufacturer's protocol. The following reagents were used for siRNA transfection. All transfections were done as reverse transfections in 60 mm dishes using 10nM siRNA in a total volume of 4mL. BT549: $4x10^5$ cells, 8µL Dharmafect1, MDA-MB-468: $12.8x10^5$ cells, 4 µL Dharmafect3, MDA-MB-157: $8x10^5$ cells, 4 µL Dharmafect1, MDA-MB-231: $8x10^5$ cells, 8 µL Dharmafect1, MDA-MB-453: $1.6x10^6$ cells, 10µL Dharmafect1, HCC1806: $1.5x10^6$ cells, 6µL Dharmafect1, A549: $3x10^5$ cells, 8µL Dharmafect1, H157: $6x10^5$ cells, 8µL Dharmafect1, U2OS: $3x10^5$ cells, 6.4µL Dharmafect1, CAL120: $5x10^5$ cells, 8µL RNAi Max, SW527: $12.8x10^5$ cells, 8µL Dharmafect4, MDA-MB-436: $1.3x10^6$ cells, 10µL Dharmafect1, HeLa: $3x10^5$ cells, 6.4µL RNAi Max, RPE: $2.4x10^5$ cells,

6.4µL RNAi Max, 293T:(35mm dish) $1x10^6$ cells, 5µL RNAi Max. Plasmid transfections were also done following the manufacturer's protocol. 293T: PEI, HeLa: Lipofectamine, U2OS: Fugene.

Reagents

The following compounds were acquired from the listed company. VX-970, BMN673, JQ1, iBET726 were purchased from Selleck Chemicals. Hydroxyurea, Gemcitabine, and Camptothecin were purchased from Sigma. Cisplatin is from Calbiochem. AZD7762 can be obtained from Selleck Chemicals. AlamarBlue is from Invitrogen.

ATR Kinase Assay

293T cells were transfected with 3µg Flag-ATR + 1µg HA-ATRIP (pDC720) per dish using PEI. 2-10cm dishes were transfected per condition. The next day each plate was expanded into a 15cm dish. The next day the cells were left to grow and the following day harvested for nuclear extracts. Cell pellets cannot be frozen. Cells were harvested with 5mL of PBS per dish and centrifuged. The pellet was resuspended in 1mL PBS and transferred to a 1.5mL tube. Cells were then resuspended in 1mL cold hypotonic buffer by gentle pipetting and centrifuged at 2500xg for 3 minutes at 4 degrees. The cells were then resuspended in 400µL cold hypotonic buffer and allowed to swell on ice for 10 minutes and then dounce homogenized. The lysate was centrifuged for 6 minutes at 3300xg at 4 degrees. The supernatant was discarded. 250µL of High salt buffer was added in

increments to the pellet, stopping to drag tube along rack to thoroughly mix. The sample was incubated for 30 minutes on a rotator in the cold room.

During the 30 minute incubation, 25µL of HA bead slurry was washed with No salt buffer per IP. Samples were centrifuged at maximum speed for 10 minutes at 4 degrees and 200µL No salt buffer was added. Samples were centrifuged at maximum speed for 5 minutes in the cold room. Extract can be flash frozen and stored at -80 degrees until ready to be used. Extract was added to the prepared beads and the IP was done at 4 degrees for 3 hours. Beads were washed 3x quickly in TGN lysis buffer with phosphatase and protease inhibitors, once in TGN + LiCl (prepare fresh, 500 mM LiCl in TGN buffer), and 2x with 1x kinase buffer. The beads were resuspended in 400µL kinase buffer and split evenly into two eppendorf tubes. The beads may be split into 6-8 tubes. Kinase assays were carried out with the ATR-ATRIP complex on the beads. Kinase reaction contained the following with a total volume of 30µL: 1µg GST-MCM2, 0.5µL γ^{32}P-ATP, 10µM cold ATP, 10pmol GST or GST-AAD, and 15µL 2x kinase buffer. Reactions were carried out at 30 degrees for 20 minutes with mixing every 3-4 minutes by gentle flicking. Reactions were stopped by adding 30µL 2X sample buffer. Samples can be stored at -80 until ready to use. Samples were separated on two 4-12% gradient gels with MOPs buffer, loading 15µL of sample per gel. One gel was stained with coomassie blue, dried overnight, and exposed with the phosphor imager screen for ~2 hours.

Hypotonic Buffer: 20mM Hepes pH 7.9, 1.5mM MgCl2, 10mM KCl, 0.2mM PMSF, 0.5mM DTT. No Salt Buffer: 20mM Hepes pH 7.9, 20% glycerol, 0.2mM PMSF, 0.1% Tween20. High Salt Buffer: 20mM Hepes pH 7.9, 25% glycerol, 1.5mM $MgCl_2$, 350mM NaCl, 0.2mM PMSF, 0.5mM DTT, 1mM NaF, 1mM Na Vanadate, 10mM B-

glycerolphosphate, Aprotinin, and Leupeptin. 2X Kinase Buffer: 20mM Hepes pH 7.5, 100mM NaCl, 20mM $MgCl_2$, 20mM $MnCl_2$, 100mM β-glycerolphosphate, 2mM DTT. TGN Buffer: 50mM Tris pH 7.5, 150mM NaCl, 10% Glycerol, 1% Tween20, 0.2mM PMSF, 0.5mM DTT, 1mM NaF, 1mM Na Vanadate, 10mM β-glycerolphosphate, Aprotinin, Leuopeptin.

Chromatin Fractionation

This is the protocol followed for all included experiments and was adapted from Mendez and Stillman [201]. All steps were done with cold, freshly made buffers and kept on ice. $3x10^6$ 293T cells were used per sample or $1.5\ x10^6$ U20S cells. With the U2OS cells, buffer volumes can be cut in half. After washing the cells with PBS, they were resuspended in 200μL Buffer A and left on ice for 5 minutes. Samples were then centrifuged at 1300xg for 4 minutes and the supernatant removed. This is the cytoplasmic/soluble fraction. The nuclei are in the pellet. Nuclei were resuspended again with 1mL of Buffer A, centrifuged at 1300xg for 4 minutes, and the supernatant discarded. The nuclei were lysed in 200μL Buffer B for 10 minutes on ice and centrifuged at 1700xg for 4 minutes. The supernatant is the soluble nuclear fraction. The pellet is the chromatin fraction. The chromatin fraction was resuspended with 1mL of Buffer B but the pellet does not go into solution so do not try pipetting. Samples were centrifuged at 10,000xg for 1 minute and the supernatant discarded. The pellet was resuspended in 200μL 2X SDS sample buffer and boiled for 5 minutes. The sample was sonicated until easily pipetteable.

Buffer A: 10mM HEPES pH 7.9, 10mM KCl, 1.5mM $MgCl_2$, 0.34M sucrose, 10% glycerol, 0.1% Triton X-100, 1mM DTT, 1mM NaF, 1mM Na_2VO_3, Aprotinin, Leupeptin.

Buffer B: 3mM EDTA, 0.2mM EGTA, 1mM DTT, 1mM NaF, 1mM Na_2VO_3, Aprotinin, Leupeptin.

Chromatin Fractionation: Alternative Method

This method was adapted from Lee *et al.* [202]. $3x10^6$ 293T cells per sample were harvested. After washing with PBS, cells were resuspended in 200µL Buffer A and incubated on ice for 5 minutes. Samples were centrifuged at 1300xg for 4 minutes and the supernatant removed. This is the "soluble fraction". The pellet was resuspended again in 1mL of Buffer A and samples were centrifuged at 1300xg for 4 minutes. The supernatant was discarded. The nuclei were resuspended in 200µL Buffer B and incubated on ice for 10 minutes. Samples were then sonicated until easy to pipette, incubated on ice an additional 10 minutes and centrifuged at 10,000xg for 1 minute. This is the "insoluble fraction".

Buffer A: 100mM NaCl, 300mM Sucrose, 3mM $MgCl_2$, 10mM Pipes pH 6.8, 1mM EGTA, 0.2% Triton X-100, 1mM DTT, 1mM NaF, 1mM Na_2VO_3, Aprotinin, Leupeptin. Buffer B: 50mM Tris-HCl pH 7.5, 150mM NaCl, 5mM EDTA, 1% Triton X-100, 0.1% SDS, 1mM DTT, 1mM NaF, 1mM Na_2VO_3, Aprotinin, Leupeptin.

DNA Fiber Labeling

Cells were plated in a 6-well dish the day before to be 60-70% confluent the next day and at least one extra well was plated for a dilution step with non-labeled cells later in the protocol. Media and HBSS were equilibrated overnight. Cells were labeled with 20µM IdU for 20 minutes and washed 2x with equilibrated HBSS (2mLs per wash). Cells were

then treated with a damaging agent if desired and washed again with 2x equilibrated HBSS. Cells were then labeled with 100µM CldU for 20 minutes and washed 2x with equilibrated HBSS. Cells were harvested by trypsinization at room temperature (300 µL/well for a 6-well plate), centrifuged and resuspended in ice cold PBS for a concentration of $1x10^6$ cells/mL. Labeled cells were diluted 1:3 with non-labeled cells before spreading. 2µL of cell suspension was added to each slide near the white frosted end and 10µL of spreading buffer was added to the cells. Cells were allowed to lyse for 6 minutes at room temperature. (Spreading Buffer: 0.5% SDS, 200mM Tris-HCl pH 7.4, 50mM EDTA) Slides were then tilted to 15 degrees to allow the DNA to spread and slides were allowed to air dry. Make sure drop runs straight and slowly. Do not allow drop to sit at the top for too long as the DNA gets tangled. Slides were fixed for 2 minutes in 3:1 methanol:acetic acid in a coplin jar. Do not screw the lid onto the coplin jar. Slides were air dried and stored overnight at 4 degrees for a maximum of 5 days.

The next day, the slides were treated with 2.5M HCl for 30 minutes in a coplin jar and rinsed 3x in PBS in the coplin jars. Slides were blocked with 10% goat serum/ PBSTw (0.1% Triton in PBS) in a coplin jar for 1 hour. 10% serum/PBSTw was sterile filtered to reduce background staining. Primary antibody was incubated on the slide for 1 hour with rat monoclonal anti-BrdU (anti-CldU) and mouse anti-BrdU (anti-IdU) 1/100 diluted in 10% goat serum/ PBSTw. 200µL of antibody was added to the parafilm and slides inverted on top. All incubations are done in the dark. Optional: Can use an anti-DNA antibody (mouse) 1/300 to check continuity of DNA fibers. Slides were rinsed 3x with PBS in coplin jar. Secondary antibody was incubated on the slides for 30 minutes same as primary, goat anti-rat IgG Alexa Fluor 594 and Goat anti-mouse Alexa Fluor 488 1:350 in 10% goat

serum/PBSTw. Slides were rinsed 3x in PBS and air dried in the dark. Whole slide coverslips were mounted with ~110 µL Prolong Gold with no DAPI. It is recommended to prepare 5 slides per condition and take a minimum of 20 images.

Flow Cytometry

Tips: Add yellow tip to end of 1 mL tip to aspirate. Rack tubes across tube rack to loosen pellet before adding next solution. Before the cells are harvested, label them with 10µM BrdU for 20 minutes when desired. $5x10^5$ cells were harvested per sample in 300µL PBS on ice. 700µL of ice cold Ethanol was added and mixed gently by inverting tube. Cells were fixed for at least 2 hours on ice or at -20 degrees. Cells were centrifuged, aspirated, and resuspended in 1mL 0.5% BSA/PBS. If the cells were BrdU labeled: 1mL 2N HCl + 0.5% triton-x-100/PBS (5mL 4N HCl, 5mL PBS, 500µL 10% Triton-X-100) was added and the samples were incubated for 30 minutes at room temperature. Samples were centrifuged, aspirated, and the remaining HCl was quenched with 1mL Na-Borate incubated for 2 minutes. Samples were pelleted, aspirated, and resuspended in 1mL 0.5%BSA/PBS. Followed by resuspension in 100uL of BrdU antibody (1:20 BrdU-488 in 0.5% BSA/PBS/0.5% Tween) and a 30 minute incubation at room temperature. Cells were washed with 1mL 0.5% BSA/PBS, and incubated with 500 µL PBS + Propidium Iodide and RNAase A. Stock PI at 5mg/mL, add 5µL per mL PBS. Use RNAase from miniprep kit (Sigma) adding 5µL per mL PBS. Protect from light, PI is light sensitive. Samples were incubated at 37 degrees for 30 minutes and then stored at 4 degrees until ready to use. Cells were filtered right before use.

Immunofluorescence

When desired: Cells were labeled with EdU for 20 minutes. Cells were plated in a 12-well or 6-well dish with coverslips the day before. HCT116 cells should be plated 2 days before. Cells were very gently rinsed with PBS. When desired, cells were pre-extracted by adding triton solution gently to the cells for 5 minutes on ice or at 4 degrees. Cells were fixed with paraformaldehyde solution for 10 min at room temperature and washed 3x PBS. Next, the cells were permeabilized with triton solution for 10 minutes on ice and followed with 4x PBS washes. When staining for PCNA: after the fixation, cells were permeabilized with ice cold acetone for 2 minutes. 5% BSA-PBS solution was used to block the cells for 15 minutes. When cells were pulsed with EdU, proceed with a click reaction for 30 minutes at room temperature in the dark and follow with a PBS wash. Next, cells were incubated with primary antibody for 30 minutes at 37 degrees in a humidified incubator. Antibodies were diluted in 1% BSA-PBS. The wells were rinsed 3x PBS before proceeding to secondary antibodies. All Alexafluor secondary antibodies were diluted 1:500 in 1% BSA-PBS and incubated with cells for 20 minutes in the dark at room temperature. Cells were rinsed three times with PBS before mounting the coverslips with pro-long gold with DAPI. Cell images were quantified using Cell Profiler or ImageExpress.

Triton-X-100 Solution: 20mM HEPES, 50mM NaCl, 3mM MgCl2, 300mM sucrose, 0.5% Triton X-100. Paraformaldehyde:15g of paraformaldehyde was dissolved in 250mL water. The solution was incubated 20 minutes at 65 degrees in a water bath and then 3 drops of 10N NaOH were added. The solution was left in the water bath for an additional 5 minutes to allow the powder to completely dissolve. Then 50mL of 10X PBS

and 10g of sucrose was added and the solution was brought to a final volume of 500mL with distilled water. The solution was sterile filtered, aliquoted into single use tubes, and stored at -20 degrees. Click Reaction Solution: The following reagents were mixed in order: 875µL PBS, 5µL Alexa Fluor 488 or 594 conjugated to azide, 100µL 20mg/mL Na Ascorbate, and 20µL 100mM Copper Sulfate.

Genetic Complementation of ATR Flox/- Cells

DNA backbone used to make all the cell lines: pCDNA5/TO HA-FLAG-ATR. First, 10µg of the DNA was linearized using Fsp1. The reaction was incubated at 37 degrees for 1-2 hours. Next, the DNA was precipitated and resuspended in 20µL. The DNA was confirmed to be linearized on an agarose gel. Next, 5 x 10^6 4TR-9 ATR flox/- HCT 116 cells were transfected with 8µg DNA in duplicate by reverse transfection using lipofectamine 2000 in a 60 mm dish. The next day, the cells were plated for colonies by splitting the transfected wells 1:6 or 1:12 into a 10 cm dish. Selection for cells containing the cDNA was done by adding 10µg/mL of Blasticidin and 300µg/mL HygromycinB to each dish and the media was changed twice a week. Colonies were ready in 3 weeks. Single colonies were expanded in a 12-well dish. At least 100 colonies were expanded per condition. When cells grew to be more than 60% confluent, they were split into a new dish and into a 96-well plate. The colonies were screened for expression of FLAG-HA-ATR using in cell analysis.

In Cell Analysis

Cells were plated in a 96-well plate the day before and fixed with 3% formaldehyde in PBS for 20 minutes at room temperature with no shaking. Cells were washed 5 times with PBS + 0.1% triton-x-100 for 5 minutes on shaker. Odyssey blocking buffer was added for 1.5 hours at room temperature on a shaker. Primary antibody was incubated on cells overnight at 4 degrees, followed by 5x PBS washes. Secondary antibody was added to cells for 1 hour at room temperature, followed by 5x PBS washes. After the last wash, the plate was turned over and tapped dry. The Licor Odyssey scanner was set to a resolution of 169µm with 30 mm focus offset.

Adenovirus Infection of ATR Flox/- cells

1 x 10^6 cells per 10cm dish were plated 24 hours before AdCRE infection. The next day 0.42µL of AdCre virus was added to cells in 10mL total media. 2µL of the stock virus was diluted into 20mL of growth media and then 4.2mL of the dilution was added per 10cm dish. The growth media was brought to a final volume of 10mL by adding 5.8mL of regular media to each plate. Pen/Strep was added to the media to prevent any bacterial growth. After 24 hours, the media was changed. After an additional 24 hours, the cells were split and plated for colonies. Viral infection of AdGFP should be used as a control. Colonies were picked, expanded, and PCR genotyped using the following primars: Sfiloxpseq: CAGCGGGAGCAGGCATTTC and ATR88961: GTCTACCACTGGCATAACAGC. PCR genotyping was done using 5µL of harvested genomic DNA and Platinum Taq (Invitrogen). The following PCR protocol was used for a total of 33 cycles: 95 degrees for 2 minutes, 95 degrees for 45 seconds, 58 degrees for 45

seconds, 72 degrees for 1 minute and 10 seconds, after 33 cycles end with 72 degrees for 5 minutes.

Purification of GST tagged protein from bacteria

Note: This protocol was used to purify any GST tagged protein, including the TopBP1-AAD for the ATR kinase assays. BL21 cells were transformed with pBG101 by electroporation. A fresh colony was picked and used to inoculate 4mL of LB and grown overnight. The next day, 2.5mL of the overnight culture was used to inoculate 225 mL of LB (no antibiotics). The target starting OD600 was 0.05-0.1. Cultures were grown at 37 degrees on a shaker and the OD600 was periodically checked. Once the OD600 reached ~0.6 (about 2 hours), the bacteria were induced with 200µL of 1M IPTG to give a final concentration of 1mM IPTG. Note: IPTG should be made fresh. The cultures were then grown at 25 degrees for 4 hours. Then, the bacteria were pelleted by centrifugation at 5000xg for 15 minutes at 4 degrees and the pellet was stored at -20 degrees.

Purification of protein: NET Buffer: 25mM Tris pH 8.0, 50mM NaCl, 0.1mM EDTA, 5% Glycerol, 1mM DTT, 0.1mM PMSF, Aprotinin, Leupeptin. The pellet was resuspended in 20mL pre-chilled NET buffer and transferred to a round bottom 40mL tube. The suspension was sonicated 3x on ice with on setting 4, Duty cycle 90 for 20 seconds. The suspension was incubated on ice for 1 minute between sonications. 20% Triton X-100 was added to the lysate to give a 1% final concentration and incubated on ice for 30 minutes. Meanwhile, 200µL glutathione sepharose bead slurry was aliquoted into microcentrifuge tubes. The beads were washed 2x with 1mL of NET buffer. After washes, the beads were centrifuged at 500xg for 1 minute.

After the 30-minute incubation, the lysate was centrifuged at 5000xg for 10 minutes at 4 degrees and the supernatant (cleared lysate) was transferred to a new tube. A 20µL sample of cleared lysate and a 20µL sample of pellet was taken to be analyze by SDS-PAGE. The pellet was then stored at -20 degrees. The cleared lysate was incubated with the washed glutathione beads on a rotator in cold room for 2.5 hours. The beads were washed 3x with 10mL of NET buffer containing additives. For each wash, the beads were incubated for 5 minutes with the buffer on a rotator at 4 degrees. Then the beads were centrifuged at 1000 rpm for 3 minutes at 4 degrees. Meanwhile, the elution buffer was prepared: 75mM Tris pH8.0, 15mM Glutathione, and 0.1µg/µL leupeptin. After the washes, the beads were transferred to a microfuge tube and centrifuged for 30 seconds at 1000xg and the supernatant removed.

A 10µL sample of beads was taken and the protein was then eluted from the beads. Three elutions were done with 200µL elution buffer for a 200µL bead slurry (equal volumes) for each elution and the samples were incubated on a rotator for 5 minutes at room temperature. The beads were then centrifuged at 500xg for 30-60 seconds. Each elution was stored on ice and kept separate. A 20µL sample of each elution was taken. After the elutions, a 10µL sample of the beads was taken and remaining beads stored on ice. Each collected sample, 7 in total was analyzed by SDS-PAGE and the gel stained with coomassie brilliant blue. The desired elutions were then combined and dialysized. Dialysis: The sample was dialyzed in 50mM NaCl, 20mM HEPES-KOH pH7.5. The buffer was changed after 3 hours and dialysis continued overnight at 4 degrees. The sample was aliquoted and stored at -80 degrees.

Whole Genome siRNA Screen

Day 1: The siRNA plates were thawed at room temperature and centrifuged at 1000xg for 3 minutes before removing the foil seal. 5µL of Optimem, containing 0.05µL of Dharmafect1, was added to each well (EL406-Peripump) and the plates were incubated at room temperature for 20 minutes. U2OS cells were harvested and counted and 800 cells in 40µL of media was added to each well (EL406-Syringe A). All the plates were returned to the incubator for 72 hours. To dilute the Dharmafect: 1.5mL of Dharmafect1 was added to 150mL of Optimem (3-50 mL conical tubes). To dilute the U2OS cells properly, $1.08x10^7$ cells were added to each 500mL bottle of DMEM containing 40mLs of FBS to a total of 2 bottles.

Day 4: On this day, each 384-well plate was split into four new 384-well plates and the appropriate drugs were added. To trypsinize the cells, the wells were washed with 80µL of PBS per well (EL406-Washer B) and then 15µL of trypsine was added to each well (EL406-peripump). The plates were then incubated on a rocking platform at room temperature for 5 minutes. 85µL of DMEM (Syringe A) was added to each well for a total volume of 100µL as some PBS was left in the wells to avoid suctioning cells. The Bravo was used to resuspend the cells and split them into 4 new 384-well plates by adding approximately 20µL of cell suspension to each well per plate. The plates were then returned to the incubator until all the plates were split. The EL406 was then used to add the ATRi, CHKi, HU, cisplatin, ATRi/cisplatin, or media to the appropriate plates. Syringe A added 30µL of media containing drug and syringe B was used for wells receiving media with no drug. Plates were then returned to the incubator for 72 more hours. Additionally, 500µL Amphotericin B and 5mL of Pen/Strep was added to each bottle of media. To dilute

the ATRi, 1.8µL of 50mM ATRi was added to each bottle of media. For cisplatin, 180µL of 2.5mM Cisplatin was added to each bottle and for the combination treatment, 900µL of 50µM ATRi and 36µL of 2.5mM Cisplatin was added to each bottle. Overall, the assay required two bottles of media for each drug condition.

Day 7: AlamarBlue was diluted in fresh media and added to the plates in groups of 40 plates every two hours. 50µL of diluted alamarBlue was added to each well (EL406-Syringe A). Plates were incubated at 37 degrees for 4 hours. Each stack took 2 hours and 2 minutes to read on the plate reader. To dilute the alamarBlue, 60mL of alamarBlue was added to each bottle of media to a total of 9 bottles.

Data Analysis: First the average cell death siRNA alamarBlue reading was subtracted from the raw values. This was done as a method of subtracting the background as the siCelldeath wells were empty of cells at this point in the protocol. Then, a percent viability was calculated by dividing the alamarBlue values (siRNA +drug)/(siRNA untreated) and a percent viability from the siRNA effect alone was calculated (siGeneX/siNT). Any siRNA which resulted in a percent viability of under 20% without drug was excluded from further analysis. We then calculated the robust Z-score using the log10(percent viability) value and the median and median absolute deviation for each plate.

Secondary Validation Screens

The screening methodology was identical to the primary screen. We also included the following drug conditions: 3.0mM high dose HU, 10nM BMN673, 10µM camptothecin, and 10nM gemcitabine. Cells were treated with high dose HU and camptothecin for only 24 hours. These cells were then released into fresh media for the

remainder of the assay. Cells were treated with BMN673, camptothecin, and gemcitabine for 96 hours instead of 72 hours.

Data analysis: A percent viability was calculated the same as the primary screen as well as a plating effect. The plating effect accounted for uneven splitting of the cells by the Bravo. To calculate this, every plate had cells transfected with non-targeting siRNA that received no drug. The alamarBlue value from the untreated control siRNA from the drug plate was divided by the alamarblue siNT on the untreated plate. The percent viability was then divided by the plating effect ratio. False discovery rate was corrected for using the Benjamini-Hochberg method [203].

Dose Response Assays

Cells were transfected with siRNA in 60mm dishes. 72 hours after transfection, cells were plated into a 96-well plate. Drug was added to the plate at the indicated increasing doses. After 72 hours or three population doublings, cell viability was measured using alamarBlue. The cell numbers plated and the length of the assay for each cell line tested is listed in table 4.1.

Clonogenic Assays

Cells were plated at multiple dilutions depending on cell type. Typically, cells were treated with drug for 24 hours, released into fresh media and allowed to form colonies. Colonies were stained with MethyleneBlue.

G2/M Checkpoint

HCT116 were plated in a 10cm dish the day before, ~$2x10^6$ cells per plate. Cells were treated with 8Gy IR and allowed to recover for 30 minutes and released into media containing nocodazole at 1µg/mL. The media and cells were harvested for flow cytometry after 8 hours. Cells were prepared for flow cytometry following the normal protocol but with an added incubation with phosphor-S10 histone H3 at 1:20 for 1.5 hours at room temperature, flicking the tube every 15-30 minutes. The cells in mitosis were positive for pS10 H3 and had a 4N DNA content. The remaining cells with a 4N DNA content are in G2 phase.

Completion of S-phase

$9x10^5$ HCT116 cells were plated in a 60mm dish the day before. The cells were treated with 2mM HU for 24 hours or 50J/m^2 UV. The cells were released into media containing 1µg/mL nocodazole and harvested at the indicated time points. Cells were fixed and stained for flow cytometry following the normal protocol.

Generation of CRISPR/Cas Null Cells

4-6 guide RNAs were designed per gene that were 50-150 base pairs apart targeting the N-terminus of the gene with forward and reverse overhangs for pX330. The guide RNAs for the BRD3 null cells deleted the start codon by generating an internal exon deletion. The ATRIP guide RNAs targeted exon 4 and resulted in an intra-exon deletion. The guide RNAs were inserted into pSPCas9(BB)-2A–Puro. Each oligo pair was phosphorylated and annealed. Each oligo pair was diluted 1:250, digested and ligated into

the plasmid. 1-2µL of the final product was transformed into competent cells and the resulting plasmid sequenced. 1µg of the plasmid was transfected into the desired cell line, U2OS or 293T. The next day, puromycin was added for 48 hours or until the control plate was dead. A fraction of the cells were harvested for PCR genotyping and the rest plated for colonies. The resulting colonies were expanded and confirmed for null status by western blot.

ATR Purification for Mass Spectrometry

Overexpressed Flag-ATR was purified from 293T nuclear extracts or from whole cell lysates. Cells were treated with 2mM HU for 2 hours prior to harvest. Anti-FLAG agarose beads were used. ATR was eluted from the beads using 300µg/mL FLAG peptide and TCA precipitated or the beads were boiled in 2X sample buffer and the sample separated by SDS-PAGE. The purified ATR was submitted to the Vanderbilt Mass Spectrometry Core. They digested the sample with trypsin and used LC-MS-MS to identify phosphorylation sites. Other digestion conditions were tried as well as phosphopeptide enrichment using titanium dioxide beads. The best conditions for detection of the S1333 peptide was trypsin digestion of FLAG-eluted ATR.

FLAG Purification of Screen Hits for Mass Spectrometry

4µg of cDNA was transfected into each 10cm dish. Typically, 20-30 dishes of 293T cells were transfected using PEI and then expanded into 15cm dishes the day after transfection. After 3 days, nuclear extracts were prepared as described in Current Protocols in Molecular Biology. After washing the cells with PBS, the pack cell volume (PCV) was

measured. The cells were resuspended in 5x the PCV with cold hypotonic buffer. The cells were centrifuged at 2500xg for 3 minutes at 4 degrees and the supernatant discarded. The cells were then resuspended in 3x PCV with cold hypotonic buffer and allowed to swell on ice for 10 minutes. The cells were dounce homogenized with 15 up and down strokes, centrifuged for 15 minutes at 3300x g at 4 degrees, and the supernatant discarded. The packed nuclear volume (PNV) was measured, the tube flicked to loosen the pellet, and the cells resuspended in 0.5x PNV low salt buffer. 0.5x PNV of high salt buffer was added slowly and with continuous flicking. The samples were incubated at 4 degrees for 30 minutes on a rotator.

The extract was then centrifuged at full speed for 30 minutes at 4 degrees and the supernatant was transferred to a new tube. The samples were dialyzed for 1 hour in 500mL dialysis buffer. The extract was precleared with Protein A agarose beads. The desired protein was purified using the anti-FLAG agarose beads for 3 hours at 4 degrees on a rotator. The beads were washed 4x with 0.5% NP-40 lysis buffer. Then the protein was eluted with FLAG peptide for 1 hour, gently flicking the tube every 15 minutes. The sample was TCA precipitated and submitted to the Vanderbilt Mass Spectrometry core. They digested the samples with trypsin and used LC-MS-MS to identify co-purifying proteins.

Hypotonic Buffer: 10mM HEPES pH7.5, 1.5mM $MgCl_2$, 10mM KCl, 0.2mM PMSF, 0.5mM DTT. Low Salt Buffer: 20mM HEPES pH7.9, 25% glycerol, 1.5mM $MgCl_2$, 0.2mM EDTA, 0.2mM PMSF, 0.5mM DTT. High Salt Buffer: 20mM HEPES pH7.9, 25% glycerol, 1.5mM $MgCl_2$, 1.2M KCl, 0.2mM EDTA, 0.2mM PMSF, 0.5mM

DTT. Dialysis Buffer: 20mM HEPES pH7.9, 20% glycerol, 100mM KCl, 0.2mM EDTA, 0.2mM PMSF, 0.5mM DTT.

CHAPTER III

MUTATION OF ATR S1333 CREATES A HYPERACTIVE KINASE[1]

Introduction

Nucleotide imbalances, hard to replicate DNA sequences, and damage to the template strand create challenges for complete and accurate DNA replication. The replication stress response maintains genome integrity through sensing and overcoming these challenges by promoting the repair of the damaged DNA, stabilizing stalled replication forks, and activating cell cycle checkpoints [26]. The PI3K-related protein kinases (PIKKs), including ATM and Rad3-related (ATR), are primary regulators of the replication stress response [28].

PIKK kinases are large proteins with significant sequence homology and shared domain architecture. The N-terminus of these proteins consist of dozens of Huntington, Elongation factor 3, Protein phosphatase 2A, and PI3K TOR1 (HEAT) repeats; each containing two interacting anti-parallel alpha-helices connected by a flexible loop [114]. The kinase domain is located at the C-terminus and is flanked by the FRAP, ATM, TRRAP (FAT) domain [120], the PIKK regulatory domain (PRD) [51], and FAT C-terminus (FATC) domain [204]. The PIKKs preferentially phosphorylate serine or threonine residues followed by a glutamine (S/TQ), giving these kinases many overlapping substrates.

[1]This chapter was published in [1]

PIKK family members promote repair of different types of damaged DNA [205]. Ataxia-telangiectasia mutated (ATM) is activated by DNA double strand breaks, but ATR signals in response to a variety of DNA lesions, including double strand breaks, base adducts, and crosslinks. The common feature of these lesions is the generation of single stranded DNA either directly or as a consequence of enzymatic processing. Unlike ATM, ATR is essential for the viability of replicating human and mouse cells and is activated every S-phase to regulate replication origin firing, repair stalled replication forks, and prevent early entry into mitosis [2-4,108,206]. Rare, hypomorphic mutations in ATR are associated with Seckel syndrome, a disorder characterized by microcephaly, growth retardation, and other developmental problems [29]. Cancer cells have an increased dependence on the ATR pathway due to high levels of oncogene-induced replication stress and frequent loss of the G_1 checkpoint [194,197,207]. This dependence makes the ATR pathway a promising cancer therapeutic target.

Generation of single stranded DNA gaps initiates ATR activation, which involves recruitment of a signaling complex containing multiple proteins including ATR, ATR-interacting protein (ATRIP), RAD9-HUS1-RAD1, and BRCT repeat protein topoisomerase binding protein 1 (TOPBP1) to the stalled fork [208]. This recruitment is largely mediated by the single-stranded DNA binding protein, replication protein A (RPA). TOPBP1 binds to the ATR-ATRIP complex promoting a conformational change that likely increases its affinity towards substrates [53,136]. Subcellular localization to specific DNA lesions and additional protein activators are key regulatory elements for the PIKK family members.

Additionally, PIKKs are regulated by post-translational modifications. ATM auto-phosphorylation induces the transition from an inactive dimer to an active monomer [119]. Several ATR auto-phosphorylation sites have been identified, including threonine 1989 [164,165]. However, T1989 is not evolutionarily conserved and there are conflicting data about how important its phosphorylation is to the ATR activation process [164,165]. Finally, several other proteins have been suggested to regulate ATR activation, but their precise roles may be dependent on the type of initiating signal.

In the process of studying how ATR phosphorylation regulates its activity, we discovered that a single mutation at serine 1333 creates a hyperactive kinase. Both the basal activity level and TOPBP1-stimulated activity of the S1333A protein are significantly increased compared to the wild type protein. Additionally, S1333 mutations to glycine, arginine, or lysine also create hyperactive kinases. Conversely, a S1333D mutation decreases ATR activity. While we find no evidence that S1333 is phosphorylated in cultured cells, our studies indicate that mutation of a single serine in the large, HEAT repeat region of this 2,644 amino acid protein is sufficient to greatly alter its activity. The exact mechanism mediating this change will require a high-resolution structural analysis; however, these mutants provide useful tools for studying the ATR pathway.

Results

Mutation of Serine 1333 alters ATR kinase activity

ATR preferentially phosphorylates S/TQs. ATR contains 19 of these putative phosphorylation sites. Sixteen of them are conserved in mice. To identify which of these serines may be functionally important, we mutated all sixteen conserved S/TQs to alanine

within one cDNA. We then tested the kinase activity of the 16A-ATR protein using an *in vitro* kinase assay. The 16A-ATR mutations create a hyperactive kinase compared to wild type in kinase assays containing the AAD of TOPBP1 (Figure 3.1A, [30]). Even when considerably less of the 16A-ATR was purified and added to the reaction compared to the wild type protein, it had significantly higher activity levels.

To determine which of the mutations in the 16A protein caused this hyperactivity, we tested a series of ATR proteins with subsets of these mutations. A 6A-ATR protein (S1333/S1348/T1376/S1782/T1890/S2143A) retained the elevated activity (Figure 3.1A). The small difference between the 16A and 6A activities seen in this representative experiment is not reproducible. We further narrowed the relevant mutations to a 3A-ATR (S1333/S1348/S1376A) protein (Figure 3.1B). Finally, a single alanine mutation, revealed S1333A as the primary mutation inducing the hyperactivity (Figure 3.1B). The small difference between the S1333A and 3A protein activities in this experiment is due to the reduced amount of 3A protein purified and was not observed in replicate experiments (data not shown).

We created additional amino acid mutations at S1333 and tested their kinase activities. First, we created an aspartic acid mutation, to mimic phosphorylation. S1333D-ATR had less kinase activity than wild type ATR upon stimulation by TOPBP1 and less activity than wild type without stimulation (Figure 3.1C). Conversely, S1333A-ATR is more active than wild type ATR with or without the addition of TOPBP1. Next, we mutated S1333 to glycine, further reducing the size of the amino acid occupying this position from the alanine mutation. We also created arginine and lysine mutations to

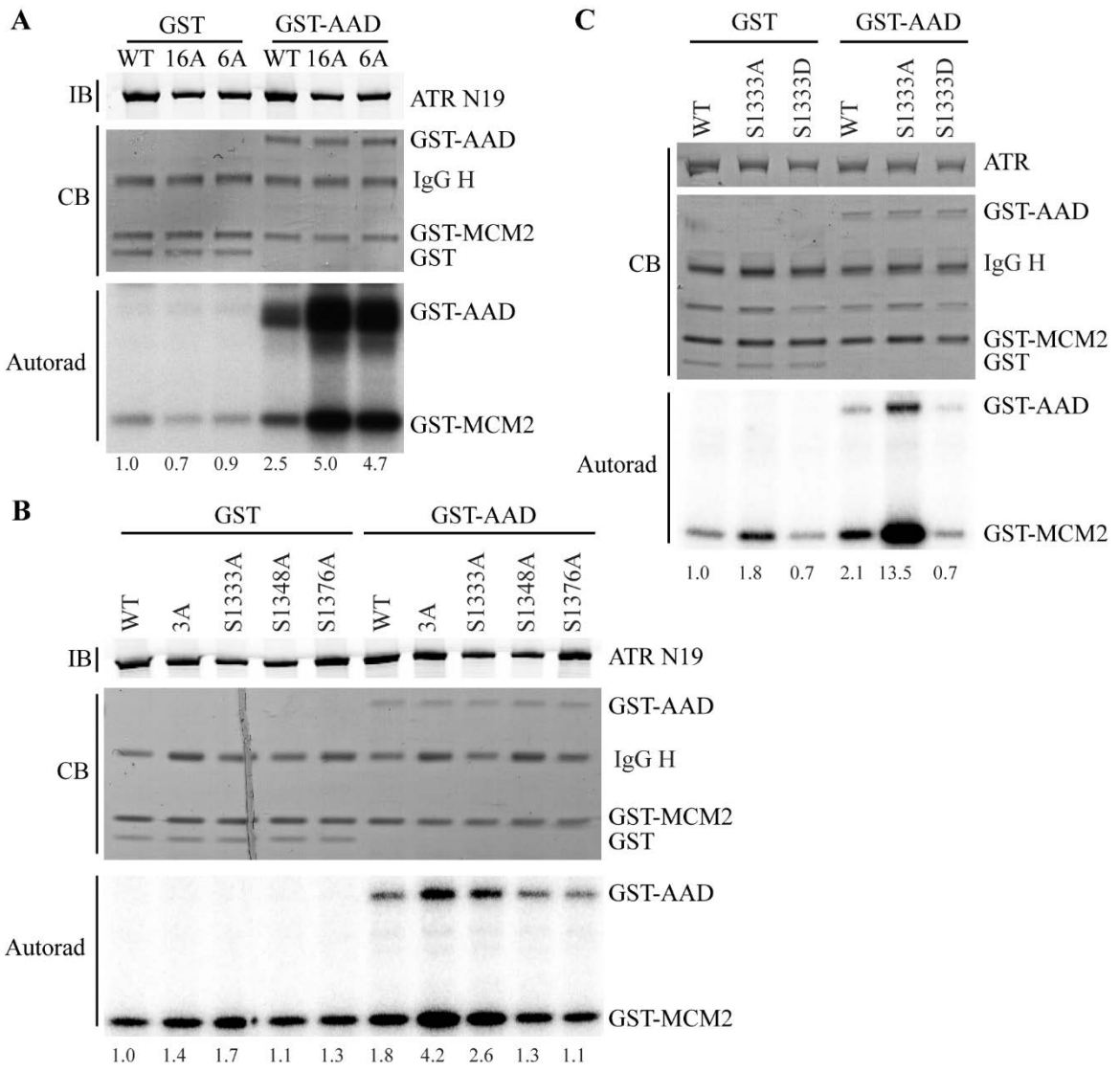

Figure 3.1. Mutation of S1333 to alanine creates a hyperactive ATR kinase. A-C. The indicated ATR mutant or wild type proteins complexed with ATRIP were purified from HEK293T cells and incubated with GST-MCM2 substrate, [γ-^{32}P]-ATP, and GST-TOPBP1-AAD (GST-AAD) or GST. Kinase reactions were separated by SDS-PAGE and [^{32}P]-MCM2 and [^{32}P]-GST-TOPBP1 detected by autoradiography. Quantitation of the fold activation compared to the wild type protein incubated with GST was measured by a phosphorimager and is indicated below each lane. The amount of ATR, TOPBP1, MCM2, and GST proteins in each reaction was detected with Coomassie blue (CB) or immunoblotting (IB) as indicated. Each mutant was tested at least three times and representative experiments are shown.

create a positive charge at this position. All of these mutations created a hyperactive kinase similar to activity levels of S1333A-ATR, with TOPBP1 (Figure 3.2). They also exhibited slightly elevated kinase activities without TOPBP1 although with some variability in the magnitude (Figure 3.2). Thus, all mutations of S1333 tested altered ATR kinase activity, with most increasing activity and the S1333D mutation decreasing activity.

Additionally, we tested select mutations in this ATR region identified through cancer genome sequencing efforts. Q1334E is a mutation found in colorectal cancer and V1338L was found in cancer of the pleura. Neither of these mutations changed ATR kinase activity *in vitro* (Figure 3.2).

ATR is a large protein containing 45 HEAT repeats [114]. S1333 is located within HEAT repeat 27 of ATR (Figure 3.3A-B and [114]). A Clustal W2 sequence alignment shows conservation of S1333 in vertebrates (Figure 3.3B). Using Phyre2 to predict the structure of HEAT repeat 27, S1333 is located on the predicted, polar exterior of helix one (Figure 3.3C). This region of ATR has not previously been implicated in its regulation.

S1333 is unlikely to be phosphorylated in cultured cells

Our *in vitro* data indicated that changing S1333 to a non-phosphorylateable residue activated ATR, while changing it to a phospho-mimetic decreased its activity. Since S1333 is followed by a glutamine, creating a consensus site for ATR auto-phosphorylation, we entertained the possibility that S1333 phosphorylation regulates ATR. To investigate whether S1333 is phosphorylated, we used three approaches: mass spectrometry, generation of a phospho-peptide specific antibody, and *in vitro* phosphorylation.

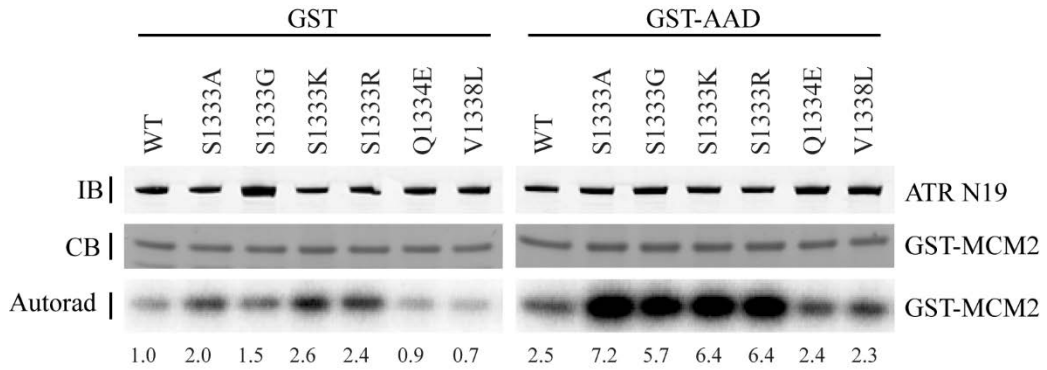

Figure 3.2. Additional S1333 mutations alter ATR kinase activity. The indicated ATR mutant or wild type proteins complexed with ATRIP were purified and incubated with GST-MCM2 substrate, [γ-^{32}P]-ATP, and GST-TOPBP1-AAD (GST-AAD) or GST. Kinase reactions were separated by SDS-PAGE and [^{32}P]-MCM2 detected by autoradiography. Quantitation of the fold activation compared to wild type protein incubated with GST measured by a phosphorimager is indicated below each lane. The amount of ATR and MCM2 present was detected by Coomassie blue (CB) or immunoblotting (IB) as indicated. Each mutant was tested at least three times and a representative experiment is shown.

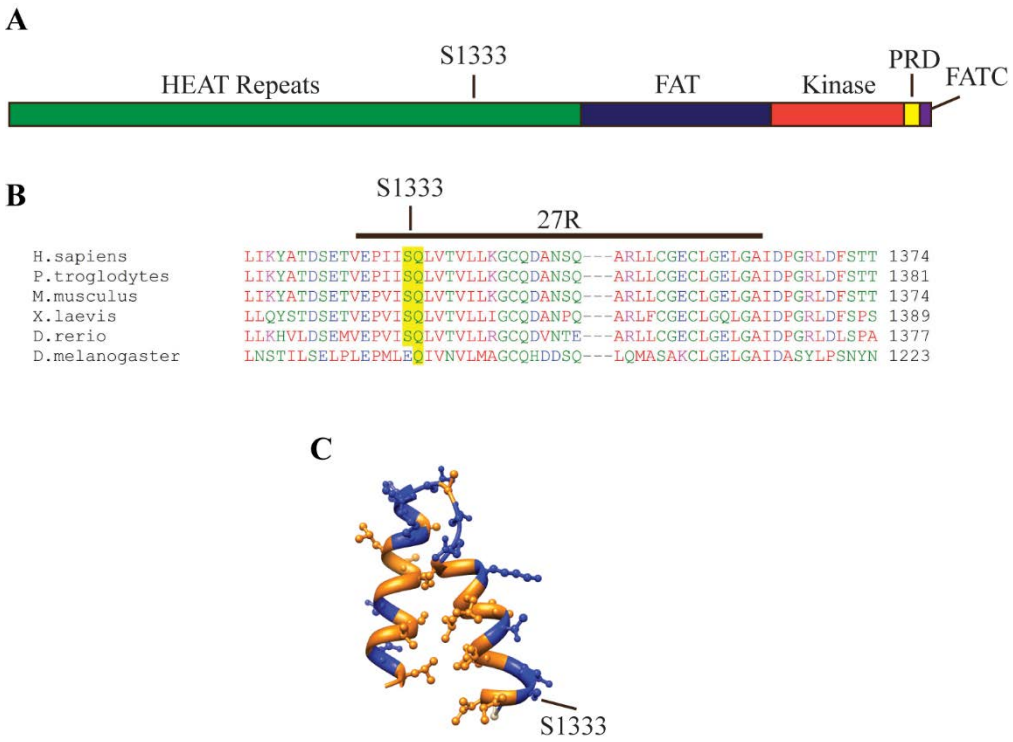

Figure 3.3. S1333 is a conserved amino acid within HEAT repeat 27 of ATR. A. Schematic representation of the ATR protein. **B.** Sequences of ATR orthologs were aligned using ClustalW2. **C.** Phyre2 was used to predict the structure of HEAT repeat 27. Polar amino acids are colored blue.

LC-MS-MS analysis of ATR purified from undamaged, HU, or IR treated HEK293T cells detected multiple phosphorylation sites, including T1989 (Table 3.1, [21]). However, we failed to detect a peptide with modifications to S1333 despite observing the unmodified peptide repeatedly (Figure 3.4). We then tried to generate a phospho-peptide specific antibody to S1333. We immunized four rabbits and none yielded a purified antibody that recognized ATR in immunoblots or immunoprecipitation experiments (data not shown). Finally, we generated a short ATR protein fragment containing S1333 and tested whether this recombinant protein was phosphorylated on S1333 by purified ATR in an *in vitro* kinase assay. Again, we failed to detect significant S1333 phosphorylation (data not shown). Thus, while these negative data do not exclude the possibility that S1333 is phosphorylated, we do not have evidence that it is phosphorylated either in cultured human cells or during *in vitro* kinase assays.

Generation of cells expressing only S1333A or S1333D-ATR

The hyperactive S1333A-ATR protein can be a useful research tool since its increased activity, which is still regulated by TOPBP1, may facilitate *in vitro* biochemical reactions. To test if the mutant retained hyperactivity when expressed in cells and to analyze the functional consequences of mutating S1333, we utilized a genetic complementation assay using HCT116 $ATR^{flox/-}$ cells. These cells contain one conditional ATR allele and the second allele disrupted by a neomycin cassette [164]. Additionally, the cells express the tetracycline repressor. Wild type ATR, S1333A-ATR or S1333D-ATR expression vectors, containing a tetracycline response promoter and an N-terminal FLAG-HA_3 tag, were transfected into the $ATR^{flox/-}$ cells. After selection, we screened stable clones

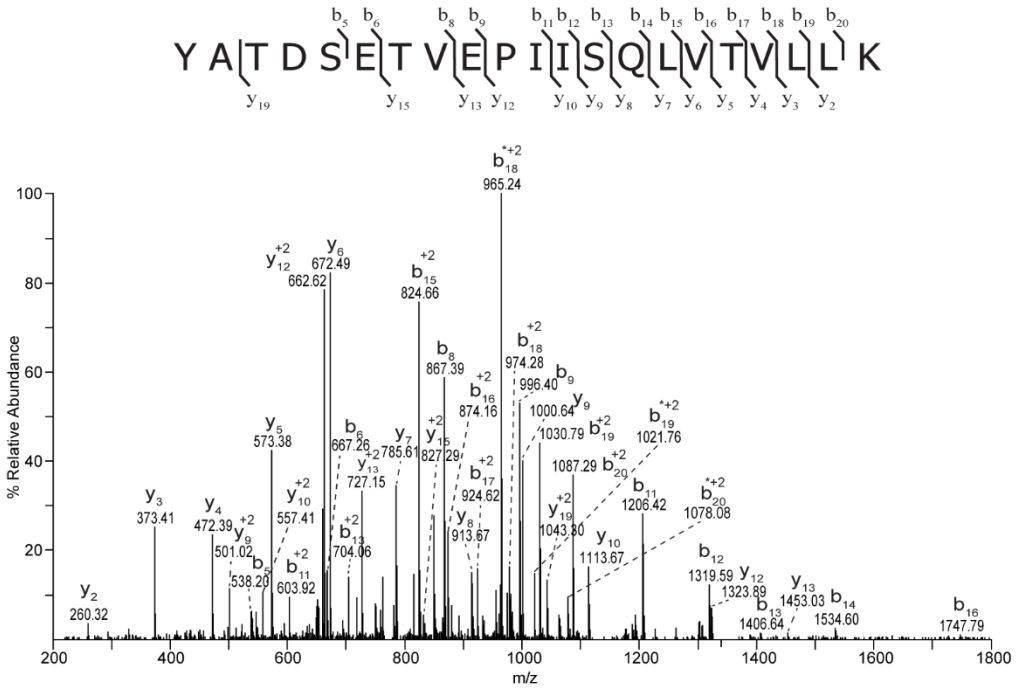

Figure 3.4. The peptide containing unphosphorylated S1333 can be detected by mass spectrometry. MS/MS spectrum of ATR peptide, residues 1321-1341, is shown. The [M+3H]+3 precursor ion with m/z 773.76 was selected for fragmentation. The observed singly and doubly protonated b- and y-type product ions are assigned to their corresponding m/z peaks in the tandem mass spectrum. The amino acid sequence is provided above the annotated spectrum, and the interresidue-placed brackets denote sites of amide bond fragmentation that occurred with collision-induced dissociation (CID). b-type product ions correspond to the resulting fragment ions that contain the N-terminus of the peptide, and y-type ions correspond to C-terminal peptide fragments. Asterisks indicate product ions for which neutral loss of water has occurred.

for equal levels of inducible ATR. Then, we infected the cell lines with adenovirus encoding the Cre recombinase to delete the remaining intact endogenous ATR allele. The exogenous ATR protein expression was maintained with tetracycline. Stable clones were screened again for equal ATR expression and deletion of the floxed ATR allele (Figure 3.5A-B). PCR genotyping to confirm Cre excision of the remaining intact ATR allele was performed as previously described [3]. Additionally, we checked for equal cell cycle distribution across the cell lines. All clones had similar distributions (Figure 3.5C) and had similar population doubling times (data not shown). Additionally, all clones expressed nearly equal levels of ATRIP, which co-immunoprecipitated with the wild type and mutant ATR proteins with equal efficiencies (Figure 3.5D). Thus, mutation of S1333 does not alter the stability of the ATR-ATRIP complex or the growth of unperturbed cells. Multiple clonal isolates of each cell type were analyzed in all subsequent experiments to ensure results were not due to clonal variations.

S1333A-ATR cell lines have elevated phosphorylation of ATR substrates

In vitro, the basal kinase activity of S1333A-ATR is higher than wild type (Figure 3.1C). To test if this is true in cells, we analyzed basal phosphorylation levels of multiple ATR substrates in three wild type, three S1333A, and three S1333D clonal cell lines without any added genotoxic stress. Phosphorylation levels were analyzed by calculating the ratio of phosphorylated protein to total protein and then normalized to wild type ATR. S1333A-ATR cells contain higher levels of phosphorylated CHK1 compared to wild type and S1333D-ATR (Figure 3.6A). We also observed increased phosphorylation of ATR and MCM2 in the S1333A-ATR cell line and slightly decreased MCM2 phosphorylation

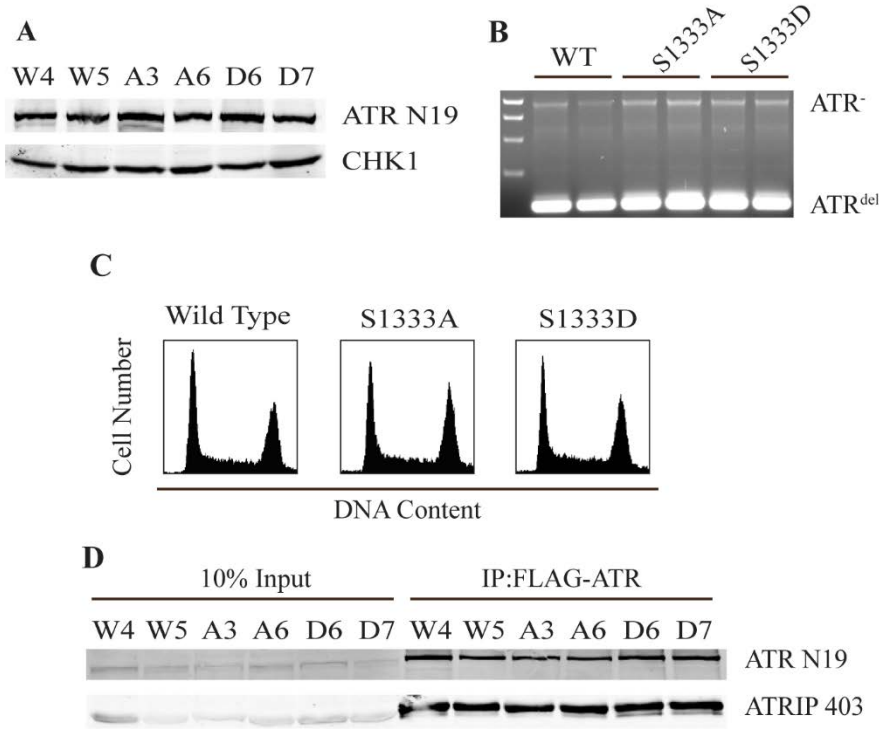

Figure 3.5. S1333A and S1333D-ATR cell lines express ATR at similar levels and maintain a normal cell cycle. ATR flox/- cells expressing wild type (WT), S1333A, or S1333D-ATR proteins were cultured in tetracycline media and infected with Cre-expressing adenovirus to delete the floxed ATR allele. Infected cells were plated at low density and several surviving colonies expanded. **A.** Cell lysates were separated by SDS-PAGE and immunoblotted to determine ATR expression levels. **B.** PCR genotyping confirmed deletion of the floxed allele. ATR^- is the PCR product derived from the neomycin-disrupted allele, ATR^{del} is the PCR product derived from the Cre excised exon 2 allele. **C.** Wild type, S1333A or S1333D-ATR asynchronously growing cells were fixed, stained with propidium iodide, and examined for DNA content by flow cytometry. **D.** Clonal isolates of ATR flox/- cells expressing wild type (W4 or W5), S1333A (A3 or A6), or S1333D (D6 or D7) ATR proteins were lysed, Flag-immunoprecipitated, separated by SDS-PAGE, and immunoblotted to detect the ATR-ATRIP complex.

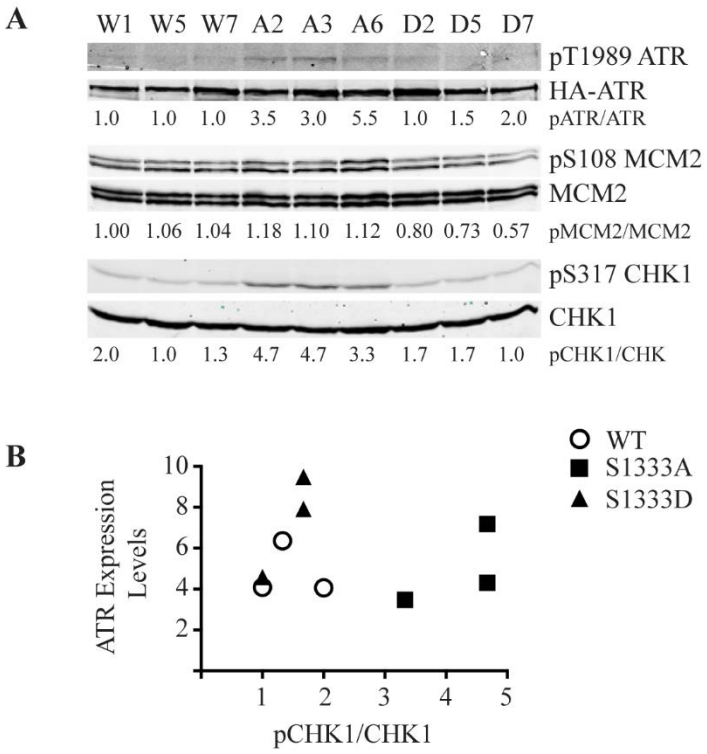

Figure 3.6. S1333A-ATR expressing cell lines contain elevated levels of phosphorylated ATR substrates. A. Lysates from ATR-/- cell clones expressing wild type (W1, W5, W7), S1333A (A2, A3, A6), or S1333D (D2, D5, D7) ATR proteins were separated by SDS-PAGE and immunoblotted with the indicated antibodies. Quantitative immunoblotting was used and the ratio of phosphorylated protein to total protein normalized to wild type (W1) is listed below each lane. Note that three clonal isolates for each ATR protein were analyzed to ensure results were not due to clonal variation. All cell lines were examined multiple times and a representative experiment is shown. **B.** The ratio of pCHK1/CHK1 and the expression levels of ATR are compared to show that the small differences in ATR expression levels in different cell lines do not account for the change in substrate phosphorylation.

in the S1333D cell line (Figure 3.6A). However, we did not detect significantly decreased levels of pCHK1 and pATR in the S1333D-ATR cells. Figure 3.6B illustrates that the difference in pCHK1 levels in the cells is not due to small differences in ATR expression levels since there was no correlation between ATR protein expression and the pCHK1/CHK1 ratio measured by immunoblotting.

S1333 mutation to aspartic acid causes modest defects in ATR checkpoint function

Next, we used our mutant cell lines to study if ATR activation is perturbed in response to DNA damage. Initially, we treated cells with 2 mM HU for varying lengths of time. S1333A-ATR expressing cells had elevated basal levels of CHK1 phosphorylation as expected and the levels at early time points after HU addition were also higher than in the wild type ATR or S1333D-ATR expressing cells. However, there were no significant differences in the maximum level of CHK1 phosphorylation achieved after 2h between S1333A, S1333D, and wild type ATR cell lines (Figure 3.7).

Next, we examined ATR signaling as a function of the amount of replication stress. We treated cells with increasing doses of HU and UV. With no treatment, pCHK1 is elevated in the S1333A-ATR cell line. At the lowest dose of UV and HU, pCHK1 levels in S1333A-ATR expressing cells continue to be elevated compared to wild type (Figure 3.8A-C). This difference reduces with higher doses of HU and UV as phosphorylation becomes saturating. This same pattern is observed on an additional CHK1 phosphorylation site (Figure 3.8C) and with MCM2 phosphorylation although it is not as striking since the basal level of MCM2 phosphorylation is quite high (Figure 3.8B).

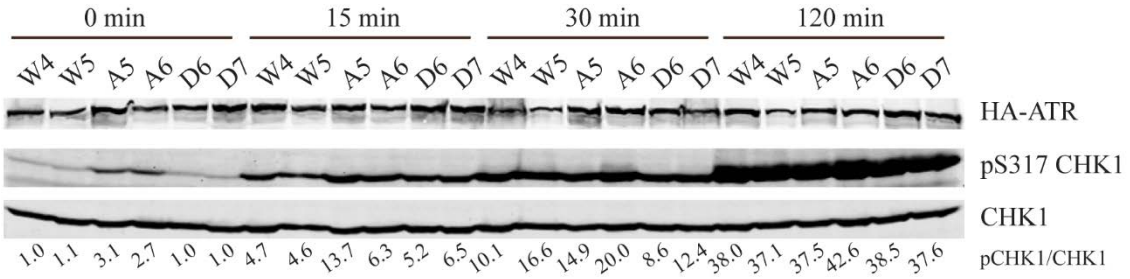

Figure 3.7. S1333A-ATR expressing cell lines maintain elevated levels of phosphorylated substrate at early time points after replication stress induction.
Cell lysates were separated by SDS-PAGE and analyzed by quantitative immunoblotting using the indicated antibodies. Quantitative immunoblotting was used and the ratio of phosphorylated protein to total protein and then normalized to wild type is listed below each lane. ATR-/- cell clones expressing wild type (W4 or W5), S1333A (A5 or A6), or S1333D (D6 or D7) ATR proteins were challenged with 2 mM HU for increasing lengths of time. Experiment is a representative images of at least two replicates.

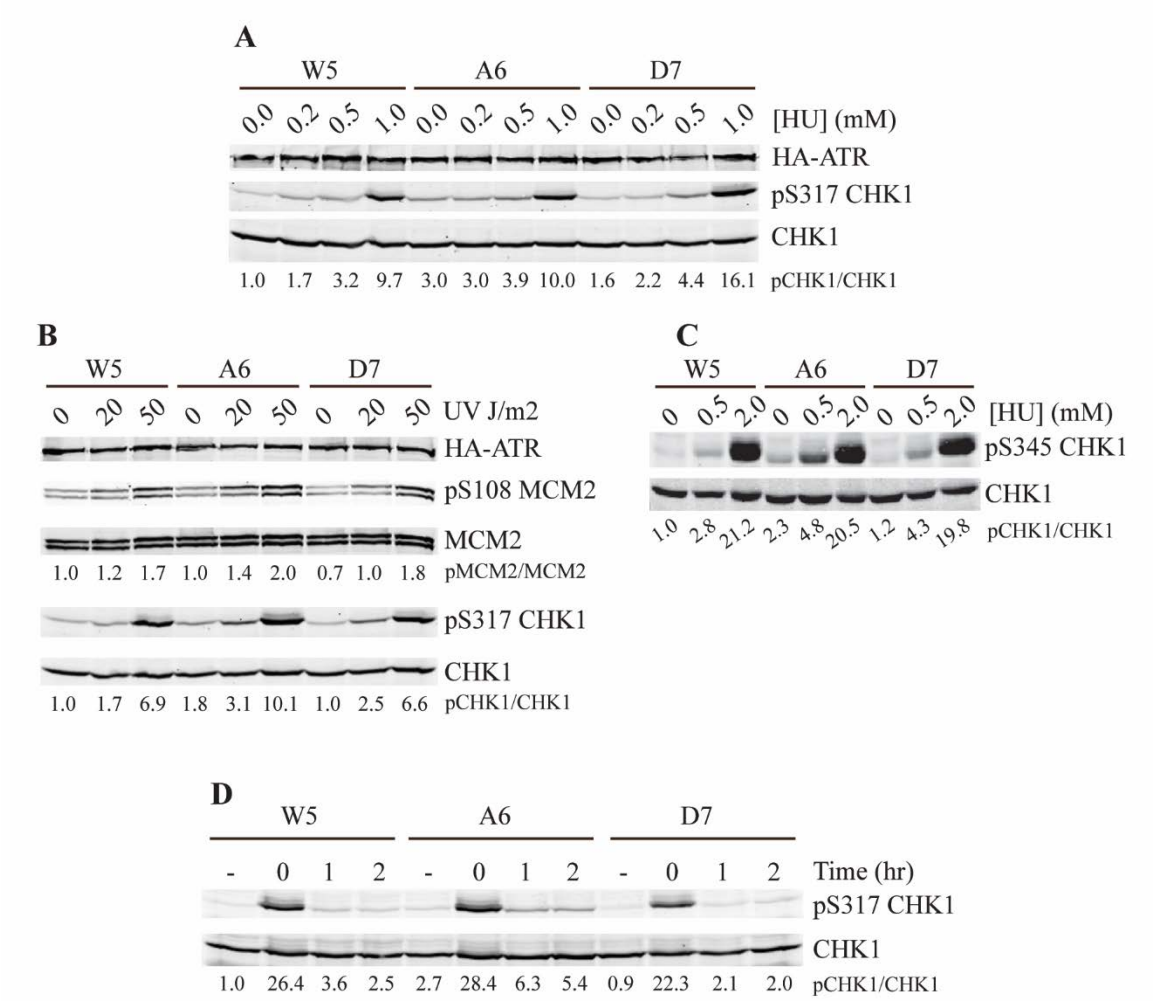

Figure 3.8. S1333A-ATR expressing cell lines maintain elevated levels of phosphorylated substrate at low replication stress levels. A-D. Cell lysates were separated by SDS-PAGE and analyzed by quantitative immunoblotting using the indicated antibodies. Quantitative immunoblotting was used and the ratio of phosphorylated protein to total protein and then normalized to wild type is listed below each lane. **A.** ATR-/- cell clones expressing wild type (W4 or W5), S1333A (A5 or A6), or S1333D (D6 or D7) ATR proteins were challenged with increasing concentrations of HU for 4 hours, or **B.** increasing doses of UV and allowed to recover for 2 hours. **C.** Cells were treated with increasing doses of HU for 2 hours. **D.** Cells were challenged with 2 mM HU for 2 hours and allowed to recover for 0, 1, or 2 hours. (-) indicates untreated cells. All experiments are representative images of at least two replicates.

Finally, we monitored ATR signaling after release from HU treatment to see if the S1333 mutations alter how quickly the pathway turns off. In this recovery assay, two hours after release from HU, the wild type and S1333D lines contain slightly elevated pCHK1 compared to untreated cells. The S1333A-ATR cell lines have higher phosphorylation levels of CHK1 after recovery, but the fold difference is the same as that observed before treatment (Figure 3.8D). Thus, the S1333A-ATR cell lines recover to a higher level of pCHK1 because the basal level of ATR signaling is higher. These assays did not indicate any problems with the cell lines turning off ATR signaling after replication stress.

ATR is essential for completion of S-phase, recovery from replication stress, and maintaining the G_2 checkpoint [3,110,208]. To test if the mutant ATR cell lines can complete S-phase following a replication challenge by HU, we treated the cells with HU for 24 hours. We then released the cells into media containing nocodazole for 0, 4, or 10 hrs. S-phase progression was monitored by flow cytometry with propidium iodide staining for DNA content. Both the S1333A and S1333D cell lines recovered and progressed through S-phase similarly to the wild type ATR cell lines (Figure 3.9A). However, when the three cell lines were treated with 50 J/m^2 UV, the S1333D-ATR cell lines had more difficulty in completing S-phase as compared to wild type or S1333A-ATR cell lines (Figure 3.9B).

ATR is also needed to maintain the G_2 checkpoint in response to ionizing radiation (IR) [3,110]. In an initial test of this checkpoint at 6h after IR we found no difference between wild type and S1333A-ATR cells but did see a small increase in the number of mitotic cells in the S1333D-ATR cell line although it was not statistically significant (data not shown). We repeated the assay at a longer time point and indeed found that the

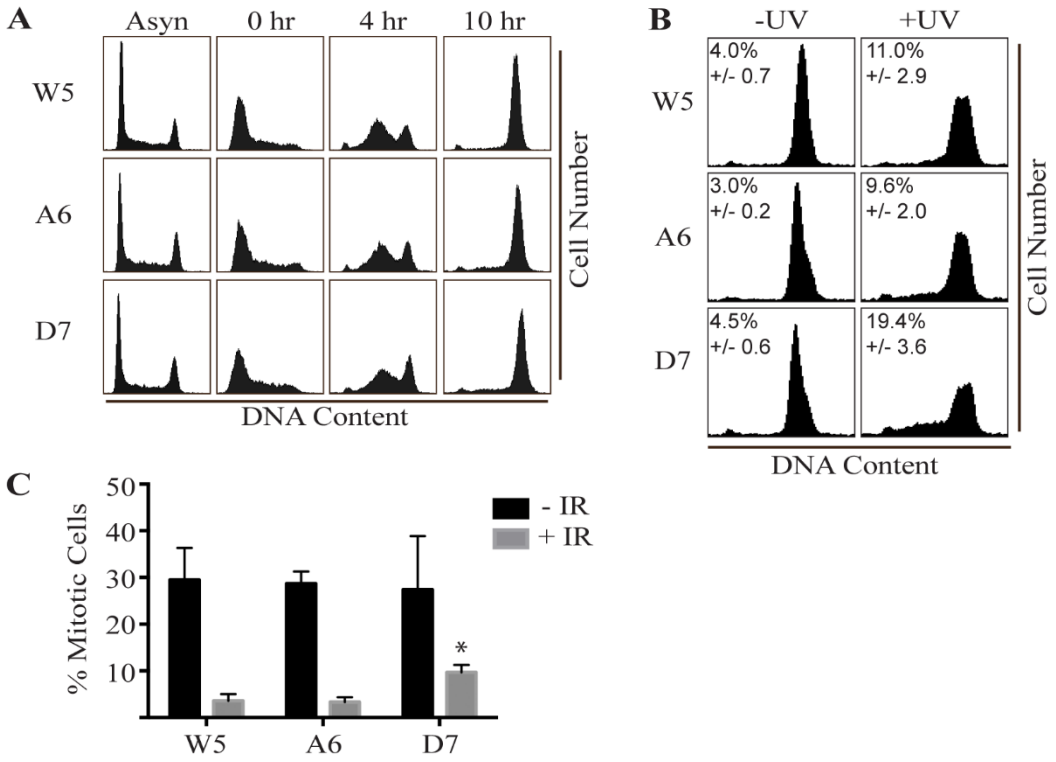

Figure 3.9. Mutation of S1333 to aspartic acid causes modest defects in completing DNA synthesis following UV radiation and in maintenance of the G_2 checkpoint. A-B. The indicated wild type, S1333A, or S1333D-ATR expressing cell lines were treated as indicated below, fixed, stained with propidium iodide, and DNA content analyzed by flow cytometry. **A.** Cells were treated with HU for 24 hrs, released into media containing nocodazole for 0, 4, or 10 hrs, and harvested, along with asynchronously growing cells. **B.** Cells were treated with or without 50 J/m^2 UV and incubated with nocodazole for 16 hrs. The percentage of cells in S-phase was quantitated in three experiments and the mean and standard error are shown. **C.** Cells were treated with or without 8 Gy IR and incubated with nocodazole for 16 hrs. The integrity of the G_2 checkpoint was analyzed by measuring mitotic cells using flow cytometry for DNA content and phospho-specific antibody to histone H3 S10. Error bars represent the standard error of three independent experiments. The difference between IR-treated A6 and D7 cells is statistically significant (one-way Anova, p=0.0137).

S1333D-ATR cells did have a modest defect in maintaining the G_2 checkpoint in response to IR (Figure 3.9C). Thus, while the hyperactive S1333A mutation alters both the *in vitro* and cellular activity of ATR, the elevated kinase activity does not alter ATR function in the S or G_2-phase checkpoint. In contrast, the less active S1333D-ATR has sufficiently altered kinase activity to cause modest defects..

Discussion

Our data indicate that a single amino acid change at position 1333, in a region outside of the known regulatory domains, is sufficient to alter ATR kinase activities. *In vitro* and in cells, S1333A-ATR is hyperactive compared to wild type ATR while S1333D-ATR is less active. Initially, we hypothesized this amino acid is an auto-phosphorylation site regulating ATR kinase activity. However, we were unable to obtain evidence of phosphorylation in cultured cells or in *in vitro* kinase reactions. Thus, how the mutations alter kinase activity is not clear, but we hypothesize they alter ATR structure enough to change its ability to bind substrates.

S1333 is located within the N-terminal HEAT repeats of ATR. The mechanistic role of the HEAT repeats within PIKK kinases is not known, but HEAT repeats have been shown to serve as protein-protein interaction domains and can also bind DNA [116]. In the structure of DNA-dependent protein kinase, a PIKK family member, the HEAT repeats fold into a double solenoid and form a platform on which the kinase and other C-terminal domains sit [115]. Thus, it is possible that small changes in the HEAT repeat structure are transmitted to the kinase domain, yielding a relatively large and unexpected change in activity.

ATRIP also binds to ATR through its HEAT repeats [118]. ATRIP has several functions in ATR signaling including stabilizing the ATR protein, targeting ATR to replication stress sites, and contributing to the interaction with the TOPBP1 protein [3,38,51,209]. TOPBP1 binding to the ATR-ATRIP complex activates ATR by inducing an unknown structural change within ATR that increases ATR substrate affinity [136]. The mutations creating a hyperactive kinase may partly mimic the effect of TOPBP1 binding to ATR-ATRIP and potentiate the ability of TOPBP1 to promote the change in ATR conformation needed for its increased activity.

In summary, we identified single amino acid mutations within the ATR HEAT repeats that alter its kinase activity. Cells expressing S1333A-ATR have elevated basal phosphorylation levels of ATR substrates but no noticeable checkpoint or replication defects in cultured cells. Thus, cells can tolerate elevated basal ATR kinase activity. The small decrease in ATR activity caused by the S1333D mutation is enough to cause modest defects in some ATR checkpoint functions. S1333 is not in a region of ATR previously known to be involved in regulation of the kinase. Future high-resolution structural studies will aid in understanding why this region is important to regulate ATR activity levels.

Table 3.1: Identified ATR phosphorylation sites

Amino Acid	Peptide
S20	ELG(p)SATPEEYNTVVQKPR
T22	ELGSA(p)TPEEYNTVVQKPR
T415	MESMEIIEEIQCQ(p)TQQENLSSNSDGISPK
T422	MESMEIIEEIQCQTQQENLS(p)SNSDGISPK
S424	MESMEIIEEIQCQTQQENLSSN(p)SDGISPK
S435	RL(p)SSSLNPSK
S436	RLS(p)SSLNPSKR
S484	ASCVSGFFILLQQQN(p)SCNR
T868	NNELKD(p)TLILTTGDIGR
T952	KPICQFLVESLHSSQMTALPN(p)TPCQNADVR
T1620	NKVDSMVS(p)TVDYEDYQSVTR
S1876	LHMLCELEHSIKPLFQHSPGDS(p)SQEDSLNWVAR
T1989	GVELCFPENE(p)TPPEGK
T2180	VFLAYPQQAMWMM(p)TAVSK
T2383	TYAVIPLNDECGIIEWVNN(p)TAGLRPILTK
T2504	GE(p)TFEVPEIVPFR
Y2637	VTGLPSIEGHVHYLIQEATDENLLCQM(p)YLGWTPYM

CHAPTER IV

WHOLE GENOME SYNTHETIC LETHAL SCREENS IDENTIFY PATHWAYS THAT SENSITIZE CANCER CELLS TO ATR INHIBITION

Introduction

Early in tumorigenesis, activated oncogenes induce replicative stress and DNA damage. In response, the DNA damage response (DDR) activates and creates a barrier for tumor progression. To breach this barrier, cancer cells must inactivate one or more DDR pathways [166-168]. Deregulated DDR pathways present exploitable defects for anti-cancer therapeutics through generation of DNA damage the cancer cell cannot repair or through the concept of synthetic lethality [172]. Synthetic lethality is when a combination of mutations results in cell death but as single mutations the cell maintains viability. Therefore, if a cancer cell contains a mutation in one pathway or gene, treating that cancer with an inhibitor to a compensatory pathway will induce cell death. Treatment of cancer through synthetic lethality will preferentially target the cancer cells and spare the normal cells, reducing side effects for the patient [177].

Targeting DNA repair enzymes is a new paradigm in cancer therapy. These inhibitors have promising potential to preferentially target cancer cells with minimal patient toxicity [172,210]. One challenge remaining for these compounds is the identification of synthetic lethal pathways. The field has tried to tackle this problem through synthetic lethal genetic screens. Genetic screens with siRNA or shRNA can rapidly and in an unbiased fashion test the whole genome for synthetic lethal relationships

with an inhibitor. Additionally, the reverse screen with a library of small molecule inhibitors will identify compounds which selective kill cancers with a specific genetic mutation. These screens can also be used to identify mechanisms of resistance.

There are also many caveats and disadvantages of performing a genetic screen to identify synthetic lethal relationships. First, whole genome screening is very costly and the purchased siRNA may not efficiently knockdown the gene target and may have off-target effects. Most whole genome screens use pooled siRNA or shRNA and so all identified genes must be validated in a secondary screen using individual siRNAs, further increasing the cost. Additionally, the cell line used in the screen, most likely being a cancer cell line, may yield results specific to that cell line. Whole genome screening generates an abundance of data and the most biologically relevant result may not give a strong phenotype. Also, the identified gene or pathway synthetic lethal with an inhibitor of interest may not be frequently mutated in cancer and therefore not applicable in the cancer clinic [177,211,212]. Despite these pitfalls, synthetic lethal genetic screens have identified clinically actionable relationships.

One great success has been with the PARP inhibitors (PARPi). Two groups identified the PARPi as being synthetic lethal with mutations in BRCA1 or BRCA2 [179,180]. Mutations in these genes impair repair of double strand breaks (DSBs) by homologous recombination (HR). One PARPi synthetic lethality screen identified a regulator of BRCA1 and the other components of HR also induce synthetic lethality [212,213]. These findings expanded the clinical utility of the PARPi as patient deficient for HR through a variety of mechanisms can be treated. Olaparib is the first PARPi to

achieve FDA approval and is approved for treatment of BRCA-mutated advanced ovarian cancer [214].

There is great therapeutic interest in developing ATR specific inhibitors due to ATR activating in response to a variety replication stressors to promote genomic stability. AstraZeneca and Vertex Pharmaceuticals developed ATR-specific inhibitors and the Fernandez-Capetillo lab developed a dual mTOR/ ATR inhibitor [181,182,197]. One avenue of clinical utility for the ATR inhibitor is through the identification of synthetic lethal relationships. The proposed synthetic lethal relationships with the ATRi include loss of ATM, p53, POLD1, BRCA2, ERCC1, XRCC3, and RAD51 [191,193,195-199]. However, so far only ATM deficiency translated into the clinic as a patient selection strategy. There is still a need to identify clinically actionable synthetic lethal relationships with the ATRi.

To answer this question, we completed a whole genome siRNA screen with the ATRi to identify pathways or proteins, when lost, which sensitize cancer cells to the ATRi. In the cancer clinic, patients receive the ATRi in combination with traditional chemotherapies, not as a monotherapy. Because of this, we conducted the whole genome screen in the presence of ATRi and cisplatin, as well as cisplatin alone. The ATRi synergizes best with platinum drugs [184]. We also wanted to utilize this screening methodology to identify and characterize new ATR pathway genes. To do this, we also conducted the screen in the presence of CHK inhibitor (CHKi) and hydroxyurea (HU). We used sensitivity to ATRi, HU, and CHKi as a strong indicator of a genes placement in the ATR pathway. Validation and characterization of these genes are described in Chapter V. The whole genome screen identified knockdown of DNA replication and the ATR pathway

as the top synthetic lethal relationships with ATRi and the combination treatment of ATRi and cisplatin. We extensively validated these findings with siRNA, shRNA, and isogenic cell lines. Our data indicate cancers with DNA replication and ATR pathway defects are the optimal cancers to treat with the ATRi and cisplatin.

Results

Whole Genome siRNA Synthetic Lethality Screens

To identify clinically actionable synthetic lethal relationships with ATR inhibition, we conducted a whole genome siRNA screen with the ATRi, cisplatin, and a combination treatment of ATRi and cisplatin. The whole genome siRNA library (Dharmacon ON-TARGETplus SMARTpool) comprised of four siRNAs per gene per well to ~18,000 genes across 57-384-well plates. U2OS cells were transfected within the plates. After three days, we split each 384-well plate into four new 384-well plates and left one plate untreated and treated the remaining three with the ATRi, cisplatin, or ATRi and cisplatin. After an additional three days, cell viability was measured using alamarBlue (Figure 4.1A). We optimized the drug concentrations used in the screen to maximally kill cells transfected with ATR siRNA (siATR) and minimally kill cells transfected with non-targeting siRNA (siNT) (Figure 4.1B). The resulting Z-factors fom these drug concentrations are 0.59 for ATRi, 0.30 for ATRi/cisplatin, and 0.34 for cisplatin. A Z-factor of >0 is an acceptable assay and >0.5 is a very good assay [215]. siATR, siNT, and siCellDeath control siRNAs were present on each plate.

We conducted this screen in duplicate and verified the two replicates produced reproducible data by calculating the spearman correlation for each drug condition (Figure

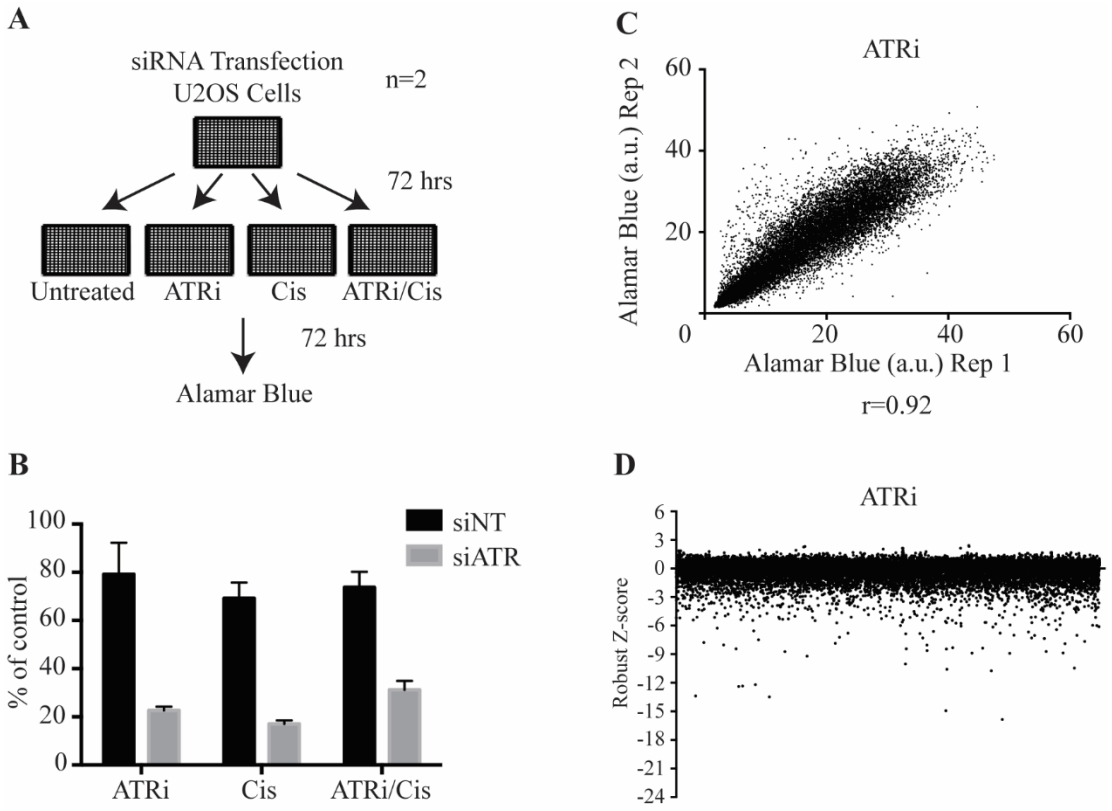

Figure 4.1. Whole genome siRNA screens identify pathways synthetic lethal with ATR inhibition and cisplatin. **A.** Schematic of the whole genome screen. U2OS cells were transfected with siRNAs and left untreated or treated with 0.1 μM ATRi (VX-970), 0.5 μM cisplatin, or 0.05 μM ATRi and 0.1 μM cisplatin. Cell viability was measured by alamarBlue. n=2 **B.** Viability of the control siRNAs, Non-targeting (NT) or ATR siRNA during the screen. The values represent the mean ±SD of the control wells on a representative plate of the screen. Z-factor ATRi=0.59, Cis=0.34, and ATRi/Cis=0.30 **C.** AlamarBlue values for replicate one vs replicate two for all the genes in the ATRi screen. Spearman correlation was calculated. R=0.92 D. Mean ATRi robust z-score for each gene graphed by plate and by row.

4.1C and Appendix A). To calculate the cell viability after drug treatment for each gene we compared the alamarBlue values from the drug treated siRNA to the untreated siRNA. This controlled for any reduced cell viability or alterations in cell growth rate due to the siRNA. We used the percent viability to calculate a robust Z-score by plate for each gene in each drug condition. The mean robust Z-score for the ATR inhibitor and for each drug condition plotted by plate and by row showed no obvious plate or row effects (Figure 4.1D and Appendix A).

We postulated this screening methodology could also be used to identify new ATR pathway genes. Therefore, we also included a Chk1/2 inhibitor (AZD7762, [216]) and HU as further pathway validation. We completed two additional replicates of the whole genome screen in the presence of the CHKi, HU and the ATRi (Figure 4.2A). We optimized the drug concentration used in these screens similarly to the first two replicates, which resulted in a Z-factor of 0.29 for the ATRi, 0.63 for the CHKi, and 0.65 for HU (Figure 4.2B). Again, we calculated the robust Z-score for each gene in each drug condition. We determined genes when knocked down in the presence of a drug resulting in a robust Z-score of -2.0 or less as synthetic lethal with that specific drug.

ATRi, CHKi, and HU Whole Genome Screen Data Analysis

Upon analysis and comparison of the identified synthetic lethal genes from the ATRi, CHKi, and HU, the whole genome screen identified knockdown of the ATR pathway as synthetic lethal with the ATRi, CHKi, and HU (Figure 4.3A). Using gene ontology pathway analysis, no additional pathways were enriched as synthetic lethal with

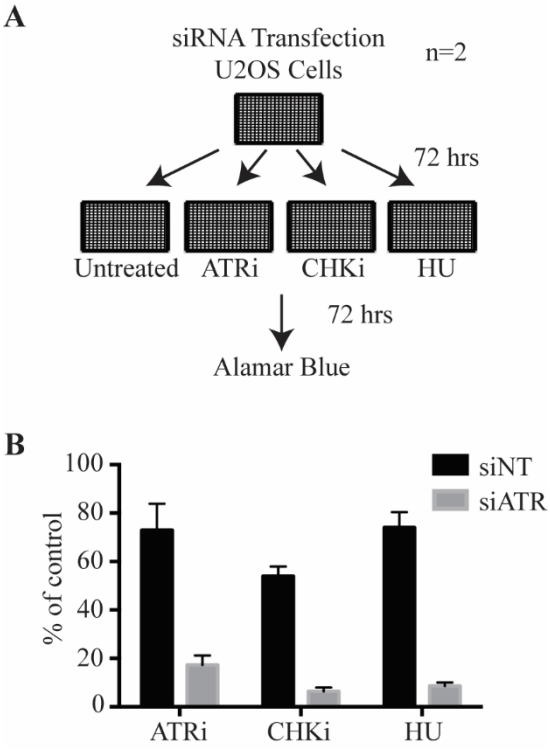

Figure 4.2. Whole genome siRNA screens identify synthetic lethal pathways with ATR inhibition, CHK1 inhibition, and hydroxyurea. A. Schematic of the whole genome screen. U2OS cells were transfected with siRNAs and left untreated or treated with 0.1 μM ATRi (VX-970), 0.05 μM CHKi (AZD7762), or 0.2 mM HU. Cell viability was measured by alamarBlue. n=2. **B.** Viability of non-targeting (NT) or ATR siRNA using the screen conditions. The values represent the mean ±SD of the control wells on a representative plate of the screen. Z-factor ATRi=0.29, CHKi=0.63, HU=0.65.

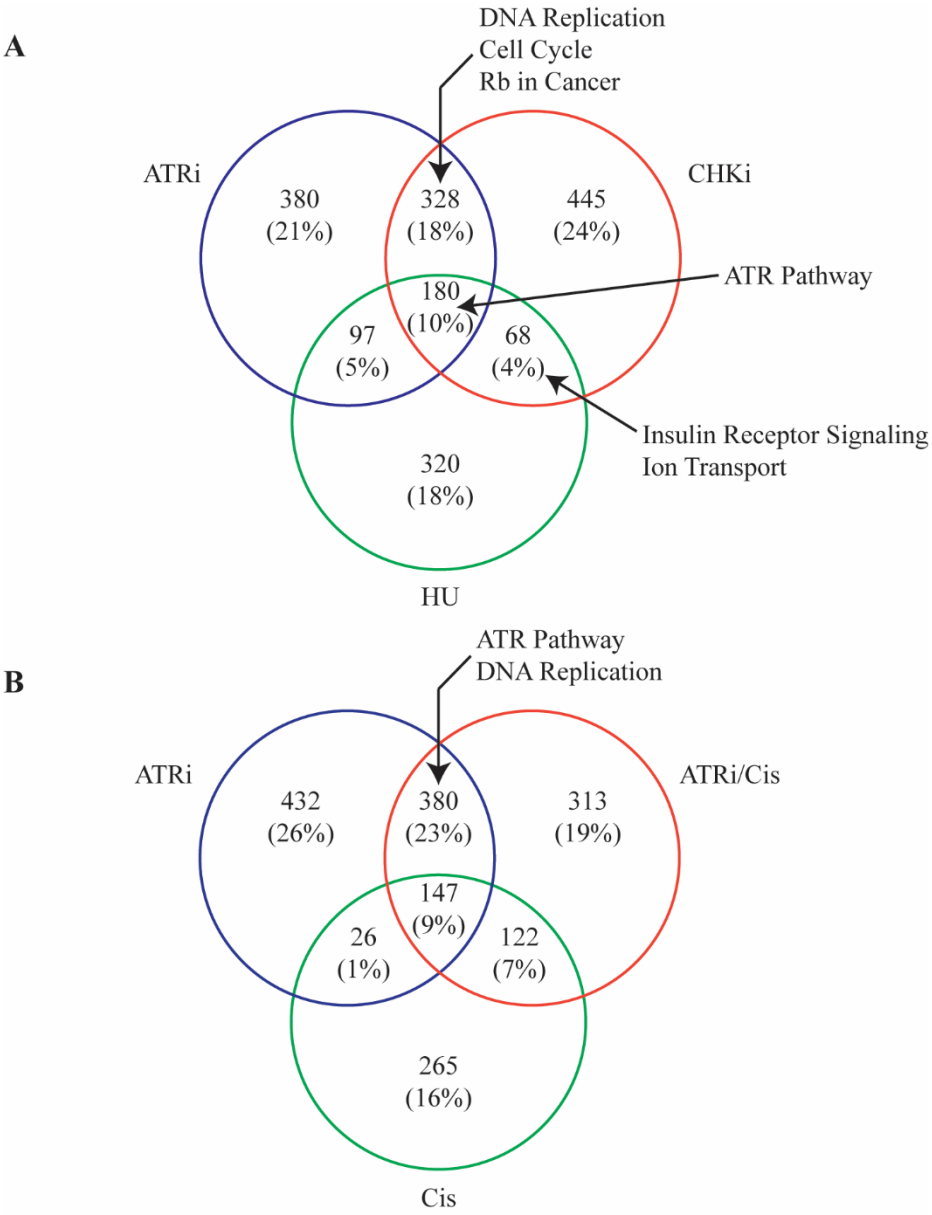

Figure 4.3. The ATR pathway and DNA replication when knocked down have synthetic lethal relationships with the ATRi alone and ATRi with cisplatin. Summary of the synthetic lethal relationships overlap in the whole genome screen treated with ATRi, CHKi, and HU **(A)** or with ATRi, cisplatin, or ATRi and cisplatin **(B)** using a robust Z-score cut off of -2.0. Numbers indicate the number of genes in that category. Percentage is of all the genes that hit in all three drug conditions.

all three drug conditions [217]. Our data identified 180 genes as synthetic lethal with all three of these drugs. We hypothesized within the 180 genes were additional, yet undescribed ATR pathway genes. Further validation and characterization of the potential new ATR pathway genes are discussed in Chapter V.

Analysis of the whole genome screen data generated from treatment with ATRi, CHKi, or HU reveals some additional intriguing results (Figure 4.3A). These screens identified knockdown of DNA replication genes as synthetic lethal with the ATRi and CHKi but not HU. Knockdown of DNA replication genes in the presence of HU results in a cell viability of about 70% of control. The dose of HU used results in slowed DNA replication. This activates the S-phase checkpoint, which results in reduced origin firing. Cells depleted for core replisome proteins would benefit from this environment as reduced origin firing results in less replication forks and thus a lower need of replisome components.

Pathways enriched as synthetic lethal with both the ATRi and CHKi included genes involved in the cell cycle and the RB/E2F pathway (Figure 4.3A). The genes in the RB/E2F pathway include transcriptional targets of E2F such as DNA replication, cell cycle, and nucleotide biosynthesis genes [218]. In addition to the DNA replication genes present in the cell cycle category, there are 12 mitosis specific genes. Most of these genes are associated with the centromeres or centrosomes, which ensure proper chromosome segregation. We also identified two components of the anaphase-promoting complex. ATR has one described function in mitosis. The Costanzo lab reported ATR and ATM activate in response to DSBs during mitosis, phosphorylate CEP63, and prevent spindle assembly [219]. One explanation of the screen data is loss of mitotic proteins creates

problems during chromosome segregation, causing DSBs, other chromosome aberrations, and genomic instability. This would result in an increased dependence on ATR potentially in mitosis but also during the next cell cycle. When ATR is inhibited under these genetic contexts, the increased genomic instability induces cell death.

There is a second explanation for why loss of centrosome proteins is synthetic lethal with the ATRi and CHKi. ATR and CHK1 localize to centrosomes and CHK1 localized at the centrosome prevents premature centrosome separation by shielding CDK1 from early activation by Cdc25 [220,221]. Additionally, mutation of centrosome proteins results in reduced ATR pathway signaling and causes the ATR-associated disease, Seckel syndrome [222-225]. This link between ATR, CHK1, and the centrosome is not fully understood, but explains the enrichment of these genes in the dataset.

The last enriched pathway identified in the ATRi, CHKi, and HU screen data sets was insulin receptor signaling and ion transport, which upon knockdown are synthetic lethal with CHKi and HU (Figure 4.3A). The three proteins identified in these pathways were subunits of V-ATPase: ATP6V1G1, E1, and D. Several other subunits of V-ATPase were sensitive to these drugs but did not have a robust Z-score less than -2.0. Most of the V-ATPase subunits are moderately sensitive to ATRi. V-ATPase regulates the pH of lysosomes, the golgi, and endosomes by pumping in protons from the cytoplasm and thereby also regulates the pH of the cytoplasm [226]. Localization of V-ATPase is shown to be regulated by glucose activation of PI3K [227]. In *S. cerevisiae*, knockdown of various subunits of this complex results in deregulation of cytoplasmic pH and higher levels of DNA damage after treatment with cisplatin, as measured by an increased induction of the DNA damage checkpoint. Knockdown of this complex also sensitized the cells to UV,

HU, and methyl methanesulfonate. It is predicted acidification of the cytoplasm may alter DNA structure, rendering it more prone to DNA damage [228].

ATRi and ATRi/Cisplatin Whole Genome Screen Data Analysis

To identify pathways when knocked down that are synthetic lethal with ATR inhibition or the ATRi and cisplatin, we compared genes with a robust Z-score of -2.0 or less for each of the screen drug conditions (Figure 4.3B) [229]. Using gene ontology analysis, we found the DNA replication and ATR pathway genes as being enriched and as having synthetic lethal relationships with the ATRi and ATRi/cisplatin [217]. No other pathways were significantly enriched in the Venn diagram breakdown of the results. Gene ontology analysis of all the hits for ATRi alone identified DNA replication, ATR pathway, cell cycle genes, as well as mismatch repair and RB in cancer (Figure 4.4A and B). A table of all the genes identified in these pathways is in Appendix A. The cell cycle genes and RB in cancer genes are nearly identical to those found in the ATRi and CHKi data sets, described above. Previous studies of mismatch repair demonstrated short term knockdown (siRNA) of mismatch repair genes as synthetic lethal with the ATRi but isogenic cell lines did not support this finding [183].

The list of the top fifteen synthetic lethal genes with the ATRi or the combination treatment of ATRi/cisplatin contains a striking number of genes in the DNA replication and ATR pathway (Figure 4.4C and D). The other genes ranked in the top 15 did not validate in secondary screening. These tables clearly demonstrate that the strongest synthetic lethal relationships with the ATRi alone or in combination with cisplatin are the ATR pathway and DNA replication.

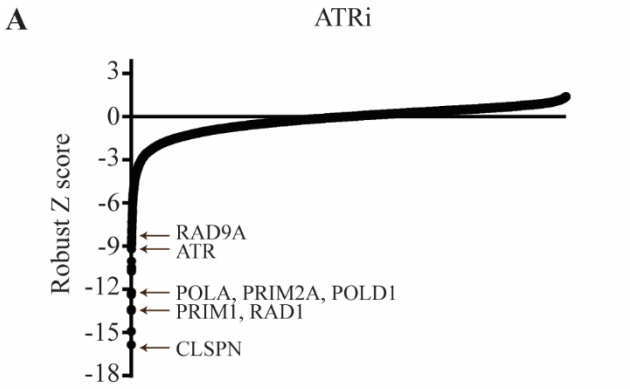

C

Rank	Gene	Gene ID	ATRi Avg
1	CLSPN	63967	-15.85
2*	HMGB3	3149	-14.93
3	PRIM1	5557	-13.48
4	RAD1	5810	-13.39
5	POLA	5422	-12.38
6	PRIM2A	5558	-12.35
7	POLD1	5424	-12.20
8*	SEZ6	124925	-10.75
9	TIMELESS	8914	-10.58
10*	EGFL3	1953	-10.46
11*	KERA	11081	-10.04
12	ATR	545	-9.20
13*	ZNF553	197407	-8.91
14*	LMNB1	4001	-8.88
15*	DPY19L2	283417	-8.87

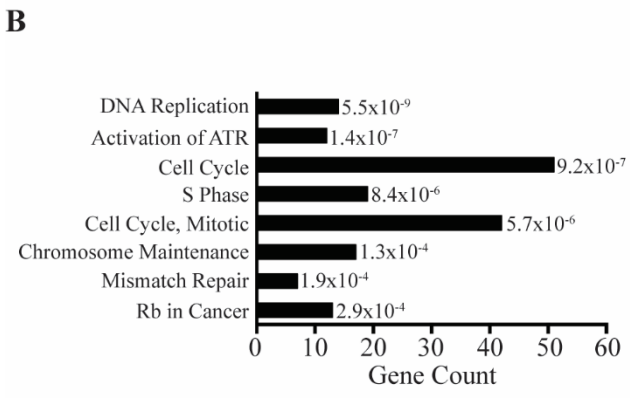

D

Rank	Gene	Gene #	ATRi/C Avg
1	CLSPN	63967	-18.83
2	POLA	5422	-14.00
3	RAD1	5810	-12.49
4*	HMGB3	3149	-11.46
5*	ZNF553	197407	-11.41
6	PRIM2A	5558	-11.24
7	POLD1	5424	-10.97
8	ATR	545	-10.63
9*	EGFL3	1953	-9.73
10	RAD9A	5883	-9.29
11*	PATE3	100169851	-8.92
12*	SEZ6	124925	-8.44
13*	CENPL	91687	-8.24
14	PRIM1	5557	-8.05
15*	KERA	11081	-8.02

Figure 4.4. DNA replication and the ATR pathway are the top synthetic lethal pathways. A. The mean robust Z-score from all four replicates of the ATRi screen for each gene is graphed by rank. **B.** Gene ontology analysis of the ATRi dataset by Toppgene using a robust z-score cutoff of -2.0. C and D. The top 15 genes synthetic lethal with ATRi **(C)** or ATRi and cisplatin **(D)** listed with their mean robust Z-score and rank. ATR pathway genes are highlighted in blue. DNA replication genes are highlighted in gold. Genes with asterisks are not in either pathway and did not validate when testing four individual siRNAs for increased sensitivity to the ATRi or ATRi/cisplatin.

Validation of the ATR Pathway and DNA Replication

To verify these findings, we sought to validate the genes from the DNA replication and ATR pathways by testing four individual siRNAs for each gene. We tested each siRNA for inducing increased sensitivity to the ATRi. The validation assays followed the same methodology as the whole genome screen and were previously described [183,191]. The ATR pathway strongly validated as being synthetic lethal with the ATR inhibitor (Figure 4.5A). A variety of DNA replication genes also validated including the main DNA polymerases involved in leading and lagging strand DNA synthesis and all of the replication MCMs (Figure 4.5B-D). MCM8 and 9 knockdown did not sensitize cells to the ATRi. These two MCMs have been implicated as having a function in HR instead of DNA replication [230,231].

Additionally, we tested genes involved in nucleotide metabolism for synthetic lethality with the ATRi. Previous findings identified knockdown of ribonucleotide reductase M1 (RRM1) and ribonucleotide reductase M2 (RRM2) as being synthetic lethal with the ATRi and the ATRi is synergistic with gemcitabine and HU, inhibitors of ribonucleotide reductase [183,186]. Ribonucleotide reductase converts ribonucleotides into deoxyribonucleotides. In the nucleotide biosynthesis pathway, we identified knockdown of the genes involved in the addition of the phosphates to the nucleotides as synthetic lethal with the ATRi (Figure 4.5E). Based on our primary and secondary screen data, siRNA to proteins involved in synthesis of the nucleotide base either strongly kill cells or do not significantly increase sensitivity to the ATRi. The pathway synthesizing the nucleotide base leads to the generation of ribonucleotides as well as deoxyribonucleotides, explaining why knockdown of these genes results in high levels of

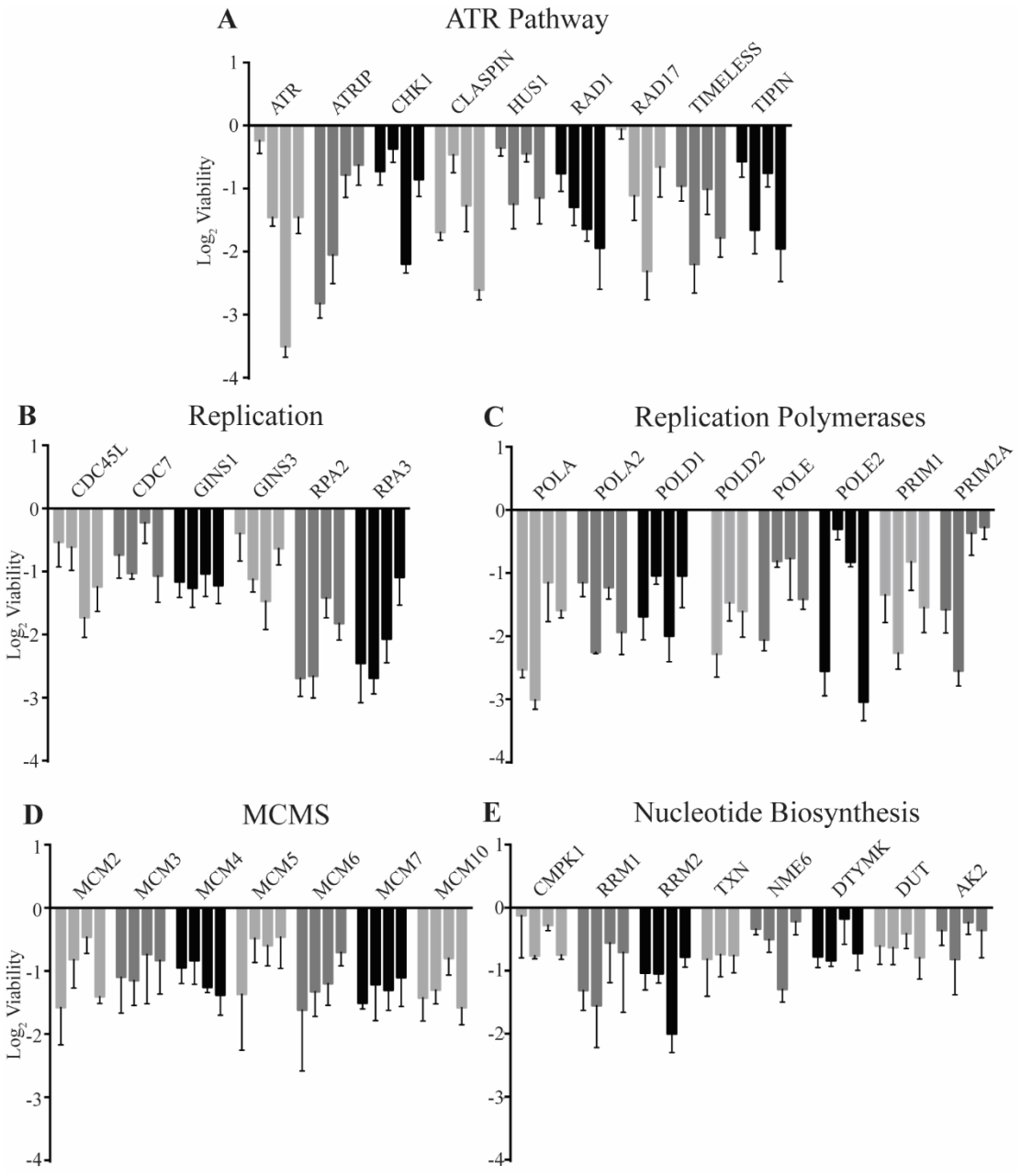

Figure 4.5 The ATR pathway and DNA replication pathways validated using four individual siRNAs. A-E. Four siRNAs per gene and one gene per well were transfected into U2OS cells and treated with the ATR inhibitor (VE-821) at 1 μM. Cell viability was measured by alamarBlue comparing untreated to treated siRNA. Log2 percent viability is graphed for each siRNA. Majority of this data is previously published in Mohni *et al.* 2014. Any siRNAs after transfection resulting in less than 1% cell viability were excluded from the graph. Tested genes were from a small custom siRNA library. Only genes that validated, percent viability of 60% or less after ATRi treatment, were included in this figure.

cell lethality and lack of synthetic lethality with the ATRi. Knockdown of RNA metabolism genes were not identified as synthetic lethal with the ATRi.

We performed the whole genome screens and validation screens with U2OS cells. To test if this synthetic lethality is universal or U2OS cell specific, we knocked down ATR in a panel of TNBC cell lines, as well as a NSCLC line. Transfection conditions were optimized using a cell death siRNA but knockdown of ATR was not verified in this experiment. A subset of the tested cell lines were exceptional responders and knockdown of ATR exquisitely sensitized these cells to the inhibitor (Figure 4.6A). The other subset of cell lines did not have as dramatic sensitization to the ATRi (Figure 4.6B). There are a number of explanations for what could be occurring. These cells could be metabolizing the drug faster or have upregulated efflux. These cells may have increased expression of DNA repair genes or increased origin firing to circumvent inhibition of ATR. These cells could have upregulated the ATR pathway in response to treatment or be more resistant to apoptosis driven by increased DNA damage. All of these are common mechanisms of resistance to a chemotherapeutic [232]. The best way to determine which mechanisms provide resistance to the ATRi would be to do a survival screen, looking for increased survival after drug treatment. Overall, we conclude knockdown of the ATR pathway sensitizes cells to the ATRi.

Our previous work showed long-term knockdown of ATR and CHK1 sensitized cells to the ATRi. Additionally, a cell line with edited ATR alleles resulting in reduced ATR expression was more sensitive to the ATRi than the parental cell line [191]. To further test that long-term knockdown of ATR pathway genes confers sensitivity to the ATRi, we employed CRISPR/Cas to edit the ATRIP alleles to reduce ATRIP expression

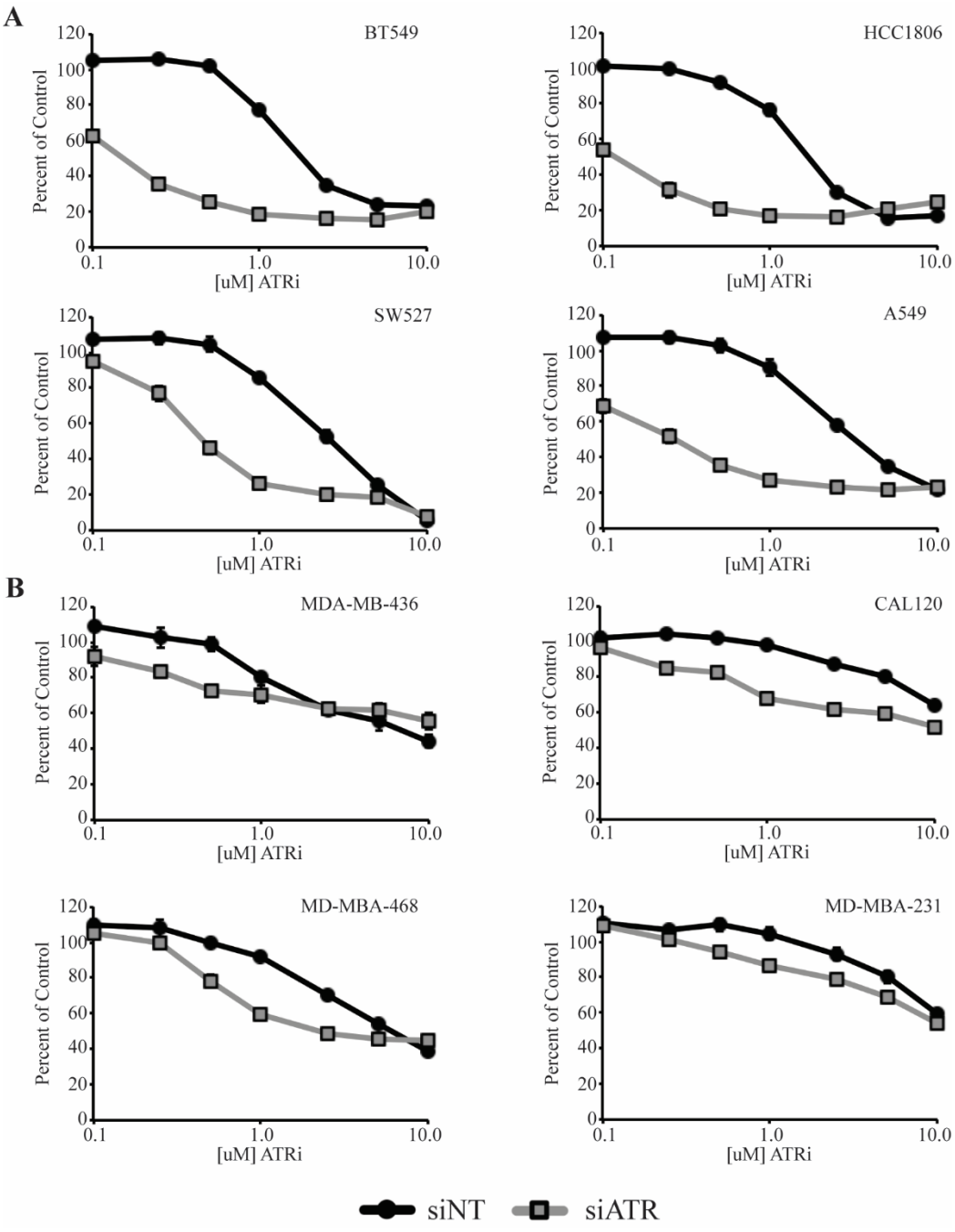

Figure 4.6. ATR depletion sensitizes triple-negative breast cancer and non-small cell lung cancer cell lines to ATRi. A panel of cell lines were transfected with the indicated control or ATR siRNA and then treated with the ATR inhibitor. After 72 hours, cell viability was measured using alamarBlue and reported as percent of untreated cells. **A.** Cell lines strongly sensitized to the ATRi after ATR knockdown. **B.** Cell lines weakly sensitized to the ATRi after ATR knockdown.

in U2OS cells [233-235]. We targeted exon 4, one exon downstream of the start codon, with two guide RNAs, deleting a small portion of coding sequence. The resulting clones either had reduced ATRIP expression (clone 26), thereby also reducing ATR expression (Figure 4.7A), or the ATRIP alleles gained a small internal deletion yielding a slightly smaller ATRIP protein and reduced ATR expression (clone 7,13 Figure 4.7B). Reduction of ATRIP expression will also reduce ATR protein levels as ATR and ATRIP are obligate binding partners. Loss of one results in loss of the other [3]. We tested two clones containing the small internal deletion and one clone with reduced ATRIP expression for increased sensitivity to the ATRi. All three clones had increased sensitivity to the ATRi in comparison to wild-type U2OS cells (Figure 4.7C). We were not able to generate ATRIP-null cells. This is not unexpected as ATR is essential [3].

We next wanted to test if the activity level of the ATR pathway was reflective of sensitivity to the ATRi. We used cell line models containing single point mutations in ATR, which alter the basal kinase activity, as previously discussed in Chapter III. Mutation of serine 1333 in the HEAT repeats of ATR generates a hyperactive kinase both *in vitro* and in cells. Conversely, mutation of serine 1333 to aspartic acid reduces the kinase activity of ATR [1]. These cell lines provided an excellent model for alterations in ATR pathway signaling as all three-cell lines expressed similar levels of ATR protein. The hyperactive kinase cell line (S1333A) was more resistant to the inhibitor compared to the wild-type cell line and the less active kinase cell line (S1333D) was more sensitive to the inhibitor (Figure 4.7D). This experiment beautifully demonstrates that ATR pathway activity inversely correlates with sensitivity to the ATRi.

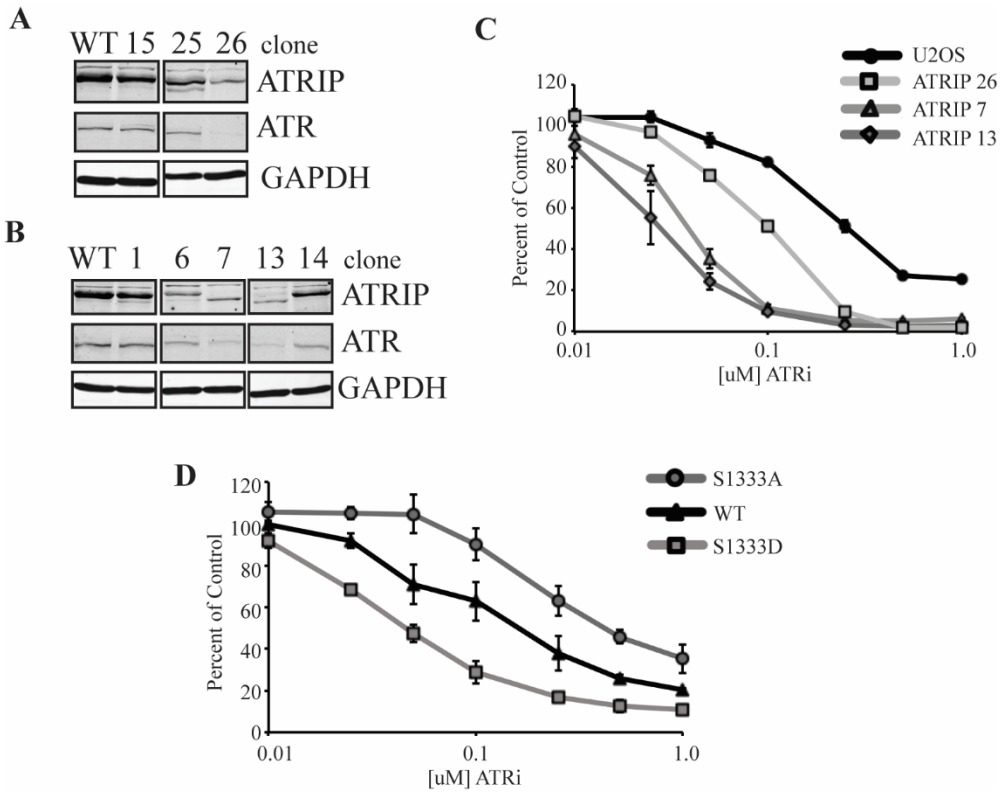

Figure 4.7. Genetic alteration of the ATRIP or ATR gene sensitizes cells to the ATRi. A-B. Using Crispr/Cas the gene alleles for ATRIP were edited in U2OS cells. Editing resulted in reduced ATRIP expression, clone 26 (**A)** or a small internal deletion within the ATRIP gene, clone 7 and 13 **(B). C.** Clones 26, 7, and 13 and (**D)** HCT-116 cells expressing FLAG-ATR, FLAG-S1333A-ATR, or FLAG-S1333D-ATR were treated with the ATRi (VX-970) for 72 hours and cell viability was measured using alamarBlue and reported as percent of untreated cells.

Identification of Cancer Cell Lines with Reduced ATR Pathway Function

We next wanted to verify that reduced ATR pathway function is synthetic lethal with the ATRi in cancer cell line models. To identify cancer cell lines with ATR pathway defects, we consulted the TCGA data using the cBioPortal interface and evaluated the mutation frequency and type across the known major ATR pathway genes [236,237]. The most striking result was the prevalence of ATRIP gene deletion in a subset of cancers. This was surprising as we know that that ATR/ATRIP complex is essential. However, these cancers may be expressing ATRIP at very low levels and thereby have reduced pathway functionality. We also found a frameshift mutation in the ATR and CHK1 genes occurring in mismatch repair deficient cancers due to microsatellite instability [238-240]. Additionally, we identified cancer cell lines with low expression of ATR pathway genes using CNV and mRNA levels in the CCLE [241]. The cell lines acquired for the following studies had a wide range of doubling times. To account for this, we adjusted the length of the ATRi dose response assays to three population doublings (Table 4.1). The cell viability was calculated using alamarBlue.

There is no clear relationship between ATRIP levels and ATRi IC50

ATRIP is located on chromosome 3p21. This chromosome region is most frequently lost in lung, breast, and renal cancers [242-244]. Additionally, renal cancers with chromosome 3p LOH are predicted to have defects in nucleotide metabolism [245]. This prediction fits well with our screen data as knockdown of nucleotide metabolism genes sensitize cells to the ATRi (Figure 4.5E). Using the CCLE dataset, we identified cancer cell lines marked as having a deep deletion of the ATRIP gene (Figure

Table 4.1: Lists all the cell lines tested, the cancer type, calculated doubling times, adjusted dose response assay length, and the number of cells plated in a 96-well plate.

Cell Line	Cancer Type	Doubling Time	Assay Length	Cells/well 96 well
A549	NSCLC	24 hr	3 day	3,000
H157	NSCLC	18 hr	2 day	5,300
HCC827	NSCLC	30 hr	4 day	8,600
H441	NSCLC	34 hr	4 day	19,000
H1869	NSCLC	24 hr	3 day	6,000
H2172	NSCLC	24 hr	3 day	5,500
A704	Renal	48 hr	6 day	3,000
DMS53	SCLC	33 hr	4 day	14,000
H520	Lung	24 hr	3 day	16,000
A673	Ewing	24 hr	3 day	15,000
MDA-MB-415	Breast	53 hr	7 day	3,300
H810	NSCLC	30 hr	4 day	19,000
H2126	NSCLC	48 hr	6 day	5,000
HCC1187	Breast	41 hr	5 day	n/a
MDA-MB-436	TNBC	29 hr	4 day	7,000
HDQP1	TNBC	31 hr	4 day	4,000
HCC1806	TNBC	26 hr	3 day	15,000
BT549	TNBC	30 hr	4 day	2,000
Cal51	TNBC	25 hr	3 day	12,800
MDA-MB-231	TNBC	29 hr	4 day	7000
Hec59	Endometrial	23 hr	3 day	8,000
IGROV-1	Evarian	30 hr	4 day	3,000
BT20	Breast	58 hr	7 day	9,000
LN319	Brain	40 hr	5 day	14,000
HEC-1-A	Endometrial	28 hr	3 day	6,000
HCT116	Colon	25 hr	3 day	4,000
TE5	Oral	32 hr	4 day	3,000
GP2D	Colon	24 hr	3 day	15,000
HCC2218	Breast	78 hr	10 day	10,000

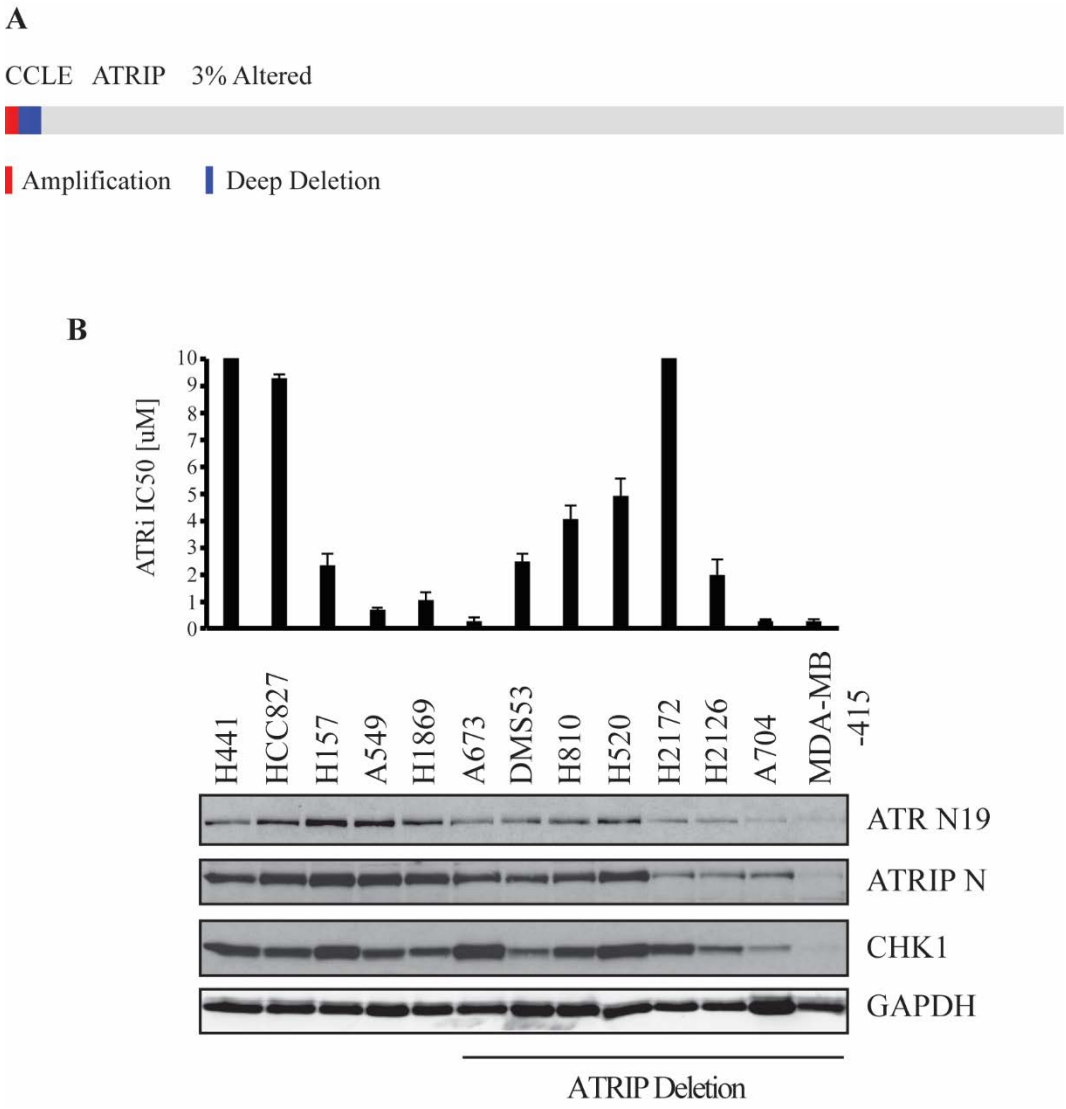

Figure 4.8. Identified ATRIP deletion cell lines still express ATRIP and have varied sensitivity to the ATRi. A. The TCGA data analysis of the cell lines within the CCLE. 3% of the cell lines have amplified (red bar) or deleted (blue bar) ATRIP alleles. **B.** Western blot of ATR and ATRIP protein levels across a panel of the ATRIP deletion cell lines identified within the CCLE and additional control lung cancer cell lines. The calculated ATRi IC50 for each cell line is graphed about the western blot. IC50 was calculated from ATRi dose response curves using GraphPad Prism.

4.8A)[241]. We examined ATRIP and ATR protein levels in each cell line by western blot and tested their sensitivity to the ATRi. Cell lines containing an ATRIP gene deletion expressed a wide range of ATRIP protein and there was no clear correlation between ATRIP or ATR protein levels and sensitivity to the ATRi based on these cell lines (Figure 4.8B).

There is no clear relationship between cancer cell lines with ATR signaling defects and ATRi sensitivity.

Next, we obtained cell lines containing the frameshift mutation in ATR or CHK1 (Figure 4.9A). The CHK1 frameshift occurs much less frequently. The TCGA data identified 34 cases of the ATR frameshift but only 10 cases of the CHK1 frameshift. This mutation arises in mismatch repair deficient cell lines experiencing microsatellite instability. The mutation arises from an expansion or contraction of a three-adenine repeat within the gene. In a study of the ATR frameshift, cell lines containing the frameshift had reduced phosphorylated CHK1 (pCHK1) after DNA damage. These cell lines also had decreased ATR protein levels and under this genetic context, ATR is reported to be a dose-dependent tumor suppressor [238,246]. However, presence of this mutation does not correlate with overall patient survival or disease free survival [247]. We tested cell lines containing the ATR or CHK1 frameshift for the ability to phosphorylate CHK1 after replication stress. These cells only had a minor reduction in pCHK1 levels compared to cell lines with wild-type ATR (Figure 4.9B).

Next, we utilized the CCLE data to identify cells expressing low levels of key ATR pathway genes in expectation that they would have ATR pathway defects. The CCLE

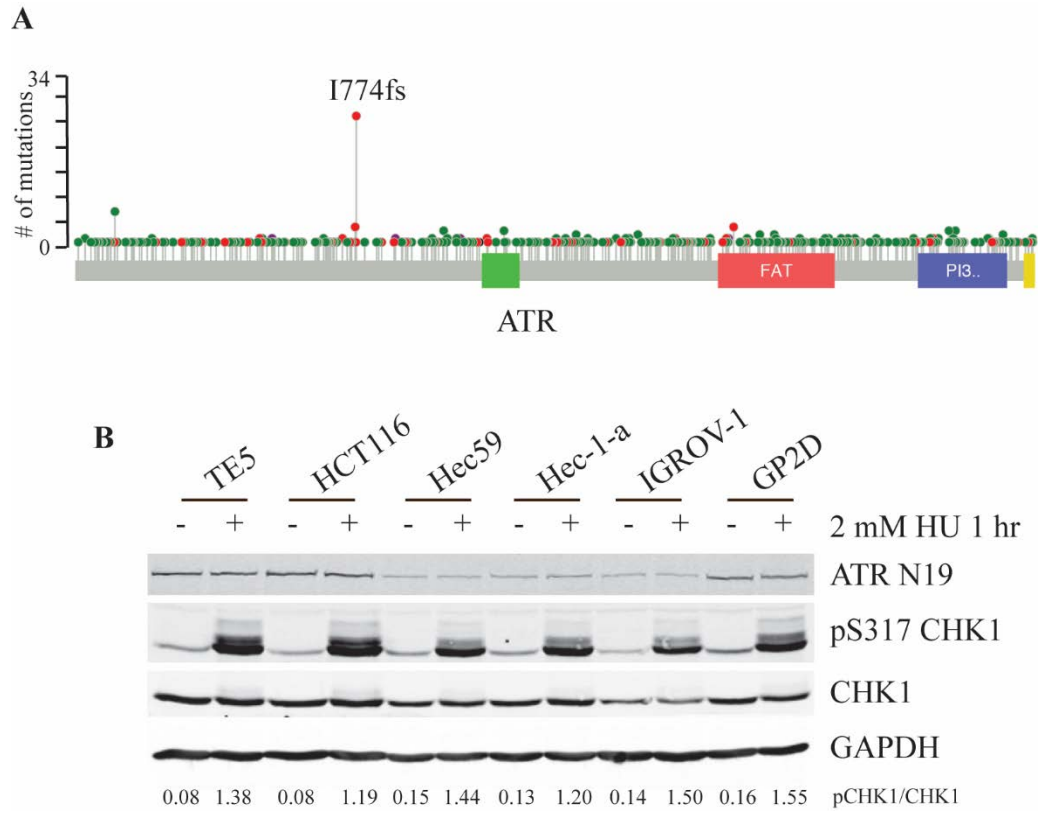

Figure 4.9. ATR and CHK1 frameshift mutations moderately decrease pCHK1 after HU treatment. A. The TCGA data showing the frequency of mutation across the ATR gene. Green spots are missense mutations and red spots are frameshift, splice, or nonsense mutations. Frequency of the mutation is graphed on the y-axis. I774fs is the identified frameshift mutation. **B.** Western blot analysis of ATR frameshift cell lines (Hec59, Hec-1-a, and GP2D), CHK1 frameshift cell line (IGROV-1) and control cell lines (TE5 and HCT116). Cells were left untreated or treated with 2 mM HU for 1 hr. Western blot analysis of pS317 CHK1, total CHK1 and total ATR are shown. pCHK1/CHK1 ratios were calculated and listed below each lane.

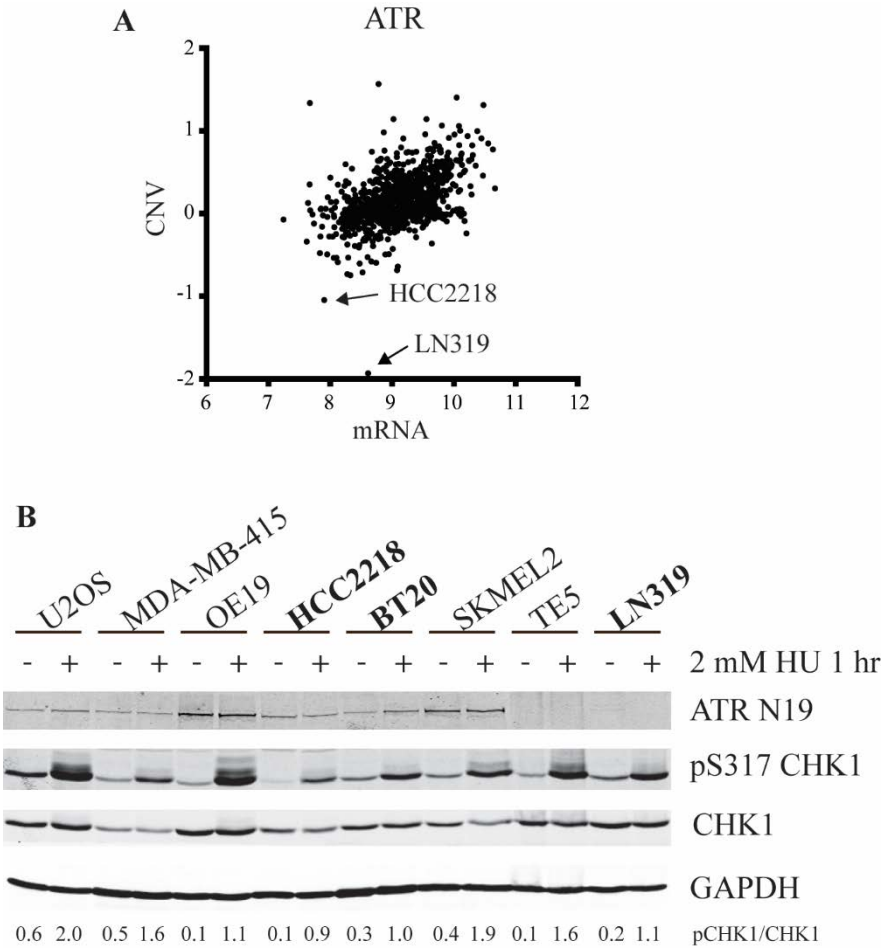

Figure 4.10. The CCLE data of copy number variation and mRNA levels of the ATR pathway genes identifies cell lines with ATR signaling defects. A. Graphs were generated for each ATR pathway gene. ATR is depicted as a representative graph. CNV vs mRNA levels were graphed to identify outliers with low CNV and low mRNA levels. **B.** Acquired outlier cell lines were examined by western blot for pS317 CHK1 levels before and after treatment with 2 mM HU for 1 hr compared to the control cell line, U2OS. Cell line names bolded were identified as having significantly reduced pCHK levels. pCHK1/CHK1 ratios are listed below each lane.

contains data on ~950 cell lines. We graphed each cell lines copy number variation (CNV) and mRNA level for the key ATR pathway genes. From the graphs, we identified outlier cell lines containing both low CNV and mRNA levels for the specified gene (Figure 4.10A). We obtained seven cell lines and tested ATR pathway function using the readout of pCHK1 levels after replication stress (Figure 4.10B). Three of the acquired lines,HCC2218, BT20, and LN319, had significantly reduced pCHK1 compared to the control U2OS cells.

We then tested the obtained ATR and CHK1 frameshift cell lines and the outlier cell lines with reduced pCHK1 for increased sensitivity to the ATRi. Additional control cell lines, HCT116 and TE5, which robustly phosphorylated Chk1 after HU treatment, were also included in the analysis. We treated the cells with increasing concentrations of the ATRi and measured the cell viability by alamarBlue after three population doublings (Figure 4.11). In comparison to the control cell lines (orange lines), the ATR frameshift (green lines), CHK1 frameshift (blue line) and ATR pathway deficient cell lines (black lines) displayed a wide range of sensitivities to the ATRi. From this data, there is no clear observable relationship between mutations in the ATR pathway and sensitivity to the ATRi.

To analyze the data further, we graphed the IC50 for the ATR pathway defective cell lines in comparison to all other cell lines tested including the ATRIP deletion cell lines (Figure 4.11B). Overall, the IC50 values ranged between >0.1-10μM. Of note, the calculation of the IC50 for the three most resistant ATR defect cell lines is lacking in complete accuracy as the full dose response curve was not captured in the assay (Figure 4.11A). We hypothesized the ATR defect cell lines would have an overall decrease in

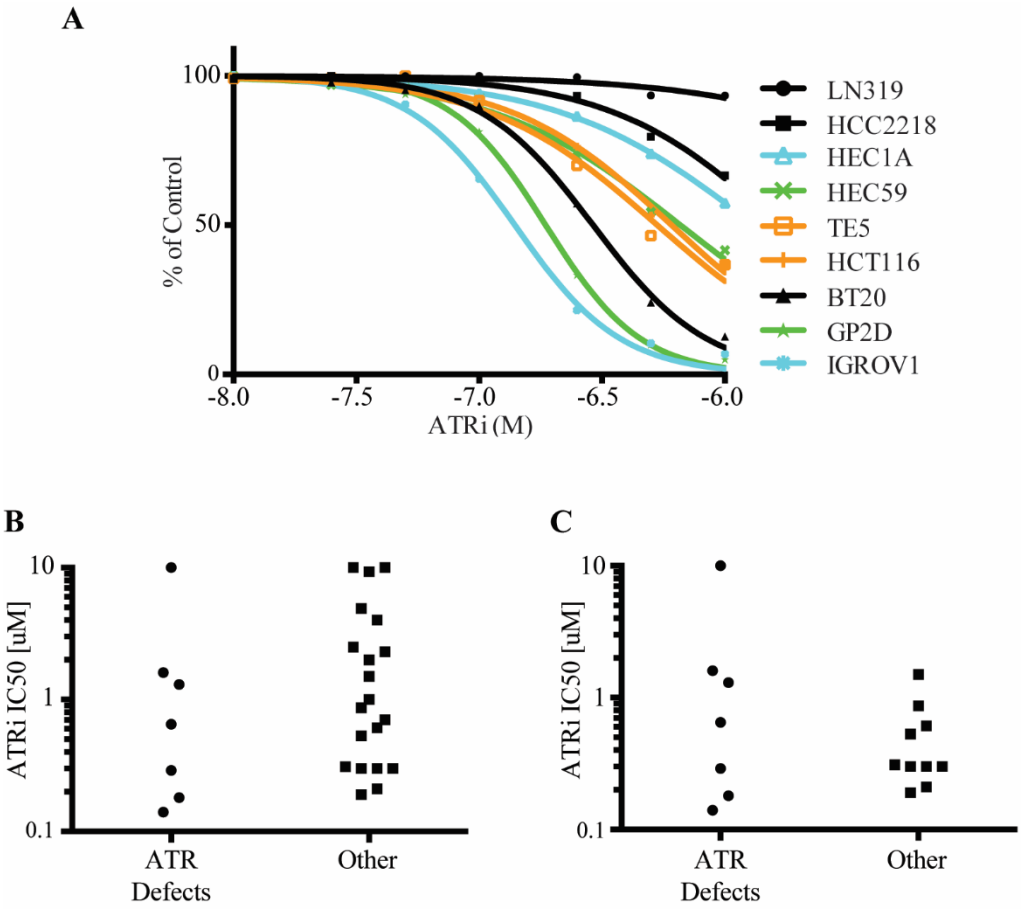

Figure 4.11. Identified cell lines with ATR defects have varied sensitivities to the ATRi. A. ATRi dose response curves. Cells were treated with ATRi for three population doublings. Cell viability was calculated using alamarBlue and comparing untreated to treated cells. GraphPad Prism was used to graph the dose response curves. Black lines (LN319, HCC2218, BT20) were identified from the CNV vs mRNA graphs and have reduced pCHK1 after HU. Green lines (HEC-1-a, HEC59, GP2D) contain the ATR frameshift mutation. The blue line (IGROV-1) contains the CHK1 frameshift mutation. Control cell lines (TE5, HCT116) are in orange. **B.** Graph comparing calculated ATRi IC50 from ATR defect cell lines to all other cell lines tested. **C.** Graph shown in B but with lung cancer cell lines removed.

average IC50 in comparison to all other cell lines tested, such as observed when comparing ATRi IC50 in ALT positive and negative cells lines [200]. The lung cancer cell lines tended to have higher IC50 values and as such, we removed them from a second comparison graph (Figure 4.11C). This also did not reveal any significant differences between the two populations. The siRNA, shRNA, and isogenic cell lines strongly supported our hypothesis, including cell lines with demonstrated alterations in ATR kinase activity. However, the cancer cell line models yielded no clear relationships between ATR pathway protein expression levels or ATR signaling defects and sensitivity to the ATRi.

Discussion

The newly developed ATR inhibitors are currently entering phase II clinical trials. These inhibitors have shown promising pre-clinical results in combination with DNA damaging chemotherapies such as platinums, PARP inhibitors, topoisomerase poisons, and gemcitabine [183,184,195]. In the clinic, the ATRi is also being combined with taxanes and the newly FDA approved anti-PDL1 therapy. However, there is no clear indication of which patient populations would best benefit from treatment with the ATRi. In this study, we conducted a whole genome siRNA screen to identify genetic determinants for sensitivity to the ATR inhibitor. As the ATRi is only used in combination with traditional chemotherapies in the clinic and not as a monotherapy, we also performed the whole genome screen in the presence of ATRi and cisplatin. ATR inhibition alone or in combination with cisplatin is most synthetic lethal with loss of ATR pathway genes and DNA replication genes. ATR inhibition is also synthetic lethal with loss of nucleotide biosynthesis genes.

Reduction in ATR activity increases the dependence on the remaining kinase activity

We validated reduction of ATR pathway genes as being synthetic lethal with ATR inhibition by siRNA, shRNA, and isogenic cell lines, both in this study and previous work [183]. We also showed overall ATR kinase activity is reflective of sensitivity to the inhibitor using an isogenic cell line. We initially hypothesized knockdown of ATR sensitizes cells to the ATRi because there was less total protein in the cell. However, this hypothesis does not explain why knockdown of the other ATR pathway genes also sensitizes cells as ATR levels are unaffected. We do know ATR is activated every S-phase to overcome replication stresses and regulates origin firing, facilitates repair of replication forks, and prevents premature onset of mitosis [28]. In the presence of replication stress when ATR is inhibited the replication forks collapse into double strand breaks [96]. We hypothesize cells with reduced ATR pathway function have higher levels of replication stress and thus a higher dependence on the remaining ATR functionality to maintain cell viability. If ATR is inhibited is those cells, a significant reduction in remaining ATR function occurs, and the cells die.

The ATR pathway is not frequently mutated in cancer.

Identifying cancers with reduced ATR pathway function proved challenging. The most prevalent alteration of the ATR pathway is deletion of the ATRIP gene. However, all of the ATRIP deletion cell lines we acquired expressed some level of ATRIP protein and those protein levels did not correlate with ATRi IC50. These cells also had a wide range of growth rates, which could alter sensitivity to the inhibitor. We corrected for this by altering the length of the dose response assay to accommodate for three population

doublings. Additional work on cell lines with ATR or CHK1 frameshift mutations or low expression of a key pathway gene did not reveal an obvious correlation between having ATR pathway defects and sensitivity to the ATRi. The tested cell lines came from a wide variety of cancers containing innumerable genetic differences.

In addition to identifying genetic alterations which sensitize cells to the ATRi, it is also crucial to know genetic alterations which promote resistance. Key future studies need to identify these alterations so patients not to treat can be properly identified. These mechanisms could include ATM upregulation as ATR and ATM share many substrates, increased origin firing to compensate for collapsing replication forks, or upregulation of ATR expression upon exposure to the drug. Additionally, we never tested if the ATRi is effectively inhibiting ATR in each of the tested cell lines. Increased efflux, decreased influx, or increased metabolism of the drug are all pathways the cancer cells could have employed to resist the ATRi treatment.

There is no good biomarker for ATR activity

To test for ATR pathway defects in our acquired cell lines, we used phosphorylated CHK1 levels after HU treatment as a readout of ATR activity. This is a poor biomarker because CHK1 gene expression is cell cycle regulated and each cell line had a different cell cycle distribution. Resources also limited this study. There are only a few good antibodies for phosphorylated ATR substrates. Additionally, ATM phosphorylates many of the same substrates, and the availability of reagents does not correct for the cell cycle and cell doubling time differences. Cell lines with fewer cells actively replicating DNA

would not have as big of an induction of pCHK1 after HU treatment because HU only effects S-phase cells. These limitations proved a challenge in this study.

This is further shown by the data from the S1333 mutant ATR lines. *In vitro*, S1333A-ATR is hyperactive but in cells expressing S1333A-ATR, there is only slightly increased basal pCHK1. At low doses of replication stress, S1333-ATR maintains higher levels of pCHK1 but at higher doses of HU, all differences in pCHK1 levels disappear. Conversely, S1333D-ATR is less active *in vitro*, but in cells there are no alterations in pCHK1 levels. However, these cell lines had very different sensitivities to the ATRi, which is reflective of the ATR mutant's *in vitro* kinase activity. Using a pCHK1 readout after HU would not have predicted this. Therefore, the cell lines identified as having ATR pathway defects may have been incorrectly labeled. However, there is no clear way to fix this. In order to effectively identify which cancers are sensitive to the ATRi, which are not, and why, a large cell line panel would need to be tested. Discussed below are some other ways our data and others may help direct the ATRi in the clinic.

ATRi synergizes with the CHKi

Consistent with our work, the Helleday group recently published the ATRi synergizes with the CHKi in cancer cells [192]. However, the CHK inhibitors used in that study did poorly in the clinic and most studies with a CHKi have been terminated due to patient toxicity as well as for business reasons [248]. Many of these early CHK1 inhibitors also equally inhibit CHK2 and have other off-target effects such as inhibition of Src family kinases [216]. Two newly developed CHK1 inhibitors are more selective for CHK1 and

are currently in phase I and phase II clinical trials [249]. It remains to be seen if a CHK1i will gain FDA approval.

DNA polymerase D1 and E are mutated in cancer

Recently, a group published loss of DNA Polymerase D1 as being synthetic lethal with reduced ATR functionality [198]. We previously published this finding prior to their work and the whole genome screen also identified knockdown of POLD1 as being synthetic lethal with the ATRi [183]. While POLD1 is not commonly lost in cancer, a point mutation within the exonuclease domain can occur. A point mutation in the same domain of POLE also occurs. These mutations effect the polymerases proofreading activity leading to an increase in DNA mismatches [250,251]. Loss of polymerase proofreading will increase the mutation rate of the DNA but will not necessarily alter the processivity of the replication fork or increase replication stress levels. Our screen and their work identified loss of the polymerase as synthetic lethal with the ATRi not loss of proofreading. Additional work needs to be done to test if these exonuclease domain mutations will confer sensitivity to the ATRi.

ATRi synergizes with anti-metabolites

Our previous work found RRM1 and RRM2 knockdown as synthetic lethal with the ATRi [183]. In this study, we decided to further examine the synthetic lethal relationship with nucleotide metabolism. During the validation screening, we found the enzymes involved in addition of the phosphates as being synthetic lethal with ATRi (Figure 4.5E). This process is tightly regulated and distortions in the nucleotide pool can greatly

impact the replication fork [206,252]. A commonly used drug in the lab, hydroxyurea, inhibits ribonucleotide reductase. HU and the clinical compound gemcitabine synergize with the ATRi to kill cells (data not shown and [184]). In early stages of cancer development, overexpression of oncogenes or viral proteins induces genomic instability through depletion of the nucleotide pools [169] and the TCGA does identify some nucleotide metabolism genes as being deleted. Deletion of chromosome 3p, commonly occurring in ccRCC, results in the loss of NME6, and is predicted to disturb nucleotide biosynthesis [245]. However, it remains to be tested if ccRCC has depleted or imbalanced nucleotide pools. In the clinical trials, the ATRi is combined with gemcitabine. The CHKi is also commonly combined with gemcitabine.

Conclusions

We conducted a whole genome siRNA screen with ATR inhibition to identify clinically actionable synthetic lethal relationships. The top identified pathways included DNA replication and the ATR pathway. We extensively validated that reduction in ATR pathway genes or signaling sensitizes cells to the ATRi by siRNA, shRNA, and isogenic cell lines. However, identifying cancer cell lines with ATR pathway defects proved challenging, and we were not able to validate our findings in cell culture models. A large cell line panel needs to be tested to identify the genetic determinants of ATRi sensitivity or resistance. Phase II clinical trials are commencing for this drug. These trials present an opportunity for researchers to identify the genetic differences between responders and non-responders directly from patient samples.

CHAPTER V

siRNA SCREENING IDENTIFIES POTENTIAL NEW ATR PATHWAY OR DNA DAMAGE RESPONSE GENES

Introduction

The canonical ATR activation pathway involves ATR localization through ATRIP binding to RPA, loading of the 9-1-1 complex onto dsDNA:ssDNA junctions, and the recruitment of the ATR activator TOPBP1. Once activated, ATR phosphorylates hundreds of downstream proteins, most of which remain uncharacterized [28]. More recent studies of the ATR activation pathway identified additional proteins necessary for full ATR activation, such as the MRN complex and RHINO [67,68,84,85]. Our lab has also recently identified a new ATR activator, ETAA1 (Appendix C). While we understand the basic ATR activation pathway, there is still much to learn.

We conducted three whole genome siRNA screens with the ATRi, CHKi, or hyrdroxyurea (HU), discussed in Chapter IV. Comparison of the top synthetic lethal genes from each of the screens identified the ATR pathway genes, among 180 genes, as synthetic lethal with all three drugs (Figure 4.3A). We hypothesized within those 180 genes, were additional, yet uncharacterized ATR pathway genes. Using the data generated from the whole genome screens as well as other genetic and proteomic screen data, we selected genes to validate in the secondary screens with the goal of identifying a new ATR pathway gene.

In this chapter, I will discuss the secondary validation screens and work on three genes of interest, RNF208, ARID3B, and BRD3. I examined localization of the proteins, γH2AX levels and ATR signaling after knockdown, and co-immunoprecipitating proteins identified by IP-mass spectrometry. From this data, we selected BRD3 for further characterization. Ultimately, we concluded the siRNA to BRD3 had off-target effects and knockdown of BRD3 does not sensitize cells to the ATRi. My collaborator, Kareem Mohni, has continued work on this project characterizing a new gene of interest, HMCES. Work on HMCES will not be discussed in this chapter but should be published in the coming year.

RESULTS

Secondary screens tested selected genes for synthetic lethality with several inhibitors

After completing the primary screen, we selected genes for validation using a wide variety of criteria. Preliminarily, we identified the top synthetic lethal genes with each inhibitor as well as those synthetic lethal with multiple inhibitors. We then used the published literature and other genomic and proteomic datasets to modify our selections. In the primary screen, 71 genes with synthetic lethal relationships with the ATRi are enriched at replication forks by iPOND [103]. Of those, 29 have no known functions. Many of those genes were included in our secondary screen. We did not select genes for the secondary screens with well-characterized functions in the ATR pathway, DNA replication, transcription, or mRNA maturation.

In the secondary screen, we purchased 4 individual siRNAs per gene, with one siRNA plated per well (Dharmacon siGENOME). Additionally, we screened a collection

of siRNAs purchased for a secondary validation screen previously done in the lab, as many of our genes of interest were within this collection. Overall, the secondary screen comprised of 11-384 well plates. The results from our secondary screen utilizing the previously purchased siRNA collection was published in Kavanaugh *et al.* [253].

We used the same methodology for the secondary screens as the primary screens. We used U2OS cells, and after transfection, we allowed the cells to grow for 72 hours. On day 3, we split the cells into 4 new 384-well plates and left one plate untreated and treated the remaining three plates with the selected inhibitors. After an additional 72 hours, cell viability was measured using alamarBlue. In addition to the conditions tested in the primary screen, we decided to include a high dose of HU. We treated the cells with high dose HU for only 24 hours and then released them into fresh media for the remaining 48 hours before measuring cell viability. Arm 1 of the screen comprised of CHKi, low dose HU, and high dose HU (Figure 5.1A), and Arm 2 of the screen comprised of the ATRi, cisplatin, and ATRi/cisplatin (Figure 5.1B).

Data analysis differed from the primary screen. We calculated cell viability for each siRNA by comparing the alamarBlue value from the treated plate to the untreated plate. These values were then normalized to correct for plate-to-plate variation. Any siRNA resulting in a viability reduction of 15% or greater after drug treatment was considered to have validated and approximately 36% of siRNAs validated in the ATRi secondary screen. We also included a statistical analysis to correct for false discovery rate [203]. The siRNAs that validated with the ATRi are listed in Appendix B and asterisks denote statistically validated siRNAs. For a gene to validate, 2 of 4 siRNAs must have reached the biological and statistical threshold. Additionally, we utilized the GESS

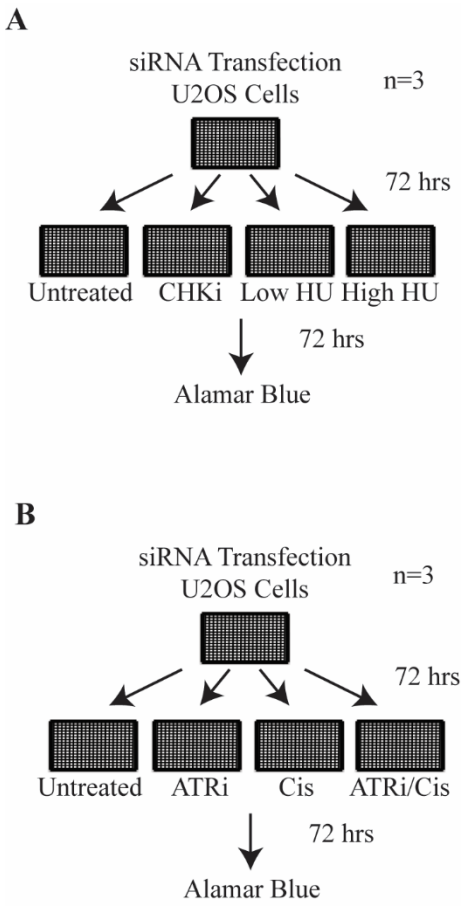

Figure 5.1. siRNA synthetic lethality secondary screens included six drug conditions. A-C. Schematic of the siRNA screens. U2OS cells were transfected with siRNAs and left untreated or treated with drug. Cell viability was measured by alamarBlue. n=3 **A.** Cells were treated with 0.05 μM CHKi (AZD7762), 0.2 mM Low dose HU, and 3.0 mM High dose HU. Cells were treated with CHKi and Low HU for 72 hours. Cells were treated with High dose HU for 24 hours and released into fresh media for the remaining 48 hours. **B.** Cells were treated with 0.1 μM ATRi (VX-970), 0.5 μM cisplatin, and 0.05 μM ATRi/ 0.1 μM cisplatin for 72 hours.

analysis to identify any significant off-target effects for each siRNA [254,255]. This analysis compares the siRNA sequence to the 3'-UTR region of genes and determines if the siRNA has any off-target miRNA-like effects but no off-target effects were identified.

Characterization of RNF208, ARID3B, and BRD3

We identified three candidate proteins for further study, RNF208, ARID3B, and BRD3. Initial characterization of these proteins utilized several assays. We looked for co-localization with the replication fork by immunofluorescence and IPOND. After knockdown, we looked for induction of γH2AX with and without replication stress to determine if loss of these proteins increases DNA damage or replication stress and we looked for defects in ATR signaling to see if these proteins function in the activation of ATR. Last, we identified protein interactors by IP-mass spectrometry to gain understanding of potential pathways in which these proteins might function.

RNF208 is a ring finger protein with no published function. The RING finger domain can facilitate protein dimerization [256]. In the secondary screens, RNF208 knockdown sensitized cells to low dose HU, the CHKi, and the ATRi. Additionally, RNF208 was identified and validated in a replication stress response screen also done in the lab [253]. In this screen, after siRNA transfection, cells were measured for their ability to recover from replication stress by monitoring γH2AX levels and incorporation of the thymidine analog EdU after release from HU. The identification of RNF208 in this screen suggests RNF208 might function in the replication stress response.

To test if RNF208 is in the ATR activation pathway, we examined phospho-CHK1 (pCHK1) levels after knockdown of RNF208 before and after replication stress induced by

HU. Without replication stress, knockdown of RNF208 results in elevated levels of pCHK1 (Figure 5.2A). This finding suggests RNF208 is not involved in ATR activation but instead, loss of RNF208 induces replication stress. We also examined γH2AX levels in EdU positive cells after knockdown of RNF208, and loss of RNF208 significantly elevates γH2AX levels (Figure 5.2B). After replication stress, we observed no significant alterations in pCHK1 or γH2AX comparing the control cells and cells lacking RNF208 (Figure 5.2A,B). By immunofluorescence, RNF208 localizes to the nucleus but did not co-localize with RPA foci after treatment with HU and ATRi (Figure 5.3C). Additionally, RNF208 was not found at the replication fork by iPOND [103]. These findings suggest RNF208 promotes genomic stability during DNA replication away from the replication fork.

The next gene, ARID3B is a member of the ARID protein family. There are seven subgroups of ARID proteins and they are involved in chromatin remodeling, histone methylation, and transcription activation. The ARID domain binds the major groove of AT-rich DNA [257,258]. ARID3B binds ARID3A to promote ARID3A localization to the nucleus [259]. ARID3A has been shown to bind E2F1 and ARID3B can bind hypophosphorylated RB [260,261]. Both proteins are implicated in regulating gene expression but further studies are needed. Overexpression of ARID3A and 3B promotes tumorigenesis through escape from senescence [260,262]. In the secondary screens, ARID3B validated with the ATRi as well as HU. We also examined ARID3A in our studies due to their known interaction. ARID3A knockdown sensitized cells to the CHKi and HU. An initial experiment did not implicate ARID3B or 3A as functioning in the ATR activation pathway as knockdown did not result in alterations in pCHK1 levels (Figure

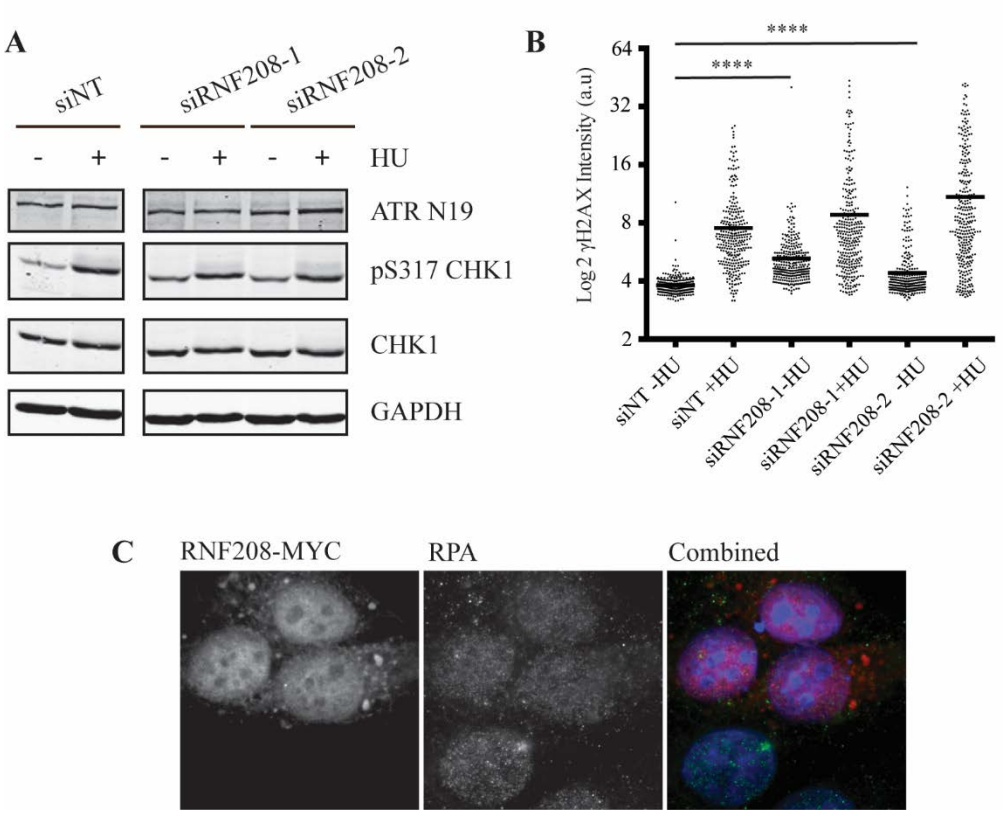

Figure 5.2. RNF208 localizes to the nucleus and knockdown induces elevated levels of γH2AX and pCHK1. A. U2OS cells were transfected with the indicated siRNA. After 72 hours, cells were left untreated or treated with 2mM HU for 2 hours. Lysates were separated by SDS-PAGE and immunoblotted with the indicated antibody. Western blot was cropped to exclude extra lanes. **B.** U2OS cells were transfected with non-targeting or RNF208 siRNA. Cells were labeled with EdU for 10 mins and then left untreated or treated with 2 mM HU for 2 hours. Cells were fixed, stained for EdU and γH2AX, imaged and γH2AX intensity measured in EdU positive cells using the ImageExpress. siNT vs siRNF208-1 –HU $p>0.0001$. siNT vs siRNF208-2 –HU $p>0.0001$ (one-way anova) **C.** U2OS cells were transfected with RNF208-MYC cDNA and treated with 3mM HU + 3μM ATRi (VE-821) for 2 hours. Cells were then fixed, extracted, and stained for MYC and RPA. The data in panel C were generated by Kareem Mohni.

5.3). However, in a recent proteomic screen ARID3B and 3A were identified as enriched at replication forks [103]. We overexpressed each protein in U2OS cells and they both form very small foci like structures but they did not convincingly co-localize with sites of DNA replication (Figure 5.4A). These foci did not change with cell cycle stage or in the presence of replication stress (data not shown). Knockdown of ARID3B caused a minor increase in γH2AX in replicating cells in the presence or absence of replication stress but only for 1 of 2 siRNAs tested (Figure 5.4B). Knockdown of ARID3A by two different siRNAs did not yield consistent results (Figure 5.4C).

The last gene we selected to follow was BRD3. BRD3 is a BET family protein along with BRD2, BRD4, and BRDT [263]. Of the BET proteins, BRD4 is the best characterized, but there are two main findings on BRD3 function. First, BRD3, in complex with BRD2, binds hyperacetylated chromatin throughout actively transcribed genes and preferentially associated with histones acetylated on H4K5, H4K12, and H3K14. This binding promotes passage of RNA Polymerase II through nucleosomes [264]. Second, BRD3 binds to acetylated GATA1, a transcription factor, and recruits it to chromatin [265]. BRD2, 3, and 4 are enriched at replication forks as well as on chromatin, as identified by iPOND [103]. Additionally, histones deposited on newly synthesized DNA contain acetylation marks on H4K5 and H4K12, the identified BRD3 binding sites [266-268]. BRD3s enrichment at replication forks as well as its ability to bind newly deposited histones presented compelling reasons to continue study of this protein.

In the secondary screen, knockdown of BRD3 sensitized cells to the ATRi as well as minor sensitization to HU and CHKi. Expression of HA-BRD3 in U2OS cells revealed distinctive nuclear foci (Figure 5.5A). While some of these foci co-localized with sites of

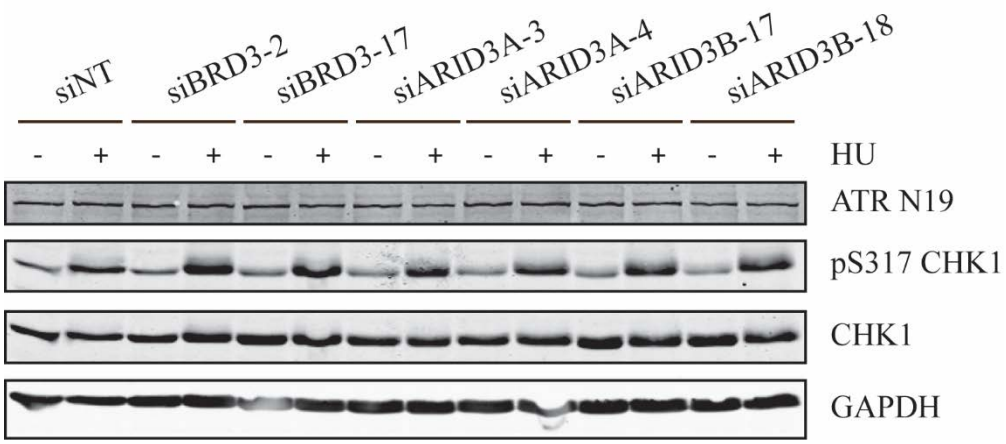

Figure 5.3. Knockdown of BRD3 or ARID3A/3B results in no alterations in ATR signaling. U2OS cells were transfected with the indicated siRNA. After 72 hours, cells were left untreated or treated with 2mM HU for 2 hours. Lysates were separated by SDS-PAGE and immunoblotted with the indicated antibody.

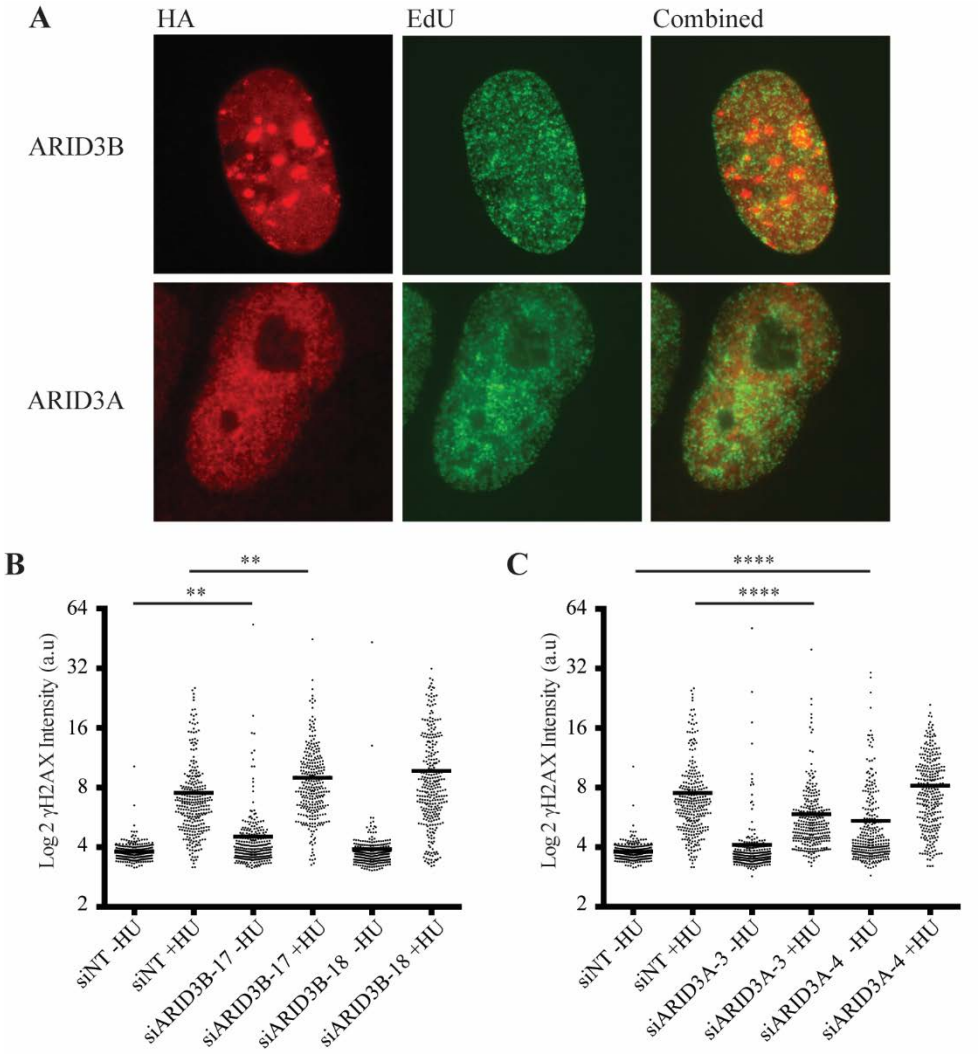

Figure 5.4. ARID3B localizes to the nucleus and knockdown slightly induces γH2AX. **A.** U2OS cells were transfected with HA-ARID3B or HA-ARID3A cDNA and labeled with EdU for 20 minutes. Cells were fixed and stained for HA, EdU and DAPI. **B-C.** U2OS cells were transfected with the indicated siRNA. Cells were labeled with EdU for 10 mins and then left untreated or treated with 2mM HU for 2 hours. Cells were fixed, stained for EdU and γH2AX, imaged and γH2AX intensity measured in EdU positive cells using the ImageExpress. **B.** siNT vs siARID3B-17 –HU p=0.0011. siNT vs siARID3B-17 +HU p=0.0012. (one-way anova) **C.** siNT vs siARID3A-3 +HU p>0.0001. siNT vs siARID3A-4 –HU p>0.0001. (one-way anova)

DNA replication, many did not. Additionally, there was no change in patterning of the foci throughout the cell cycle or co-localization with RPA after treatment with HU (data not shown). Knockdown of BRD3 did not alter pCHK1 levels but did result in slight decreases in γH2AX (Figure 5.3 and 5.5B). However, the two siRNAs induced inconsistent alterations in γH2AX levels.

Initial experiments with RNF208, ARID3B, and BRD3 did not result in convincing data these proteins are involved in the ATR pathway. At this junction, only RNF208 seemed to be functioning in a pathway promoting genomic integrity in unperturbed replicating cells. However, we decided to proceed with IP-mass spectrometry to identify co-precipitating protein complexes and gain a better understanding of the potential functions of these proteins.

Identification of protein interactors for RNF208, ARID3B/3A, and BRD3

To identify novel protein interactors, we overexpressed FLAG-tagged RNF208, BRD3, ARID3B, or ARID3A in 293T cells, and purified the proteins using anti-FLAG agarose beads. We analyzed the purified protein complexes by LC-MS-MS to identify co-purifying proteins. A non-transfected control IP was also included to identify non-specific interactions. We also cross-compared identified interactors between the samples to further eliminate non-specific proteins.

Of interest, we identified the FACT (facilitates chromatin transcription) complex, comprised of SSRP1 and SUPT16H, and PARP1 as interacting with ARID3B and 3A (Figure 5.6A). The FACT complex remodels Histone H2A/B dimers to promote transcription and DNA replication [269]. Additionally, PARP mediates the poly-ADP-

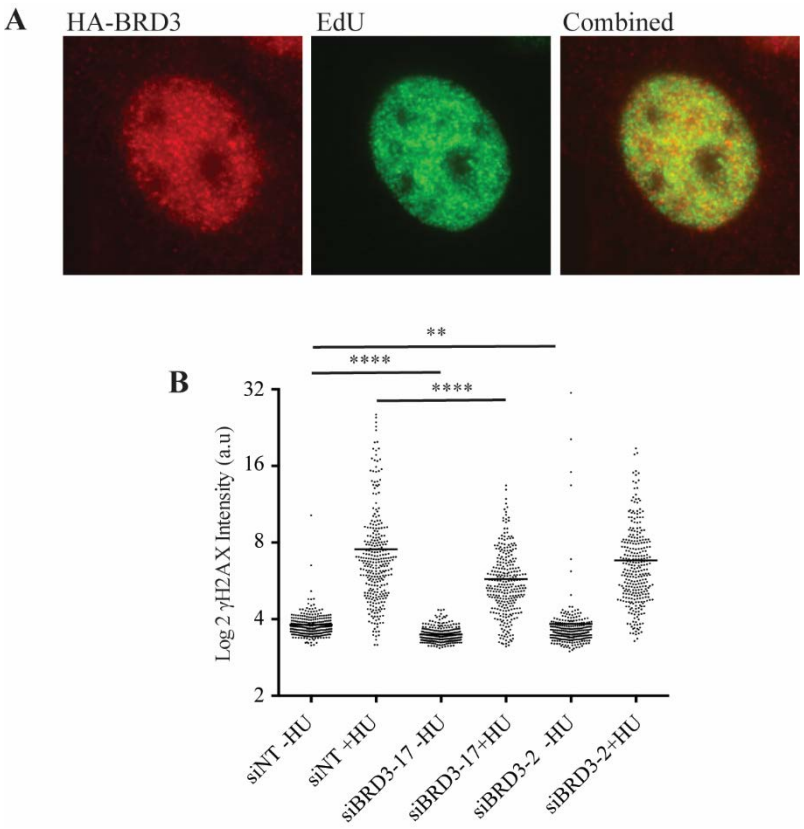

Figure 5.5. BRD3 localizes to small foci in the nucleus. A. U2OS cells were transfected with HA-BRD3 cDNA and labeled with EdU for 20 minutes. Cells were fixed and stained for HA, EdU and DAPI. **B.** U2OS cells were transfected with non-targeting or BRD3 siRNA. Cells were labeled with EdU for 10 mins and then left untreated or treated with 2mM HU for 2 hours. Cells were fixed, stained for EdU and γH2AX, imaged and γH2AX intensity measured in EdU positive cells using the ImageExpress. siNT vs siBRD3-17 –HU $p>0.0001$. siNT vs siBRD3-17 +HU $p>0.0001$. siNT vs siBRD3-2 –HU $p=0.0011$. (one-way anova)

ribosylation of FACT after replication stress to inhibit removal of γH2AX [270]. We hypothesized ARID3A and 3B could be functioning with the FACT complex. However, multiple other experiments done in the lab identified the FACT complex by IP-mass spectrometry. This diminishes our certainty that FACT is a real ARID3B interactor and this complex may just be a non-specific binder to anti-FLAG agarose beads.

We identified only seven proteins interactors for RNF208 (Figure 5.6B). We identified two components of the SCF complex, SKP1 and FBXO3. Two RING finger proteins, RBX1 and RBX2 are also part of the SCF complex [271]. RNF208 could be a novel SCF complex protein or is ubiquitinated by this complex. We also identified RALGAPB and RALGAPA1. RALGAPB forms a heterodimeric complex with RALGAPA1 or A2 and increases the GTP hydrolysis rate of Ral GTPases [272]. We did not identify RALGAPA2. Little is known about this complex, but one group published RALGAPB is a mitotic regulator. During mitosis, RALGAPB localizes to the mitotic spindle to promote proper chromosome alignment [273]. This fits with our screen data as loss of mitotic regulators sensitizes cells to the ATRi (Figure 4.5B).

Finally, our BRD3 IP data yielded the most exciting results (Figure 5.7A). In accordance with the published literature, we identified BRD2 as a BRD3 interactor [264]. Additionally, BRD9 co-precipitates but has no known function. We also found components of chromatin remodeling and modifying complexes (the Ino80 and the Swi/Snf complexes) and transcription initiation factors (TAF1-10). This is consistent with the known functions of BRD3 and other BET proteins in regulating transcription. However, we also identified the ATAD5/RFC2-5 complex, and we verified this finding by IP-WB (Figure 5.7B). This complex unloads PCNA from chromatin [274,275]. Additional groups

A

Identified Proteins	ARID3A	ARID3B	Ctl
ARID3B	22	233	0
ARID3A	199	36	0
PARP1	39	16	0
SSRP1	7	5	0
SUPT16H	15	2	0
NOLC1	20	14	0
FHL2	0	7	0
GNB2L1	8	6	0
YWHAE	1	6	0
TMPO	11	5	0
PPP3CA	0	4	0
TPM3	7	3	0
NAT10	7	2	0
NPM1	7	1	0

B

Identified Proteins	RNF208	Ctl
RNF208	89	0
RALGAPB	42	0
RALGAPA1	32	0
DDX21	15	1
SKP1	5	0
BAG6	4	0
FBXO3	3	0
LMNB1	3	0

Figure 5.6. ARID3B interacts with the FACT complex and RNF208 interacts with the RALGAP complex. A. FLAG-ARID3B or **B.** FLAG-RNF208 cDNA was transfected into 293T cells. FLAG IPs were performed from the nuclear extracts. Co-immunoprecipitating complexes were identified by LC-MS-MS and peptide counts are listed.

A

Identified Proteins	BRD3	Ctl
BRD3	216	6
BRD9	19	0
BRD2	15	0
RFC4	7	0
RFC2	5	0
RFC3	5	0
RFC5	4	0
ATAD5	30	0
TAF6	24	0
TAF1	24	0
TAF4	23	3
TAF5	21	0
TAF2	11	0
TAF8	11	0
TAF7	10	1
TAF9	10	0
TAF9B	7	0
TAF3	3	0
TAF10	4	0
INO80B	5	0
INO80	17	0
INO80D	3	0
INO80C	3	0
ACTR5	3	0
SMARCC1	31	2
SMARCA4	34	2
SMARCD1	15	0
ACTL6A	13	0

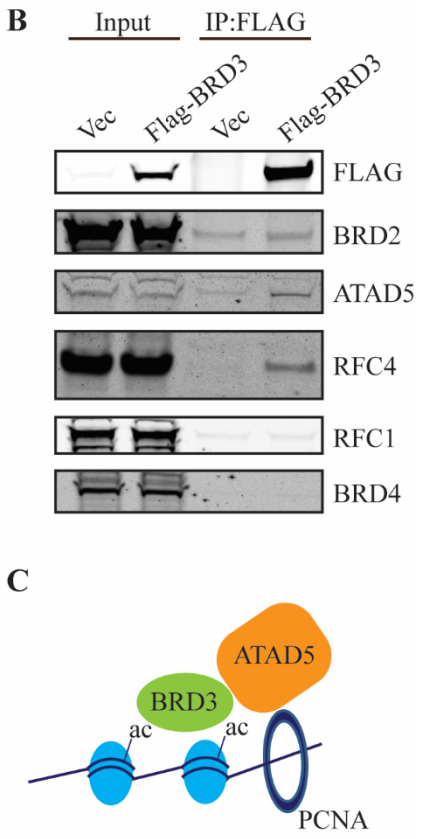

Figure 5.7. BRD3 interacts with the ATAD5/RFC2-5 complex. A. FLAG-BRD3 cDNA was transfected into 293T cells. FLAG IPs were performed from the nuclear extracts. Co-immunoprecipitating complexes were identified by LC-MS-MS and peptide counts are listed. **B.** Some of the mass spectrometry results were confirmed by western blot. IPs were performed as in **A. C.** Model for BRD3 regulating PCNA levels on chromatin.

have also found BRD3, as well as BRD2 and BRD4, as interacting with ATAD5 [276-278]. However, there is no documented follow up on this interaction. Knowing BRD3 is present at replication forks, can bind the acetylation mark on newly deposited histones, and can interact with ATAD5, we hypothesized Brd3 binds the acetylated histones on nascent DNA and recruits ATAD5 to unload PCNA (Figure 5.7C). This finding and hypothesis was very intriguing and as such, we stopped work on ARID3A/3B and RNF208 and focused on BRD3.

To verify our findings from the screen, we obtained two siRNAs to BRD3 and tested for increased sensitivity to the ATRi, CHKi, and HU. Knockdown of BRD3 in U2OS cells did cause increased sensitivity to the ATRi (Figure 5.8A) but we did not see sensitization to HU or CHKi (data not shown). We also tested for sensitization to these inhibitors in a long-term viability assay. In Figure 5.7B, we knocked down BRD3, BRD2, and ATAD5 and treated these cells with the ATRi, CHKi, or HU for 24 hrs. We then released the cells into fresh media and allowed them to form colonies. As seen in the short-term assay, knockdown of BRD3 sensitized the cells to the ATRi and there was only slight sensitization to the CHKi and HU. Knockdown of ATAD5 phenocopied the BRD3 results and knockdown of BRD2 did not sensitize cells to any of the tested inhibitors. Thereby, loss of ATAD5 function sensitizes cells to the ATRi, suggesting accumulation of PCNA on chromatin induces replication stress and an increased reliance on ATR.

BRD3 does not regulate PCNA levels on chromatin.

Inhibitors for BET proteins (BETi) are available and were developed as anti-cancer reagents [279,280]. These inhibitors prevent binding of the bromodomain to acetylation

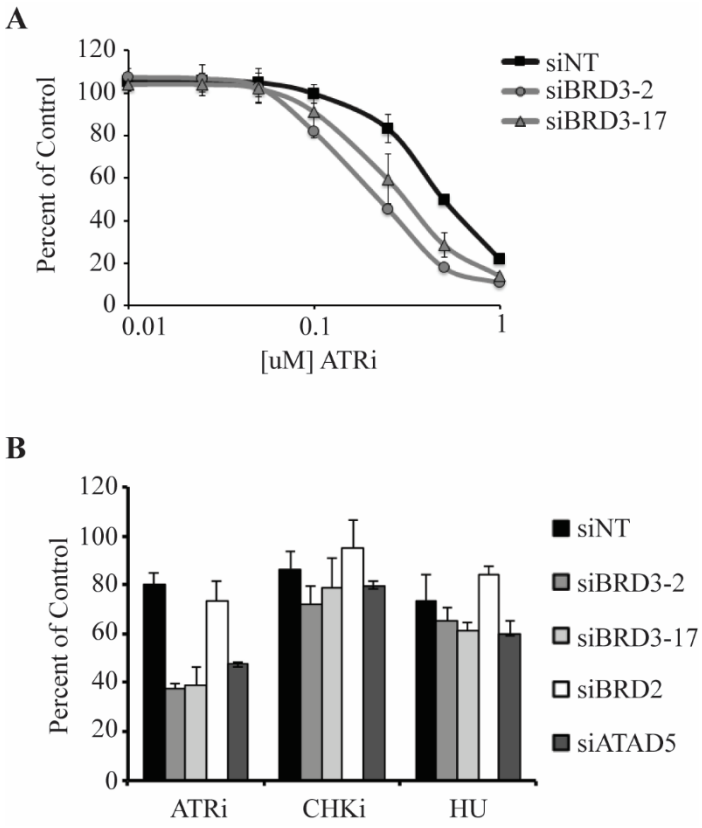

Figure 5.8. Knockdown of BRD3 sensitizes cells to the ATRi. A. Cells were transfected with BRD3 or non-targeting (NT) siRNA. After 72 hours, cells were treated with increasing dose of ATRi (VX-970) for an additional 72 hours. Cell viability was measured using alamarBlue and comparing non-treated cells to treated cells. Error bars are the standard deviation n=3. **B.** Cells were transfected with siRNA to BRD2, BRD3, ATAD5, or non-targeting siRNA. Cells were plated for colonies, treated with 100 nM ATRi (VX-970), 50 nM CHKi (AZD7762), or 1 mM HU for 24 hours, released into fresh media, and allowed to form colonies. Error bars represent the standard deviation n=3. The data in panel B and A were generated by Kareem Mohni.

marks. We acquired two BETi: JQ1, which preferentially targets BRD4 but will also inhibit BRD3, and I-BET762, which inhibits BRD3, BRD2, and BRD4. To test if BRD3 regulates ATAD5 unloading of PCNA, we looked for increased PCNA levels on chromatin after BRD3 knockdown or inhibition. In Figure 5.9A, we knocked down BRD3 and ATAD5 in U2OS cells and monitored PCNA levels on chromatin. ATAD5 knockdown resulted in the expected increase in PCNA levels. However, knockdown of BRD3 caused a slight decrease in PCNA on chromatin in comparison to cells transfected with non-targeting siRNA. We also treated the cells with HU and I-BET762. The control cells had the expected decrease in PCNA after HU treatment, but the BETi did not affect PCNA levels. In cells knocked down for ATAD5 or BRD3, there were very slight decreases in PCNA levels with HU treatment and there were no changes in PCNA with BET inhibition. This experiment did not yield any evidence BRD3 regulates PCNA unloading.

We next wanted to try an experiment with JQ1 alone and in combination with the ATRi or HU (Figure 5.9B). We did this experiment in Kasumi-1 cells, an AML cancer line more sensitive to the BETi than U2OS cells. HU treatment alone causes a decrease in PCNA and increase in RPA on chromatin, and the ATRi alone increased the amount of PCNA bound to chromatin. This is consistent with the increase in origin firing observed under ATR inhibition [96]. Co-treatment of JQ1 and HU prevented the drop in PCNA levels induced by HU alone. There is even a slight increase in PCNA and RPA. The ATRi and JQ1 treatment induced higher levels of PCNA on chromatin compared to the JQ1 and HU treatment. This data suggests JQ1 in combination with ATRi or HU perturbs DNA replication more than any reagent alone. However, JQ1 alone did not increase PCNA levels on chromatin and did not support our hypothesis.

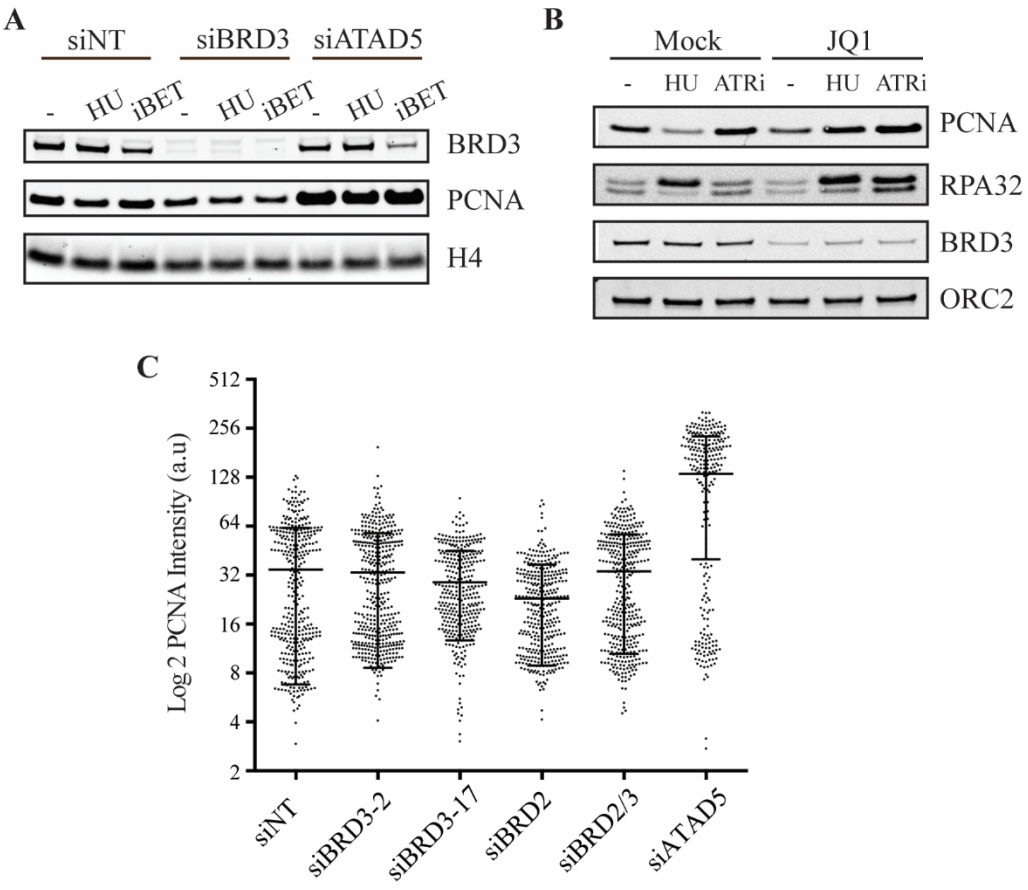

Figure 5.9. Knockdown or inhibition of BRD3 does not increase PCNA levels on chromatin. A. Cells were transfected with BRD3, ATAD5, or non-targeting siRNA. Cells were then treated with 2 mM HU, 10 μM BETi (iBET762), or left untreated (-) for 2 hours. Chromatin fractionation was performed and the nuclear insoluble fraction was subjected to SDS-PAGE. Levels of BRD3, PCNA and Histone H4 were measured by western blot. **B.** Cells were treated with 1 μM iBET (JQ1), 3mM HU, 250 nM ATRi (VX-970), treated with a combination, or left untreated for 1 hour. Cells were fractionated and the nuclear insoluable fraction was separated by SDS-PAGE and PCNA, RPA32, BRD3, or ORC2 levels were visualized by western blot. **C.** Cells were transfected with BRD3, BRD2, ATAD5, or non-targeting siRNA and labeled for 10 minutes with EdU. Cells were then extracted, fixed, and stained for PCNA and EdU. PCNA intensity in EdU positive cells was quantified using CellProfiler. The data in panel B were generated by Kareem Mohni.

Finally, we also looked for increased levels of PCNA on the chromatin on a single cell basis using immunofluorescence (Figure 5.9C). In this experiment, we knocked down BRD3, BRD2, ATAD5 and BRD3/2. Knockdown of ATAD5 resulted in the expected increase in PCNA on chromatin. However, knockdown of BRD3 and BRD2 did not nor did knockdown of both. This experiment also did not support our hypothesis. ATAD5 has also been shown to regulate PCNA ubiquitination [202]. We never observed alterations in PCNA ubiquitination after knockdown of BRD3 or after BET inhibtion, with or without DNA damage (data not shown).

BRD3 knockdown slows DNA replication.

We next wanted to test if BRD3 promotes replication fork processivity. We did this by testing if knockdown of BRD3 slows DNA replication on a single molecule level (Figure 5.10A). We transfected cells with non-targeting or BRD3 siRNA and labeled the cells for 20 minute with IdU and then CldU. We observed a modest decrease in replication rates in cells lacking BRD3. We next wanted to verify our findings with the BETi. We pretreated Kasumi-1 cells with JQ1 for 2 hours and then labeled the cells for 20 minutes with IdU and then CldU (Figure 5.10B). In this experiment, we did not observe any slowing of the replication fork after BET inhibition. This was concerning that the BETi could not reproduce the phenotype observed with the siRNA.

We hypothesized if loss of BRD3 increases sensitivity to the ATRi than the ATRi and the BETi will be synergistic. To test this, we synchronized U2OS cells overnight in thymidine and released the next day for 2 hours to allow progression into S-phase. Cells were than treated with JQ1 for 1 hour followed by ATRi for 2 hrs and released to form

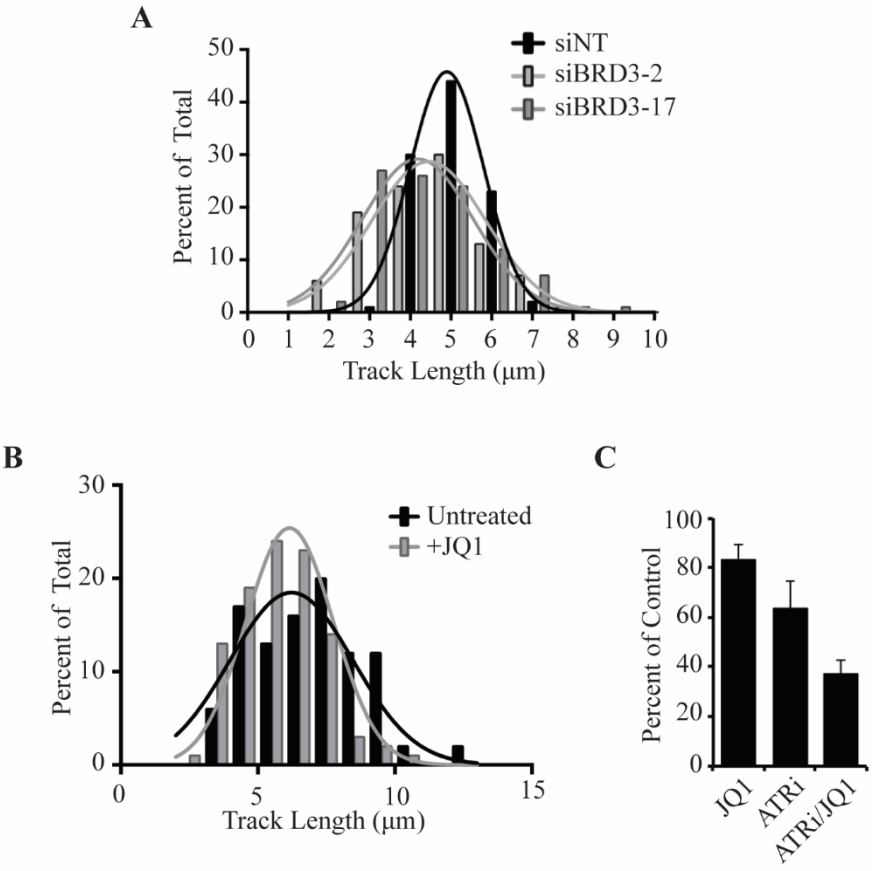

Figure 5.10. Knockdown but not inhibition of BRD3 slows DNA replication. A. Cells were transfected with BRD3 or non-targeting siRNA. The cells were labeled with IdU and then CldU for 20 minutes before harvesting for DNA fiber labeling. Quantification of the IdU track in dual-labeled DNA tracks is shown. **B.** Cells were pretreated with 1 μM BETi (JQ1) for 2 hours. With JQ1 still present in the media, cells were labeled with IdU and then CldU for 20 minutes before being harvested for DNA fiber labeling analysis. The quantification of the IdU track in dual-labeled DNA tracks is shown. **C.** Cells were synchronized using a thymidine block overnight. Cell were released into fresh media for 24 hours and then treated with 1 μM BETi (JQ1) for 2 hours followed by 100 nM ATRi (VX-970) for an additional 2 hours or treated with just BETi or just ATRi. Cells were then released and allowed to form colonies. Error bars are the standard deviation n=3. The data in panel C were generated by Kareem Mohni.

colonies (Figure 5.10C). JQ1 modestly reduced cell viability compared to untreated cells and the ATRi reduced cell viability by 60%. However, the combination treatment was exactly additive. We obtained similar results in the short-term dose response assay.

siBRD3 off-target effects creates the sensitivity to the ATRi.

At most, the BET inhibitors reduce BRD3 bound to the chromatin by 50%. It is possible the inhibitors did not phenocopy the siRNA because half of the BRD3 still bound to the chromatin. Therefore, we generated BRD3 null U2OS cells using CRISPR/Cas. We used two guide RNAs to target exon 2 and deleted the start codon. We verified the cells were null by western blot using an antibody to the c-terminus of the protein (Figure 5.11A) and by PCR genotyping (data not shown). We tested two clones for increased sensitivity to the ATRi compared to wild type U2OS cells (Figure 5.11B). However, the BRD3 null cells were just as sensitive to the ATRi as wild type U2OS cells. We hypothesized the clones could have adopted a compensation mechanism. However, we wanted to verify the siRNAs did not have off-target effects creating the ATRi sensitivity. So we transfected the two BRD3 null clones with the two siRNAs to BRD3 and tested for increased sensitivity to the ATRi. Very unfortunately, both siRNAs still conferred sensitivity to the ATRi in a BRD3 null background (Figure 5.11C-E, data not shown). Thus, we concluded the siRNA to BRD3 has off target effects creating the sensitivity to the ATRi. All four siRNAs in the secondary screen resulted in increased sensitivity to the ATRi to similar extents. We only purchased and tested two of the four. We used BLAST with the siRNA sequence to try and identify any potential off-target effects, but this analysis only yielded BRD3. The identification of the off-target gene remains unknown.

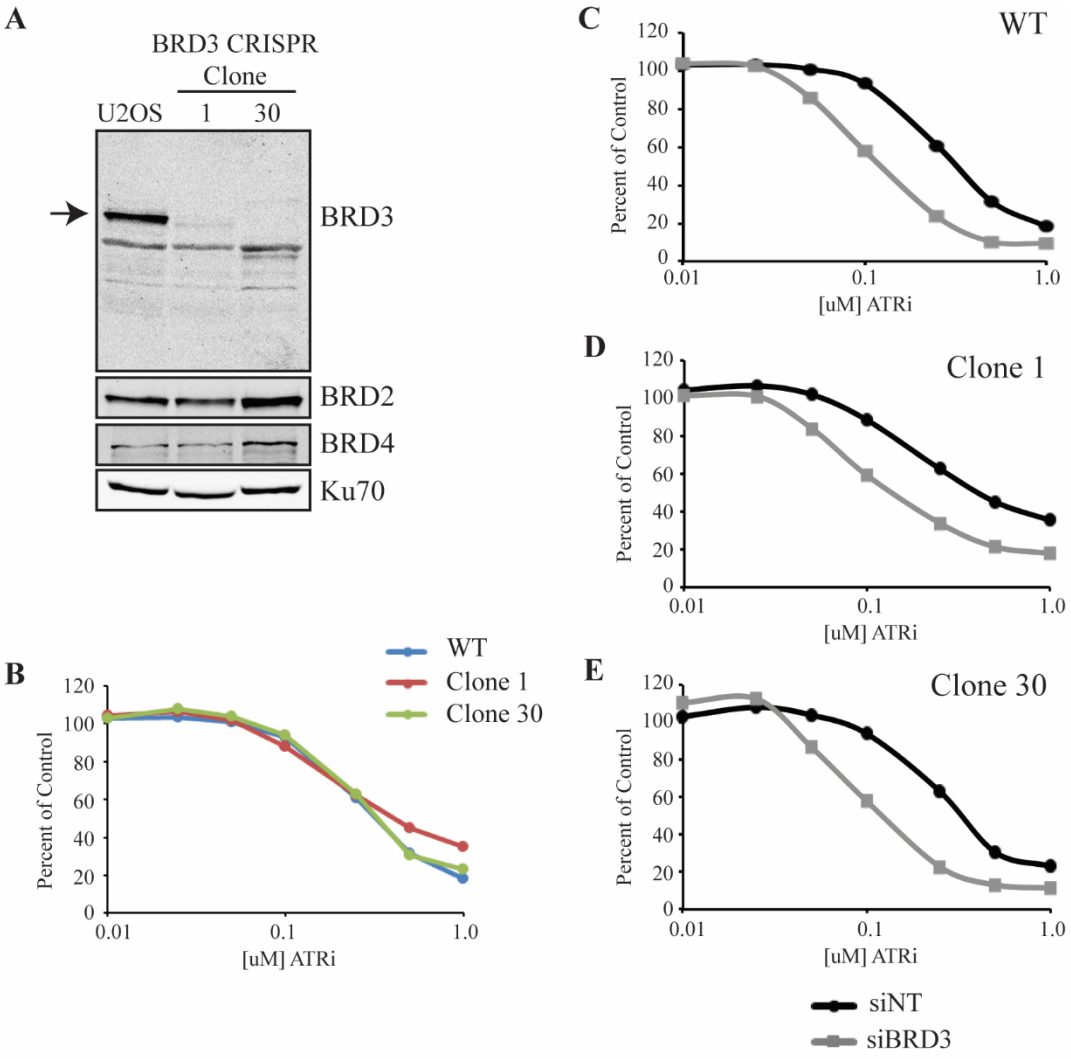

Figure 5.11. BRD3 null cell lines are not sensitive to the ATRi. **A.** Crispr/Cas was used to target the BRD3 gene. The resulting clones did not express BRD3 as shown by western blot. BRD2 and BRD4 protein levels were not affected. **B.** Two BRD3 null cell lines were tested for increased sensitivity to the ATRi (VX-970) compared to the wild type U2OS cell line. Cells were treated with the inhibitor for 72 hours and cell viability was measured by alamarBlue. **C.** Wild type U2OS cells, **D.** BRD3 null cell line 1, and **E.** BRD3 null cell line 30 were transfected with ATR or non-targeting siRNA and tested for sensitivity to the ATRi (VX-970). Cells were treated for 72 hours and cell viability was measured by alamarBlue and comparing untreated to drug treated cells. The data in panel A were generated by Kareem Mohni.

DISCUSSION

The recent development of ATR inhibitors provided a useful tool for studying the ATR pathway. Our genetic screens in combination with ATR inhibition identified the ATR pathway as one of the top synthetic lethal pathways. Therefore, we proposed to use this screening methodology to discover new ATR pathway genes. We selected 435 genes from our primary screen for validation in the secondary screens. 36% of the siRNAs validated in the ATRi validation screen and from there, we selected three genes of interest: ARID3B, RNF208, and BRD3. IP mass spectrometry data lead us to investigate the relationship between BRD3 and the ATAD5:RFC2-5 complex. However, our siRNA to BRD3 proved to have off target effects, and we were never able to generate data supporting our hypothesis. From there, research focus has shifted to studying HMCES and should be published in the coming year by my collaborator, Kareem.

RNF208 could be a novel mitotic regulator.

RNF208 is a ring finger protein with no known function. Knockdown of RNF208 sensitized cells to HU, CHKi, and the ATRi. This gene was also found in a replication stress response screen, which identified genes that promote recovery from long-term treatment with HU. We identified RNF208 as interacting with the SCF complex as well as the heterodimeric RALGAP complex. Ring finger proteins RBX1 and RBX2 are part of the SCF complex [271] and may be directing ubiquitination of RNF208. The RALGAP complex, comprised of RALGAPB and RALGAPA1, is not as well characterized. One group characterized RALGAPB as having a role in the spindle assembly checkpoint during mitosis [273]. Centromere, centrosome, and mitotic checkpoint proteins were enriched as inducing increased sensitivity to the ATRi in the primary screen. Though currently, ATR

has only one characterized function during mitosis. When DSBs occur during mitosis, ATM and ATR phosphorylate CEP63, which inhibits spindle assembly [219]. Conversely, mutation of centrosome proteins reduces ATR signaling and replication through centromeric DNA might be stressed when a core centromere protein is lost [223]. Suggesting the reliance on ATR is most likely during interphase when these proteins are lost. The function of the RNF208: RALGAPB/A interaction remains unknown. RNF208 might be regulating RALGAP ubiqutination by the SCF complex leading to degradation of these proteins. This would cause an increase in RALGAP protein levels, which has already been shown to cause multinucleation and cell death [273].

ARID3B could aid in histone remodeling to promote replication processivity.

ARID3B belongs in the ARID protein family. The ARID domain can directly bind DNA and ARID proteins are involved in regulating transcription through modifying chromatin structure, histone methylation, and inhibition of transcription factors [257]. ARID3B can exist in complex with ARID3A to block 3A nuclear export [259]. From our data, knockdown of ARID3B sensitizes cells to HU and the ATRi and ARID3B/3A is enriched at replication forks [103]. Our mass spectrometry data revealed ARID3B and 3A to be interacting with PARP1 and the FACT complex. FACT remodels histone H2A/B to allow processivity of the transcription and replication machinery [269]. PARP1 inhibits FACT to prevent removal of γH2AX to allow continued DNA damage signaling [270]. Knockdown of either subunit of the FACT complex sensitizes cells to the ATRi [183]. ARID3B could be aiding in localization of FACT to the fork to remodel histones and promote replication fork processivity. However, other IP-mass spectrometry experiments

done in the lab have also identified the FACT complex as a protein interactor for other genes of interest. If the FACT complex is a real ARID3B/3A interactor remains to be determined. Further work is needed to confirm this interaction and to understand how ARID3B is functioning with FACT.

BRD3 siRNA is off target, but BRD3 may still function during DNA replication stress.

BRD3 is a member of the BET protein family with BRD2, 4, and T. BRD3 binds acetylated histones and promotes RNA polymerase II processivity [264]. Knockdown of BRD3 sensitized cells to the ATRi. However, we concluded the siRNA had off-target effects. Our IP-mass spectrometry data identified BRD3 as interacting with ATAD5:RFC2-5. Additional groups identified this interaction but no further study was published [276-278]. ATAD5 has a well-documented function in unloading PCNA from the chromatin [202,274]. Newly deposited histones contain the acetylation marks BRD3 preferentially binds and BRD3 travels with the replication fork [103,266-268]. We hypothesized BRD3 aids in ATAD5 localization and promotes unloading of PCNA but our data did not support this theory. ATAD5 could have additional functions yet unknown, which require BRD3.

From our chromatin fractionation experiments, BET inhibition, in combination with HU or ATRi, does seem to be impacting DNA replication. Our DNA fiber labeling experiments with JQ1 did not reveal any slowing of the replication fork. However, JQ1 only reduces the amount of BRD3 on chromatin by at most 50%. Additionally, we did not analyze DNA replication during treatment with JQ1 and a replication stress reagent because the Kasumi-1 cells were exquisitely sensitive to HU. Therefore, BRD3 or BET

proteins in general may still have a function during replication stress. We also identified BRD3 as interacting with chromatin remodeling complexes such as INO80. INO80 is important for replication stress recovery [281]. BRD3 function during replication stress may be independent of the ATAD5 interaction and more due to regulation of chromatin remodelers.

ATRi screening identifies the major ATR pathway genes as well as other pathways.

We proposed siRNA screening in combination with the ATRi could be used to identify new ATR pathway genes and that screening with the CHKi and HU provides further pathway validation. However, we have not yet identified a new ATR pathway gene within this dataset. However, the ATR pathway was not the only pathway synthetic lethal with ATR inhibition. Loss of chromatin remodeling or DNA replication genes and genes associated with mitosis are synthetic lethal with the ATRi. I believe RNF208, ARID3B, and BRD3 are in those pathways. However, knockdown of genes regulating transcription, such as chromatin remodelers, can produce synthetic lethal events due to decreased transcription of genes that are synthetic lethal with the ATRi. It is hard to rule out transcriptional changes as being the root of the synthetic lethality for ARID3B or BRD3. In fact, a group has published that BET inhibition synergizes with the ATRi because of transcriptional alterations [190]. However, in our hands, these two inhibitors had at most an additive effect.

There are still new ATR pathway genes to find. Our secondary screen identified knockdown of HMCES as sensitizing cells to the ATRi. HMCES also travels with the replication fork and may be involved in repair of methylated DNA bases. My collaborator,

Kareem Mohni, is further characterizing the function of this protein and work is still ongoing.

Conclusions

Our secondary screen included four siRNAs to a selection of genes. We identified three genes for further study but in the end, we were thwarted by siRNA off-target effects. However, our IP-mass spectrometry data revealed potential new functions for RNF208, ARID3B, and BRD3 in need of further characterization. Additionally, our work identifying HMCES and its function to promote genome integrity should be published in the coming year.

CHAPTER VI

SUMMARY AND FUTURE DIRECTIONS

Summary

DNA damage occurs daily from a variety of sources such as by reactive oxygen species generated during metabolism or UV light from the sun. It is critical that cells are able to respond and repair the damage in order to maintain genomic integrity and prevent disease such as cancer. Cells are able to achieve this through the activation of the DNA Damage Response (DDR). A major kinase regulator of the DDR is ATR. ATR is a member of the PIKK family along with two other major regulators of the DDR, ATM and DNA-PKcs. Once activated, ATR regulates origin firing, stabilizes the replication fork, promotes DNA repair, and activates cell cycle checkpoints through phosphorylation of hundreds of downstream targets [28]. In recent years, two pharmaceutical companies developed ATR-specific inhibitors and these inhibitors serve as a useful tool for studying ATR function [181,182].

In my dissertation work, I completed several projects, which revolved around modulation of ATR kinase activity. I examined ATR regulation through autophosphorylation and characterized an ATR point mutation that altered the kinase activity levels. Using the newly developed ATR inhibitors (ATRi), I conducted a whole genome siRNA screen to identify pathways when lost that are synthetic lethal with the ATRi. This screen served two purposes. One goal was to identify a clinically actionable patient population in the cancer clinic to treat with the ATRi. The second goal was to

identify a new ATR pathway or DNA repair gene. Additional work which contributed to other projects in the lab included analysis of ATR function at the replication fork on a single molecule level and the identification of a new ATR activator.

Regulation and Activation of ATR

ATR activates in response to a variety of replication stressors through a multistep process involving ATRIP, RPA, TOPBP1, and the 9-1-1 complex [28]. However, there are many examples in the literature describing alternative activation pathways, additional proteins needed, and post-translational modifications regulating ATR activation. It is becoming increasing clear activation of ATR is more complicated than the current canonical pathway. More work is necessary to understand all the complexities of this pathway. The mechanisms of regulation for the other PIKK kinases as well as the *S. cerevisiae* ATR orthologue MEC1 can serve as a guide for elucidating these details.

ATR and the other PIKK kinases have similar mechanisms of regulation. They localize to a specific subcellular region through a binding partner, they activate through protein-protein interactions, and post-translational modifications alter their kinase activity [282]. ATM and DNA-PKcs auto-phosphorylate during activation and these autophosphorylation events are important for upregulation of kinase activity and promotion of DNA repair [119,144,145,147-149,151,154]. The longstanding hypothesis in the field is that ATR also undergoes autophosphorylation. Following the examples of ATM and DNA-PKcs, autophosphorylation would increase ATR kinase activity and mutation of these sites would impair ATR activation and checkpoint signaling.

Conflicting evidence of ATR regulation by autophoshorylation

A previous graduate student in the lab, Edward Nam, identified T1989 as a phosphorylation site on ATR [164]. His work demonstrated T1989 is a DNA damage inducible, ATR kinase activity-dependent phosphorylation site. However, phosphorylation of T1989 does not increase kinase activity and may not be a true autophosphorylation site. Additionally, mutation of this site does not impair phosphorylation of downstream substrates or activation of the checkpoint in response to DNA damage [164]. The Lee lab also published ATR is phosphorylated on T1989 and they claim T1989 is an autophosphorylation site and facilitates ATR interaction with TOPBP1 [165]. In this work, the T1989A mutation resulted in impaired phosphorylation of CHK1 after UV. These findings are in direct contrast to the work done in our lab.

There are inherent differences between the two studies, which may explain the contrasting results. The two studies examined two different CHK1 phosphorylation sites under different replication stress conditions, hydroxyurea verses UV. Phosphorylation of T1989 may influence ATR activity under specific contexts. Both groups used the HCT116 flox/- ATR cell line to generate a pooled collection of cells solely expressing T1989A or T1989E-ATR after Ade-Cre infection. The pooled collection of cells can then be plated for colonies to examine cell viability. Dr. Nam was able to generate colonies expressing T1989A-ATR while the Zou group was not. This suggests the cells used for the two studies contained differences, which may explain the opposing results. However, the Zou group did not include a control adenovirus infection in the colony formation assay and therefore, their result could be due to experimental error. Since these studies were completed, the CRISPR/Cas system for gene editing was published and this system allows for direct

mutation of the endogenous ATR alleles [233-235]. This presents an excellent alternative and perhaps more biological method for studying the functional importance of ATR T1989 phosphorylation and for resolving the differences between the two studies.

Regulation of ATR by Phosphorylation

I examined regulation of ATR by autophosphorylation using site-directed mutagenesis and mass spectrometry. Mutation of the conserved serine 1333 to alanine within ATR created a hyperactive kinase while the phosphomimetic, aspartic acid, decreased kinase activity. This result suggested S1333 is an inhibitory phosphorylation site. However, I was never able to obtain evidence of this phosphorylation event. Despite my findings, there is still potential this site is phosphorylated. Instances where ATR downregulation is needed in the cell may occur at very specific times or under specific contexts. S1333 phosphorylation could be cell cycle regulated or occur at a specific time during recovery from DNA damage. I initially postulated this site is phosphorylated under normal growth conditions, to prevent aberrant kinase activity, but the ATR protein I purified from unperturbed cells was not phosphorylated on S1333. Additionally, phosphorylation of S1333 may not occur in cell culture models and I never purified ATR protein from another source.

There is compelling evidence ATR activity is not regulated by autophosphorylation. When ATR is purified from cells after DNA damage, the kinase activity is similar to that of ATR protein purified from undamaged cells. Whereas ATM purified from cells after DNA damage is more active then ATM purified from unperturbed cells [283,284]. If ATR activity is upregulated after DNA damage through

autophosphorylation, it should be possible to purify a more active kinase. However, to achieve an active form of ATR *in vitro* TOPBP1 must be added to the reaction and even the S1333A-ATR, which has increased kinase activity, is activated by TOPBP1.

While the question of if ATR activity is regulated by autophosphorylation remains unanswered, there is new evidence phosphorylation of ATR regulates DNA repair. Numerous groups identified ATR phosphorylation on S435, including our lab [165,285,286]. However, mutation of S435 does not impair ATR signaling or checkpoint activation so this site was thought not to have functional significance [165,285]. The D'Orazio group identified cAMP-dependent protein kinase as the kinase which phosphorylates ATR on S435. This phosphorylation does not alter kinase activity but rather promotes ATR binding to XPA. This increased binding results in faster recruitment of XPA to damage sites and thus faster repair of UV damaged DNA [163,287]. This study demonstrates that ATR phosphorylation sites could have other functional significance beyond regulating kinase activity.

In my search for phosphorylation of S1333, I identified 12 new potential ATR phosphorylation sites by mass spectrometry (Table 3.1). Of these sites, two are located on an S/TQ motif and three are located on S/TP motifs, the CDK consensus sequence. One of the phosphorylated S/TQ sites is conserved in mice and was mutated in the 16A-ATR [30]. These newly identified sites could be regulatory phosphorylation or autophosphorylation sites and warrant further study. However, future study of these sites needs to be more expansive than previous work. Similar to S435 phosphorylation, the functional significance of these new phosphorylation sites may not alter kinase activity but instead promote a specific activity. It will be important to identify the kinase which

phosphorylates that site and to study the point mutations under a wide array of DNA damaging agents and assays.

PIKK kinases undergo conformational changes when activated.

While there is still potential phosphorylation occurs on S1333, I hypothesize S1333 makes critical interactions within ATR holding the kinase in an inactive conformation. PIKK kinases, including ATM and DNA-PKcs, undergo conformational changes upon activation. ATM transitions from an inactive dimer to an active monomer when activated by the MRN complex, and under conditions of oxidative stress, ATM activates through formation of new disulfide bonds within the dimer [119,129]. DNA-PKcs also undergoes a conformation change upon phosphorylation, releasing it from the DNA ends to allow repair by NHEJ [157,158].

ATR is also postulated to undergo a conformational change upon activation by TOPBP1. This alteration in structure increases ATR substrate affinity [136]. In the *in vitro* kinase assays without TOPBP1, ATR phosphorylates the substrate and itself at low levels. Upon addition of TOPBP1, there is a large increase in phosphorylation levels of the substrate but not ATR or ATRIP (Figure 6.1). Additionally, as substrate concentration increases in the assay, TOPBP1-induced increase in substrate phosphorylation diminishes [136]. Therefore, as substrate concentrations approach saturation, TOPBP1 effect on ATR declines. TOPBP1 does not induce ATR or ATRIP phosphorylation as these two proteins are in close proximity to the kinase domain, appearing to this domain as being at high concentration. These results suggest TOPBP1 binding to ATR induces a conformation change, which increases ATR substrate affinity.

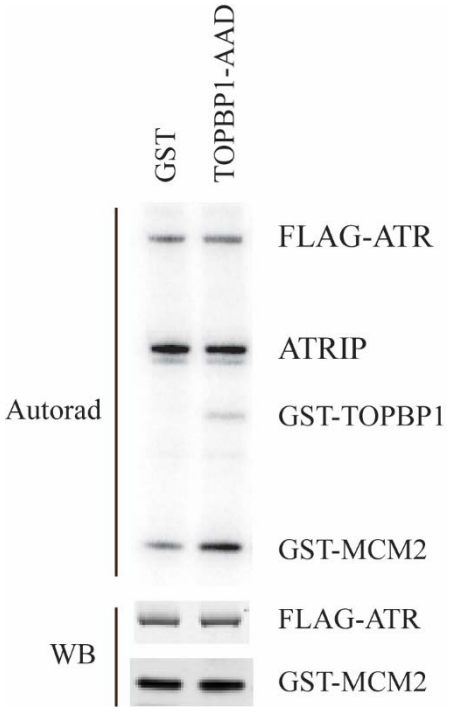

Figure 6.1. Activation of ATR *in vitro* increases phosphorylation of the ATR substrate MCM2 but not ATR or ATRIP. The ATR/ATRIP complex was purified from HEK293T cells and incubated with GST-MCM2 substrate, [γ-^{32}P]-ATP and GST-TOPBP1-AAD or GST. Kinase reactions were separated by SDS-PAGE and [^{32}P]-MCM2, [^{32}P]-TOBBP1-AAD, [^{32}P]-HA-ATRIP, and [^{32}P]-FLAG-ATR detected by autoradiography. The amount of ATR and GST-MCM2 was detected by western blot.

It is easy to envision that S1333 maintains critical interactions keeping ATR in the inactive form. By mutation of this site, a partial conformational change towards the active form of the kinase occurs. TOPBP1 binding then induces the remaining conformational change (Figure 6.2). This model fits the in cell data. Conversely, mutation of S1333 could increase ATR substrate affinity independent of the TOPBP1-induced mechanism. In the *in vitro* experiments including TOPBP1, the S1333A-ATR protein phosphorylated the MCM2 substrate more than wild-type ATR. This suggests even after activation by TOPBP1, S1333A-ATR has increased substrate affinity.

The clearest way to determine why mutation of S1333 alters kinase activity is to solve the structure of the ATR/ATRIP complex as well as ATR/ATRIP bound by TOPBP1. However, it is difficult to purify large quantities of ATR due to its large size. Very recently, the structure of MEC1 was resolved at low resolution by negative stain electron microscopy. The Zhang groups show the MEC1/DDC2 (ATR/ATRIP) complex in a dimer, with the main dimerization contacts occurring within the HEAT repeats. In contrast to their TEL1 (ATM) structure, the two MEC1 kinase domains are in close proximity, possibly preventing substrate access. This structure supports the need for a conformational change to separate the two kinase domains in order for ATR to phosphorylate its substrate [117]. The kinase domains within the TEL1 dimer are further apart and have ample room for substrates to bind. This supports the reports in the literature that ATM can exist as an active dimer or monomer [119,129].

This model of the MEC1 structure supports my hypothesis that S1333, located in the HEAT repeats, maintains specific interactions keeping ATR in an inactive form. Potentially, mutation of S1333 could disrupt the stability of the dimer, allowing substrate

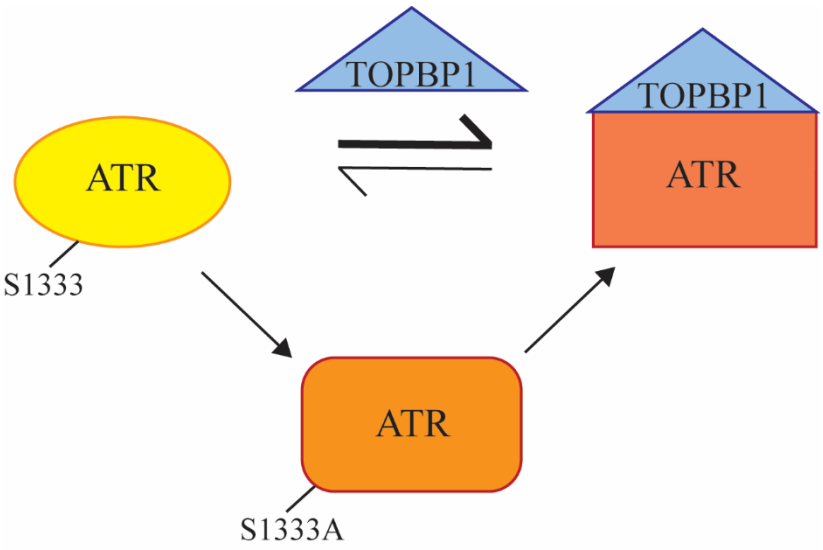

Figure 6.2. Mutation of S1333 induces a partial activating conformational change within ATR. When ATR is activated by TOPBP1, it is predicted ATR undergoes a conformational change, increasing ATR's substrate affinity. I hypothesize mutation of S1333 to alanine induces a partial conformational change toward the active ATR structure.

access to the kinase domain. Dimerization of the ATR/ATRIP complex utilizes contacts within ATR and ATRIP and disruption of ATRIP oligomerization impairs ATR checkpoint signaling [37]. It is possible, mutation of S1333 disrupts the dimer interface between the two ATR molecules, increasing substrate access to the kinase domain, but without altering the ATRIP dimerization, allowing continued checkpoint signaling.

Activators of ATR

In *S. cerevisiae*, there are three proteins which can activate MEC1, Dpb11 (orthologue of TOPBP1), Ddc1 (RAD9 orthologue), and Dna2 [77-80]. However, in mammalian cells, the only protein identified to activate ATR is TOPBP1. Mouse studies using a TOPBP1 mutant which can no longer activate ATR, showed this mutation is embryonic lethal [288]. This work suggests TOPBP1 is the only major ATR activator in mammalian cells. However, there was still a possibility other proteins could activate ATR as well.

Recently, a graduate student in the lab, Thomas Bass, identified ETAA1 as a novel RPA and ATR interactor using IP-mass spectrometry. He found knockdown of this protein results in reduced phosphorylation of RPA after DNA damage. These results suggested ETAA1 could be involved in ATR activation. Using the *in vitro* kinase assays, I determined that ETAA1 directly activates ATR, independently of TOPBP1 (Appendix C). These initial results are very exciting. However, there is much we still do not understand about this gene. How is ETAA1 regulated? Under what conditions does it act as an ATR activator? It is clear this protein is only a minor activator of ATR and therefore must be activating ATR in specific contexts. ETAA1 is enriched at replication forks by iPOND

and colocalizes with RPA at sites of DNA damage. If ETAA1 and ATR/ATRIP bind RPA and travel with the replication fork, what prevents ETAA1 from constitutively activating ATR? The initial study of ETAA1 will be published soon in Nature Cell Biology.

Utilization of the ATRi to study the ATR pathway

The development of ATR-specific inhibitors created a useful tool for studying ATR and its downstream functions. These inhibitors allowed us to gain better insight on how ATR functions at the replication fork. I demonstrated inhibition of ATR rapidly slows DNA replication rates and deregulates origin firing. This is most likely a result of ATR not activating CHK1. Inhibition of CHK1 also slows the replication fork and increases origin firing, and CHK1 directly inhibits Cdc25, regulating origin firing [95,98]. Replication fork restart is challenged when ATR is inhibited during replication stress and this is in part due to ATR preventing aberrant processing of stalled replication forks [96]. Furthermore, inhibition of ATR does not affect replisome stability at stalled forks, contrary to previous studies [103]. These findings are a direct result of the availability of ATR-specific inhibitors. In my dissertation work, I proposed to use the ATRi to identify new ATR pathway or DNA repair genes.

Whole genome siRNA screens aimed to identify new ATR pathway or DNA repair genes.

I proposed to use whole genome siRNA screens in combination with the ATRi, CHKi, or HU to identify new ATR pathway genes. The whole genome screens identified the ATR pathway as synthetic lethal with all three inhibitors. Overall, 180 genes were identified as synthetic lethal with all three inhibitors as well. I hypothesized there were

new ATR pathway genes to be discovered within those 180 genes. After the secondary validation screens of a selection of genes, I selected three genes of interest for further characterization, BRD3, RNF208, and ARID3B. While ultimately work was discontinued on all three genes, I identified novel protein interactors for each protein suggestive of potential new functions.

I and several other groups identified BRD3 interacting with the ATAD5/RFC2-5 complex, which unloads PCNA from chromatin [276-278]. Additionally, we found BRD3 is enriched at the replication forks by iPOND and the histone acetylation marks BRD3 preferentially binds are present on newly deposited histones on nascent DNA [103,264,266]. While I never generated data in support of my initial hypothesis, all of these observations remain true. Why BRD3 interacts with ATAD5 remains unknown. ATAD5 may have additional unknown functions at the replication fork or BRD3 functions with ATAD5 under specific contexts. When we combined the BET inhibitor with HU, PCNA levels on chromatin did not decrease as typical during HU treatment. There was also a larger increase in RPA on the chromatin after HU with the BETi. These results are suggestive the BET proteins are functioning in some way in response to replication stress. We only ever examined DNA replication rates after treatment with the BETi in unperturbed cells. A follow up experiment using DNA fiber labeling in combination with HU and the BETi would determine if the BET proteins have a replication stress response function.

All of the experiments using the BET inhibitors were done at short time points to avoid transcriptional changes. However, since completeing this work another lab published the BETi synergizes with the ATRi because of reduction in transcription of DNA replication genes [190]. In my hands, the effect of treating cells with the BETi and the

ATRi was at most additive. This could be due to differences in the cell lines tested, dosing schedules, as well as the compounds used. Their reported synergy with JQ1, the compound used in most of our work, was in combination with a pan-PIKK kinase inhibitor. The synergy they observe with VE-821 was with a BET inhibitor we did not use, RVX2135, and they only observed synergy at very high concentrations of both drugs. Overall, their work utilizes three ATR inhibitors which inhibit other members of the PIKK family to varying extents. More work is needed to clarify their findings and better elucidate if this is a viable treatment option in the cancer clinic.

My studies of the ARID3B/3A complex identified the FACT complex as an interactor, and we identified both complexes as being enriched at the replication fork [103]. There is a high probability the FACT complex is a non-specific binder to the FLAG-agarose beads, but evidence in the literature suggests this interaction may be real, as the two complexes have similar described functions. ARID family proteins modulate chromatin structure and promote transcriptional activation of genes [257,258]. The FACT complex reorganizes the chromatin to promote transcriptional initiation and elongation as well as DNA replication and repair [270,289,290]. It is conceivable these two proteins work together at the replication fork to promote fork processivity, but it is also possible they work together to promote transcription. Further experiments examining effects on the replication fork after knockdown of these complexes would test this hypothesis. However, the FACT:ARID3B interaction needs to be validated by IP using a different tag.

My IP-mass spectrometry data for RNF208 contained one interaction of interest: the RALGAPA/B complex. RALGAPs regulate the function of Ral GTPases, which are involved in cytokinesis [291]. RALGAPB localizes to the mitotic spindle during mitosis

promoting chromosome alignment and deregulation of RALGAPB is predicted to cause genomic instability [273]. Further work is needed characterizing RALGAP function in mitosis. Why RNF208 interacts with RALGAPA/B is unclear, but knockdown of RNF208 slightly elevated replication stress levels as measured by pCHK1 and γH2AX in unperturbed cells. Key future experiments would test if RNF208 knockdown causes mitotic defects. Mitotic genes are enriched in the top synthetic lethal genes with ATR inhibition so RNF208 functioning in mitosis would fit this data.

ATR, Mitosis, and the Centrosomes

Enrichment of mitosis genes in the ATRi whole genome screen results went unexplored and unvalidated. Within this gene subset, there are multiple components of the centrosome and centromere (Table A.2). The presence of multiple components adds strength the centrosome and centromere would validate and this finding is biological. These genes include MIS18BP1, CENPQ, CENPL, SPC24 at the centromere and CETN2, OFD1, CEP290, ODF2 at the centrosome.

Previous reports link the centrosome with the ATR pathway. Mutation of centrosome proteins results in the ATR-linked disease Seckel syndrome and cells from these patients have increased centrosome numbers and defective ATR checkpoint signaling [222-225]. Seckel syndrome caused by ATR hypomorphic mutations also have increased centrosome numbers and knockdown of ATR results in increased numbers of centrosomes [35,292]. ATM, ATR, CHK2, and CHK1 all localize to centrosomes and CHK1 localization prevents early activation of CDK1 [220,221,293]. How and why mutations of centrosome proteins results in reduced ATR pathway signaling remains unknown.

However, this fits with our overall findings in the whole genome screen, reduction in ATR pathway signaling sensitizes cells to the ATRi.

The proteins identified at the centromere are all components of the kinetochore and the other mitosis genes identified are involved in various aspects of proper chromosome alignment and separation. All of these genes hint ATR may function in mitosis and there is some evidence in the literature linking ATR and mitosis as well. ATR localizes to the centrosome during mitosis and associates with γ-tubulin [220]. This association raises the potential ATR regulates nucleation of tubulin during mitosis. ATR and ATM phosphorylate centrosome and centromere proteins and phosphorylation of CEP63, induced by double strand breaks occurring during mitosis, delocalizes CEP63 from the centrosome preventing spindle assembly [27,219,294,295]. More extensive work is needed to validate these findings and elucidate how or if ATR is functioning in mitosis. Potentially, ATR and ATM could be preventing progression through mitosis in the presence of aberrant DNA structures.

ATR Inhibitors in the Cancer Clinic

The versatility of ATR makes it a promising target for anti-cancer therapies. Our lab and others identified DNA damaging chemotherapies as being synergistic with the ATRi, including platinums, topoisomerase poisons, PARP inhibitors, and gemcitabine [183,184,186,187,194,195]. Additionally, we found the ATRi can resensitize cisplatin resistant cells to cisplatin [183,189]. This is a promising preclinical result as most patients in the clinical trials will have already received a platinum-based therapy and became

resistant to it. This provides an excellent opportunity for the ATRi to be beneficial in patients.

The inhibitors are currently entering phase II clinical trials, and in those trials, trials, Astra Zeneca and Vertex Pharmaceuticals are recruiting patients with a wide range of tumor types such as HPV negative head and neck cancer, non-small cell lung cancer with brain metastasis or ATM deficiency, gastric, urothelial, ovarian, or small cell lung cancer, or anyone with a solid malignant tumor. Because the ATRi synergizes with many chemotherapies, these trials will use the ATRi in combination with platinums, radiation, PARP inhibitors, taxanes, topoisomerase inhibitors, and gemcitabine (clinicaltrials.gov). The phase II trials very clearly have little directionality on who should be treated with the ATRi or how they should be treated. This leaves a bigger opportunity for these drugs to fail when they might be very beneficial for specific patients.

A whole genome siRNA screen identifies synthetic lethal relationships with the ATRi

To identify a clinically actionable patient population, we and many other groups worked extensively to identify synthetic lethal relationships with the ATRi. Synthetic lethality is when cells can compensate for loss or mutation of one protein or pathway by increasing reliance on a separate protein or pathway to maintain cell viability. However, if the second pathway is lost, or inhibited by a small molecule, cell death occurs (Figure 6.3). There has been mild success in identifying synthetic lethal relationships with the ATRi. However, the only finding which has translated into the clinic so far as is ATM deficiency [194]. In our hands at least, knockdown of ATM only results in mild sensitization to the ATRi [183,191].

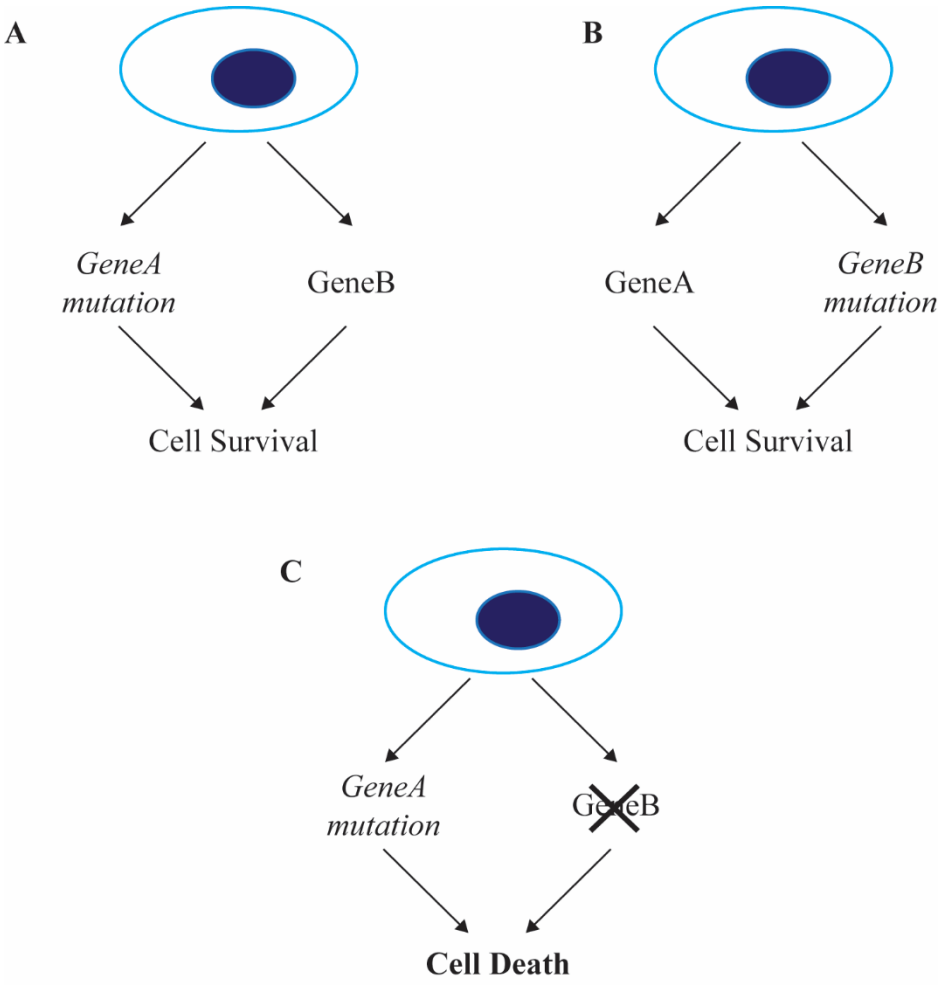

Figure 6.3. Synthetic Lethality. Synthetic lethality is defined by the presence of two or more mutations which induce cell death but alone the cell maintains viability. **A.** Mutation of GeneA is compensated for by GeneB and the cell survives. **B.** Mutation of GeneB is compensated for by GeneA and the cell survives. **C.** Mutation of GeneA combined with mutation or inhibition of GeneB induces cell death by synthetic lethality.

Other identified synthetic lethal relationships with the ATRi include deficiencies in ERCC1, XRCC1, homologous recombination (HR), and p53 [191,193,194,196,197,199]. However, there are conflicting reports if deficiencies in HR are synthetic lethal with the ATRi. We and others have found BRCA status does not correlate with sensitivity [183,187]. Additional work done in the lab identified knockdown of the translesion polymerase ζ catalytic subunit REV3 as synthetic lethal with ATRi/cisplatin. This synthetic lethal relationship is potentially clinically useful as REV3 is mutated in 17% of lung cancer and 7% of B cell lymphomas have homozygous deletions of REV3 according to the TCGA [236]. This work still needs validation in isogenic cell lines as well as in cancer cells. The Zou lab found cells maintaining their telomeres using the ALT (alternative lengthening of telomeres) pathway as hypersensitive to the ATRi and that ATR is required for ALT [200]. This finding has potential to translate into the clinic.

To identify a clinically actionable patient population, I, in collaboration with a post-doctoral fellow in the lab Kareem Mohni, conducted a whole genome siRNA screen in combination with the ATRi, cisplatin and the ATRi/cisplatin. These conditions were included as the ATRi is not being used as a monotherapy in the clinic and the ATRi synergizes best with platinum therapies [184]. The top two enriched pathways identified as synthetic lethal with the ATRi alone and in combination with cisplatin was DNA replication and the ATR pathway. We validated each component in the ATR activation pathway as well as DNA replication using individual siRNAs, long-term knockdown by shRNA, and isogenic cell lines. The final experiment in the validation process used the S1333A and S1333D-ATR cell lines. This experiment demonstrated that the level of ATR kinase activity present in a cell inversely correlates with sensitivity to the ATRi. In

agreement with our findings, the Helleday lab identified the CHK1i inhibitors as being synergistic with the ATRi, and the Gallmeir lab found POLD1 deficiency sensitizes cells to the ATRi [192,198].

Depletion of ATR pathway proteins sensitizes cells to the ATRi

Early work in the lab identified ATR knockdown as sensitizing cells to the ATRi. Our initial hypothesis on why this was true was that knockdown of ATR shifts the ATR protein to ATRi ratio, creating less protein for the inhibitor to target. However, this does not hold true for knockdown of the other components involved in activating ATR, except for ATRIP. Knockdown of ATRIP results in knockdown of ATR as the two are obligatory binding partners and stabilize each other [3]. My hypothesis for what is occurring stems back to ATR being essential in S-phase and playing a key role in overcoming replication stress (Figure 6.4A). When ATR cannot fully activate, due to loss of a component of the pathway, cells are not able to overcome replication stress, which is particularly high in cancer cells due to the overexpression of oncogenes [20]. This increases the replication stress load, further activating and increasing the reliance on the remaining ATR functionality (Figure 6.4B). Therefore, if ATR is inhibited in cells with a higher dependence on ATR due to reduced ATR function, the ATRi induces cell death (Figure 6.4C).

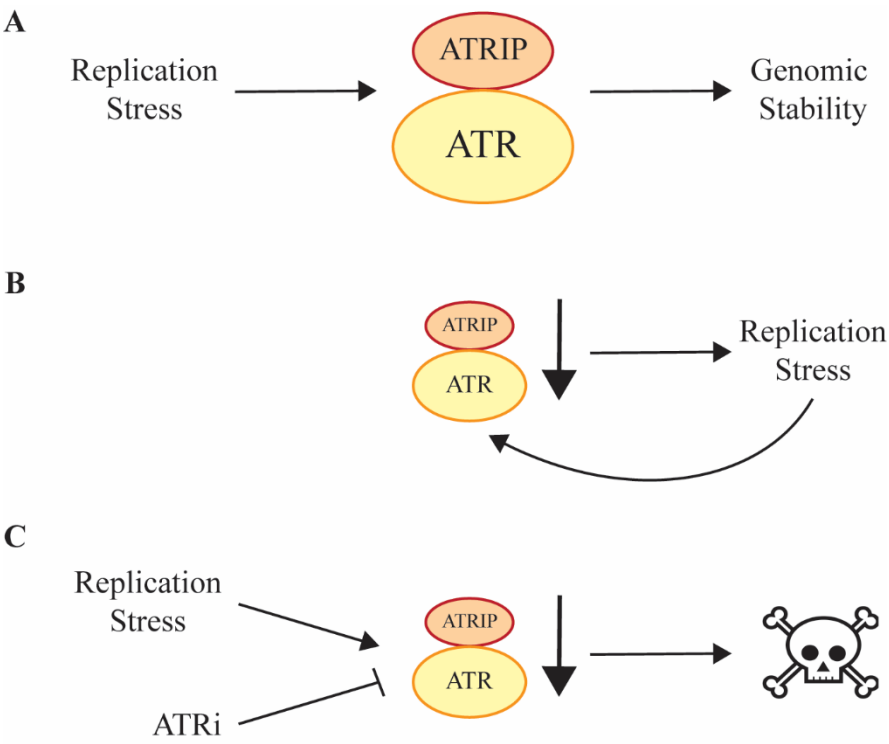

Figure 6.4. ATR is essential in S-phase for overcoming replication stress. A. In the presence of replication stress, ATR activates promoting genomic stability. **B.** If ATR function is reduced, cells have elevated levels of replication stress. The remaining ATR activity is needed to overcome this stress and maintain cell viability. **C.** In cells with reduced ATR function and elevated levels of replication stress, if they are treated with the ATR inhibitor, the cells will die.

ATRIP gene deletion and ATR and CHK1 frameshift mutations occur in cancer

The ATR pathway is not frequently mutated in cancer. However, the TCGA identified two potential patient populations with ATR pathway defects. First, there is a subset of cancers containing chromosome 3p21 deletions [242-244]. This region of the chromosome, while also containing other tumor suppressors, contains the ATRIP gene. These patients potentially express lower levels of ATRIP and may have defects in ATR activation and signaling. With the PARPi, levels of CDK12, which regulate BRCA1 levels, directly correlate with sensitivity to the inhibitor [296]. I hypothesized ATR/ATRIP protein levels would correlate with sensitivity to the inhibitor. Based on the cell lines I acquired containing the ATRIP deletion, I did not observe any easily identifiable relationship between ATR/ATRIP protein levels and sensitivity to the inhibitor.

The cell lines I obtained came from a variety of cancers, contained innumerable genetic differences, and represent a much more complicated system then isogenic cell lines. There is evidence in the literature ATR is a dose dependent tumor suppressor in mismatch repair deficient cancers which leaves the chance in some cases ATR protein levels will inversely correlate with sensitivity to the ATRi [246]. However, only one group published this finding and there have been no follow up studies. One potential pitfall in my analysis of the ATRIP deletion lines is I never tested ATR functionality. These lines expressed varying levels of ATRIP and ATR, but it is unclear how much ATR/ATRIP is needed in a cell to still have full functionality of the pathway. Considering this, some of the cell lines may have reduced pathway function while others may not.

The second patient population identified were those with mismatch repair deficient cancers. Mismatch repair deficiency causes microsatellite instability. The ATR and CHK1 genes contain a three-adenine repeat which can be expanded or contracted in these cancers,

introducing a frameshift mutation. It was previously published that the ATR frameshift reduces ATR signaling [238]. However, the cell lines I obtained only had a very minimal decrease in pCHK1 levels after HU treatment and these cell lines had a range of sensitivities to the ATRi. The Cliby group tested ATR signaling after treatment with UV, IR, and a topoisomerase inhibitor in two cells lines containing the ATR frameshift. The two cell lines did have reduced pCHK1 levels, but they did not have equal loading and no additional publications exist claiming this frameshift reduces ATR functionality. It could be that a subset of cancers with this mutation result in reduced ATR functionality. However, this mutation is not frequently occurring. Further work on a larger cell line panel is needed to fully understand the impact of this mutation on ATR.

Measuring ATR activity in cells

When analyzing the cell lines containing the ATR or CHK1 frameshifts or the outlier cell lines from the CNV vs mRNA graphs, I measured ATR functionality through levels of pCHK1 before and after replication stress induced by HU. However, this measurement is flawed. First, CHK1 protein levels are cell cycle regulated [297]. If a particular cell line has a large percentage of the cell population in G1, the overall CHK1 levels will be decreased. Additionally, phosphorylation of CHK1 arises from ATR activating in response to replication stress. In my analysis, I induced replication stress with HU, which only effects cells actively replicating DNA. A cell line could have reduced pCHK1 before or after HU treatment just by having fewer cells in S-phase or fewer replication forks. Perhaps the better way to measure ATR activation would have been to measure ATR phosphorylation on T1989 and to use a different DNA damaging reagent.

This would improve the readout for ATR activity but still have some problems if a large number of cells were in G1.

The S1333A and S1333D-ATR cells lines sensitivity to the ATRi inversely correlated with the measured *in vitro* ATR kinase activity. These two mutations within ATR only resulted in slight signaling differences in cells. S1333A-ATR had increased pCHK1 basally and after low levels of replication stress. The S1333D-ATR line only had slight recovery and checkpoint defects after treatment with IR and UV but not HU. I tested the acquired cancer cell lines for ATR defects by measuring pCHK1 after high levels of replication stress. Using this same assay, the S1333A and S1333D-ATR cell lines are identical to the wild-type ATR cell line. This assay is not sensitive enough to detect the differences in kinase activity levels and therefore, may have been the incorrect way to screen the cancer cell lines for ATR pathway defects. The S1333D-ATR cell line only had slight checkpoint defects and therefore, the better way to screen the cancer cell lines might have been through checkpoint activation assays. These assays may become difficult to interpret when coming cell lines growing at different rates and with different cell cycle distributions. However, I selected cancer cell lines based off of their genetic data and the genetics did not predict sensitivity to the inhibitor.

Alternative approaches for identifying a clinically actionable patient population

The next approach to identifying a clinically actionable patient population would be to screen a large cell line panel and identify the genetic similarities which confer sensitivity or resistance to the ATRi. However, doing this has potential pitfalls. During my work, I noticed the cell doubling time alters the observed sensitivity to the ATRi. With

cells that double in ~24 hours, the dose response curves are identical whether the cells were treated for 24 hours or 72 hours with the ATRi (Figure 6.5A). This highlights that the cells only need to progress through S-phase once to experience the lethal event. However, a slower growing cell line (~48 hour doubling time) treated for three days with the ATRi looked sick and had progressed through S-phase at least once during the assay, but still maintained a high enough viability to reduce the alamarBlue (Figure 6.5B). This data suggested that while the lethal event occurred, the slower growing cells needed more time to commit to apoptosis and die. Therefore in my experiments, I altered the dose response assay for each cell line based on their doubling time to accommodate for three population doublings. This would not be a practical alteration when screening a large panel and the resulting data from the panel may end up being more reflective of cell growth rate than resistance or sensitization mechanisms.

Recently, other groups have also noticed that cell growth rates impact calculated IC50 values and that IC50 data generated does not replicate in other labs due to small differences in assay lengths or cell growth rates. Both the Sorger and Tyson groups proposed to fix this by included a correction for cell doubling time in the IC50 calculation [298,299]. To do this, instead of using a reagent such as alamarBlue as an indirect read out of cell number and viability, they propose it is better to count the actual cell numbers at the beginning and end of the assay, in the presence and absence of drug. From those cell numbers both groups proposed to calculate a growth rate correction value. This method saves a lot of time from how I conducted my experiments and eliminates the need to

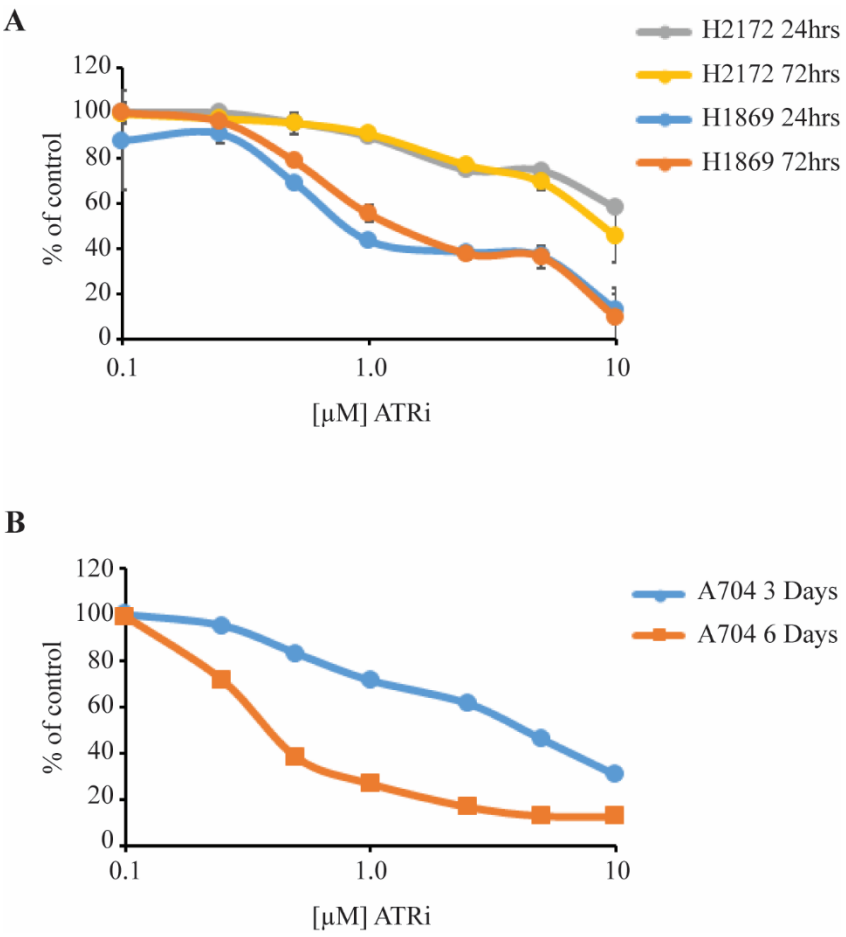

Figure 6.5. The lethal event with ATR inhibition occurs within the first cell cycle but the cells need time to continue to cycle in order to die. A. H2172 and H1869 cells have a doubling time around 24 hours. These cell lines were treated with ATRi (VX-970) at increasing doses for 24 hours or 72 hours. After three days, cell viability was measured by alamarBlue and calculated as a percent of control. **B.** A704 cells double approximately every 48 hours. A704 cells were incubated with the ATRi (VX-970) at increasing dose for three or six days. Cell viability was measured by alamarBlue and calculated as a percent of control. n=3

calculate cell-doubling times of all the different cell lines before performing the dose response assays. These new methods make large cell line panel screening more feasible.

Identification of the genetic determinants of sensitivity to the inhibitor is important, but it is also important to understand resistance mechanisms. Multiple approaches can be used to identify mechanisms of resistance. A siRNA or shRNA whole genome screen can be designed to identify genes when knocked down that allow the cells to continue to grow in the presence of the ATRi. A newly arising alternative screening method uses CRISPR/Cas to generate loss-of-function alleles and can be used to perform negative and positive selection screens by methodology similar to shRNA screening [300]. The field is rapidly developing Cas9 enzymes with fewer off target events [301]. This new methodology is very promising, and hopefully, it will prove to be a better technique then siRNA or shRNA screening.

From my experiments and others published in the literature, many cell lines have already been identified as resistant to the ATRi. Study of these cell lines might easily identify resistance mechanisms. First, the cells need to be tested if the ATRi is inhibiting ATR at the concentrations used in the assay. We know ATR inhibition deregulates origin firing [96]. Additionally, ATR prevents aberrant processing of stalled forks and RPA exhaustion in the presence of the ATRi and replication stress causes replication catastrophe [94,96]. Potential mechanisms of resistance could include upregulation of RPA, upregulation of ATR, mechanisms re-regulating fork processing enzymes, or prevention of excess origin firing during ATR inhibition. All of these mechanisms are easily testable. In the generation of ATRi resistant cells in the lab, we found this resistance to be transient, suggesting there is a transcription upregulation of some protein or process. This

upregulation is easily identifiable through RNA-sequencing experiments or even western blotting of candidate genes.

Another approach to identify mechanisms of resistance or sensitivity is through use of the patient samples acquired in the phase II clinical trials. Once the trials are completed, these samples will have clinical records identifying responders and non-responders. DNA and RNA sequencing of these samples is perhaps the best way to identify genetic determinants of resistance and sensitivity. However, analyzing and making conclusions from this type of data can be difficult and this information may come too late as the drug may fail in phase II.

Directed use of the ATRi in the cancer clinic

Based on the data from my whole genome screen, other experiments conducted, and the published data on the ATRi, there are two ways the ATRi should be used in the cancer clinic. First, the ATRi should be and is being used in combination with traditional DNA damaging chemotherapies (Figure 6.6A). The ATRi synergizes with a range of chemotherapies, and this reflects on the versatility of ATR. ATR responds to a multitude of problems encountered during DNA replication, which allows for use of the inhibitor with a range of reagents creating DNA lesions. Additionally, we showed the ATRi can resensitize cancer cells already resistant to these therapies. Second, the data from my screen and the follow up work suggests cancers with ATR signaling defects will be particularly sensitive to the ATRi alone or in combination with cisplatin (Figure 6.6B). The remaining challenge is to properly identify cancers with ATR signaling defects.

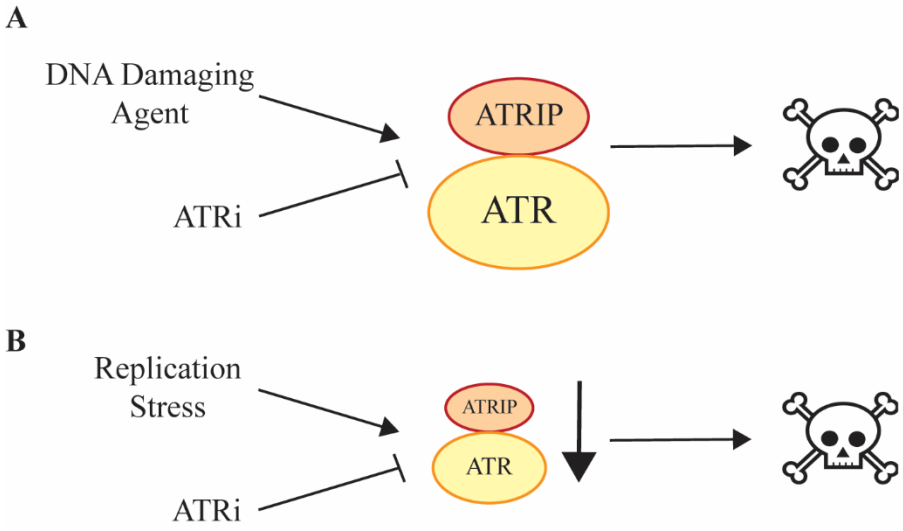

Figure 6.6. Directed use of the ATRi in the cancer clinic. A. The ATRi synergizes with DNA damaging chemotherapies. As such, patients should be treated with the DNA damaging chemotherapy first and then the ATRi to most effectively kill the cancer cells. **B.** Cancers with reduced ATR functionality should be treated with the ATRi. Reduced ATR function results in increased replication stress and increased dependence on the remaining ATR function. If ATR is inhibited in these cells, the cells will die.

APPENDIX A

WHOLE GENOME SCREENS DATA AND EXTRA FIGURES

This appendix contains table A.2 with the top genes synthetic lethal with the ATRi, correlation graphs, and Z-score graphs for each drug condition. The ATRi screen table includes the percent of control for each gene after treatment with ATRi and the calculated robust Z-score. The table also includes the percent viability after gene knockdown and the corresponding robust Z-score. siRNAs which resulted in a percent viability less than 20% were not included in the robust Z-score calculations. All four replicates of the whole genome screen with the ATRi are listed as well as the calculated average. A gene was considered synthetic lethal and included in this table if the average robust Z-score was -2.0 or less.

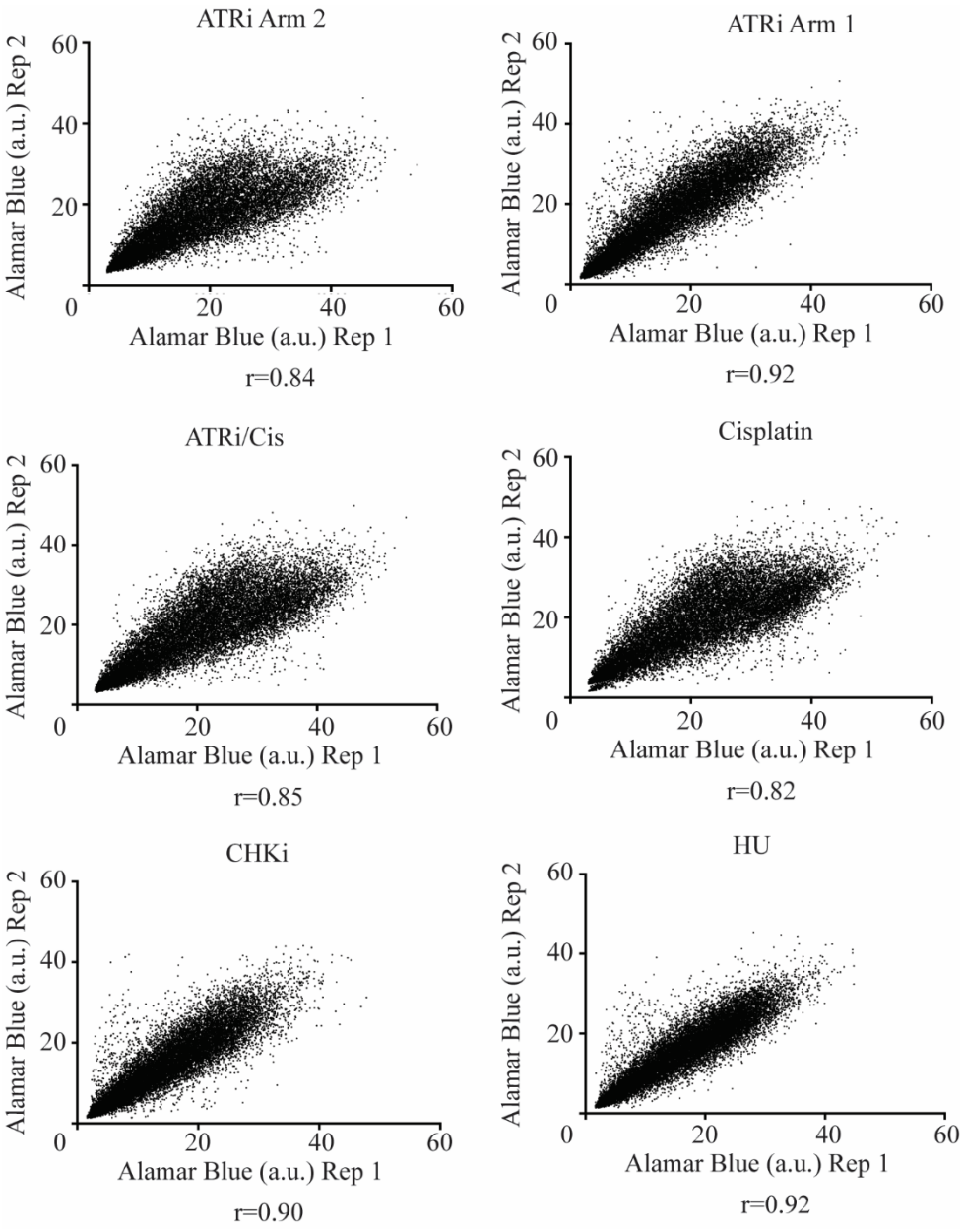

Figure AA.1. Replicate correlation graphs for the whole genome screens. The alamarBlue values for each gene, under each drug condition, for each replicate are graphed. The spearman correlation was calculated and reported on each graph. Overall, the replicates were highly correlative but Arm 1 of the screen with CHKi, HU, and ATRi were more correlative than Arm2 (ATRi, cisplatin, ATRi/cisplatin).

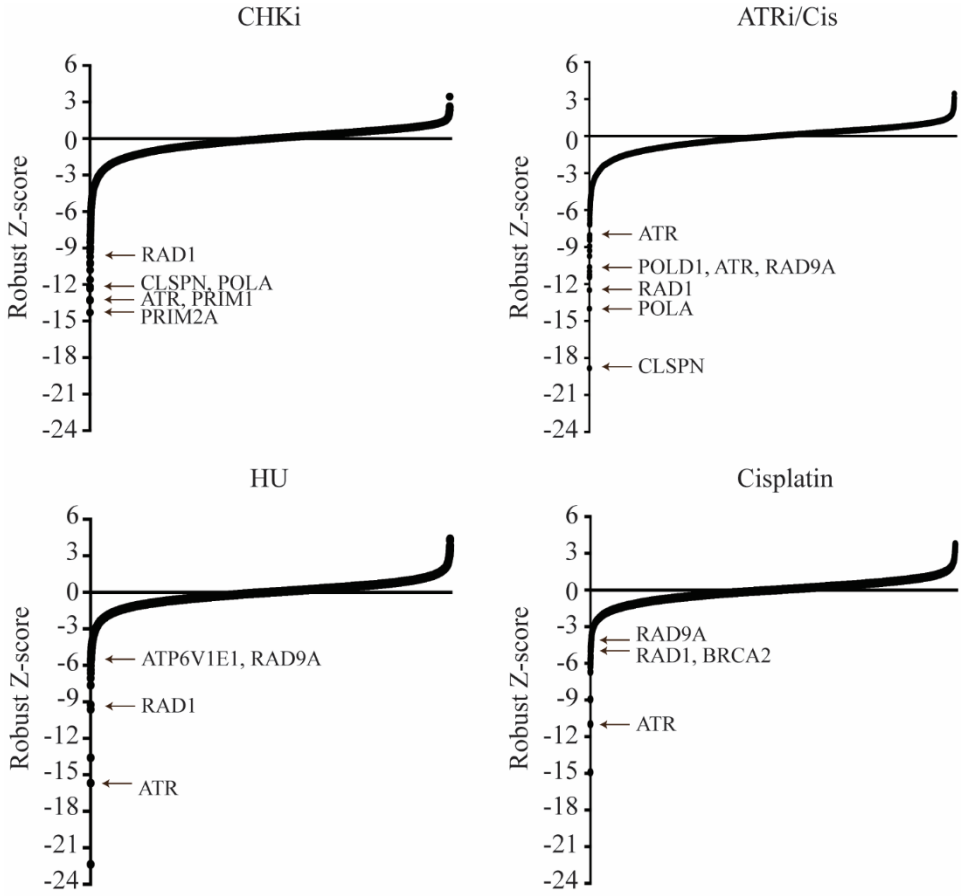

Figure AA.2. The ATR pathway was synthetic lethal with each drug condition screened in the whole genome screens. The robust Z-score for each gene is graphed by rank. ATR pathway and other genes with known functions synthetic lethal with each drug are indicated on the graphs. The ATRi graph is in Chapter IV.

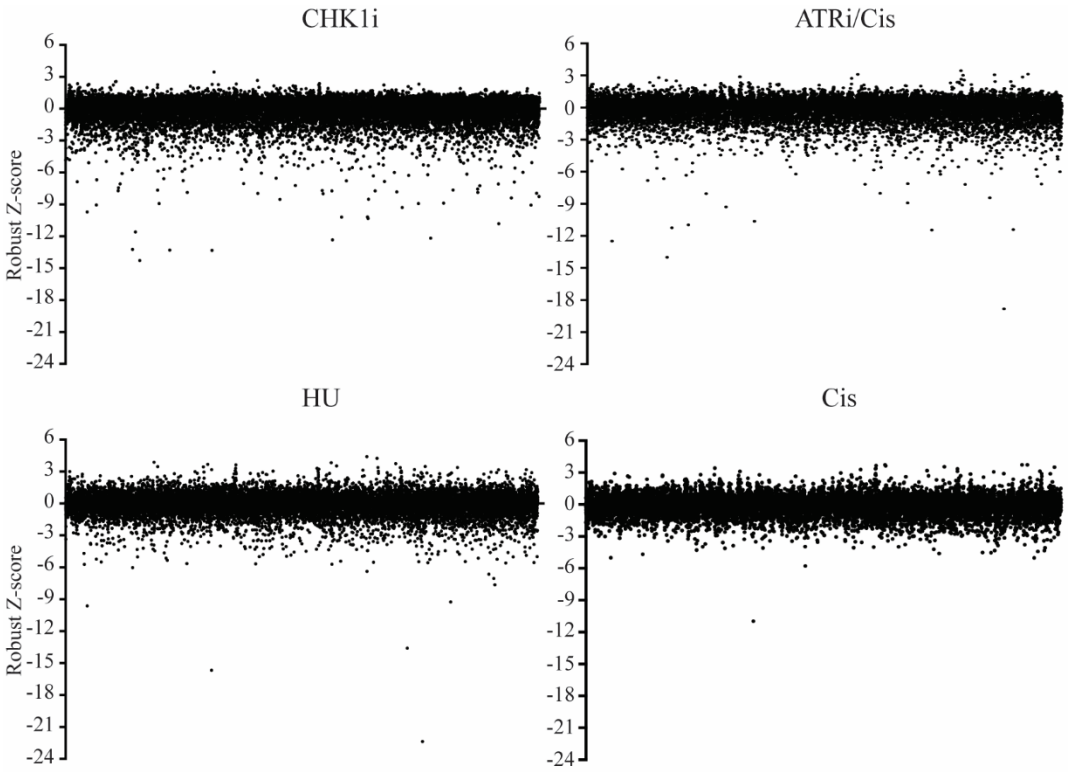

Figure AA.3. The robust Z-score average for each gene is graphed by plate and by row. The ATRi graph is in Chapter IV.

Table A.1: Pathways enriched in the ATRi whole genome screen dataset. The top synthetic lethal genes with the ATRi (robust Z-score less than -2.0) were analyzed by ToppGene to identify enriched pathways. Those pathways and the genes synthetic lethal with the ATRi are listed.

Pathway	**Genes Synthetic Lethal with ATRi**
DNA Replication	MCM3, MCM5, MCM10, CDC7, CDC45, POLD4, POLD3, POLA1, POLD1, POLE2, PRIM1, PRIM2 ,RFC4, RFC5
Activation of ATR	MCM3, MCM5, MCM10, CDC7, CDC45, CLSPN, ATR, HUS1, RAD1, RAD9A, RFC4, RFC5
Cell Cycle	MIS18BP1, MCM3, MCM5, MCM10, CDC7, CDC45, TUBB4A, FZR1, SYCP2, ANAPC10, OFD1, CEP290, GINS4, ANAPC11, SPC24, GINS2, POLD4, POLD3, CLSPN, NUDC, SMC1B, PDS5B, ATR, DIDO1, ODF2, CCNA2, CETN2, TUBA4A, HUS1, POLA1, POLD1, POLE2, PPP2R5E, CSNK2A1, CSNK2B, PRIM1, PRIM2, KNTC1, CENPL, NEK9, GINS1, RAD1, DHFR, DNA2, RAD9A, RFC4, RFC5, CENPQ, AAAS, LMNB1, BORA
S Phase	MCM3, MCM5, CDC45, FZR1, GINS4, GINS2, POLD4, POLD3, PDS5B, CCNA2, POLA1, POLD1, POLE2, PRIM1, PRIM2, GINS1, DNA2, RFC4, RFC5
Cell Cycle, Mitotic	MCM3, MCM5, MCM10, CDC7, CDC45, TUBB4A, FZR1, ANAPC10, OFD1, CEP290, GINS4, ANAPC11, SPC24, GINS2, POLD4, POLD3, NUDC, PDS5B, ODF2, CCNA2, CETN2, TUBA4A, POLA1, POLD1, POLE2, PPP2R5E, CSNK2A1, CSNK2B, PRIM1, PRIM2, KNTC1, CENPL, NEK9, GINS1, DHFR, DNA2, RFC4, RFC5, CENPQ, AAAS, LMNB1, BORA
Chromosome Maintenance	MIS18BP1, SYCP2, POLD4, POLD3, SMC1B, ATR, DIDO1, POLA1, POLD1, POLE2, PRIM1, PRIM2, DNA2, RFC4, RFC5, CENPQ, LMNB1
Mismatch Repair	MSH5, MLH3, POLD4, POLD3, POLD1, RFC4, RFC5
RB in Cancer	MCM3, CDC7, CDC45, POLD3, SAP30, CCNA2, POLA1, POLE2, PRIM1, DHFR, STMN1, RFC4, RFC5

		Mock								ATRi								
		% of Control				Robust Z-score				% of Control				Robust Z-score				
Gene Symbol	Gene ID	Rep 1	Rep 2	Rep 3	Rep 4	Rep 1	Rep 2	Rep 3	Rep 4	Rep 1	Rep 2	Rep 3	Rep 4	Rep 1	Rep 2	Rep 3	Rep 4	Average
CLSPN	63967	43.01	29.25	36.44	25.11	-1.91	-3.56	-4.13	-2.87	8.81	8.67	6.60	0.00	-13.94	-17.01	-11.52	-20.94	-15.85
HMGB3	3149	44.10	34.65	43.00	34.83	-2.86	-3.02	-3.79	-2.79	6.65	11.26	7.37	8.33	-20.12	-12.37	-16.44	-10.79	-14.93
PRIM1	5557	148.72	150.98	155.46	122.30	0.95	0.64	0.84	0.96	8.71	12.03	6.82	6.60	-13.18	-14.61	-12.19	-13.95	-13.48
RAD1	5810	124.25	153.26	157.78	116.44	0.73	0.72	1.00	0.95	9.41	12.96	5.15	8.71	-13.46	-14.41	-13.33	-12.35	-13.39
POLA	5422	31.54	27.31	24.49	21.18	-1.79	-2.27	-2.93	-2.26	9.58	9.06	7.16	9.01	-13.99	-13.97	-12.52	-9.03	-12.38
PRIM2A	5558	79.81	55.36	57.28	33.64	-0.23	-1.00	-1.05	-1.41	8.68	9.47	6.54	11.33	-14.64	-13.70	-13.04	-8.00	-12.35
POLD1	5424	81.33	82.38	69.44	28.45	-0.64	-1.19	-1.15	-2.86	6.81	12.90	5.91	9.27	-14.12	-11.88	-12.97	-9.81	-12.20
SEZ6	124925	56.72	61.14	84.86	46.05	-1.30	-1.28	-0.59	-1.39	17.50	13.93	7.39	9.70	-10.14	-12.06	-11.74	-9.05	-10.75
TIMELESS	8914	91.63	80.72	85.14	56.94	-0.66	-0.76	-1.15	-1.24	23.51	16.10	10.54	13.45	-10.03	-10.18	-13.87	-8.24	-10.58
EGFL3	1953	22.34	23.69	31.47	23.26	-3.59	-3.92	-4.49	-3.73	12.95	12.01	7.82	18.51	-9.77	-14.69	-10.45	-6.93	-10.46
KERA	11081	66.57	77.74	77.97	91.73	-1.13	-0.66	-0.81	0.16	14.40	21.14	7.04	15.60	-12.16	-9.40	-11.90	-6.68	-10.04
ATR	545	64.54	63.65	54.23	40.63	-0.72	-0.93	-1.22	-1.19	20.09	18.33	15.47	17.38	-9.45	-10.87	-9.27	-7.23	-9.20
ZNF553	197407	86.53	69.68	74.54	45.15	-0.88	-1.09	-1.11	-1.57	19.08	13.94	13.43	14.97	-8.24	-10.60	-9.41	-7.40	-8.91
LMNB1	4001	41.40	48.50	48.76	43.78	-2.13	-1.39	-1.88	-2.49	25.72	18.73	17.38	24.79	-7.95	-8.25	-11.65	-7.68	-8.88
FLJ32949	283417	23.59	21.42	32.14	17.22	-3.91	-3.75	-4.02	-4.44	16.31	22.38	17.21	14.02	-9.50	-10.70	-7.04	-8.22	-8.87
RAD9A	5883	83.36	107.00	104.39	82.81	0.01	0.21	0.15	0.32	20.90	16.67	12.74	14.01	-8.25	-11.06	-7.36	-8.27	-8.74
CETN2	1069	34.72	39.15	50.00	33.47	-2.47	-2.17	-2.25	-2.17	20.15	30.29	14.68	17.91	-10.68	-7.70	-9.17	-6.94	-8.62
MIZF	25988	20.66	19.54	27.94	14.36	-5.14	-4.55	-5.45	-5.59	28.33	30.57	15.93	13.74	-8.54	-6.27	-10.91	-8.13	-8.46
TXN	7295	48.42	55.28	52.94	31.77	-1.07	-1.00	-1.22	-1.52	18.00	20.19	17.89	11.97	-9.77	-8.95	-7.24	-7.75	-8.43
LOC644943	644943	39.40	42.15	44.94	26.11	-2.44	-2.18	-2.31	-3.35	23.38	27.42	8.49	17.00	-8.83	-7.68	-10.91	-6.28	-8.43
ZNF615	284370	79.72	79.55	97.72	66.09	-0.67	-0.53	-0.23	-0.41	26.56	13.33	12.30	17.20	-6.74	-12.73	-6.93	-7.02	-8.35
TMEM18	129787	93.93	86.76	85.60	55.06	-0.56	-0.37	-0.60	-1.24	25.03	21.23	14.88	17.59	-8.32	-8.82	-9.06	-7.08	-8.32
hCG_2036778	100169851	102.42	75.10	73.93	69.26	0.06	-0.77	-1.13	-0.55	35.69	24.99	11.89	20.10	-6.32	-9.08	-10.41	-6.35	-8.04
SLC15A2	6565	27.62	20.73	16.25	25.05	-1.94	-2.17	-2.87	-1.85	12.29	27.69	13.71	24.72	-10.38	-8.10	-8.69	-4.97	-8.04
SLD5	84296	156.66	111.75	97.57	81.92	0.45	0.05	-0.35	0.13	21.02	26.25	17.50	16.79	-7.95	-9.46	-6.96	-7.23	-7.90
KCNG4	93107	60.33	85.62	68.79	42.95	-1.10	-0.48	-0.88	-0.84	17.96	17.43	15.91	14.43	-8.76	-8.14	-6.39	-8.12	-7.85
LOC157708	157708	35.58	34.37	40.05	26.12	-1.62	-2.07	-1.95	-2.14	23.81	31.02	19.13	13.57	-6.74	-7.51	-7.01	-9.88	-7.79
PFS2	51659	71.26	57.59	55.84	52.30	-1.10	-1.76	-1.90	-1.06	24.84	24.17	9.54	16.60	-5.89	-10.03	-7.94	-6.79	-7.66
KIAA1268	54625	54.99	51.66	69.44	40.98	-0.60	-1.17	-0.45	-1.20	17.35	28.13	10.45	23.23	-8.57	-7.11	-8.43	-5.88	-7.50
LOC123169	123169	127.16	127.40	113.63	79.15	0.27	0.24	0.04	-0.16	22.90	22.64		17.83	-7.22	-8.22		-6.44	-7.30
LSM10	84967	60.03	78.72	89.73	76.12	-1.19	-0.67	-0.58	-0.34	23.23	30.13	18.86	31.10	-9.60	-7.74	-7.70	-4.12	-7.29
KIAA0317	9870	21.33	17.89	24.73	18.95			-3.19	-2.36	22.00	28.17	13.59	16.78			-7.12	-7.32	-7.22
ARS	57152	30.99	9.55	16.85	16.49	-3.47	-5.90			24.62	35.10		35.14	-7.51	-6.56			-7.03
KIAA0685	9701	78.64	66.07	99.99	64.93	-0.95	-1.34	-0.55	-0.85	22.70	33.14	11.10	23.92	-6.72	-7.08	-8.72	-5.55	-7.02
NEU2	4759	84.68	111.39	80.25	45.90	-0.57	0.02	-0.90	-1.96	37.65	18.76		17.81	-4.26	-9.62		-7.14	-7.01
SNTB2	6645	38.53	39.50	25.31	16.53	-2.50	-2.34	-3.87	-4.63	25.70	30.91	14.02	27.28	-8.18	-6.89	-8.25	-4.08	-6.85
ZDHHC14	79683	45.53	39.95	50.84	56.02	-1.99	-2.35	-2.46	-0.72	21.98	32.16	21.01	29.55	-7.74	-8.25	-7.93	-3.41	-6.83
TBC1D4	9882	67.41	75.49	111.02	67.63	-0.93	-0.93	-0.13	-0.45	24.15	27.08	17.81	25.39	-7.61	-8.48	-6.56	-4.55	-6.80
LOC653978	653978	105.94	45.89	56.57	57.79	-1.92	-4.00	-3.56	-2.50	27.91	33.43	31.12	41.14	-7.70	-10.61	-4.03	-4.82	-6.79
MGC39497	144321	90.09	62.28	83.22	25.90	-0.79	-1.88	-1.16	-3.40	30.00	26.19		15.99	-5.70	-7.29		-7.01	-6.67
CABIN1	23523	21.54	18.71	28.23	4.74	-3.62	-4.08			54.18	18.57	36.75	80.31	-2.63	-10.57			-6.60
UGT2B4	7363	23.61	32.58	36.91	19.49	-3.22	-3.98	-2.66	-3.88	26.45	32.10	14.14	22.34	-6.00	-6.55	-8.31	-5.37	-6.56
K6IRS4	121391	135.21	114.84	109.83	81.32	0.31	0.05	-0.11	-0.18	97.92	92.42		70.60	-8.67	-10.63		-0.16	-6.49
FLJ11127	54491	112.70	105.16	115.96	82.34	-0.15	-0.22	0.11	-0.13	26.21	29.84	21.48	20.08	-6.61	-7.11	-6.20	-5.75	-6.42
FOXO1A	2308	104.40	96.64	131.14	79.30	0.34	0.11	0.69	0.30	15.77	36.35	19.51	23.46	-7.99	-4.69	-7.45	-4.97	-6.27
NUDC	10726	58.48	19.93	24.84	31.25	-1.23	-3.89	-3.90	-2.33	24.07	32.30	25.81	22.07	-8.15	-6.42	-5.11	-4.89	-6.14
REC14	80349	26.75	22.79	32.23	22.00	-3.66	-5.18	-4.78	-4.08	33.43	33.02	12.00	23.37	-5.27	-7.18	-7.65	-4.33	-6.11
RUSC2	9853	83.44	78.80	68.38	48.36	-0.68	-0.56	-1.21	-1.35	26.11	31.10	20.82	20.29	-7.90	-5.35	-5.71	-5.23	-6.05
DJ383J4.3	91687	29.01	45.12	54.73	22.85	-3.46	-3.20	-2.83	-3.97	36.58	26.40	19.87	19.82	-4.72	-8.86	-5.39	-5.01	-5.99
MRPL35	51318	50.57	30.06	41.53	27.12	-1.82	-3.02	-2.52	-3.24	27.64	37.01	20.24	26.24	-7.68	-5.70	-6.30	-4.27	-5.99
FLJ39155	133584	67.29	52.93	48.07	30.50	-1.40	-2.74	-3.31	-3.12	26.94	24.69	19.25	37.28	-6.60	-9.36	-5.53	-2.39	-5.97
C9ORF138	158297	42.30	21.79	19.94	6.45	-2.61	-3.76			26.85	32.30	30.89	28.59	-6.37	-5.49			-5.93
PRO1580	55374	25.12	33.01	45.97	18.47	-3.55	-3.44	-3.13	-4.45	40.25	27.36	16.26	26.93	-4.09	-7.70	-7.61	-4.27	-5.92
FLJ31052	127943	55.82	39.33	23.87	34.53	-2.15	-4.10	-5.81	-3.87	45.18	41.51	20.59	19.35	-3.69	-5.89	-6.77	-7.18	-5.88
C2ORF28	51374	58.62	52.54	82.95	64.18	-1.23	-1.93	-1.18	-0.57	38.64	35.74	22.62	16.03	-4.66	-6.40	-5.36	-6.88	-5.82
NTNG2	84628	33.91	10.99	19.90	9.27	-2.94	-4.81			27.79	39.45	18.46	31.15	-7.47	-4.06			-5.76
ZNF674	641339	58.21	65.22	68.82	43.85	-1.75	-0.99	-1.23	-1.91	46.17	30.83	21.35	23.59	-3.98	-6.47	-7.00	-5.54	-5.75
UBE2N	7334	32.64	18.52	15.13	15.58	-2.09	-3.40			28.61	28.53	25.69	31.62	-5.90	-5.55			-5.72
KIAA0195	9772	75.35	36.05	56.04	58.81	-1.25	-2.91	-2.77	-1.14	34.43	48.32	21.66	32.20	-6.98	-3.47	-8.71	-3.60	-5.69
FLJ13154	79650	40.96	18.81	26.03	14.90	-3.20	-5.42	-5.62	-4.99	23.60	30.25		30.58	-7.05	-6.37		-3.64	-5.69
C22ORF16	400916	27.67	29.33	28.15	17.57	-3.19	-2.93	-3.52	-3.67	38.39	23.89	23.53	24.03	-4.59	-8.69	-4.10	-5.29	-5.67
CDC45L	8318	65.94	68.47	85.56	44.54	-1.12	-0.89	-0.58	-1.38	32.84	33.66	19.05	21.71	-5.50	-6.33	-5.02	-5.82	-5.67
BAGE4	85317	43.12	56.74	43.80	55.99	-2.22	-1.44	-2.38	-1.22	38.15	37.58	21.40	20.65	-5.47	-5.60	-6.00	-5.38	-5.61
BIK	638	129.92	128.22	119.10	92.00	0.39	0.48	0.15	0.27	31.81	39.92	36.89	24.41	-7.61	-4.64	-4.90	-5.07	-5.55
HUS1	3364	132.70	109.17	101.94	118.79	0.45	0.30	0.17	1.03	35.62	21.13	20.04	20.49	-3.79	-7.89	-5.39	-4.86	-5.48
SDOS	84309	98.44	51.71	56.16	51.67	-0.45	-2.19	-2.43	-1.48	37.06	32.03	24.36	22.62	-4.58	-6.62	-5.56	-5.15	-5.48
GPC6	10082	59.99	33.69	50.07	32.10	-1.67	-2.42	-2.14	-2.83	31.25	45.78	24.17	27.05	-6.75	-3.97	-6.30	-4.83	-5.46
TCOF1	6949	96.40	88.90	94.83	58.00	-0.29	-0.97	-0.41	-0.94	26.78	64.15	20.98	15.56	-5.93	-2.50	-6.20	-7.20	-5.46
JUP	3728	30.56	21.84	40.01	27.28	-2.76	-3.43	-2.89	-2.63	34.28	47.33	25.18	28.47	-6.63	-4.51	-5.99	-4.57	-5.42
CARD4	10392	92.68	126.86	128.25	91.94	0.12	0.32	0.48	0.34	51.89	41.04	24.45	18.07	-3.19	-5.60	-4.95	-7.88	-5.40
OR5A1	219982	80.29	75.41	61.33	53.13	-0.66	-0.74	-1.46	-1.36	37.05	46.52	22.81	17.77	-5.67	-4.19	-5.66	-6.07	-5.40
CCNA2	890	30.25	23.89	22.04	13.18	-1.86	-2.51			38.49	32.14	29.37	29.76	-4.70	-6.04			-5.37
MGC2747	79086	147.66	122.91	132.10	95.24	0.55	0.24	0.48	0.35	84.47	100.47		66.26	-8.07	-7.46		-0.49	-5.34
SHMT1	6470	30.82	37.91	58.87	28.03	-1.61	-1.68	-1.10	-1.64	30.75	32.39	24.34	28.33	-5.96	-6.59	-4.31	-4.46	-5.33
FZD4	8322	26.02	26.63	34.09	19.58	-2.38	-3.28	-2.92	-3.34	39.54	49.63	19.12	24.12	-6.33	-3.39	-5.55	-5.93	-5.30
CHMP1.5	57132	42.62	71.04	86.58	19.23	-2.35	-1.31	-0.92	-4.34	36.24	33.85	23.85	25.75	-4.71	-6.25	-5.67	-4.50	-5.28
APRIN	23047	27.98	42.80	52.69	23.73	-2.32	-1.60	-1.39	-2.16	31.32	27.62	24.47	25.37	-4.56	-7.20	-4.59	-4.73	-5.27
FGF11	2256	23.80	27.78	25.04	42.93	-2.19	-2.74	-2.42	-1.33	37.69	35.13	18.03	40.76	-4.93	-7.06	-5.57	-3.49	-5.26
BTN3A3	10384	36.50	52.52	51.49	29.47	-3.43	-1.91	-3.09	-3.32	48.29	39.63	24.26	29.64	-4.28	-4.68	-7.90	-4.04	-5.22
RFC5	5985	71.49	59.94	82.05	51.47	-0.80	-1.73	-0.81	-1.54	34.21	61.92	25.41	23.75	-5.32	-2.94	-6.27	-6.25	-5.20
HIRA	7290	80.32	70.99	84.97	77.49	-0.53	-1.18	-0.70	-0.14	32.20	48.17	26.60	34.06	-5.75	-4.62	-5.95	-4.36	-5.17
ODF2	4957	36.45	37.02	48.97	42.40	-1.88	-1.84	-1.89	-1.63	31.28	31.59	24.56	31.11	-5.37	-6.07	-4.92	-4.30	-5.17
ACP6	51205	144.20	124.05	128.37	113.75	0.58	0.52	0.64	0.95	25.04	32.41	20.34	23.00	-5.57	-5.39	-5.32	-4.36	-5.16
RALY	22913	44.32	38.11	34.58	3.33	-1.85	-2.82			43.85	35.51	23.21	-80.25	-3.86	-6.45			-5.16
UNC45B	146862	57.10	44.95	32.60	26.81	-0.92	-1.32	-2.09	-1.49	39.30	30.89	23.84	25.61	-4.21	-6.11	-5.28	-4.95	-5.14
KRTHA3B	3884	37.31	50.43	43.73	23.32	-3.49	-2.50	-3.63	-3.70	35.42	35.91		21.99	-4.77	-5.28		-5.35	-5.13
FLJ43374	377007	43.76	57.61	51.02	39.68	-2.45	-2.49	-3.09	-2.35	35.41	31.98	25.18	26.22	-4.92	-7.42	-4.32	-3.85	-5.13
GNA13	10672	27.46	20.18	25.22	15.96	-1.91	-2.60	-2.31	-2.98	28.93	48.08	22.73	17.82	-4.67	-3.07	-6.48	-6.29	-5.13
SERPINA6	866	71.39	79.55	82.28	51.38	-0.43	-0.65	-0.65	-1.17	37.09	36.09	29.79	30.08	-5.21	-6.58	-3.89	-4.75	-5.11
SAP30	8819	28.50	38.58	36.49	20.96	-1.89	-2.04	-1.76	-2.78	45.41	38.92	27.87	23.85	-3.72	-6.27	-3.62	-6.82	-5.11
RNF43	54894	18.09	24.70	26.00	17.44	-7.25	-5.90	-6.49	-7.09	41.88	44.11	26.59	49.79	-4.67	-7.65	-4.75	-3.36	-5.11

		Mock								ATRi								
		% of Control				Robust Z-score				% of Control				Robust Z-score				
Gene Symbol	Gene ID	Rep 1	Rep 2	Rep 3	Rep 4	Rep 1	Rep 2	Rep 3	Rep 4	Rep 1	Rep 2	Rep 3	Rep 4	Rep 1	Rep 2	Rep 3	Rep 4	Average
KRT6B	3854	41.71	32.46	41.36	17.40	-2.07	-2.80	-3.17	-2.05	40.46	31.49	28.25	28.37	-4.61	-6.98	-5.67	-3.17	-5.11
FLJ33620	151790	68.11	64.00	60.42	40.93	-1.43	-1.28	-1.72	-2.14	54.02	31.22		21.83	-2.63	-7.46		-5.21	-5.10
B4GALT2	8704	21.51	19.17	15.80	15.52	-2.61	-2.87			37.49	40.21	36.90	50.49	-5.23	-4.92			-5.07
HTR2A	3356	144.72	141.30	116.61	113.81	0.69	0.62	0.26	0.83	9.33	72.60	58.90	53.63	-17.82	-0.86	0.04	-1.43	-5.02
BIRC1	4671	32.39	33.62	21.71	25.51	-1.39	-1.94	-2.41	-2.13	31.33	36.05	24.13	27.06	-5.07	-5.50	-4.37	-5.05	-5.00
NR2C2	7182	76.60	79.64	81.24	62.70	-0.18	-0.07	-0.15	-0.23	25.70	41.04	31.02	26.64	-6.14	-5.26	-3.93	-4.60	-4.98
MSI2	124540	38.55	41.51	43.52	20.27	-2.35	-2.07	-2.40	-3.30	29.46	51.07	28.69	20.61	-5.68	-3.63	-4.18	-6.42	-4.98
THG-1	81628	181.00	167.24	147.82	117.00	1.09	1.09	0.84	1.05	87.55	97.70		78.75	-9.38	-5.92		0.42	-4.96
KIAA0746	23231	58.03	54.54	48.93	18.01	-1.43	-1.61	-2.59	-3.17	48.47	30.77	35.55	28.31	-2.87	-8.62	-4.65	-3.62	-4.94
XAB1	11321	31.50	28.97	29.75	19.58	-3.12	-2.72	-3.63	-3.93	44.44	37.72	20.48	19.75	-4.21	-4.30	-5.78	-5.36	-4.91
SLC12A8	84561	66.59	73.69	78.78	68.20	-0.95	-1.00	-1.36	-0.42	35.28	37.91	31.17	24.85	-5.23	-5.96	-3.76	-4.66	-4.90
USP50	373509	61.73	92.90	88.42	63.77	-1.12	-0.32	-0.62	-0.74	54.86	44.62	20.85	29.76	-3.04	-4.93	-7.10	-4.34	-4.85
GPC3	2719	76.94	105.31	92.03	38.00	-0.72	-0.12	-0.51	-1.41	30.07	46.65	35.07	19.69	-4.82	-4.46	-3.27	-6.83	-4.84
BIN2	51411	136.48	113.28	97.54	59.82	0.50	0.07	-0.31	-1.10	53.90	26.95		26.53	-2.37	-7.24		-4.92	-4.84
LETM2	137994	54.15	28.61	32.90	44.46	-1.65	-3.14	-3.16	-1.86	32.88	62.62	18.16	29.18	-6.49	-2.23	-6.88	-3.77	-4.84
GABARAPL2	11345	68.57	43.72	35.39	46.18	-0.37	-1.01	-1.55	-0.77	35.36	38.23	22.79	34.12	-4.31	-5.77	-5.73	-3.37	-4.80
SYMPK	8189	47.29	38.89	51.14	35.34	-1.91	-2.41	-2.45	-1.71	31.82	46.56	30.93	32.86	-5.46	-5.19	-5.52	-2.90	-4.77
KCNJ2	3759	10.15	27.20	44.48	29.01			-2.27	-1.88	24.52	35.64	25.65	17.55			-4.46	-5.06	-4.76
CYP2A13	1553	80.47	88.18	94.98	76.97	-0.10	-0.30	-0.04	0.01	31.62	45.26	28.72	34.72	-5.53	-4.81	-4.31	-4.22	-4.72
UCP2	7351	133.66	156.82	139.67	103.67	0.76	0.95	0.81	0.85	30.10	34.54	29.80	25.07	-4.45	-4.98	-4.75	-4.65	-4.71
GPR63	81491	46.05	60.53	74.11	36.82	-1.35	-1.36	-0.91	-1.84	44.34	40.24	25.21	31.55	-5.42	-4.78	-4.18	-4.41	-4.70
MGC14560	51184	48.30	25.38	41.50	37.73	-2.26	-3.36	-3.18	-2.14	35.40	39.05	38.97	27.39	-4.77	-6.35	-3.00	-4.55	-4.67
ASB9	140462	42.90	74.87	54.15	33.99	-1.69	-0.70	-1.66	-1.81	34.89	32.53	27.67	33.84	-4.16	-6.24	-5.08	-3.05	-4.63
FLJ32028	201799	17.35	17.28	14.55	25.80			-7.12	-3.44	28.68	42.21	18.63	38.40			-6.17	-2.99	-4.58
SLC17A1	6568	67.24	62.76	78.95	75.72	-0.45	-0.81	-0.37	-0.56	46.08	38.49	31.25	35.08	-3.88	-5.20	-4.10	-5.12	-4.58
CXCL3	2921	70.74	60.72	116.72	43.27	-0.35	-0.96	0.14	-0.96	43.31	32.09	27.78	23.36	-2.93	-6.23	-3.99	-5.13	-4.57
KIRREL2	84063	72.55	81.43	85.30	12.48	-0.77	-0.66	-0.70	-2.58	36.02	39.54	33.30	31.26	-5.40	-5.43	-4.67	-2.75	-4.56
WDR4	10785	40.08	20.42	37.58	18.26	-2.29	-3.94	-3.43	-3.14	28.85	58.36	35.08	26.30	-6.06	-3.31	-4.74	-3.97	-4.52
WASF1	8936	48.45	44.40	41.34	28.28	-2.28	-2.12	-2.85	-2.83	48.29	43.70	25.67	21.32	-3.14	-3.66	-5.73	-5.48	-4.50
MAPKAPK5	8550	35.09	33.78	28.71	26.59	-1.57	-1.73	-2.37	-1.83	34.23	34.17	25.81	21.49	-3.99	-5.08	-4.22	-4.65	-4.49
ARMET	7873	81.23	130.45	107.50	79.76	-0.68	0.22	-0.19	0.00	25.86	36.60	38.10	41.00	-6.48	-5.91	-2.71	-2.78	-4.47
KIAA1720	80851	148.84	157.55	125.81	106.57	0.54	0.43	0.22	0.54	79.99	7.43	65.68	75.52	0.10	-18.38	-0.03	0.53	-4.45
ADAM29	11086	13.29	19.52	35.32	32.20			-2.73	-1.66	31.42	59.31	25.66	20.55			-4.46	-4.41	-4.43
ANAPC10	10393	35.52	36.66	35.72	34.48	-2.48	-3.34	-3.26	-2.91	48.43	48.24	27.44	33.31	-2.90	-4.61	-5.74	-4.48	-4.43
ITGAV	3685	37.85	38.46	36.60	24.74	-1.50	-1.84	-2.14	-2.25	49.34	47.60	21.60	33.60	-2.56	-4.35	-6.29	-4.44	-4.41
RP11-564C4.1	653308	67.19	72.90	73.08	48.88	-1.54	-1.21	-1.42	-1.90	40.77	42.61		24.49	-3.20	-4.21		-5.71	-4.37
SP110	3431	57.80	39.52	54.95	19.83	-1.60	-2.05	-1.84	-3.89	40.52	42.31	25.72	25.63	-4.85	-3.68	-4.72	-4.18	-4.36
SYCP2	10388	147.89	97.69	136.68	63.93	0.48	-0.29	0.59	-0.29	45.98	43.66	30.08	23.61	-2.62	-4.93	-4.06	-5.80	-4.35
FEM1B	10116	37.43	31.39	28.91	19.46	-1.50	-2.02	-2.56	-2.42	34.17	42.17	31.80	29.87	-5.49	-4.34	-3.93	-3.65	-4.35
LOC129521	129521	79.18	68.34	52.19	28.29	-0.94	-1.26	-2.76	-3.18	36.10	44.85	24.81	34.38	-4.20	-4.80	-4.75	-3.59	-4.34
OBP2A	29991	36.04	28.83	35.51	19.17	-2.89	-2.86	0.25	0.39	33.02	24.57		16.82	-5.24	-7.50		-0.26	-4.33
IRX2	153572	164.17	152.24	142.51	119.39	1.09	0.94	1.08	1.03	41.42	49.10	29.61	26.41	-4.58	-3.34	-4.13	-5.28	-4.33
ECRG4	84417	22.56	19.59	24.68	15.30	-4.44	-4.86			52.60	39.37		37.53	-3.10	-5.55			-4.33
LBP	3929	35.08	13.18	25.94	11.99	-1.64	-4.03			29.57	56.04	47.97	37.56	-5.50	-3.15			-4.32
FLJ33516	139221	24.47	34.22	22.03	24.51	-3.06	-2.99	-4.68	-2.68	48.71	35.44	18.76	27.54	-2.33	-6.59	-5.13	-3.22	-4.32
FLJ45235	339416	107.87	126.42	122.02	80.23	-0.29	0.31	0.23	-0.23	83.75	89.99		65.64	-7.06	-5.28		-0.54	-4.29
WNT8B	7479	37.16	33.70	38.00	43.56	-3.05	-2.52	-3.41	-2.08	42.52	35.39	28.53	38.13	-4.40	-5.22	-4.31	-3.24	-4.29
CSNK2B	1460	104.24	112.04	98.89	64.52	0.00	0.17	0.00	-0.31	49.17	45.33	36.58	24.81	-3.44	-4.53	-3.86	-5.34	-4.29
SETD1A	9739	84.41	91.29	70.55	45.98	-0.56	-0.36	-0.83	-0.72	28.15	48.63	32.54	24.59	-5.99	-2.74	-3.08	-5.28	-4.27
CLEC2	51266	53.44	65.03	47.49	50.88	-0.84	-0.77	-1.58	-0.74	40.97	46.80	30.38	32.12	-3.63	-4.48	-4.27	-4.71	-4.27
ALS2CR7	65061	88.39	76.20	69.73	73.23	-0.10	-0.42	-0.77	-0.25	33.14	59.13	28.61	25.43	-5.45	-2.24	-4.59	-4.80	-4.27
C14ORF123	29082	39.36	51.69	62.55	46.20	-2.71	-2.81	-2.34	-1.91	36.20	48.18	25.09	28.18	-4.78	-4.34	-4.34	-3.55	-4.25
MK-STYX	51657	120.34	103.34	95.52	52.82	0.30	0.20	0.04	-0.52	33.89	45.88	18.79	25.53	-4.04	-3.37	-5.69	-3.91	-4.25
FOXD4L1	200350	64.23	44.72	52.89	37.04	-1.53	-1.87	-2.29	-2.59	33.41	61.02	21.59	38.76	-6.05	-2.09	-5.67	-3.15	-4.24
OR13C9	286362	164.26	116.41	149.43	93.49	0.66	0.34	0.77	0.65	42.70	45.47	36.17	23.87	-3.10	-3.84	-4.07	-5.94	-4.24
INS-IGF2	723961	52.91	55.77	82.56	55.58	-1.44	-1.50	-0.67	-0.93	51.18	39.44	23.76	32.75	-3.43	-5.08	-5.55	-2.89	-4.24
RFC4	5984	94.15	129.82	100.92	80.53	0.00	0.09	-0.33	-0.15	42.31	56.90	31.09	35.38	-3.39	-3.69	-5.71	-4.15	-4.24
DPYSL3	1809	17.35	33.10	19.76	22.14	-3.97	-3.84	-5.20	-4.03	56.52	39.78	41.38	31.92	-1.87	-6.76	-3.52	-4.78	-4.23
DATF1	11083	49.92	50.73	63.41	33.76	-1.90	-2.01	-2.10	-2.68	43.43	50.83	22.92	27.93	-3.20	-3.86	-5.14	-4.71	-4.23
CATSPER1	117144	26.80	20.06	14.43	12.09	-2.41	-3.25			29.39	48.85	48.61	37.05	-5.73	-2.72			-4.22
PADI1	29943	80.43	58.96	68.76	39.72	-0.37	-2.18	-1.48	-2.28	47.54	53.74	35.12	30.62	-2.78	-4.18	-4.78	-5.04	-4.20
OSTBETA	123264	14.72	24.79	25.27	23.14			-3.85	-3.07	66.36	45.30	31.89	24.56			-3.99	-4.34	-4.17
RPAP1	26015	89.81	68.70	69.90	53.69	-0.43	-1.08	-1.28	-0.67	27.65	56.76	27.29	33.82	-5.26	-3.06	-4.57	-3.77	-4.16
KIAA0963	22904	128.49	126.48	112.46	76.44	0.15	0.30	0.00	-0.34	42.59	44.89	39.22	21.48	-3.76	-4.32	-3.14	-5.41	-4.16
PIK3R4	30849	82.00	84.92	74.16	50.69	-0.36	-0.37	-0.59	-0.77	43.38	41.89	43.53	29.16	-4.28	-5.08	-2.76	-4.49	-4.15
DKFZP434I116	25962	79.95	81.74	70.99	33.01	-0.74	-0.76	-1.22	-1.98	45.27	44.02	16.58	27.75	-2.73	-5.00	-5.67	-3.19	-4.15
MGC42367	343990	53.93	55.69	46.19	41.34	-2.13	-1.96	-2.89	-2.47	53.00	49.80		25.49	-3.05	-3.89		-5.50	-4.15
PRO2730	80335	117.61	95.79	108.58	67.91	-0.08	-0.44	0.01	-0.40	31.15	60.31	24.41	24.49	-4.69	-2.96	-3.98	-4.95	-4.15
KIR2DL4	3805	55.38	43.87	34.27	17.19	-1.71	-1.82	-3.22	-4.30	35.44	42.41	34.86	28.10	-5.78	-3.67	-3.31	-3.76	-4.13
ALG12	79087	134.54	158.13	140.69	112.63	0.79	1.01	0.78	0.80	36.57	66.13	24.95	22.79	-4.12	-1.81	-5.20	-5.38	-4.13
PCBD	5092	35.96	37.84	38.26	41.91	-1.23	-1.73	-1.45	-1.16	34.38	46.26	17.14	47.08	-4.51	-3.89	-6.03	-2.03	-4.11
FLJ27505	389320	67.48	87.79	90.67	53.88	-1.09	-0.58	-0.61	-0.94	25.02	50.10	37.17	38.50	-6.68	-3.76	-2.83	-3.11	-4.10
GSH-2	170825	41.80	71.84	64.78	39.62	-2.57	-1.85	-2.21	-2.36	33.84	48.18	27.43	33.25	-5.20	-4.34	-3.94	-2.87	-4.09
SNX6	58533	19.52	28.15	31.83	24.17	-3.81	-2.88	-3.54	-2.90	40.39	45.18	37.32	43.27	-5.38	-4.84	-3.68	-2.43	-4.08
PIGB	9488	116.46	120.24	103.10	58.06	0.10	-0.06	-0.21	-0.94	18.70	76.07	33.08	36.37	-8.07	-1.51	-3.77	-2.91	-4.06
DXYS155E	8227	94.58	99.91	89.46	73.41	-0.56	-0.30	-0.93	-0.50	35.77	41.18	28.31	42.54	-4.25	-5.44	-4.10	-2.44	-4.06
GCKR	2646	47.85	58.84	59.90	35.46	-0.90	-0.88	-1.07	-1.21	39.14	48.79	28.85	29.13	-4.52	-3.83	-3.51	-4.31	-4.04
FLJ14904	84944	97.99	62.05	50.90	38.99	-0.53	-1.89	-3.05	-2.21	38.01	37.12		36.91	-4.37	-5.07		-2.66	-4.03
XKRX	402415	43.86	46.40	43.84	22.68	-2.04	-2.52	-2.71	-4.22	45.75	47.58		24.56	-3.23	-3.50		-5.35	-4.03
NDUFV3	4731	33.71	40.69	38.60	29.40	-2.64	-2.11	-2.70	-2.40	44.36	51.27	26.24	28.65	-3.18	-3.60	-4.65	-4.68	-4.03
OR2V2	285659	58.67	66.81	67.33	34.09	-0.94	-0.47	-1.25	-1.36	49.27	30.53	31.72	34.74	-2.22	-6.00	-4.98	-2.87	-4.02
LPHN2	23266	24.75	40.71	35.19	35.72	-2.46	-2.28	-2.84	-1.91	50.36	48.52	34.10	26.27	-4.41	-3.54	-2.68	-5.45	-4.02
KIAA0186	9837	91.61	88.73	82.48	50.25	-0.48	-0.55	-0.77	-1.01	38.41	36.85	27.76	31.65	-3.63	-6.31	-3.42	-2.66	-4.00
PRKCH	5583	59.81	54.04	41.99	39.24	-0.84	-1.25	-1.75	-1.26	46.43	43.17	33.04	40.09	-3.82	-4.87	-4.50	-2.80	-4.00
FLJ10375	55129	91.95	107.72	86.07	36.66	-0.64	-0.68	-1.17	-2.58	35.57	43.49	26.12	42.91	-4.89	-5.11	-4.16	-1.81	-3.99
RAP2C	57826	21.93	31.74	31.24	24.49	-3.42	-3.96	-3.83	-3.73	51.56	57.12	38.74	26.57	-2.35	-3.66	-4.03	-5.92	-3.99
RABGGTA	5875	38.45	36.61	37.69	30.19	-1.45	-1.70	-1.71	-2.10	56.45	44.06	22.59	32.91	-2.77	-4.02	-5.24	-3.91	-3.99
MCM3	4172	41.23	42.45	32.95	36.61	-1.24	-1.56	-1.94	-1.50	49.28	40.37	39.05	31.82	-2.89	-5.66	-2.62	-4.73	-3.97
KIAA1533	57655	23.66	28.82	37.69	20.46	-3.68	-3.81	-3.83	-4.16	33.74	49.96	34.15	32.49	-5.13	-3.59	-3.85	-3.32	-3.97
FLJ40160	128209	74.41	63.78	68.75	67.50	-1.35	-2.23	-1.88	-1.09	51.06	41.30	36.51	39.30	-2.94	-5.93	-3.67	-3.35	-3.97
GALNTL4	374378	30.52	36.92	57.22	22.88	-1.63	-1.73	-1.17	-2.00	39.65	49.45	26.02	33.00	-4.45	-3.74	-4.00	-3.64	-3.95

		Mock								ATRi								
		% of Control				Robust Z-score				% of Control				Robust Z-score				
Gene Symbol	Gene ID	Rep 1	Rep 2	Rep 3	Rep 4	Rep 1	Rep 2	Rep 3	Rep 4	Rep 1	Rep 2	Rep 3	Rep 4	Rep 1	Rep 2	Rep 3	Rep 4	Average
ATP6V0D1	9114	34.82	28.03	32.25	28.50	-1.63	-2.22	-2.32	-1.72	37.90	55.67	24.63	34.58	-4.80	-2.60	-5.40	-2.99	-3.95
GPR2	2826	63.77	57.31	64.78	42.24	-0.77	-1.48	-1.26	-1.52	43.66	52.38	27.56	37.24	-5.54	-3.03	-3.73	-3.48	-3.95
CCNB1IP1	57820	59.69	70.49	86.66	51.36	-0.91	-0.38	-0.60	-0.62	35.66	47.63	36.68	24.63	-3.97	-3.20	-4.07	-4.51	-3.94
RHOF	54509	44.90	25.86	35.61	34.45	-1.92	-4.48	-3.26	-2.91	38.17	59.42	32.03	42.04	-4.56	-3.22	-4.68	-3.26	-3.93
FLJ23657	152816	71.64	51.90	62.80	29.00	-1.09	-2.03	-1.56	-2.56	38.90	43.86	24.01	39.62	-3.52	-5.42	-4.05	-2.67	-3.92
ZNF620	253639	35.30	36.41	42.99	19.58	-2.58	-2.57	-3.00	-2.98	34.98	59.57	36.53	31.18	-4.88	-3.14	-4.48	-3.15	-3.91
SEPHS1	22929	71.36	52.09	36.67	35.33	-0.92	-2.57	-2.67	-2.28	27.78	50.83	40.10	33.46	-5.71	-3.86	-2.74	-3.33	-3.91
C14ORF28	122525	28.97	29.35	24.97	8.05	-2.25	-2.29			27.09	56.84	44.18	46.44	-5.28	-2.53			-3.91
ITGAL	3683	24.88	45.82	42.50	35.48	-1.78	-1.38	-1.28	-1.48	56.22	49.80	24.03	21.96	-1.59	-3.41	-4.39	-6.19	-3.89
SLC2A12	154091	69.28	61.53	51.14	18.79	-0.72	-2.06	-2.36	-4.52	63.70	43.50	31.43	44.87	-1.24	-5.99	-5.63	-2.68	-3.89
GALNAC4S-6ST	51363	22.59	41.05	26.93	24.83	-2.28	-1.91	-2.29	-2.44	48.70	46.45	28.99	38.01	-3.27	-4.91	-3.44	-3.93	-3.89
NPL	80896	25.01	28.00	29.20	22.35	-2.11	-2.73	-2.15	-2.65	42.87	37.26	36.83	48.23	-4.09	-6.61	-2.37	-2.45	-3.88
CPSF3	51692	101.51	76.64	103.12	75.00	-0.31	-1.09	-0.40	-0.18	39.51	37.39	22.11	47.61	-5.30	-5.34	-3.61	-1.24	-3.87
PTP4A1	7803	91.59	73.20	63.54	65.58	-0.19	-1.00	-1.10	-0.59	37.18	48.54	37.52	42.15	-4.89	-4.01	-3.50	-3.06	-3.87
CPR8	9236	15.92	26.75	18.01	10.71	-4.58	-4.02			50.74	40.70	24.64	33.11	-2.73	-4.99			-3.86
CYGB	114757	21.85	14.58	24.24	47.46			-3.70	-2.20	63.75	52.29	48.44	48.29			-4.71	-2.99	-3.85
ZNF383	163087	26.33	28.92	21.64	17.44	-3.75	-3.11			74.39	25.53	46.59	33.82	-0.77	-6.92			-3.85
TIGD7	91151	84.42	37.16	55.84	32.21	-0.82	-2.21	-1.83	-2.82	44.62	54.86	32.20	33.94	-4.23	-2.83	-4.66	-3.64	-3.84
LOC120237	120237	15.10	12.58	23.86	29.84			-5.81	-4.47	38.13	33.94	27.67	46.02			-5.17	-2.50	-3.83
C1orf162	128346	67.65	71.92	84.64	59.08	-1.06	-0.77	-0.61	-0.68	47.28	37.90	23.31	43.33	-3.37	-5.51	-4.14	-2.25	-3.82
ZNF297B	23099	47.39	13.32	38.07	11.81	-2.37	-5.09	-3.07	-5.71	41.67	36.57		53.02	-4.24	-6.24		-0.97	-3.82
GALGT2	124872	29.64	31.24	42.43	19.03	-1.96	-2.27	-1.82	-2.81	35.00	58.86	34.03	34.25	-4.53	-2.79	-3.60	-4.33	-3.81
SYTL3	94120	38.18	43.33	47.57	26.78	-5.00	-4.18	-4.21	-5.45	49.04	54.53	37.40	51.20	-3.50	-5.38	-3.19	-3.14	-3.80
LOC340267	340267	31.68	42.05	26.81	20.97	-3.72	-3.84	-5.38	-5.93	46.23	43.89	36.71	45.93	-3.55	-5.44	-3.64	-2.51	-3.78
MGC14126	84984	45.99	36.37	45.37	26.74	-2.38	-2.53	-2.89	-3.15	46.73	41.52	31.21	42.85	-3.07	-5.87	-4.10	-2.10	-3.78
MGC2198	192286	146.73	104.71	126.07	97.57	0.53	-0.31	0.37	0.44	39.93	48.09	33.66	51.75	-4.44	-4.72	-4.11	-1.86	-3.78
CHST6	4166	38.36	59.30	49.98	26.34	-1.26	-0.86	-1.46	-1.75	48.60	55.14	28.62	24.13	-3.24	-3.00	-3.55	-5.33	-3.78
CGI-119	51643	31.96	29.82	44.80	23.57	-3.52	-3.69	-2.99	-4.38	55.65	44.37		32.61	-3.34	-3.78		-4.21	-3.78
MGC26988	153745	14.74	49.87	40.95	8.34	-5.12	-2.91	-3.90	-6.91	46.67	35.72	25.74	52.16	-3.22	-6.59	-4.23	-1.00	-3.76
UBE2M	9040	80.63	50.30	58.09	35.68	-0.63	-1.49	-1.26	-1.19	39.85	41.04	31.32	29.92	-3.86	-3.64	-3.25	-4.24	-3.75
FZR1	51343	36.20	55.70	55.40	45.11	-2.40	-1.54	-2.17	-0.54	26.06	65.53	38.48	40.56	-7.59	-1.99	-3.79	-1.62	-3.75
HTR3E	285242	112.17	142.75	78.78	63.56	-0.10	0.50	-0.58	-0.12	33.89	38.40	36.36	34.23	-4.85	-3.99	-2.56	-3.53	-3.73
LOC653192	653192	77.76	81.49	58.09	73.32	-2.85	-2.24	-3.46	-1.59	52.81	62.13	38.77	40.45	-2.95	-3.98	-3.03	-4.95	-3.73
DUX1	26584	134.55	86.38	88.17	82.26	0.79	0.06	-0.01	0.25	42.48	53.42	34.60	24.84	-3.26	-3.35	-3.29	-4.95	-3.71
SSTK-IP	128229	66.29	42.91	47.98	34.41	-1.50	-2.25	-2.39	-2.64	47.89	44.84		34.07	-3.37	-4.68		-3.08	-3.71
LOC165186	165186	110.23	37.65	55.67	19.93	-0.30	-2.50	-1.97	-3.76	50.14	41.53	27.41	36.43	-2.94	-3.97	-5.36	-2.58	-3.71
NAV1	89796	70.33	86.64	87.13	58.80	-0.27	-0.18	-0.25	-0.30	48.55	49.75	25.17	32.46	-3.25	-3.69	-4.15	-3.73	-3.70
CNGA1	1259	123.66	75.71	85.47	72.51	0.06	-0.71	-0.39	0.12	46.47	37.21	26.79	32.70	-2.92	-4.15	-3.98	-3.77	-3.70
MDS006	56985	132.41	82.41	89.70	70.02	0.06	-0.65	-0.63	-0.33	52.60	40.24	41.75	32.03	-2.34	-6.11	-2.66	-3.70	-3.70
POLE2	5427	80.28	76.40	77.97	64.15	-0.04	-0.47	-0.25	-0.33	44.73	37.90	37.51	30.47	-2.95	-5.18	-2.22	-4.40	-3.69
WBSCR27	155368	33.47	20.45	24.64	15.88	-1.52	-2.75	-2.65	-3.40	44.12	47.95	33.50	35.21	-3.37	-3.75	-3.67	-3.96	-3.69
FOXJ2	55810	19.21	24.46	30.93	24.56	-2.82	-2.45	-2.23	-3.91	45.94	49.18	31.57	47.56	-3.90	-3.60	-4.04	-3.16	-3.68
ADAMTS15	170689	27.44	51.73	89.88	47.44	-0.66	-1.24	-0.85	-0.84	28.16	46.04	35.88	29.15	-3.80	-4.96	-2.96	-2.96	-3.67
LOC115548	115548	38.76	33.34	12.39	18.77	-3.16	-4.74			42.39	57.78	43.34	26.92	-4.08	-3.26			-3.67
PEF1	553115	51.55	57.93	48.70	45.31	-1.50	-1.41	-2.09	-1.43	65.34	48.81	30.76	21.89	-1.90	-3.65	-4.18	-4.93	-3.67
PROK1	84432	27.00	48.65	46.70	32.99	-1.66	-1.28	-1.12	-1.63	41.85	50.82	27.17	31.56	-3.35	-3.28	-3.79	-4.21	-3.66
CLIC3	9022	88.44	56.04	57.83	31.42	-0.48	-1.29	-1.27	-1.42	38.51	45.64	33.76	28.12	-4.07	-3.08	-2.90	-4.57	-3.66
ANAPC11	51529	54.91	35.26	48.29	28.07	-3.90	-4.81	-4.16	-5.27	49.79	53.28	34.18	59.42	-3.38	-5.63	-3.60	-2.00	-3.65
MGC4707	79096	51.33	107.95	60.64	40.26	-2.06	-0.67	-2.46	-2.31	40.94	43.19	34.79	35.93	-4.03	-5.16	-2.87	-2.55	-3.65
C21ORF106	23181	99.96	100.79	121.03	68.79	0.00	-0.03	0.34	-0.55	33.18	53.79	43.98	47.25	-5.54	-3.88	-2.50	-2.65	-3.64
SOX18	54345	72.48	69.77	61.75	43.85	-0.17	-0.50	-0.73	-1.19	52.03	47.79	33.47	31.50	-2.46	-3.77	-3.68	-4.64	-3.64
NPHS2	7827	35.54	29.54	24.35	29.27	-1.48	-1.94	-2.38	-1.74	32.07	47.74	34.93	31.35	-4.11	-3.11	-3.73	-3.57	-3.63
RKHD3	84206	117.42	101.76	82.10	70.19	-1.61	-1.56	-2.16	-1.76	46.29	64.39	34.77	49.15	-3.93	-3.60	-3.52	-3.46	-3.63
AHCY	191	26.89	20.92	21.22	14.18	-2.06	-2.75			48.90	43.46	34.66	36.11	-3.10	-4.15			-3.63
LOC113730	113730	24.96	16.69	21.07	13.29	-3.83	-6.09			52.63	45.54	35.62	58.16	-2.48	-4.76			-3.62
TRIM31	11074	32.60	29.69	30.42	30.75	-5.47	-5.34	-5.90	-4.92	69.69	52.73	40.68	39.93	-0.88	-5.74	-2.81	-5.05	-3.62
FSHB	2488	24.53	24.06	12.90	4.53	-2.52	-2.34			50.61	40.08	29.52	65.70	-2.69	-4.54			-3.62
MAF1	84232	144.23	154.70	121.74	113.30	0.84	0.84	0.52	0.93	51.14	46.12	32.56	35.13	-3.02	-4.38	-4.80	-2.25	-3.61
KIAA1049	22980	83.86	91.49	95.46	65.36	-0.96	-0.58	-0.56	-0.92	79.80	86.29		59.68	-4.79	-4.99		-1.04	-3.61
IRAK2	3656	43.19	55.75	47.81	42.06	-1.33	-1.19	-1.48	-1.12	54.94	50.54	38.39	29.57	-2.69	-3.76	-3.55	-4.41	-3.61
MCM10	55388	129.37	107.42	104.16	78.78	0.42	-0.01	-0.17	0.02	37.38	56.19	41.91	34.87	-4.47	-3.63	-3.63	-2.62	-3.59
BRD3	8019	134.71	124.10	119.32	81.43	0.66	0.50	0.50	-0.01	39.74	52.24	38.76	29.14	-4.32	-3.02	-2.95	-4.05	-3.58
LOC388284	388284	124.16	107.02	107.12	91.86	0.49	-0.02	0.08	0.60	37.84	42.65	45.56	40.77	-5.06	-4.91	-2.76	-1.60	-3.58
SDBCAG84	51614	62.77	48.64	90.70	79.26	-1.66	-1.86	-0.59	0.03	41.58	34.86	41.98	55.94	-3.78	-7.24	-2.63	-0.64	-3.57
GPR77	27202	62.37	28.74	41.54	30.96	-0.73	-2.25	-2.00	-2.14	50.70	54.40	39.11	21.37	-2.80	-2.76	-2.90	-5.74	-3.55
RAG1	5896	30.74	49.21	54.44	57.31	-5.65	-3.79	-3.71	-2.54	71.01	54.32	37.37	41.26	-0.74	-5.42	-3.19	-4.80	-3.54
PLA2G4D	283748	35.64	32.18	33.55	28.85	-1.41	-1.92	-2.00	-2.11	34.34	60.06	39.55	32.48	-4.75	-2.24	-2.69	-4.46	-3.53
FLJ14639	84901	43.35	40.85	37.66	25.78	-1.94	-2.54	-3.09	-2.56	34.76	55.50	21.54	35.90	-4.17	-3.29	-4.53	-2.14	-3.53
SDS3	64426	42.40	37.38	53.56	38.04	-2.91	-4.29	-2.81	-3.47	44.61	58.78	31.19	44.37	-3.76	-3.12	-4.52	-2.69	-3.52
IL17R	23765	21.22	30.83	35.89	8.40	-2.46	-2.05	-2.08	-3.95	42.96	56.73	34.27	26.72	-3.96	-2.49	-3.50	-4.15	-3.52
SLC22A12	116085	24.20	23.11	25.75	11.89	-2.14	-2.62			47.53	50.92	45.29	44.85	-3.11	-3.94			-3.52
FLJ20203	54856	45.59	0.23	-2.48	0.71	-2.47	-14.93			54.94	45.76		33.49	-2.52	-4.52			-3.52
PHLDA1	22822	28.64	22.63	13.84	7.83	-3.06	-3.70			51.87	50.10	46.23	54.46	-2.45	-4.58			-3.51
LOC100130958	100130958	43.44	73.27	84.29	55.07	-1.38	-0.62	-0.49	-0.48	32.50	50.21	30.10	38.43	-4.37	-3.34	-3.60	-2.72	-3.51
LOC340578	340578	88.01	98.06	92.14	62.81	-0.55	-0.30	-0.45	-0.49	35.57	49.24	30.07	31.01	-4.04	-4.17	-3.07	-2.74	-3.51
LOC51136	51136	29.65	45.34	30.17	25.49	-5.76	-4.04	-5.93	-5.64	55.84	49.14	47.84	52.64	-2.53	-6.49	-2.06	-2.93	-3.50
TIGD3	220359	20.11	14.72	27.24	30.91			-3.40	-3.72	71.91	84.96	51.27	50.55			-4.33	-2.67	-3.50
LAP1B	26092	87.64	85.92	81.52	60.08	-0.87	-0.92	-1.24	-0.96	45.11	46.88		31.62	-3.40	-3.58		-3.46	-3.48
IQCA	79781	85.07	53.35	52.21	30.96	-0.38	-1.51	-2.12	-2.35	40.65	60.72	32.95	52.23	-5.33	-2.72	-4.41	-1.46	-3.48
C15ORF24	56851	87.00	96.87	89.25	64.44	-0.13	-0.07	-0.07	-0.01	42.92	45.30	36.18	35.02	-3.68	-3.80	-3.16	-3.25	-3.47
TBL2	26608	104.12	80.78	78.11	65.49	-0.01	-0.57	-0.80	-0.78	66.75	47.30	26.70	32.04	-1.63	-4.08	-4.83	-3.34	-3.47
ZNF517	340385	36.51	22.80	21.96	12.96	-2.91	-3.27			46.78	53.07	54.20	45.97	-3.89	-3.04			-3.47
CRISP3	10321	72.03	90.41	91.08	63.56	-0.79	-0.41	-0.47	0.01	47.61	49.68	35.03	36.28	-3.51	-3.87	-4.36	-2.11	-3.46
SCA2	6311	100.66	98.17	94.68	62.74	-0.43	-0.35	-0.73	-0.94	54.53	43.01	30.62	38.17	-1.96	-5.12	-3.72	-3.03	-3.46
CCL3L3	414062	38.04	29.56	23.15	10.46	-2.86	-3.06			42.80	47.89	37.56	38.89	-3.81	-3.10			-3.45
UHRF1	29128	113.34	79.22	74.13	58.46	-1.72	-2.33	-2.54	-2.46	48.95	61.52	44.06	47.22	-3.51	-4.09	-2.44	-3.76	-3.45
CYBASC3	220002	52.99	31.43	73.16	29.34	-1.87	-3.84	-1.71	-2.61	50.27	61.89	15.53	33.06	-3.65	-2.21	-4.94	-2.97	-3.44
MRPL11	65003	74.83	67.63	33.27	33.01	-0.95	-0.89	-3.30	-2.44	48.00	46.13	35.59	28.77	-3.67	-3.21	-3.22	-3.65	-3.44
CACNG6	59285	43.83	31.97	30.64	24.97	-1.62	-2.36	-2.71	-1.85	39.43	39.32	38.98	33.86	-3.92	-3.86	-2.24	-3.58	-3.40
GLRA1	2741	31.47	20.70	18.82	11.23	-2.15	-3.18			39.57	47.36	34.48	30.77	-3.90	-2.88			-3.39
CEI	153571	40.65	42.56	45.99	32.27	-2.46	-2.73	-3.13	-2.84	54.53	53.69	38.99	23.57	-2.31	-3.10	-3.17	-4.94	-3.38

		Mock								ATRi								
		% of Control				Robust Z-score				% of Control				Robust Z-score				
Gene Symbol	Gene ID	Rep 1	Rep 2	Rep 3	Rep 4	Rep 1	Rep 2	Rep 3	Rep 4	Rep 1	Rep 2	Rep 3	Rep 4	Rep 1	Rep 2	Rep 3	Rep 4	Average
LCT	3938	35.67	54.47	28.61	31.98	-1.24	-1.07	-1.94	-1.69	30.35	45.11	48.66	37.63	-5.25	-4.05	-0.96	-3.25	-3.38
TCFL1	6944	36.07	26.49	27.50	20.74	-1.59	-2.60	-2.74	-2.63	44.97	48.39	35.39	44.18	-3.09	-4.23	-3.37	-2.80	-3.37
GAGEC1	9506	71.95	78.18	92.42	66.55	-1.48	-1.20	-0.76	-0.66	45.07	40.65		40.51	-3.41	-4.49		-2.17	-3.36
HT014	57095	43.35	41.70	40.83	23.33	-2.10	-2.60	-2.79	-3.11	53.52	50.52	22.15	38.04	-1.83	-4.33	-4.39	-2.87	-3.35
LOC645037	645037	18.56	32.47	25.88	18.98	-3.61	-2.75	-3.78	-3.55	57.35	58.01	26.14	31.13	-2.72	-2.49	-5.05	-3.14	-3.35
FLJ21908	79657	140.63	93.51	113.22	98.53	0.58	-0.29	0.18	0.47	44.77	62.27	37.06	26.77	-4.26	-2.02	-3.20	-3.91	-3.35
GLRA4	441509	21.36	29.72	24.74	17.59	-2.78	-2.50	-3.19	-2.49	36.91	42.28	37.94	36.48	-4.33	-3.48	-2.36	-3.19	-3.34
BRI3	25798	103.77	76.01	115.56	60.75	-0.13	-0.86	-0.01	-0.65	40.83	55.23	34.59	36.81	-3.69	-3.10	-3.21	-3.35	-3.33
OPTC	26254	52.43	51.41	46.97	66.46	-1.94	-1.58	-0.46	0.01	44.33	33.57		30.73	-3.57	-5.56		-0.88	-3.33
OR3A2	4995	28.91	22.54	30.53	13.99	-2.79	-4.28	-4.76	-4.30	50.17	76.13	50.57	12.27	-3.02	-0.74	-1.34	-8.24	-3.33
DNA2L	1763	92.41	81.14	108.89	69.58	0.07	-0.23	0.41	-0.14	46.52	62.62	27.10	35.54	-3.85	-1.74	-4.24	-3.49	-3.33
MCM5	4174	79.30	104.26	93.55	57.86	-0.12	0.25	0.08	-0.34	36.03	39.46	36.84	41.36	-3.47	-4.21	-3.39	-2.24	-3.33
TMEM43	79188	31.45	23.55	39.91	27.72	-2.52	-3.50	-2.62	-2.63	51.01	53.87	27.43	38.57	-3.45	-2.99	-4.79	-2.06	-3.32
DYRK1B	9149	14.87	39.65	24.90	13.74	-2.93	-1.85			47.46	56.62	35.79	36.24	-3.68	-2.97			-3.32
PLA2R1	22925	84.80	75.90	60.36	89.48	-0.01	-0.48	-0.90	-0.06	48.80	40.09	35.59	62.05	-3.51	-4.94	-3.37	-1.45	-3.32
SLC16A11	162515	68.36	50.36	77.53	53.22	-0.91	-2.30	-0.97	-1.42	45.57	66.05	29.18	52.55	-3.33	-2.51	-5.32	-2.10	-3.31
CYP4F2	8529	20.24	22.77	23.65	72.82	-2.72	-2.57	-2.77	-0.68	54.51	47.62	44.36	38.58	-2.79	-3.81	-2.13	-4.51	-3.31
MGC16279	85002	53.33	45.66	52.13	58.54	-2.16	-2.51	-2.50	-1.29	49.64	49.80		44.68	-3.49	-3.89		-2.56	-3.31
DDHD1	80821	109.62	116.56	104.82	78.35	0.36	-0.22	-0.22	-0.24	31.65	78.66	44.05	34.25	-4.92	-0.92	-3.05	-4.35	-3.31
CDH1	999	43.04	35.94	36.93	21.68	-2.12	-2.60	-3.49	-2.77	44.09	57.34	37.47	39.73	-3.45	-3.46	-4.33	-2.00	-3.31
MGC52022	375346	54.72	22.96	52.40	21.69	-1.97	-3.59	-2.41	-3.77	48.63	58.31	28.91	38.38	-2.82	-3.21	-4.48	-2.71	-3.30
SIRPB2	55423	103.50	83.90	57.36	47.95	-0.35	-1.40	-2.66	-1.80	48.67	46.52	27.74	43.62	-2.96	-4.60	-3.89	-1.74	-3.30
FLJ22624	79866	19.96	19.15	23.70	16.35			-5.45	-4.72	44.67	51.78	23.92	49.34			-4.93	-1.64	-3.29
CARF	55602	104.23	95.85	122.95	77.27	-0.38	-0.45	0.25	-0.35	74.99	86.03		53.00	-4.40	-3.80		-1.66	-3.29
LOC399940	399940	46.84	56.68	42.28	36.00	-4.38	-3.35	-4.66	-4.31	52.37	71.23	31.31	48.14	-3.01	-2.52	-4.01	-3.62	-3.29
CPNE4	131034	143.11	136.49	129.76	98.05	0.70	0.69	0.76	0.43	59.94	43.63	31.95	37.64	-2.04	-4.02	-3.76	-3.31	-3.28
ARCH	339487	26.81	14.81	8.24	8.28	-3.07	-5.30			63.82	42.53	26.82	44.84	-0.90	-5.66			-3.28
KRT6A	3853	30.10	31.60	28.49	51.37	-3.12	-2.89	-3.55	-1.46	44.31	50.50	43.57	36.27	-4.44	-3.65	-2.23	-2.76	-3.27
KRTHA3A	3883	17.97	19.76	24.06	18.55			-5.93	-4.36	63.03	53.92		32.82				-3.27	-3.27
ZNF100	163227	83.58	94.87	71.39	68.65	-0.44	-0.30	-1.31	0.13	45.80	46.80	43.94	36.80	-3.77	-4.28	-2.98	-2.05	-3.27
HSPA6	3310	26.29	45.18	40.49	45.77	-2.00	-1.46	-1.57	-1.04	40.42	65.06	29.85	44.38	-4.07	-2.13	-4.09	-2.78	-3.27
FY	2532	14.38	14.55	26.11	13.99			-3.10	-3.90	40.48	68.89	37.38	32.97			-3.15	-3.38	-3.26
UNC5D	137970	38.55	27.38	22.76	14.99	-1.70	-1.97			41.34	46.45	60.07	56.75	-3.17	-3.36			-3.26
MBNL1	4154	38.24	35.97	57.42	52.82	-2.79	-2.28	-1.75	-1.36	51.16	40.62	38.43	52.01	-3.26	-4.73	-3.66	-1.40	-3.26
HBLD1	122961	42.68	57.98	38.09	57.72	-2.89	-2.60	-4.07	-1.74	60.91	52.69	42.29	32.87	-1.86	-3.99	-2.87	-4.31	-3.26
HCFC1	3054	19.41	15.79	28.31	16.74			-3.29	-4.28	55.46	53.82	31.84	39.17			-3.97	-2.53	-3.25
DOCK11	139818	49.92	64.20	94.29	70.59	-1.29	-0.76	-0.34	-0.19	50.18	46.43	33.66	37.69	-2.53	-3.81	-3.32	-3.34	-3.25
OR2B6	26212	124.68	118.93	113.01	101.67	0.39	0.35	0.30	0.50	46.38	46.18	68.19	46.59	-4.03	-3.33	-2.40	-3.24	-3.25
ASCL4	121549	24.18	23.48	49.28	24.11	-3.35	-3.55	-2.57	-1.53	49.45	43.40	48.61	32.77	-3.25	-4.79	-2.37	-2.55	-3.24
STARD7	56910	21.56	18.44	27.62	17.30	-5.01	-4.70	-5.50	-5.00	59.22	73.98	33.13	31.25	-2.65	-0.87	-5.67	-3.76	-3.24
ANKRD15	23189	60.77	33.75	63.82	24.94	-1.15	-3.16	-2.12	-2.89	61.91	51.74	41.90	21.73	-1.70	-3.63	-2.28	-5.34	-3.24
TRIAD3	54476	122.05	120.61	103.52	84.45	-1.49	-1.04	-1.28	-1.05	60.61	58.14	37.20	51.59	-1.92	-4.69	-3.22	-3.08	-3.23
MGC24975	163154	25.17	25.99	35.27	12.74	-2.55	-2.51	-2.16	-3.40	39.86	41.89	40.24	37.67	-3.35	-4.51	-2.21	-2.82	-3.22
FLJ25070	55599	47.97	47.36	76.02	34.05	-2.23	-3.06	-1.63	-2.80	48.26	51.15	26.18	42.73	-3.01	-3.89	-4.15	-1.83	-3.22
LRRC24	441381	20.33	21.35	23.20	26.58	-4.22	-3.38	-4.35	-3.06	60.99	33.76	34.25	36.62	-2.01	-4.90	-3.39	-2.56	-3.22
LOC389834	389834	58.64	29.42	47.83	18.65	-1.24	-2.79	-2.37	-3.48	39.88	54.78	41.92	58.30	-5.47	-3.46	-2.99	-0.90	-3.21
ZNF650	130507	42.28	40.65	50.27	30.61	-4.69	-4.37	-4.01	-4.94	83.53	49.19	53.41	38.92	0.47	-6.48	-1.56	-5.25	-3.20
CCL18	6362	57.41	47.56	57.21	24.41	-1.87	-1.97	-1.89	-3.22	62.27	34.84	38.15	36.64	-1.75	-5.03	-3.48	-2.55	-3.20
HSF2	3298	30.90	33.77	35.68	37.85	-2.82	-3.60	-3.26	-2.59	41.79	69.45	41.21	38.56	-3.93	-2.18	-2.95	-3.72	-3.19
C10ORF9	219771	53.48	52.89	61.08	48.06	-2.27	-2.95	-2.32	-2.50	64.98	54.79	30.75	41.74	-1.47	-3.68	-4.60	-3.02	-3.19
SMARCD1	6602	31.80	35.29	34.92	29.52	-1.61	-1.75	-1.92	-2.06	52.74	61.56	32.48	32.58	-2.38	-2.08	-3.85	-4.44	-3.19
LOC83468	83468	46.70	47.61	53.10	35.81	-1.11	-1.21	-1.02	-1.70	33.25	69.13	37.30	35.91	-5.72	-1.10	-2.49	-3.44	-3.19
TNFRSF25	8718	20.45	31.02	23.94	31.27	-6.88	-5.20	-6.80	-4.85	71.62	45.87	54.64	49.78	-0.67	-7.23	-1.46	-3.36	-3.18
RAI	10848	97.36	58.72	86.00	41.53	-0.65	-1.43	-0.77	-1.86	47.79	58.55	40.01	31.78	-2.93	-3.18	-2.87	-3.74	-3.18
SDFR1	27020	46.83	55.78	55.65	43.31	-0.84	-1.03	-0.82	-1.09	36.81	56.74	26.55	46.20	-4.11	-2.56	-3.90	-2.13	-3.18
MGC4189	84268	51.39	26.66	39.09	33.96	-2.16	-3.41	-3.00	-2.67	84.92	43.82		23.55	0.18	-4.86		-4.85	-3.17
FLJ10315	55116	96.78	95.97	91.94	75.73	-0.58	-0.45	-0.68	-0.42	62.50	81.98		49.57	-4.86	-2.61		-2.01	-3.16
SECTM1	6398	16.62	15.65	37.26	14.38			-2.78	-4.16	76.66	49.31	23.51	43.62			-4.10	-2.22	-3.16
SEL1L	6400	91.39	60.72	63.80	46.27	-0.75	-1.40	-1.57	-1.51	46.53	55.91	28.23	41.08	-3.35	-2.16	-5.19	-1.93	-3.16
WDR33	55339	30.23	34.18	34.69	19.48	-2.69	-3.12	-4.30	-3.49	52.48	55.56	44.31	24.45	-2.73	-3.10	-2.00	-4.74	-3.14
GTF2E2	2961	44.40	62.59	63.77	39.26	-1.95	-1.59	-1.55	-2.46	50.17	41.51	51.34	45.50	-2.66	-5.61	-1.44	-2.85	-3.14
ABCB1	5243	47.23	59.63	58.91	29.57	-0.92	-0.85	-1.10	-1.54	60.04	45.31	36.92	31.39	-1.98	-4.32	-2.35	-3.91	-3.14
SLC26A7	115111	125.35	156.44	113.98	70.34	0.08	0.67	0.26	0.07	34.06	51.48	38.89	37.48	-4.82	-2.44	-2.25	-3.04	-3.14
IMP-2	10644	31.85	27.64	19.51	11.38	-3.23	-4.62			48.11	55.82	34.95	52.94	-3.03	-3.23			-3.13
PITPNM2	57605	20.13	25.64	26.18	20.85	-2.09	-2.42	-2.09	-2.52	44.79	45.30	34.32	40.04	-2.94	-4.02	-2.66	-2.91	-3.13
PPP2R5E	5529	146.19	106.09	106.45	73.95	0.67	-0.17	0.12	-0.29	54.72	54.04	39.22	38.48	-2.44	-3.28	-3.22	-3.57	-3.13
RODH-4	8608	38.13	28.58	36.50	43.05	-3.21	-5.33	-4.23	-2.95	47.16	70.17	35.87	37.48	-3.43	-1.71	-3.76	-3.60	-3.13
IFI16	3428	57.96	73.61	60.37	74.13	-1.14	-1.55	-1.87	-0.40	41.59	74.70	45.47	31.60	-3.48	-1.37	-2.80	-4.85	-3.12
MSL3L1	10943	21.89	26.20	26.38	22.37	-4.97	-3.76	-5.68	-4.19	48.54	50.06	51.86	39.27	-4.24	-3.26	-2.46	-2.54	-3.12
KIAA1447	57597	37.47	34.52	33.75	12.37	-2.98	-2.78	-3.43	-5.58	59.48	47.09		34.52	-2.03	-4.30		-3.02	-3.12
SYN1	6853	71.22	82.83	78.76	62.51	-0.81	-0.67	-0.93	-0.87	47.29	59.40	36.37	49.95	-3.07	-3.22	-3.81	-2.36	-3.12
HCN2	610	36.47	45.70	50.02	30.21	-1.91	-1.67	-1.60	-1.49	41.41	43.70	33.80	40.49	-3.62	-3.31	-2.90	-2.63	-3.11
GRK1	6011	35.30	43.11	50.79	28.28	-1.83	-2.15	-1.89	-2.47	86.15	40.74	24.83	38.16	-0.14	-4.70	-4.25	-3.34	-3.11
ST8SIA3	51046	121.43	35.19	101.47	37.12	0.67	-1.81	0.14	-2.68	59.97	45.58	33.01	53.88	-2.17	-4.10	-3.79	-2.36	-3.10
VEGFB	7423	52.34	32.02	35.23	31.56	-0.83	-2.05	-1.82	-1.80	48.33	57.60	32.82	44.26	-3.01	-3.03	-3.57	-2.80	-3.10
EED	8726	55.84	65.27	83.08	45.09	-0.72	-0.82	-0.28	-1.07	60.58	55.75	30.74	39.26	-1.67	-3.27	-3.93	-3.50	-3.09
SERPINF2	5345	57.65	45.85	51.71	27.10	-1.67	-2.68	-3.04	-2.81	40.42	55.04	34.56	37.71	-5.14	-2.94	-1.94	-2.35	-3.09
FGD4	121512	120.08	68.21	94.68	47.26	0.09	-1.45	-0.72	-1.37	47.30	52.28	28.48	37.57	-4.07	-3.26	-2.66	-2.36	-3.09
MGC22793	221908	12.38	21.43	44.51	5.95			-2.62	-7.69	92.74	49.83		34.05				-3.08	-3.08
FLJ13912	64785	73.22	94.41	98.07	49.69	-1.12	-0.52	-0.48	-1.59	40.82	44.89	42.06	49.29	-4.01	-4.32	-2.79	-1.21	-3.08
MGC45840	283229	41.84	40.79	22.14	16.22	-2.70	-2.38			46.66	58.57		41.55	-3.54	-2.63			-3.08
SEMA4B	10509	39.16	26.59	20.42	16.86	-2.29	-4.13			63.37	40.03		39.80	-1.52	-4.63			-3.08
PQBP1	10084	29.66	31.83	36.58	6.49	-2.87	-2.84	-3.59	-3.62	58.05	50.96	35.47	35.88	-2.17	-3.70	-4.28	-2.15	-3.08
GTF3C5	9328	59.50	32.56	66.57	49.79	-1.08	-3.89	-1.58	-1.60	58.68	65.74	33.03	43.60	-1.67	-2.46	-5.25	-2.86	-3.06
COL11A2	1302	97.93	132.49	93.62	45.50	-0.17	0.51	-0.33	-1.42	57.49	46.91	41.74	31.74	-2.70	-3.92	-2.57	-3.05	-3.06
SPTLC2	9517	33.06	39.14	44.66	37.49	-1.60	-1.45	-1.27	-1.23	44.22	41.35	41.76	32.86	-2.35	-3.94	-2.59	-3.34	-3.06
NARFL	64428	46.59	38.89	63.35	32.96	-2.24	-2.20	0.74	0.58	40.14	34.08		30.32	-4.13	-5.46		0.43	-3.06
LOC343637	343637	50.70	48.80	41.80	34.67	-1.87	-2.10	-3.52	-2.61	44.90	50.38	36.58	42.56	-3.02	-3.93	-2.84	-2.44	-3.06
AIM1L	55057	63.61	49.96	54.12	41.16	-1.21	-1.65	-1.79	-1.57	58.41	37.74	32.30	47.14	-2.14	-5.54	-2.72	-1.82	-3.05
LDHAL6A	160287	20.06	37.81	31.68	31.48	-3.09	-2.21	-3.07	-2.44	50.01	54.68	40.61	39.26	-3.41	-3.41	-2.22	-3.12	-3.04
FLJ37927	166979	81.99	86.24	123.71	78.36	-1.07	-0.91	0.36	-0.19	41.77	62.61		31.16	-3.84	-1.74		-3.54	-3.04

		Mock								ATRi								
		% of Control				Robust Z-score				% of Control				Robust Z-score				
Gene Symbol	Gene ID	Rep 1	Rep 2	Rep 3	Rep 4	Rep 1	Rep 2	Rep 3	Rep 4	Rep 1	Rep 2	Rep 3	Rep 4	Rep 1	Rep 2	Rep 3	Rep 4	Average
LOC348158	348158	55.05	81.95	88.70	38.15	-0.79	-0.30	-0.26	-1.34	49.70	49.29	42.15	41.32	-2.52	-4.10	-2.34	-3.20	-3.04
PLXNA3	55558	12.30	28.43	23.39	13.33	-3.30	-2.26			49.90	55.87	54.17	85.54	-2.82	-3.26			-3.04
PLA2G1B	5319	15.20	27.58	27.24	26.93			-4.24	-3.44	67.91	46.44	41.53	45.73			-3.50	-2.57	-3.03
RNF208	727800	43.69	57.47	55.61	68.26	-4.59	-3.31	-3.63	-1.87	36.63	92.04	31.18	54.56	-5.67	0.22	-4.02	-2.65	-3.03
LCE1C	353133	46.45	46.24	55.52	25.52	-1.24	-1.46	-1.29	-2.02	48.95	49.64	38.35	29.96	-2.32	-3.41	-2.44	-3.92	-3.02
COX6A1	1337	28.84	20.42	17.18	19.63	-1.86	-2.20			42.44	57.89	52.92	42.24	-3.27	-2.77			-3.02
DHCR7	1717	28.15	27.31	35.19	22.81	-1.99	-2.27	-2.13	-2.12	63.03	44.86	34.97	32.39	-1.40	-3.96	-3.38	-3.29	-3.01
ATP6V0C	527	21.99	22.60	18.99	12.68	-2.44	-2.81			47.16	48.53	45.66	35.88	-2.57	-3.44			-3.01
FLJ38608	132228	31.24	20.25	31.54	10.21	-2.76	-4.48	-3.53	-5.20	54.00	56.17	21.87	43.19	-1.78	-3.51	-4.44	-2.27	-3.00
BTN2A3	54718	22.24	27.36	52.06	22.05	-2.69	-1.97	-1.92	-2.15	41.74	57.58	34.03	39.01	-3.12	-2.00	-4.54	-2.32	-3.00
GNRH2	2797	20.80	25.98	17.20	9.39	-3.80	-3.37			56.47	53.32	74.53	56.68	-1.93	-4.06			-2.99
OGFR	11054	15.81	24.58	27.07	19.39	-2.69	-2.46	-2.80	-2.30	46.88	50.89	42.43	35.36	-3.45	-3.54	-1.69	-3.27	-2.99
NME3	4832	15.81	8.84	19.72	20.54			-3.77	-3.05	62.77	71.01	40.64	33.59			-2.69	-3.28	-2.99
OR6C6	283365	26.65	30.16	35.82	26.35	-2.97	-3.47	-4.19	-2.75	47.74	58.19	56.78	22.76	-3.33	-2.75	-0.76	-5.10	-2.98
CNTF	1270	66.25	61.37	66.38	67.68	-0.59	-1.20	-1.19	-0.46	50.54	53.32	33.63	49.24	-3.35	-3.60	-3.24	-1.73	-2.98
LRRC8	56262	23.51	26.79	69.33	69.62	-4.91	-4.37	-1.86	-0.53	48.94	48.95		36.72	-2.94	-3.31		-2.68	-2.98
SPACA3	124912	61.46	44.84	74.76	26.22	-0.67	-1.38	-0.46	-1.87	54.44	57.59	38.68	25.63	-2.38	-2.39	-2.80	-4.34	-2.98
FLJ20772	55039	51.19	42.59	48.98	33.53	-2.13	-2.17	-2.63	-2.49	56.08	48.22	35.40	45.48	-1.95	-4.70	-3.47	-1.78	-2.97
PHKG2	5261	17.08	18.09	48.24	42.93			-1.65	-1.42	100.23	59.02	45.42	30.22			-2.09	-3.86	-2.97
HNRPUL1	11100	35.85	48.60	35.82	40.25	-2.55	-1.89	-3.59	-1.43	60.41	59.88	35.86	34.41	-1.51	-3.10	-4.60	-2.68	-2.97
AQP6	363	41.91	48.45	46.18	47.60	-1.22	-0.84	-1.10	-0.72	46.22	53.17	34.42	41.61	-2.78	-3.39	-3.32	-2.38	-2.97
ZNF704	619279	56.79	25.81	33.77	22.62	-1.87	-3.13	-3.81	-4.11	49.63	47.69	42.76	42.13	-3.34	-3.51	-2.33	-2.69	-2.97
C14ORF161	79820	96.08	80.26	88.75	42.89	-0.27	-0.70	-0.68	-1.30	46.73	61.38	47.19	32.37	-3.09	-2.89	-2.89	-2.98	-2.96
SNX4	8723	57.21	66.08	57.14	33.91	-1.88	-1.21	-1.90	-2.34	50.43	49.64	35.36	39.51	-2.91	-2.88	-3.91	-2.14	-2.96
LOC200159	200159	56.33	48.10	45.42	35.20	-2.13	-3.32	-3.42	-3.79	47.77	64.11	44.76	38.41	-3.35	-2.43	-2.57	-3.47	-2.95
TRIM49	57093	118.08	111.67	108.75	82.40	-1.59	-1.27	-1.10	-1.14	55.12	58.07	47.39	56.62	-2.63	-4.70	-2.11	-2.37	-2.95
OCA2	4948	82.60	84.93	82.41	63.09	-0.01	-0.22	-0.41	-0.28	43.14	52.82	44.05	44.15	-3.33	-3.59	-2.08	-2.80	-2.95
LOC113174	113174	113.40	130.84	117.49	92.94	-0.13	-0.11	-0.03	0.14	47.11	67.71	33.77	26.30	-3.16	-1.78	-3.01	-3.84	-2.95
MDM4	4194	100.44	62.86	70.51	44.87	-2.08	-3.04	-2.73	-3.47	65.37	60.49	45.38	46.62	-1.35	-4.27	-2.31	-3.86	-2.95
ARHGEF1	9138	123.19	109.13	112.96	66.74	0.15	0.00	-0.05	-0.48	47.24	45.26	32.22	46.51	-4.08	-4.15	-2.20	-1.35	-2.94
GPR110	266977	63.78	99.64	72.01	72.76	-0.77	-0.19	-0.99	-0.23	62.07	46.56	36.38	41.58	-2.74	-3.81	-2.36	-2.86	-2.94
SPAG9	9043	38.43	48.58	31.60	20.37	-1.67	-1.19	-2.15	-1.96	52.70	50.20	29.69	44.38	-2.44	-3.18	-4.17	-1.97	-2.94
CAMK1	8536	83.68	77.91	69.92	48.41	-0.33	-0.53	-0.71	-0.86	34.98	67.08	43.31	51.67	-5.72	-1.78	-2.79	-1.46	-2.94
TSC	54997	75.15	51.35	47.26	42.53	-1.34	-2.45	-3.33	-1.96	50.68	60.21		28.09	-2.75	-1.99		-4.08	-2.94
ITGB6	3694	29.36	37.31	34.61	38.49	-1.81	-1.79	-1.85	-1.39	47.38	64.36	35.49	40.79	-3.13	-2.21	-3.14	-3.27	-2.94
BLOC1S3	388552	138.34	132.63	128.07	92.51	0.59	0.56	0.61	0.50	47.56	44.93	43.21	38.63	-3.74	-3.36	-2.31	-2.32	-2.93
SPRR1B	6699	54.47	59.78	71.44	36.86	-1.56	-1.78	-1.25	-2.66	56.30	39.54		45.36	-2.14	-4.72		-1.93	-2.93
GML	2765	93.76	95.00	80.54	53.59	0.02	-0.10	-0.28	-0.32	43.92	52.28	39.20	40.49	-3.54	-2.94	-2.76	-2.46	-2.92
DCUN1D3	123879	39.33	25.80	47.40	22.64	-1.79	-2.77	-1.72	-2.03	47.09	49.95	33.46	35.90	-2.83	-2.60	-2.95	-3.27	-2.91
SLAMF6	114836	104.39	121.95	94.23	59.31	-0.12	-0.02	-0.43	-0.88	30.76	69.64	44.88	40.23	-5.09	-2.02	-2.14	-2.40	-2.91
CDC42BPA	8476	45.00	20.73	20.55	9.11	-1.26	-3.11			43.38	69.45	51.13	42.43	-4.28	-1.54			-2.91
PIK3C2A	5286	28.55	18.35	11.65	7.50	-1.88	-2.79			55.01	39.70	45.97	41.41	-1.60	-4.21			-2.90
FAM83G	644815	24.56	23.01	20.07	16.86	-3.34	-4.55			54.56	47.58		35.68	-2.31	-3.50			-2.90
SFRS10	6434	49.84	23.69	26.21	24.34	-1.86	-3.61	-3.78	-3.55	56.47	69.48	24.44	43.28	-2.77	-1.55	-5.30	-1.94	-2.89
COX4I2	84701	37.03	62.11	30.31	17.08	-1.52	-0.79	-2.46	-2.65	69.17	27.84	43.82	45.63	-0.78	-6.94	-2.08	-1.75	-2.89
ZNF277	11179	86.79	26.98	35.88	68.43	-0.80	-3.38	-3.25	-0.66	60.51	52.69		32.56	-1.92	-3.44		-3.30	-2.89
PPP1R15A	23645	48.61	49.33	77.46	45.43	-1.34	-1.28	-0.81	-1.43	50.12	67.11	34.64	32.00	-2.53	-1.65	-3.18	-4.16	-2.88
PTBP2	58155	17.78	11.14	30.54	12.73			-3.31	-3.15	56.02	69.33	41.02	38.50			-3.37	-2.38	-2.88
GARNL1	253959	93.62	64.14	62.91	90.79	-0.26	-0.85	-1.22	0.10	43.65	57.52	56.76	61.36	-4.43	-2.13	-3.64	-1.30	-2.88
LOC115811	115811	44.63	58.44	61.23	18.62	-1.88	-1.62	-1.65	-3.32	43.15	53.02	40.69	28.12	-2.99	-3.63	-1.74	-3.14	-2.88
PRC1	9055	63.71	45.52	82.84	58.16	-1.06	-1.97	-0.66	-0.82	58.09	50.70	37.30	36.74	-2.64	-3.40	-3.16	-2.30	-2.87
CCL3	6348	44.94	23.70	47.27	24.39	-1.94	-2.78	-1.97	-4.56	61.97	59.55	49.02	49.43	-2.10	-1.94	-4.63	-2.83	-2.87
D15WSU75E	27351	65.03	65.49	60.74	48.89	-1.00	-1.07	-1.69	-1.33	62.21	57.29	43.24	35.43	-2.08	-3.14	-2.81	-3.45	-2.87
LOC256394	256394	128.91	93.15	69.44	84.03	0.22	-0.37	-1.31	-0.07	63.98	48.94		34.58	-1.58	-4.01		-3.01	-2.86
EVC	2121	54.84	76.60	88.28	57.98	-1.34	-0.83	-0.63	-0.50	59.50	55.61	42.95	28.42	-1.28	-3.20	-2.22	-4.75	-2.86
ANXA5	308	28.47	27.80	35.63	26.87	-2.93	-2.91	-3.22	-2.66	52.71	55.25	44.38	46.64	-3.35	-3.40	-2.66	-2.04	-2.86
DCP1B	196513	42.81	32.01	55.52	21.61	-2.14	-2.88	-2.18	-2.77	57.30	42.80	42.20	58.76	-1.84	-5.88	-3.59	-0.13	-2.86
C5ORF19	51308	31.77	30.10	24.96	26.68	-3.41	-3.11	-4.32	-3.37	49.31	53.19		42.67	-3.19	-3.37		-2.00	-2.86
C6ORF139	55166	44.70	74.60	77.96	53.34	-1.88	-1.00	-0.94	-0.87	39.05	59.52	32.57	33.78	-3.53	-2.78	-2.72	-2.39	-2.86
LOC116236	116236	82.43	72.71	76.65	37.65	-0.62	-0.93	-1.15	-1.58	59.52	58.11	39.39	36.14	-1.60	-3.35	-4.01	-2.45	-2.85
ZNF528	84436	58.49	46.76	27.37	21.29	-1.22	-1.94	-3.89	-2.66	42.30	51.12	50.96	37.26	-3.05	-3.80	-1.33	-3.22	-2.85
C2ORF16	84226	51.19	42.18	47.20	27.20	-2.15	-2.24	-2.46	-2.93	54.86	61.46	30.74	35.83	-2.44	-1.59	-4.70	-2.67	-2.85
SIVA	10572	49.35	58.26	68.34	49.98	-1.69	-1.82	-1.35	-1.64	48.52	59.37	40.97	50.64	-2.89	-3.23	-2.99	-2.29	-2.85
DKFZP686O1689	341405	30.39	14.62	29.83	10.83	-3.52	-4.86	-3.79	-5.96	43.92	57.97		43.35	-3.91	-2.71		-1.93	-2.85
SLC39A3	29985	32.51	15.56	42.98	37.75	-1.82	-3.23	-1.58	-2.63	51.52	68.28	38.11	43.27	-3.16	-1.47	-2.99	-3.77	-2.85
LOC352909	352909	64.16	104.15	101.86	48.84	-1.52	-0.77	-0.55	-1.75	54.76	60.17	32.75	29.81	-2.24	-2.67	-3.15	-3.32	-2.84
PHC3	80012	28.26	38.19	50.00	32.17	-2.95	-2.23	-2.25	-2.26	66.88	62.11	27.82	48.22	-1.53	-2.56	-5.41	-1.87	-2.84
GLUL	2752	49.42	57.91	67.89	41.20	-1.51	-2.23	-1.52	-2.17	50.21	61.96	43.95	43.77	-2.49	-2.96	-3.06	-2.84	-2.84
STK25	10494	60.61	49.57	77.88	44.97	-0.78	-1.23	-0.51	-1.32	49.51	64.84	30.22	39.29	-2.95	-1.67	-4.30	-2.43	-2.84
ARPC1B	10095	37.07	37.73	70.59	15.51	-2.24	-2.85	-1.75	-4.05	61.08	57.91	33.93	31.79	-1.78	-2.79	-3.33	-3.41	-2.83
RAB43	339122	26.93	33.92	30.28	27.69	-4.34	-3.07	-5.14	-3.52	52.31	56.06	48.58	42.05	-3.64	-2.56	-2.92	-2.18	-2.83
DKFZP761B107	91050	26.22	33.27	37.90	21.92	-3.73	-2.45	-2.94	-3.96	58.96	47.87	39.81	47.29	-2.26	-3.69	-3.46	-1.90	-2.83
ILDR1	286676	78.90	84.54	72.61	42.29	-0.75	-0.65	-1.15	-1.53	43.86	59.11	34.11	46.23	-3.25	-2.63	-3.28	-2.14	-2.83
PARP10	84875	67.39	58.98	80.38	35.08	-1.38	-1.21	-0.78	-2.57	72.75	48.15	41.95	33.45	-0.77	-3.65	-3.16	-3.71	-2.82
CHRM5	1133	60.50	66.00	86.43	20.96	-0.87	-1.15	-0.51	-3.18	65.22	49.97	34.17	41.01	-2.35	-3.34	-2.67	-2.94	-2.82
LOC653404	653404	50.67	39.32	49.59	47.84	-2.29	-2.93	-2.66	-1.98	24.89	30.11		21.09	-1.05	-0.92		-6.50	-2.82
LOC727830	727830	24.89	33.94	25.94	24.34	-3.57	-3.36	-5.13	-3.66	51.07	52.00	38.33	42.17	-2.70	-3.32	-3.26	-2.00	-2.82
TUBA1	7277	103.53	133.80	118.12	105.72	0.35	0.43	0.27	0.70	47.06	67.12	42.95	35.63	-3.78	-1.84	-1.92	-3.71	-2.81
PF4	5196	36.81	28.18	52.05	32.22	-3.40	-3.57	-3.05	-3.04	60.37	57.50	46.74	35.18	-2.49	-2.41	-3.20	-3.13	-2.81
MDK	4192	48.38	24.49	22.73	20.55	-0.88	-2.42	-2.82	-2.84	49.17	53.48	35.63	47.36	-2.77	-3.02	-3.31	-2.13	-2.81
PRO1855	55379	77.86	61.54	67.16	52.88	-1.23	-2.37	-1.96	-2.10	53.25	54.08	56.00	38.89	-2.68	-3.78	-1.36	-3.41	-2.81
R3HDML	140902	110.32	86.44	102.51	47.23	-0.12	-0.72	-0.42	-1.37	25.64	60.09	47.39	64.29	-8.27	-2.39	-0.75	0.19	-2.80
TNFRSF1A	7132	37.92	35.66	46.25	32.67	-2.33	-3.43	-2.49	-3.09	38.72	69.13	42.86	54.97	-4.46	-2.21	-2.68	-1.86	-2.80
ZFP64	55734	88.40	79.75	75.99	34.68	-0.46	-0.74	-1.05	-1.61	46.41	51.50	42.38	41.58	-2.57	-3.75	-2.29	-2.60	-2.80
ATP5G3	518	11.99	6.61	22.19	18.41			-2.90	-4.77	51.68	73.95	38.43	51.68			-2.94	-2.63	-2.78
FLJ40432	151195	37.07	36.01	45.64	45.23	-2.67	-3.19	-3.16	-1.86	39.87	58.05	45.23	42.29	-4.15	-2.57	-2.42	-1.99	-2.78
CDC7	8317	38.09	30.15	52.21	35.79	-1.62	-2.16	-1.46	-1.83	42.52	67.26	33.81	41.73	-3.90	-1.44	-3.69	-2.10	-2.78
KLHL5	51088	43.67	42.91	31.06	17.04	-1.39	-1.58	-2.57	-2.31	44.31	57.77	50.84	33.60	-2.91	-2.35	-1.99	-3.87	-2.78
HMGCLL1	54511	59.40	73.52	75.25	40.08	-0.70	-0.41	-0.33	-1.44	51.72	70.38	26.15	43.05	-3.26	-0.98	-4.44	-2.44	-2.78
ZNRF4	148066	14.08	19.33	12.54	34.78			-4.96	-2.21	53.04	51.90	51.60	35.52			-1.53	-4.02	-2.78
CHURC1	91612	37.09	25.57	49.90	38.99	-2.24	-3.93	-3.00	-1.79	53.99	54.33	42.99	33.72	-2.56	-3.26	-2.15	-3.11	-2.77

		Mock								ATRi								
		% of Control				Robust Z-score				% of Control				Robust Z-score				
Gene Symbol	Gene ID	Rep 1	Rep 2	Rep 3	Rep 4	Rep 1	Rep 2	Rep 3	Rep 4	Rep 1	Rep 2	Rep 3	Rep 4	Rep 1	Rep 2	Rep 3	Rep 4	Average
CIDEB	27141	61.73	56.66	87.12	58.65	-1.12	-1.46	-0.52	-0.80	56.44	56.79	35.48	37.54	-2.82	-2.64	-3.43	-2.20	-2.77
SPTBN1	6711	37.62	36.50	35.90	37.72	-1.77	-2.28	-2.75	-1.97	44.88	78.90	47.53	28.75	-4.06	-0.60	-1.38	-5.03	-2.77
DAZ	1617	31.91	38.52	31.14	29.74	-1.70	-2.05	-2.04	-2.07	52.57	53.27	42.68	46.13	-2.77	-3.85	-1.72	-2.73	-2.77
MFN2	9927	16.06	36.13	15.44	9.32	-2.93	-1.77			44.61	63.29	43.17	42.80	-3.71	-1.80			-2.76
CTSK	1513	47.65	38.46	42.20	28.42	-1.40	-2.43	-2.07	-2.72	55.30	50.36	36.13	59.20	-2.38	-3.76	-3.73	-1.15	-2.76
AAAS	8086	108.24	99.07	120.73	71.24	0.01	0.03	0.32	0.18	60.32	40.18	47.47	40.54	-1.26	-4.62	-2.41	-2.74	-2.75
ZNF616	90317	80.44	62.57	69.79	55.97	-0.51	-1.17	-1.29	-1.03	46.21	55.11	48.18	56.51	-4.35	-3.41	-2.17	-1.06	-2.75
ARHI	9077	59.86	64.36	68.23	48.36	-0.63	-0.95	-0.65	-1.09	52.90	67.86	40.53	35.75	-2.73	-1.99	-1.95	-4.31	-2.74
PSEN1	5663	68.46	78.78	79.21	61.59	-0.37	-0.38	-0.50	-0.33	58.32	65.64	28.85	44.11	-1.60	-1.98	-4.58	-2.81	-2.74
LOC390231	390231	93.81	83.06	79.55	56.32	-2.29	-2.18	-2.28	-2.60	58.05	65.39	45.15	52.42	-2.24	-3.44	-2.33	-2.96	-2.74
IGFBP3	3486	54.17	60.31	68.39	30.77	-1.59	-1.37	-1.51	-2.01	53.47	60.32	41.31	40.18	-2.26	-3.04	-3.72	-1.94	-2.74
FLJ22419	79750	77.87	58.20	56.23	35.82	-1.16	-1.45	-2.18	-2.30	42.84	55.38	42.88	50.46	-3.60	-3.61	-2.53	-1.21	-2.74
ZC3HDC1	64761	62.12	62.09	56.44	36.21	-1.68	-1.30	-2.16	-2.26	42.44	68.60	37.21	42.73	-3.66	-1.94	-3.23	-2.12	-2.73
MGC2803	79002	65.78	64.60	53.74	33.76	-1.52	-1.26	-2.06	-2.69	49.61	52.73		46.43	-3.15	-3.44		-1.60	-2.73
SOX2	6657	20.13	27.00	29.49	52.45	-2.41	-2.24	-2.27	-0.80	27.64	65.33	55.89	43.60	-5.95	-1.68	-0.65	-2.64	-2.73
GTF2F2	2963	42.69	38.63	30.92	26.41	-1.28	-1.65	-2.41	-1.86	49.01	57.35	48.51	28.14	-3.08	-2.42	-1.49	-3.92	-2.73
RIPK2	8767	47.10	26.73	48.86	24.51	-1.24	-2.38	-1.62	-2.66	43.49	70.80	50.01	27.03	-3.76	-1.12	-1.57	-4.46	-2.73
GPS2	2874	62.22	134.59	141.36	84.77	-0.97	0.19	0.67	0.00	58.67	78.97	34.45	39.85	-1.68	-0.89	-4.93	-3.42	-2.73
FLJ36525	259173	60.99	88.42	61.98	39.81	-1.80	-0.68	-1.95	-2.60	46.30	70.69		42.39	-3.95	-1.40		-2.83	-2.73
DEAF1	10522	23.67	12.52	13.40	69.00			-5.24	-0.87	54.96	64.34	66.97	48.70			-2.52	-2.93	-2.73
LOC284123	284123	49.35	46.15	53.02	23.03	-1.69	-2.23	-2.08	-2.82	44.97	51.37	31.28	43.52	-2.77	-3.86	-2.89	-1.36	-2.72
HUMMLC2B	29895	61.86	67.37	68.06	61.35	-1.38	-1.35	-1.33	-0.66	55.79	49.82	27.29	53.03	-1.61	-4.44	-3.51	-1.30	-2.71
RP11-95H8.1	642265	89.68	51.64	68.38	33.04	-0.72	-1.81	-1.35	-2.75	41.66	62.43		44.91	-4.24	-2.14		-1.76	-2.71
DKFZP566C0424	26099	128.64	124.46	116.33	91.84	0.18	0.27	0.07	0.23	65.15	72.60		63.61	-2.73	-4.71		-0.70	-2.71
STAU2	27067	127.47	143.95	150.11	91.66	0.47	0.82	0.75	0.54	33.28	68.90	35.84	56.08	-4.99	-1.50	-3.00	-1.33	-2.71
PABPC1	26986	74.40	61.88	71.40	59.42	-0.23	-0.66	-0.41	-0.29	35.83	57.78	41.89	37.26	-3.50	-2.01	-2.57	-2.74	-2.70
SFTPD	6441	48.65	38.16	47.58	65.72	-1.71	-2.42	-2.69	0.06	59.59	56.28	37.36	38.89	-1.99	-3.02	-3.97	-1.81	-2.70
RCE1	9986	28.91	43.49	98.30	52.11	-0.59	-1.59	-0.68	-0.64	48.25	53.57	31.92	38.57	-1.67	-3.81	-3.48	-1.81	-2.69
LOC130355	130355	12.94	28.60	35.02	20.25	-4.55	-3.62	-4.27	-3.40	55.70	53.92	52.04	28.95	-2.36	-3.32	-1.19	-3.88	-2.69
MIPOL1	145282	42.95	21.68	36.11	27.70	-2.65	-3.53	-3.58	-3.49	63.60	52.90	26.29	52.14	-1.64	-2.91	-4.71	-1.50	-2.69
MGC2654	79091	76.91	43.19	69.34	28.56	-1.01	-2.69	-1.69	-3.19	48.48	56.07	43.41	39.69	-3.00	-2.80	-2.63	-2.31	-2.69
FLJ46481	389197	10.11	13.54	21.89	18.28			-3.97	-5.59	48.50	71.35	56.22	58.28			-3.71	-1.67	-2.69
ZNF610	162963	112.49	90.82	101.44	82.38	-0.11	-0.27	-0.12	-0.05	52.01	53.52	44.03	48.82	-3.14	-2.99	-2.88	-1.73	-2.69
HTR5A	3361	62.43	56.59	67.07	45.09	-0.81	-1.51	-1.17	-1.36	57.47	47.41	38.76	51.56	-3.35	-3.69	-2.04	-1.65	-2.68
SPATA11	84266	22.89	28.59	36.40	14.01	-4.04	-4.53	-4.33	-5.40	56.43	52.86	29.17	47.73	-2.05	-3.64	-3.66	-1.37	-2.68
ATP11A	23250	24.08	39.62	22.83	21.58	-2.26	-1.55	-2.71	-2.89	50.70	49.92	40.09	46.18	-3.37	-3.21	-2.09	-2.06	-2.68
LOC554235	554235	20.37	3.48	17.59	24.86			-4.30	-3.13	39.05	82.10	29.56	55.58			-3.98	-1.38	-2.68
LOC283849	283849	42.70	47.09	50.60	53.15	-2.35	-2.45	-2.79	-1.40	60.51	41.07	48.25	42.37	-1.70	-4.93	-2.09	-1.98	-2.68
OR13C4	138804	86.79	72.74	68.24	48.44	-0.13	-0.54	-0.61	-0.49	44.05	57.33	43.99	39.29	-3.52	-2.38	-2.17	-2.63	-2.68
FLJ36674	284040	54.43	36.50	28.51	9.47	-2.01	-2.65			58.43	54.39		40.67	-2.14	-3.20			-2.67
ARL6IP2	64225	33.75	53.50	69.89	36.90	-2.03	-1.12	-1.05	-2.02	48.99	49.25	39.75	48.68	-2.67	-3.47	-2.48	-2.05	-2.67
FLJ33215	259282	114.90	121.76	105.68	79.68	-0.08	0.27	-0.07	-0.22	54.41	60.04		34.83	-2.58	-2.44		-2.98	-2.67
SMC6L1	79677	137.59	105.24	104.48	77.62	0.35	-0.29	-0.32	-0.51	53.85	62.25	42.32	45.97	-2.62	-2.66	-2.87	-2.50	-2.66
SLC24A5	283652	32.04	33.19	31.64	22.65	-1.86	-2.07	-2.53	-1.82	65.51	50.00	53.69	28.24	-0.81	-3.25	-1.66	-4.92	-2.66
POPDC2	64091	6.60	35.79	11.61	15.35	-5.75	-2.53			71.91	46.20	44.37	48.71	-1.30	-4.02			-2.66
TSPAN13	27075	29.63	34.78	23.04	11.01	-3.47	-2.69			64.08	43.22	35.02	31.79	-1.59	-3.73			-2.66
TNPO3	23534	39.51	33.24	40.04	38.56	-2.44	-2.77	-2.62	-2.26	44.37	68.76	41.56	41.81	-4.43	-1.62	-2.48	-2.10	-2.66
HT017	57408	22.01	31.08	30.82	21.45	-5.11	-3.93	-4.97	-3.94	59.64	48.98		35.69	-1.83	-3.30		-2.83	-2.66
CXORF22	170063	65.33	23.39	27.53	46.62	-1.48	-3.36	-4.50	-1.87	54.45	45.48	43.17	49.04	-2.70	-3.78	-2.29	-1.84	-2.65
ARMC2	84071	84.74	96.35	86.99	60.02	0.04	-0.12	-0.43	-0.31	67.09	54.24	43.41	23.10	-0.74	-2.84	-1.85	-5.18	-2.65
CPB2	1361	70.59	97.91	66.47	55.02	-0.67	-0.35	-1.00	-1.04	61.24	70.61	44.50	30.10	-1.73	-1.47	-2.44	-4.96	-2.65
RAB4B	53916	45.79	38.04	42.05	33.01	-1.06	-1.76	-1.50	-1.71	50.23	57.78	38.95	49.23	-2.78	-3.01	-2.63	-2.17	-2.65
MGC4549	84337	40.65	77.71	71.16	32.35	-2.46	-1.06	-1.60	-2.83	57.09	47.92	39.79	45.82	-2.04	-3.88	-3.07	-1.58	-2.64
OR5BF1	127066	92.05	120.69	104.06	97.64	-0.30	0.30	-0.04	0.44	51.67	64.92	31.94	43.29	-3.37	-1.74	-3.98	-1.47	-2.64
OR10A4	283297	48.36	40.69	62.89	24.11	-1.86	-2.31	-1.78	-2.54	50.93	71.74	40.22	35.81	-2.56	-1.60	-3.88	-2.49	-2.64
KIAA0258	9827	51.24	39.82	42.22	32.27	-2.06	-2.06	-2.63	-2.81	54.28	73.57	33.36	44.15	-2.84	-0.98	-4.46	-2.26	-2.64
FLJ35779	134359	147.93	126.12	105.32	83.60	0.74	0.22	-0.25	-0.01	58.07	55.24		32.11	-1.98	-2.54		-3.38	-2.63
OLFML3	56944	84.30	71.47	91.68	65.80	-0.40	-0.88	-0.51	-0.67	61.27	57.49	36.32	53.12	-2.20	-3.11	-3.84	-1.38	-2.63
STMN1	3925	30.65	25.80	30.47	26.01	-3.95	-3.80	-5.12	-3.71	53.15	73.40	43.11	41.03	-3.51	-0.92	-3.78	-2.31	-2.63
BOK	666	88.97	72.22	55.94	40.64	-0.41	-0.76	-1.71	-1.61	44.72	59.20	33.28	47.44	-3.70	-2.43	-2.59	-1.78	-2.62
COG1	9382	82.63	95.88	118.13	75.41	-0.35	0.02	0.19	-0.01	58.16	56.42	30.72	45.38	-1.64	-2.67	-3.79	-2.40	-2.62
ST8SIA2	8128	50.62	80.77	53.71	64.71	-0.91	-0.47	-1.08	-0.50	62.61	45.83	40.89	52.43	-1.64	-5.01	-1.91	-1.93	-2.62
CHTF18	63922	122.31	95.78	107.17	81.81	0.10	-0.15	0.04	-0.07	64.74	37.91	47.23	53.57	-1.59	-5.16	-2.48	-1.25	-2.62
CDIPT	10423	87.51	103.92	93.62	82.30	0.08	0.08	0.06	0.16	47.86	51.20	33.02	48.56	-2.55	-3.23	-2.84	-1.86	-2.62
HAGHL	84264	62.65	47.38	52.41	43.14	-0.53	-0.88	-0.89	-0.89	42.13	54.74	45.39	42.52	-3.31	-3.18	-1.71	-2.28	-2.62
HAO2	51179	41.86	47.61	56.54	44.83	-1.22	-0.87	-0.76	-0.82	50.73	60.77	32.33	43.98	-2.24	-2.42	-3.69	-2.11	-2.61
PDGFB	5155	48.39	53.71	42.12	51.43	-1.56	-2.45	-2.94	-1.50	64.83	60.10	44.11	42.31	-1.15	-3.23	-3.04	-3.05	-2.61
GLI3	2737	76.67	121.37	129.47	80.38	-0.16	0.51	0.55	0.23	59.28	56.14	45.42	36.63	-1.51	-3.14	-1.89	-3.92	-2.61
IGSF6	10261	128.08	147.38	132.38	72.79	0.39	0.74	0.60	-0.16	59.25	56.81	39.64	45.92	-1.63	-3.54	-3.97	-1.30	-2.61
SLC34A1	6569	51.48	65.78	51.55	26.03	-0.97	-0.69	-1.28	-1.88	42.62	56.87	37.48	54.22	-4.02	-2.47	-2.98	-0.97	-2.61
LOC91181	91181	21.46	19.09	13.55	20.75	-4.80	-6.89			47.16	69.46	49.31	45.15	-3.43	-1.79			-2.61
TSARG6	374407	69.67	60.08	54.23	31.75	-1.42	-1.37	-2.29	-2.65	47.48	54.98	46.99	46.00	-2.97	-3.67	-2.07	-1.71	-2.61
LOC200008	200008	20.12	28.39	37.34	21.42	-3.45	-3.47	-3.12	-2.99	49.68	75.73	22.99	29.46	-2.22	-1.01	-4.24	-2.95	-2.60
EAP30	11267	69.86	89.40	84.15	64.60	-1.23	-0.67	-1.01	-0.83	64.23	46.88	44.83	37.73	-1.35	-4.02	-2.47	-2.57	-2.60
MYO1A	4640	17.49	20.00	19.57	20.82			-2.78	-2.44	40.63	72.11	33.97	50.48			-3.91	-1.28	-2.59
WARS2	10352	42.58	49.61	56.46	36.35	-1.27	-1.14	-0.90	-1.67	55.69	53.06	39.32	42.61	-2.85	-2.81	-2.20	-2.50	-2.59
FLJ10211	55095	76.74	92.63	87.19	68.74	-1.27	-0.79	-1.00	-1.01	52.64	52.59	57.18	47.36	-2.75	-4.01	-1.24	-2.34	-2.59
ADAM11	4185	77.19	76.29	86.57	62.00	0.67	-0.47	-0.93	-0.28	50.07	49.28	39.08	38.61	-1.52	-4.45	-2.57	-1.80	-2.59
IL1F8	27177	60.06	56.86	59.44	36.63	-0.68	-0.89	-0.80	-1.65	65.23	42.78	27.49	67.30	-1.96	-4.21	-4.16	0.01	-2.58
ABCB8	11194	26.26	22.77	20.82	19.67	-2.11	-2.57	-2.89	-3.11	44.01	61.85	54.22	32.94	-4.16	-1.82	-0.44	-3.91	-2.58
LOC113828	113828	84.18	68.13	96.73	62.31	-0.88	-1.13	-0.33	-0.93	55.45	63.89		32.53	-2.46	-1.96		-3.30	-2.58
LOC120224	120224	111.70	103.58	84.88	55.19	-0.19	-0.24	-0.70	-0.92	55.82	59.48	39.67	31.92	-1.61	-3.07	-1.94	-3.70	-2.58
MRPS21	54460	70.76	73.36	82.72	62.05	-0.83	-0.90	-0.80	-0.03	48.90	62.98	55.14	28.71	-3.33	-2.26	-1.60	-3.12	-2.58
MGC35308	285800	27.79	26.86	10.74	24.44	-3.43	-2.88			56.20	51.99	24.02	32.29	-2.58	-2.57			-2.57
STX4A	6810	121.79	119.63	111.32	89.03	0.05	-0.37	-0.23	0.01	52.19	57.05	37.80	39.29	-2.53	-3.07	-2.50	-2.18	-2.57
LOC203413	203413	96.29	107.48	90.90	50.65	-0.59	-0.14	-0.72	-1.78	64.77	57.32		40.34	-1.72	-2.89		-3.09	-2.57
SUMF1	285362	60.38	44.69	40.17	31.91	-0.82	-1.33	-1.67	-1.20	55.43	66.24	32.31	37.53	-2.14	-1.51	-3.74	-2.87	-2.57
NMUR2	56923	17.40	23.98	19.35	12.16	-3.10	-3.52			63.95	55.73	50.55	44.16	-2.51	-2.62			-2.56
NFIC	4782	38.34	60.16	45.64	49.88	-1.35	-0.71	-1.23	-0.65	43.75	51.40	41.96	38.42	-2.41	-2.69	-2.56	-2.59	-2.56
BCNP1	199786	76.69	87.22	62.28	54.63	-1.27	-1.02	-2.25	-1.97	58.30	60.25	56.99	35.32	-2.13	-2.92	-1.26	-3.93	-2.56
FCRH3	115352	49.10	53.71	41.94	54.50	-2.51	-2.89	-3.71	-1.98	71.88	60.37	49.89	31.79	-0.85	-2.91	-1.98	-4.49	-2.56

		Mock								ATRi								
		% of Control				Robust Z-score				% of Control				Robust Z-score				
Gene Symbol	Gene ID	Rep 1	Rep 2	Rep 3	Rep 4	Rep 1	Rep 2	Rep 3	Rep 4	Rep 1	Rep 2	Rep 3	Rep 4	Rep 1	Rep 2	Rep 3	Rep 4	Average
C6ORF134	79969	76.65	57.25	85.43	47.30	-0.89	-1.25	-0.56	-1.41	62.48	52.75	41.84	30.17	-1.84	-2.49	-2.47	-3.44	-2.56
C3orf65	646600	102.63	60.88	58.54	67.70	-0.22	-1.16	-1.94	-0.72	48.32	74.79	32.84	46.26	-3.52	-0.92	-3.62	-2.16	-2.56
ADH1C	126	36.88	19.00	25.78	60.30	-1.58	-2.88	-2.60	-1.24	55.41	49.30	51.49	51.38	-2.68	-3.59	-1.30	-2.66	-2.56
NEIL1	79661	20.48	25.09	31.92	41.06	-2.43	-2.48	-2.00	-1.26	61.68	58.17	39.39	41.72	-1.56	-2.96	-2.57	-3.14	-2.56
POLR3D	661	15.68	43.18	30.89	27.90	-3.01	-1.39	-2.11	-2.29	63.52	60.42	23.39	55.01	-2.11	-1.97	-5.05	-1.10	-2.56
FLJ35725	152992	86.71	59.75	73.28	64.16	-0.75	-1.59	-1.61	-0.88	54.60	52.06	34.33	51.27	-1.96	-3.69	-3.15	-1.43	-2.56
BRD1	23774	40.50	25.56	35.60	24.90	-2.71	-3.40	-3.30	-3.17	40.10	58.53	48.46	40.13	-4.16	-1.88	-2.12	-2.06	-2.56
FBXO24	26261	49.22	53.07	45.38	29.58	-1.43	-1.34	-2.09	-2.11	63.09	47.38	33.95	44.06	-0.78	-3.75	-3.94	-1.73	-2.55
CKLF	51192	51.49	43.56	46.24	38.93	-2.13	-2.17	-2.52	-1.97	70.19	59.12	41.29	26.74	-1.09	-1.82	-3.03	-4.26	-2.55
STMN3	50861	5.86	14.28	31.05	9.33			-3.23	-5.17	73.22	78.05	36.16	46.38			-2.98	-2.12	-2.55
ZNF499	84878	29.29	28.87	29.01	20.75	-4.23	-4.15	-5.21	-4.04	53.46	50.13		41.55	-2.45	-3.16		-2.04	-2.55
CA7	766	15.66	17.55	30.43	22.93			-1.84	-2.34	57.41	37.80	34.31	43.67			-2.66	-2.44	-2.55
IER3	8870	73.81	64.17	70.71	46.02	-0.88	-1.23	-1.41	-1.14	70.09	53.80	44.06	37.48	-0.59	-3.99	-3.32	-2.27	-2.54
C6ORF70	55780	72.52	97.84	117.96	42.66	-0.29	-0.09	0.16	-0.99	50.38	57.66	36.72	37.05	-2.17	-2.44	-2.65	-2.90	-2.54
FLJ13868	64755	93.70	62.16	49.54	52.46	-0.67	-1.88	-3.15	-1.35	70.05	41.22		39.61	-0.92	-4.40		-2.29	-2.54
TRALPUSH	116931	129.32	114.07	99.96	74.01	0.19	0.03	-0.41	-0.50	84.06	62.21		55.41	-3.90	-2.28		-1.43	-2.54
RC3	23312	33.82	37.09	40.12	27.10	-3.08	-3.77	-3.97	-3.47	56.36	78.28	20.64	39.32	-2.06	-0.69	-5.22	-2.17	-2.54
POLD3	10714	91.86	53.46	89.13	55.79	0.01	-1.06	-0.07	-0.49	70.31	60.44	41.14	22.47	-0.67	-2.09	-2.44	-4.93	-2.53
C13ORF9	51028	33.86	34.89	24.82	13.53	-3.54	-4.56			58.45	60.07	31.49	44.57	-2.12	-2.95			-2.53
MGC17301	196410	43.59	40.34	54.06	31.01	-1.17	-1.95	-1.07	-1.99	64.38	58.35	38.43	41.82	-1.46	-3.15	-2.18	-3.33	-2.53
SCARF2	91179	61.65	73.75	78.42	48.36	-0.55	-0.61	-0.38	-0.93	64.51	63.54	31.20	45.26	-1.29	-2.30	-3.85	-2.66	-2.53
LOC148213	148213	107.23	84.26	90.02	69.62	-0.25	-0.62	-0.54	-0.61	58.21	59.24		35.58	-2.16	-2.54		-2.87	-2.53
FLJ43582	389649	63.29	57.42	67.20	55.21	-1.77	-1.67	-2.06	-1.34	63.47	65.79	41.71	40.29	-2.09	-1.59	-4.02	-2.41	-2.53
TRPV4	59341	12.77	40.87	109.13	26.90	-1.65	-1.71	-0.47	-2.04	50.19	63.27	29.18	35.45	-1.51	-2.55	-3.89	-2.16	-2.53
LOC402682	402682	32.60	21.48	25.33	19.94	-3.34	-3.93	-4.27	-4.21	57.57	56.16		39.38	-2.23	-2.95		-2.39	-2.52
AP1S1	1174	24.51	32.26	43.79	21.20	-2.28	-2.13	-1.84	-1.93	53.36	61.74	38.73	41.59	-1.91	-1.93	-3.65	-2.58	-2.52
MGC2463	79037	22.71	27.10	25.89	17.13	-3.21	-3.59	-4.20	-3.51	41.63	63.97	27.19	46.01	-3.19	-2.25	-3.51	-1.14	-2.52
FSCN1	6624	16.32	11.81	16.31	36.50			-6.36	-0.87	59.33	105.68	41.13	40.26			-3.38	-1.66	-2.52
APOD	347	64.38	69.25	81.68	63.94	-0.56	-0.52	-0.16	-0.34	58.52	65.32	30.44	43.12	-2.57	-1.46	-3.61	-2.43	-2.52
NEK9	91754	68.30	59.13	73.82	65.73	-0.57	-0.89	-0.64	-0.49	59.88	55.70	42.78	33.72	-1.76	-2.62	-2.42	-3.26	-2.51
LOC646627	646627	95.68	71.08	79.72	55.50	-0.24	-0.80	-0.77	-0.84	53.29	52.91	29.35	54.78	-2.68	-3.20	-3.13	-1.04	-2.51
MS4A7	58475	24.53	41.02	27.87	16.44	-3.34	-2.88	-4.06	-5.25	39.90	64.44		44.13	-3.95	-1.50		-2.08	-2.51
SARS	6301	23.88	18.78	24.82	18.38	-2.41	-2.91	-2.67	-4.78	45.43	61.80	53.37	49.92	-3.98	-2.12	-1.09	-2.85	-2.51
RHOC	389	48.88	49.83	36.15	34.06	-1.05	-1.19	-2.07	-1.39	58.11	55.29	43.45	32.15	-1.95	-2.65	-2.13	-3.32	-2.51
LOC374920	374920	111.39	86.54	82.18	50.90	0.06	-0.23	-0.50	-0.41	65.15	51.31	44.72	36.74	-0.84	-3.09	-2.77	-3.33	-2.51
CDKL3	51265	93.23	83.20	86.92	88.46	0.00	-0.25	-0.25	0.17	64.70	56.11	43.74	30.02	-1.28	-2.57	-2.30	-3.89	-2.51
MYO15A	51168	65.64	42.15	51.26	50.37	-0.61	-1.98	-1.85	-1.23	47.02	67.29	33.62	53.81	-3.78	-1.82	-3.24	-1.19	-2.51
PCLKC	54825	167.37	95.92	89.09	71.51	0.71	-0.35	-0.58	-0.34	58.71	56.20	43.02	33.56	-2.07	-2.13	-2.79	-3.03	-2.51
ZNF599	148103	17.85	9.22	35.22	12.19			-3.64	-4.01	71.83	75.29	44.52	41.74			-3.25	-1.76	-2.51
FCN1	2219	26.69	26.29	23.84	8.38	-2.96	-3.85			55.28	59.35	45.93	7.82	-2.41	-2.60			-2.51
SPINK9	643394	37.11	52.94	55.98	32.80	-3.38	-1.88	-2.77	-2.98	62.59	54.11	46.02	45.84	-2.21	-2.78	-3.31	-1.72	-2.50
PEX7	5191	16.63	29.42	23.64	25.18	-2.81	-1.63	-2.23	-1.84	42.10	60.26	38.72	48.84	-3.31	-2.48	-2.64	-1.59	-2.50
C2ORF24	27013	69.69	44.63	57.61	56.16	-0.94	-1.55	-1.45	-1.60	62.48	57.50	88.41	35.32	-2.05	-2.13	-0.64	-5.19	-2.50
LOC155054	155054	147.74	97.91	108.82	87.23	0.32	-0.25	0.01	0.31	45.72	69.96	48.13	35.98	-3.20	-1.78	-1.95	-3.06	-2.50
FAT2	2196	33.33	54.79	48.10	26.63	-2.26	-1.59	-2.32	-2.18	38.67	47.97	53.80	53.58	-3.51	-4.26	-1.05	-1.17	-2.50
GIOT-1	92283	100.71	96.70	87.56	74.18	-0.47	-0.43	-0.84	-0.49	46.55	82.15		39.13	-3.91	-0.33		-3.25	-2.50
LIP8	116840	58.79	79.05	75.26	50.70	-2.09	-1.17	-1.54	-1.45	60.35	53.81		34.40	-1.76	-2.71		-3.02	-2.50
C11ORF8	744	81.78	139.61	133.82	103.32	-0.18	0.67	0.83	0.64	72.34	15.67	73.41	69.63	-0.48	-10.54	0.89	0.15	-2.49
CSF2RB	1439	88.22	66.75	128.82	74.96	0.06	-0.53	0.66	0.19	35.89	53.60	44.26	45.11	-3.49	-2.44	-2.22	-1.82	-2.49
TAS2R48	259294	66.42	64.69	53.24	17.08	-0.99	-1.21	-2.04	-3.13	42.70	57.35	40.35	51.07	-3.00	-2.98	-2.54	-1.44	-2.49
TNFSF8	944	55.32	67.57	57.64	32.23	-1.41	-1.09	-2.04	-1.07	58.68	45.14	54.88	39.74	-2.09	-4.53	-1.63	-1.71	-2.49
CEACAM1	634	45.54	67.17	66.47	60.88	-1.86	-1.10	-1.55	-0.06	52.22	59.53	42.58	44.10	-2.88	-2.64	-3.17	-1.26	-2.49
RIF1	55183	72.09	35.68	61.96	26.15	-0.76	-2.37	-1.63	-2.73	56.79	56.32	33.93	74.05	-2.78	-3.26	-4.24	0.32	-2.49
AMFR	267	30.10	16.13	37.91	14.50	-2.35	-3.56	-2.52	-3.62	41.90	55.98	51.12	37.75	-3.12	-2.64	-1.67	-2.51	-2.48
QIL1	125988	20.70	21.99	24.16	8.64	-4.67	-4.54			78.86	90.14		98.28	-3.40	-1.57			-2.48
KIAA1441	57592	24.39	23.07	27.71	27.15	-3.41	-3.99	-4.92	-3.30	67.98	57.68	34.46	37.55	-0.77	-2.92	-3.13	-3.11	-2.48
ICMT	23463	65.02	37.09	53.99	80.93	-0.51	-1.72	-1.12	-0.36	48.03	67.00	38.00	59.56	-3.61	-1.59	-3.00	-1.71	-2.48
HIBADH	11112	34.51	46.38	32.70	18.28	-1.64	-1.32	-2.29	-2.53	57.55	43.39	48.13	41.19	-2.01	-4.17	-1.54	-2.21	-2.48
FLJ20054	54530	34.56	38.35	47.57	42.04	-2.57	-3.07	-2.46	-2.24	66.30	47.82		39.57	-1.29	-3.46		-2.69	-2.48
MKNK2	2872	65.64	73.64	72.28	53.99	-0.64	-0.48	-0.69	-0.92	43.11	63.07	47.55	39.41	-3.81	-1.84	-1.85	-2.41	-2.48
ACRV1	56	29.09	18.20	17.66	20.51	-3.07	-4.07			44.08	71.01	57.20	47.51	-3.78	-1.17			-2.48
POLD4	57804	105.93	128.93	91.70	74.30	0.14	0.77	-0.48	-0.28	64.14	60.10	42.14	44.16	-0.95	-3.14	-2.80	-3.01	-2.47
THY1	7070	58.20	46.02	51.84	23.96	-1.80	-1.80	-2.36	-3.93	71.32	44.08	30.28	56.41	-0.85	-3.96	-4.02	-1.06	-2.47
LAMA1	284217	172.71	133.04	159.39	79.11	0.96	0.61	1.27	-0.04	54.34	68.40	36.43	29.97	-3.12	-1.58	-1.74	-3.44	-2.47
EGR3	1960	29.78	78.94	78.66	69.37	-1.67	-0.34	-0.47	0.00	45.19	72.19	38.97	37.64	-3.67	-1.19	-2.09	-2.93	-2.47
P66ALPHA	54815	47.21	37.25	35.54	39.59	-2.02	-2.78	-4.07	-2.24	63.27	66.17	24.02	46.86	-1.16	-1.89	-4.91	-1.92	-2.47
DC2	58505	77.17	55.25	66.64	28.01	-1.18	-1.77	-2.10	-3.48	66.36	51.06	46.15	45.95	-1.74	-3.13	-3.29	-1.71	-2.47
CD3D	915	45.06	64.80	54.64	43.34	-1.39	-1.08	-1.69	-1.62	70.43	48.33	50.51	39.28	-1.35	-4.35	-1.05	-3.12	-2.47
KCNK13	56659	50.58	56.08	51.76	30.24	-1.38	-1.28	-1.52	-1.49	34.66	65.06	37.63	49.73	-4.72	-1.21	-2.40	-1.54	-2.47
SRMS	6725	46.23	33.85	32.35	16.82	-1.22	-2.16	-2.28	-2.86	56.61	63.06	43.51	43.28	-2.49	-2.21	-2.76	-2.40	-2.47
MYH8	4626	43.79	69.29	66.01	56.91	-1.16	-0.79	-0.71	-0.76	57.12	53.67	41.51	51.91	-2.23	-3.80	-1.84	-1.99	-2.47
FLJ10074	55681	141.92	142.80	133.73	119.63	0.61	0.58	0.66	1.03	67.64	52.91		31.65	-1.12	-2.81		-3.46	-2.46
VHL	7428	36.95	53.01	64.42	54.40	-2.48	-1.68	-1.71	-0.78	41.51	63.56	51.79	47.81	-3.82	-2.61	-2.31	-1.11	-2.46
POU6F1	5463	51.34	52.62	51.93	31.93	-0.97	-1.09	-1.27	-1.51	44.40	56.99	51.37	38.78	-3.74	-2.46	-1.16	-2.48	-2.46
DGKB	1607	117.49	79.97	93.53	58.74	0.41	-0.33	-0.08	-0.73	50.66	70.70	39.32	35.15	-2.81	-1.13	-2.87	-3.03	-2.46
SPAP1	79368	104.88	146.07	159.37	116.12	0.35	0.69	0.96	0.83	54.55	62.98	35.91	34.49	-1.77	-1.89	-2.44	-3.72	-2.45
SERTAD1	29950	19.97	15.57	22.53	35.52			-2.61	-1.71	51.37	48.32	34.06	50.34			-2.72	-2.18	-2.45
LOC201181	201181	149.75	104.21	126.44	88.73	0.74	0.27	0.39	0.37	46.11	55.20	45.26	39.94	-2.58	-2.27	-2.75	-2.21	-2.45
LRIG2	9860	89.16	43.16	54.72	81.08	-0.69	-1.88	-1.88	-0.09	51.88	55.44	45.31	54.43	-3.16	-2.76	-2.72	-1.16	-2.45
PMVK	10654	49.92	79.79	71.03	54.96	-1.11	-0.49	-0.67	-0.62	67.91	57.94	40.64	42.28	-1.27	-2.81	-3.19	-2.52	-2.45
CALD1	800	28.98	23.44	53.28	19.53	-2.89	-3.27	-2.07	-3.38	68.15	61.94	34.85	49.43	-1.39	-2.58	-4.08	-1.75	-2.45
E(Y)2	56943	104.98	78.91	65.68	47.63	-0.31	-0.94	-1.43	-1.30	59.31	51.36	38.73	43.26	-1.29	-4.20	-2.04	-2.26	-2.45
KRT13	3860	25.97	17.12	34.84	29.01	-3.58	-5.72	-4.55	-2.64	41.68	83.55	31.47	38.73	-4.93	-0.34	-2.29	-2.22	-2.45
SCAMP1	9522	78.48	74.28	71.20	41.20	-0.17	-0.64	-0.58	-1.41	49.78	60.06	39.19	55.09	-3.12	-2.93	-2.10	-1.63	-2.44
SC4MOL	6307	92.87	103.70	98.95	92.78	0.11	0.07	0.00	0.23	48.09	64.53	45.61	46.84	-3.35	-2.38	-1.42	-2.63	-2.44
LOC93380	93380	31.27	17.85	20.38	6.76	-4.03	-5.58			58.19	52.08		55.81	-1.97	-2.91			-2.44
ATF5	22809	52.26	36.18	46.03	33.91	-0.75	-1.76	-1.64	-1.29	53.45	67.02	35.11	38.46	-2.67	-1.69	-2.58	-2.81	-2.44
SPRR1A	6698	16.75	19.80	25.61	14.71			-4.08	-3.45	79.48	68.80	51.81	34.69			-1.25	-3.63	-2.44
DPH2L1	1801	56.91	79.90	54.78	53.15	-2.10	-1.36	-2.72	-2.08	61.79	52.51	59.83	42.30	-1.78	-4.02	-1.00	-2.95	-2.44
KIAA0759	23357	86.12	77.05	76.43	71.73	-0.71	-1.00	-1.00	-0.26	60.35	51.22	35.11	46.93	-1.19	-4.22	-2.45	-1.87	-2.44
GLG1	2734	122.00	69.17	91.68	75.90	0.37	-0.41	-0.45	0.08	38.84	56.01	40.56	55.86	-3.51	-2.18	-3.44	-0.61	-2.43

		Mock								ATRi								
		% of Control				Robust Z-score				% of Control				Robust Z-score				
Gene Symbol	Gene ID	Rep 1	Rep 2	Rep 3	Rep 4	Rep 1	Rep 2	Rep 3	Rep 4	Rep 1	Rep 2	Rep 3	Rep 4	Rep 1	Rep 2	Rep 3	Rep 4	Average
ACTR3	10096	38.59	38.05	43.58	33.71	-1.78	-1.79	-2.16	-2.27	57.01	51.60	39.67	46.36	-1.76	-3.19	-2.49	-2.29	-2.43
ZNF540	163255	24.05	38.20	47.51	41.70	-3.19	-2.82	-3.18	-1.63	63.97	67.96	36.78	29.91	-1.49	-1.59	-2.93	-3.72	-2.43
TXNRD3	114112	25.09	26.00	18.34	15.39	-2.19	-2.33			51.04	64.66	45.96	79.79	-3.33	-1.53			-2.43
HNRPM	4670	71.02	31.27	43.28	20.68	-0.97	-2.93	-2.98	-2.87	52.22	72.47	40.68	39.92	-2.41	-1.52	-3.81	-1.97	-2.43
TSPAN6	7105	113.09	92.16	87.11	95.58	0.16	-0.18	-0.53	0.50	64.77	48.01	27.44	56.63	-1.54	-3.87	-3.43	-0.87	-2.43
ZNF84	7637	57.05	66.06	88.75	44.65	-1.31	-1.05	-0.61	-1.53	65.13	67.57	39.97	40.68	-1.73	-1.96	-3.27	-2.74	-2.43
CHST5	23563	17.46	25.80	19.07	22.61	-3.38	-3.00	-4.36	-3.30	57.23	72.21	52.87	28.81	-2.60	-1.28	-0.81	-5.02	-2.43
HT021	57415	83.38	81.42	59.00	41.65	-0.91	-0.70	-1.79	-2.09	71.74	51.31		36.51	-0.86	-3.65		-2.75	-2.42
FLJ38753	127707	108.78	70.73	66.91	63.88	-0.39	-1.00	-1.60	-0.60	60.00	53.97	43.22	44.97	-1.54	-3.81	-2.49	-1.84	-2.42
PSFL	83464	66.82	134.54	177.57	95.63	0.49	0.67	0.51	0.64	37.79	57.19	30.97	58.19	-2.63	-3.32	-3.62	-0.11	-2.42
FLJ37953	129450	36.46	56.90	83.58	32.27	-1.76	-1.08	-0.50	-1.55	76.56	48.81	32.60	37.31	-0.08	-3.52	-3.22	-2.86	-2.42
PTGDR	5729	36.28	37.97	24.43	21.61	-1.78	-2.45	-3.78	-3.10	60.03	63.27	34.96	45.65	-3.01	-1.78	-2.55	-2.33	-2.42
MGC4796	83931	59.59	33.54	37.52	31.80	-0.84	-2.17	-1.98	-1.65	56.06	59.45	48.87	42.84	-2.56	-2.63	-2.03	-2.45	-2.42
SPC24	147841	38.43	57.87	55.85	31.58	-2.39	-1.47	-2.16	-1.96	55.93	57.36	44.10	49.83	-1.98	-3.46	-3.31	-0.91	-2.42
GLIS2	84662	13.81	32.49	30.84	17.05	-2.91	-1.96	-2.52	-2.54	44.84	66.72	26.03	61.92	-3.72	-1.72	-3.99	-0.24	-2.42
LOC646480	646480	109.52	98.53	99.13	73.07	-0.26	-0.34	-0.58	-0.52	47.23	60.14	44.39	42.58	-2.74	-2.60	-1.88	-2.44	-2.42
NCK2	8440	110.90	92.17	84.57	62.02	0.33	-0.08	-0.18	-0.29	55.82	50.15	52.26	33.61	-2.21	-3.26	-1.07	-3.12	-2.41
TRAPPC6B	122553	66.31	92.90	81.78	80.62	-0.96	-0.35	-1.23	-0.02	48.06	68.29	38.26	41.29	-3.29	-1.55	-2.73	-2.08	-2.41
ZNF236	7776	143.99	118.45	96.89	72.71	0.83	0.26	0.09	0.20	60.65	63.23	33.53	38.68	-1.60	-1.79	-3.55	-2.71	-2.41
OR6T1	219874	26.64	30.76	32.76	30.93	-2.97	-3.42	-4.51	-2.36	69.09	61.17	43.10	27.60	-1.01	-2.38	-2.14	-4.13	-2.41
TBCE	6905	98.64	83.35	95.76	47.38	-0.44	-0.67	-0.70	-1.82	50.99	61.50	56.68	43.66	-3.84	-2.00	-1.82	-1.98	-2.41
FLJ20581	54988	30.05	55.69	39.03	25.17	-2.88	-1.99	-3.06	-3.88	67.52	58.91		31.64	-1.19	-2.09		-3.94	-2.41
FLJ13615	80184	35.99	42.07	73.45	37.11	-2.31	-2.46	-1.12	-1.71	45.95	62.16	34.79	36.41	-2.65	-2.46	-2.43	-2.09	-2.41
MT1F	4494	64.73	36.20	64.28	23.45	-1.31	-2.24	-1.39	-3.41	48.26	66.31	30.12	54.90	-3.64	-1.25	-3.99	-0.73	-2.40
GPR172B	55065	34.45	77.06	57.30	39.46	-1.47	-0.32	-0.89	-1.42	44.41	61.99	38.84	53.03	-3.33	-2.03	-2.80	-1.44	-2.40
TRIM71	131405	102.73	56.29	94.26	55.90	-2.01	-3.38	-1.64	-2.63	66.48	58.92	48.58	60.80	-1.23	-4.55	-1.99	-1.82	-2.40
RAMP2	10266	57.17	54.65	57.72	45.17	-0.59	-0.95	-0.87	-1.13	49.41	51.72	47.26	48.71	-2.74	-3.24	-1.64	-1.96	-2.40
ALOX12B	242	55.51	95.06	69.93	75.93	-1.41	-0.22	-1.28	-0.21	57.73	69.10	41.07	46.79	-1.68	-2.21	-2.98	-2.70	-2.39
DSCR4	10281	53.60	47.97	68.31	35.64	-1.45	-1.74	-1.36	-2.03	50.30	79.47	42.09	46.09	-3.70	-0.79	-2.97	-2.10	-2.39
TLR8	51311	65.38	56.28	74.41	41.36	-0.39	-0.96	-0.59	-0.93	50.16	66.74	35.27	42.77	-3.05	-1.72	-2.56	-2.24	-2.39
FBXL5	26234	69.60	59.54	71.07	38.08	-0.78	-1.12	-1.01	-1.57	55.90	54.22	39.71	40.47	-1.47	-2.85	-3.07	-2.16	-2.39
FAM36A	116228	107.05	129.60	117.58	90.41	0.14	0.43	0.40	0.57	52.80	53.56	49.02	46.12	-2.81	-3.36	-2.31	-1.07	-2.39
SHC1	6464	55.64	53.17	65.06	49.51	-1.23	-2.48	-1.64	-1.61	64.66	73.00	38.72	44.15	-1.17	-1.56	-4.03	-2.78	-2.39
C6ORF27	80737	26.43	18.09	13.25	11.95	-2.38	-2.80			77.17	39.58	54.13	37.70	-0.15	-4.62			-2.39
LOC90835	90835	26.20	20.30	36.24	25.51	-2.40	-2.61	-1.88	-1.58	42.74	56.40	49.81	45.64	-3.70	-2.48	-1.54	-1.81	-2.38
FBXO17	115290	25.00	33.98	35.50	35.01	-2.70	-2.17	-2.67	-1.75	56.80	61.89	44.59	29.47	-1.38	-1.98	-2.43	-3.75	-2.38
FLJ43860	389690	96.22	74.73	75.89	63.41	-0.20	-0.82	-0.89	-0.61	64.88	54.87	42.44	37.17	-1.95	-2.87	-2.48	-2.25	-2.38
FLJ32884	149499	105.04	83.98	92.27	74.83	-0.31	-1.40	-0.92	-0.50	59.92	58.42	37.99	36.51	-1.68	-2.89	-2.48	-2.48	-2.38
KIAA1787	84461	38.91	29.34	39.32	23.80	-2.20	-2.79	-2.94	-2.94	55.26	70.75	43.07	46.26	-2.99	-1.63	-2.83	-2.08	-2.38
NEDD5	4735	77.45	81.74	90.63	71.12	-1.17	-0.67	-0.60	-0.29	37.67	72.12	56.36	40.45	-4.38	-1.54	-1.17	-2.42	-2.38
CRYAA	1409	74.48	67.97	74.85	50.90	-0.83	-0.91	-0.94	-1.05	60.06	64.86	31.50	38.08	-1.98	-1.80	-2.83	-2.92	-2.38
RNPC1	55544	80.16	113.29	97.03	71.87	-0.86	0.00	-0.31	-0.26	50.30	64.24	32.95	44.12	-2.16	-2.47	-2.72	-2.17	-2.38
TTC1	7265	79.20	76.81	70.15	40.58	-0.91	-1.09	-1.87	-1.77	59.62	58.57	26.26	45.11	-2.48	-2.55	-2.97	-1.49	-2.37
KIAA1271	57506	39.95	51.06	52.52	25.36	-3.28	-2.46	-2.93	-3.46	53.19	54.84		41.49	-2.48	-2.58		-2.05	-2.37
HSU79303	29903	48.38	67.14	54.12	50.47	-2.55	-2.03	-2.77	-2.29	49.92	69.77	41.22	54.11	-3.08	-1.76	-3.01	-1.62	-2.37
ZNF169	169841	83.40	101.16	96.03	67.52	-0.21	0.00	0.08	0.07	64.64	41.38	35.54	56.80	-1.22	-4.35	-3.25	-0.63	-2.36
MARCH9	92979	164.27	147.84	129.48	97.90	-0.60	-0.41	-0.44	-0.48	64.90	66.14	46.41	55.48	-1.41	-3.31	-2.20	-2.53	-2.36
LOC170261	170261	27.12	26.89	32.78	25.80	-3.95	-3.98	-3.99	-4.07	96.69	84.07		89.32	-1.55	-6.61		1.08	-2.36
UNQ9372	388364	30.25	52.90	49.45	30.51	-3.13	-2.12	-2.87	-3.00	63.86	50.69	44.26	41.93	-1.39	-3.49	-2.53	-2.03	-2.36
TEX261	113419	51.80	40.46	42.43	33.75	-1.70	-2.15	-2.44	-2.06	49.89	66.22	40.86	37.22	-3.06	-1.65	-1.69	-3.04	-2.36
RBM10	8241	69.03	62.16	82.56	36.83	-0.40	-0.92	-0.53	-1.28	47.69	53.00	50.76	37.00	-2.45	-2.99	-1.10	-2.90	-2.36
MGC4809	91860	76.22	107.48	105.76	42.82	-1.10	-0.68	-0.42	-2.13	56.18	62.80	28.08	50.09	-2.08	-2.35	-3.84	-1.17	-2.36
GPR30	2852	24.44	26.20	33.27	15.71	-2.49	-3.31	-2.98	-3.86	69.62	62.02	34.07	40.48	-1.83	-1.91	-2.68	-3.01	-2.36
PKP1	5317	85.99	88.83	87.60	46.01	-0.34	-0.18	-0.36	-0.58	45.73	63.60	54.23	36.71	-2.74	-1.75	-1.60	-3.34	-2.36
NINJ2	4815	68.85	89.43	92.53	84.22	-0.96	-0.20	-0.22	-0.17	53.54	57.49	78.44	50.01	-3.07	-2.13	-1.45	-2.74	-2.35
LOC389827	389827	84.46	75.63	76.88	44.39	-0.74	-0.73	-1.04	-0.47	53.82	50.41		43.06	-2.47	-3.03		-1.55	-2.35
AMN	81693	43.26	50.36	60.14	36.12	-1.86	-1.73	-1.52	-1.98	63.87	56.21	35.05	46.14	-2.04	-2.70	-3.49	-1.15	-2.35
SLC25A23	79085	56.88	76.89	95.72	47.76	-0.62	-0.39	-0.04	-0.67	51.54	57.64	40.48	45.68	-2.89	-2.70	-1.91	-1.88	-2.35
SPATA5L1	79029	18.18	37.88	17.90	25.66	-2.75	-1.63	-3.20	-2.49	66.09	60.41	32.83	43.91	-1.89	-1.97	-3.19	-2.33	-2.35
NR4A1	3164	125.87	79.41	86.68	61.63	0.60	-0.27	-0.04	-0.42	67.92	60.42	39.46	35.53	-1.74	-1.97	-2.18	-3.50	-2.35
IQSEC1	9922	23.81	68.34	44.13	28.81	-2.67	-0.74	-1.73	-1.77	44.14	49.35	49.56	45.82	-2.84	-3.45	-1.22	-1.87	-2.34
HCST	10870	61.58	53.63	48.00	25.23	-0.86	-1.15	-1.64	-1.63	64.58	61.95	49.98	30.46	-0.89	-1.91	-2.10	-4.46	-2.34
SH3GLB1	51100	60.24	65.06	56.33	96.90	-1.27	-0.82	-1.51	0.33	72.68	32.91	72.30	62.77	-1.04	-5.18	-2.00	-1.14	-2.34
FLJ10378	55132	32.55	61.43	61.40	33.15	-2.50	-1.49	-1.65	-1.97	49.57	60.22	35.04	36.85	-2.23	-2.69	-2.40	-2.04	-2.34
GJA7	10052	60.45	29.87	47.57	20.48	-0.46	-2.15	-1.09	-2.56	53.29	55.62	36.92	43.55	-1.91	-2.69	-2.30	-2.45	-2.34
GCDH	2639	108.91	113.62	97.39	70.62	0.35	0.39	0.19	-0.10	65.75	66.23	34.08	38.34	-1.92	-1.37	-2.99	-3.08	-2.34
UCN2	90226	67.05	52.71	73.30	87.59	-1.02	-1.23	-0.82	-0.03	60.49	45.38	73.71	57.23	-2.26	-3.42	-1.87	-1.79	-2.34
GHRHR	2692	51.14	70.98	91.54	45.64	-1.17	-0.98	-0.37	-1.33	73.87	58.46	29.63	45.80	-1.36	-2.30	-3.37	-2.32	-2.34
FLJ31579	257068	18.63	24.01	23.59	16.36	-2.71	-2.48			67.21	52.53	28.44	30.20	-1.80	-2.88			-2.34
CYP4Z1	199974	19.48	20.02	23.10	37.87			-2.56	-1.58	59.85	57.79	34.01	52.35			-2.73	-1.94	-2.34
HCFC2	29915	34.30	49.38	37.15	30.32	-1.57	-1.52	-1.73	-2.03	82.75	58.07	38.23	36.93	0.17	-3.19	-2.21	-4.11	-2.33
WBSCR28	135886	47.92	68.30	66.44	39.70	-1.37	-0.64	-1.17	-1.81	49.44	68.05	37.74	45.44	-2.61	-1.57	-2.74	-2.39	-2.33
OFD1	8481	52.73	49.12	35.44	33.62	-0.90	-1.16	-1.83	-1.85	57.51	55.14	45.89	40.79	-2.67	-2.56	-1.35	-2.74	-2.33
LOC283219	283219	21.85	26.98	27.98	11.49	-4.75	-5.55			64.41	58.67	36.37	78.13	-1.52	-3.14			-2.33
ZSWIM2	151112	164.15	140.77	118.30	85.47	-0.60	-0.56	-0.78	-1.00	63.73	79.28	54.46	40.57	-1.54	-1.37	-1.47	-4.93	-2.33
VPS8	23355	88.54	55.77	91.99	48.48	-2.46	-3.40	-1.73	-3.18	59.75	63.37	56.38	57.82	-2.02	-3.77	-1.31	-2.21	-2.33
TKT	7086	83.77	108.82	84.79	90.26	-0.03	0.15	-0.22	-0.04	68.89	51.88	37.89	58.97	-1.26	-3.26	-3.02	-1.78	-2.33
MAP3K14	9020	83.63	66.49	56.68	29.19	-0.20	-0.67	-1.27	-2.28	67.00	42.68	46.28	42.64	-1.06	-4.28	-1.99	-1.98	-2.33
KIAA1893	114787	78.44	57.28	72.75	54.01	-1.14	-1.48	-1.32	-1.09	63.26	53.11	44.96	44.76	-1.22	-3.94	-2.29	-1.86	-2.33
ZNF433	163059	29.49	40.07	29.28	18.32	-2.48	-2.29	-3.70	-2.98	53.59	58.64	46.28	39.95	-1.82	-2.82	-1.83	-2.83	-2.33
ELL3	80237	32.70	38.83	73.92	19.44	-2.29	-2.36	-1.12	-2.85	49.46	65.03	35.02	48.76	-2.24	-2.08	-3.28	-1.70	-2.32
ANKRD9	122416	23.48	17.21	14.21	6.86	-2.34	-3.33			58.07	50.52	82.41	50.87	-1.46	-3.19			-2.32
EDARADD	128178	80.43	74.80	62.90	36.85	-0.53	-0.85	-1.74	-0.86	60.69	54.99	45.48	42.04	-1.86	-3.18	-2.77	-1.47	-2.32
KIAA1529	57653	57.61	75.50	63.25	49.46	-1.86	-0.90	-1.60	-1.33	54.40	47.49	56.86	37.54	-2.49	-3.15	-1.21	-2.42	-2.32
DIO2	1734	64.17	65.63	62.71	57.87	-0.49	-0.37	-0.58	-0.37	56.60	53.18	35.08	54.34	-1.62	-3.39	-3.21	-1.05	-2.32
USP18	11274	2.27	15.62	56.07	26.25			-1.80	-2.09	96.72	52.74	38.08	37.34			-2.69	-1.94	-2.32
PGA5	5222	77.22	47.54	49.85	28.88	-0.51	-1.96	-1.68	-2.68	59.91	60.14	45.85	45.96	-1.87	-2.56	-2.26	-2.58	-2.32
FLJ90652	283899	59.06	83.40	79.96	55.26	-1.34	-0.71	-0.86	-0.78	59.24	53.49	33.53	38.64	-1.26	-3.57	-2.59	-1.85	-2.32
LOC643812	643812	97.24	74.15	98.86	36.31	-0.56	-1.17	-0.45	-2.91	50.28	69.04		53.12	-2.74	-2.56		-1.65	-2.32
TIMP3	7078	22.07	23.19	21.51	11.85	-1.95	-2.60			56.67	52.43	39.52	30.58	-1.55	-3.08			-2.31
FOXE3	2301	55.79	46.65	61.07	42.98	-0.95	-1.77	-1.41	-1.64	62.07	77.15	35.41	37.66	-2.11	-0.77	-2.96	-3.37	-2.31

		Mock								ATRi								
		% of Control				Robust Z-score				% of Control				Robust Z-score				
Gene Symbol	Gene ID	Rep 1	Rep 2	Rep 3	Rep 4	Rep 1	Rep 2	Rep 3	Rep 4	Rep 1	Rep 2	Rep 3	Rep 4	Rep 1	Rep 2	Rep 3	Rep 4	Average
RBM29	84173	134.53	162.31	101.59	106.68	0.78	0.76	0.08	0.68	57.99	63.42	35.23	52.80	-1.93	-2.32	-3.18	-1.76	-2.30
SALL4	57167	87.50	61.27	95.04	63.94	-0.24	-0.85	-0.32	-0.47	47.82	56.83	41.42	54.49	-2.81	-2.63	-2.27	-1.48	-2.30
CA9	768	42.19	36.12	38.34	24.84	-1.21	-1.30	-1.42	-1.86	51.99	52.45	47.56	43.69	-2.10	-3.49	-1.44	-2.14	-2.29
DAP	1611	38.48	65.16	46.88	51.74	-1.67	-0.72	-1.36	-0.38	51.36	56.42	36.45	53.43	-2.60	-2.48	-3.13	-0.96	-2.29
SMARCC2	6601	33.29	63.98	27.16	19.50	-2.50	-1.95	-3.39	-3.87	42.95	44.68	58.20	56.41	-3.10	-4.62	-0.75	-0.69	-2.29
KIAA1068	23386	28.09	12.35	22.11	31.01	-3.51	-5.01	-5.26	-2.72	46.33	55.49	48.77	56.93	-3.12	-3.60	-1.89	-0.55	-2.29
TWIST1	7291	81.46	82.94	88.02	70.71	-0.15	-0.57	-0.48	-0.35	62.58	75.26	41.22	34.14	-2.06	-0.96	-2.14	-3.98	-2.29
MFI2	4241	124.79	74.01	103.76	63.35	0.23	-0.53	0.00	-0.02	40.01	65.55	55.68	40.86	-3.45	-1.56	-1.44	-2.69	-2.29
DSCR10	259234	97.87	68.03	74.03	44.16	-0.18	-0.91	-0.96	-1.40	68.55	46.23	37.03	48.57	-1.21	-4.13	-2.12	-1.66	-2.28
C10ORF104	119504	53.94	58.92	61.76	72.33	-1.52	-1.01	-1.27	-0.70	53.04	52.48	75.53	58.37	-3.14	-2.63	-1.71	-1.66	-2.28
TUBB4	10381	9.86	11.73	6.49	7.37	-1.72	-2.21			38.82	35.00	29.97	36.14	-3.38	-1.18			-2.28
CHRM3	1131	187.60	186.46	180.17	134.24	1.16	1.27	1.38	1.22	59.90	61.88	39.94	46.08	-3.03	-1.92	-1.89	-2.28	-2.28
KRTAP13-3	337960	38.53	51.51	52.66	23.56	-1.58	-1.23	-1.44	-1.75	57.10	50.37	46.64	47.12	-1.55	-3.21	-2.52	-1.83	-2.28
PHF21A	51317	23.70	17.79	17.79	12.07	-2.80	-3.38			61.48	48.30	49.57	71.27	-0.93	-3.62			-2.28
SYK	6850	29.23	29.63	36.69	49.92	-2.10	-2.19	-2.30	-1.09	50.18	61.80	43.13	43.38	-2.87	-1.97	-2.37	-1.89	-2.27
GPHB5	122876	83.32	46.52	60.68	42.66	-0.68	-1.70	-1.56	-1.71	55.43	71.87	40.80	33.07	-2.67	-0.81	-2.58	-3.02	-2.27
DSCR6	53820	73.16	61.40	57.55	37.91	-1.10	-1.19	0.56	0.54	50.07	42.39		30.78	-2.88	-4.10		0.16	-2.27
ACP1	52	75.00	137.57	91.72	66.62	-0.41	0.70	-0.04	-0.07	39.94	57.43	41.12	42.52	-3.21	-2.06	-2.07	-1.72	-2.27
KNTC1	9735	105.02	93.22	80.34	84.61	0.00	-0.12	-0.59	-0.15	96.75	12.29	103.53	76.08	0.86	-10.55	0.42	0.21	-2.26
MSH5	4439	70.06	91.64	85.63	56.65	-0.23	0.00	-0.05	-0.64	76.73	59.40	37.46	38.53	-0.31	-2.32	-3.01	-3.40	-2.26
FLJ12847	79648	61.46	58.42	51.80	43.13	-1.88	-2.57	-2.93	-2.95	62.59	62.72	49.49	44.17	-1.70	-2.60	-2.02	-2.72	-2.26
APPBP1	8883	69.28	117.03	120.51	102.66	-0.72	-0.21	0.20	0.57	42.61	87.10	44.81	44.68	-3.36	-0.05	-2.92	-2.71	-2.26
RPS6KA3	6197	89.64	99.77	83.92	56.22	-0.07	0.09	-0.34	-0.83	45.85	74.36	46.49	36.57	-3.43	-0.81	-1.97	-2.82	-2.26
IL31	386653	52.13	33.92	31.62	25.94	-1.10	-1.78	-2.15	-1.55	50.26	70.07	42.12	38.53	-2.73	-1.17	-2.39	-2.73	-2.26
BNIP1	662	31.61	41.67	38.58	31.83	-1.88	-1.52	-1.79	-3.14	49.54	75.95	50.20	45.85	-3.41	-0.78	-1.44	-3.40	-2.26
CLST11240	51751	67.56	48.34	50.00	50.90	-1.67	-2.63	-3.12	-1.44	66.54	48.79		40.13	-1.21	-3.33		-2.22	-2.26
PLEKHG4	25894	47.34	49.44	55.53	32.35	-1.74	-1.67	-1.95	-2.25	59.90	59.26	37.86	67.37	-2.37	-2.89	-3.59	-0.16	-2.25
PLEKHH1	57475	69.76	38.32	45.13	14.47	-0.90	-2.39	-2.50	-3.49	47.82	59.74	47.69	44.33	-2.41	-2.69	-1.68	-2.24	-2.25
ZNF514	84874	33.92	12.87	18.31	9.97	-1.91	-3.80			73.52	43.75	54.12	42.89	-0.28	-4.23			-2.25
COL14A1	7373	70.63	67.53	68.79	47.87	-0.97	-1.43	-1.36	-1.82	63.48	59.73		35.83	-1.51	-2.00		-3.24	-2.25
C20ORF46	55321	63.90	87.83	63.17	76.79	-1.42	-0.67	-2.27	-0.12	65.53	54.84	27.63	45.68	-1.83	-2.96	-2.78	-1.43	-2.25
OR8U1	219417	21.98	18.01	26.55	29.93			-3.33	-2.61	77.85	60.27	36.16	53.80			-2.96	-1.54	-2.25
SAP18	10284	21.75	40.69	26.21	15.53	-3.39	-3.31	-3.47	-4.49	56.94	47.32	51.00	44.83	-1.41	-4.28	-1.45	-1.85	-2.25
KLRA1	10748	32.83	47.36	33.08	33.04	-1.77	-1.42	-2.35	-1.65	67.42	51.74	54.42	38.25	-0.77	-3.74	-0.83	-3.66	-2.25
HACE1	57531	71.91	44.31	54.75	32.01	-0.82	-1.73	-1.40	-1.39	58.17	59.12	31.54	41.34	-1.54	-1.71	-3.22	-2.52	-2.25
ATP1A2	477	34.64	34.36	45.42	32.04	-1.42	-1.86	-1.67	-1.40	44.78	77.92	34.96	44.82	-3.73	-0.67	-2.60	-1.98	-2.25
AATK	9625	152.03	148.67	124.69	83.72	0.57	0.72	0.47	0.18	56.75	60.82	54.21	41.24	-2.47	-2.47	-1.38	-2.65	-2.24
LOC387778	387778	79.73	101.31	76.21	74.56	-0.99	-0.85	-1.62	-0.51	58.04	68.33	35.39	35.62	-1.88	-1.71	-2.80	-2.58	-2.24
FBXO4	26272	57.38	31.85	26.95	36.25	-1.14	-2.29	-3.33	-1.68	48.26	47.56	54.34	45.14	-2.31	-3.72	-1.33	-1.61	-2.24
PER1	5187	112.82	53.60	59.30	48.75	0.04	-1.45	-1.90	-1.74	70.04	71.97	37.53	33.99	-0.98	-1.14	-2.97	-3.88	-2.24
PIM2	11040	93.16	66.51	73.16	32.26	-0.01	-0.67	-0.66	-2.05	74.36	55.76	44.78	30.73	-0.42	-2.61	-2.17	-3.76	-2.24
FBLN5	10516	49.62	45.81	28.20	38.74	-1.57	-1.95	-3.55	-1.81	73.84	61.77	40.48	31.95	-1.14	-2.07	-2.73	-3.01	-2.24
PITPNB	23760	89.39	78.86	94.01	52.57	-0.62	-1.01	-0.75	-1.10	63.34	64.49	31.89	35.13	-2.06	-1.95	-2.24	-2.68	-2.24
DVL2	1856	46.96	52.13	33.17	24.20	-1.29	-1.08	-2.06	-1.66	58.42	58.35	48.34	35.72	-1.83	-2.28	-1.69	-3.14	-2.23
MIST1	168620	21.77	18.53	27.50	28.29	-3.64	-4.54	-4.95	-3.18	69.37	58.71	31.73	46.53	-0.66	-2.78	-3.54	-1.96	-2.23
CBX3	11335	25.17	28.57	41.15	22.35	-3.09	-3.62	-3.69	-3.15	60.79	54.98	48.29	38.96	-1.81	-3.17	-1.57	-2.38	-2.23
BRUNOL4	56853	90.02	117.48	98.67	82.04	-0.11	-0.20	-0.40	-0.10	67.63	60.98	45.16	49.79	-0.93	-3.10	-2.86	-2.04	-2.23
TRIM23	373	53.33	59.05	44.37	36.15	-3.99	-3.23	-4.48	-4.30	68.53	62.09	51.86	57.60	-1.00	-3.99	-1.69	-2.24	-2.23
ZNF595	152687	123.39	142.35	122.37	108.21	0.49	0.60	0.31	0.44	81.07	26.38	68.62	68.60	-0.06	-8.69	-0.09	-0.07	-2.23
MLH3	27030	56.10	72.97	63.06	53.54	-0.71	-0.62	-0.78	-0.72	54.87	75.44	40.61	41.23	-2.26	-1.03	-2.40	-3.21	-2.23
OR6K2	81448	119.48	102.52	116.68	54.47	-0.10	-0.20	0.21	-1.07	67.56	53.80	40.77	39.85	-1.30	-2.40	-3.10	-2.10	-2.22
C14ORF31	122786	63.70	53.69	57.75	40.74	-1.32	-1.94	-1.80	-1.69	49.99	56.01	38.08	55.74	-2.19	-3.53	-2.11	-1.06	-2.22
PRAMEF8	391002	56.45	49.82	74.36	32.86	-1.01	-0.96	-0.99	-1.43	63.33	57.46	41.95	35.36	-0.85	-2.02	-3.23	-2.79	-2.22
SLC40A1	30061	99.43	132.79	148.97	96.95	0.34	0.69	0.85	0.62	62.39	68.00	43.74	37.17	-1.21	-1.72	-2.12	-3.83	-2.22
C14ORF106	55320	111.89	51.25	81.22	48.58	0.08	-1.76	-0.96	-1.03	66.60	58.03	52.80	36.33	-0.91	-3.36	-2.19	-2.42	-2.22
KHSRP	8570	19.74	36.71	36.52	13.28	-2.47	-1.56	-1.64	-3.36	47.27	51.45	46.66	40.52	-1.98	-2.68	-1.88	-2.33	-2.22
AKAP5	9495	93.73	75.86	75.78	70.51	-0.35	-1.44	-0.94	-0.42	51.76	65.55	39.09	46.71	-1.98	-2.38	-2.87	-1.64	-2.22
JM1	28952	140.99	103.42	88.40	94.39	0.28	-0.24	-0.58	0.44	63.18	51.74	35.56	52.13	-0.95	-4.14	-2.40	-1.38	-2.22
ZDHHC6	64429	63.60	73.10	64.20	43.17	-1.43	-1.24	-2.21	-1.61	61.87	60.96	32.18	39.61	-2.23	-2.30	-2.21	-2.11	-2.21
MIA	8190	13.39	26.55	32.10	17.21			-3.15	-3.70	44.84	62.45	44.72	42.77			-1.87	-2.55	-2.21
STK36	27148	79.91	92.85	70.72	43.92	-0.40	-0.19	-0.68	-1.04	52.10	66.79	52.61	43.14	-3.05	-1.81	-1.57	-2.41	-2.21
DOLPP1	57171	3.31	10.73	28.03	14.13			-2.23	-3.43	55.88	92.53	51.23	40.71			-1.13	-3.29	-2.21
FLJ46247	374786	98.82	83.73	66.37	45.49	-0.46	-1.41	-2.13	-1.95	63.12	55.62	40.67	40.70	-1.36	-3.26	-2.17	-2.03	-2.21
ARID3B	10620	30.64	43.17	45.61	28.36	-3.18	-2.86	-3.52	-2.70	71.71	63.97	24.35	37.66	-1.21	-2.00	-3.25	-2.35	-2.20
KIAA0409	23378	55.13	46.12	58.98	54.23	-1.60	-1.96	-1.57	-1.31	66.95	51.53	44.21	47.30	-1.61	-3.52	-2.15	-1.53	-2.20
MGC4368	79415	25.55	21.18	12.60	43.83	-4.32	-6.49	-8.18	-2.88	48.67	64.96	51.98	55.41	-3.23	-2.32	-1.76	-1.49	-2.20
TTLL4	9654	48.90	51.40	46.41	70.36	-0.95	-0.75	-1.09	-0.03	51.23	67.84	34.70	47.56	-2.19	-1.63	-3.28	-1.72	-2.20
CLEC2L	154790	75.64	93.27	77.74	76.52	-0.81	-0.21	-0.81	-0.35	50.01	64.48	48.81	47.36	-3.61	-2.04	-1.63	-1.53	-2.20
KLK12	43849	54.45	73.18	56.42	80.66	-1.16	-1.00	-1.38	-0.07	51.60	60.07	42.04	65.05	-2.82	-2.57	-2.80	-0.62	-2.20
CAB45	51150	27.38	39.30	46.83	34.59	-3.03	-2.76	-2.40	-2.11	50.55	75.66	30.72	41.62	-2.13	-1.21	-3.01	-2.44	-2.20
BTG1	694	37.74	21.40	31.17	25.86	-1.37	-2.50	-1.93	-1.99	45.02	55.10	52.16	34.66	-2.25	-2.28	-1.17	-3.09	-2.20
LOC401429	155060	10.94	5.08	6.16	34.79			-10.05	-2.60	60.92	58.09	34.55	52.79			-3.12	-1.28	-2.20
LOC442582	442582	96.22	73.80	49.47	39.33	-0.22	-0.71	-2.03	-1.69	53.72	47.74	47.55	53.06	-2.63	-3.91	-1.03	-1.21	-2.19
RPL36AL	6166	16.54	21.24	44.39	43.55			-2.12	-1.55	93.35	72.09	39.35	50.55			-2.53	-1.86	-2.19
SNCA	6622	50.39	39.37	55.11	25.59	-1.76	-2.39	-2.21	-2.41	44.77	74.43	49.01	44.41	-3.36	-1.30	-2.65	-1.47	-2.19
CASP14	23581	53.84	66.52	95.33	45.49	-1.18	-1.21	-0.14	-1.52	71.91	61.00	41.09	45.29	-0.71	-2.46	-2.94	-2.66	-2.19
HIRIP3	8479	113.12	91.79	94.11	63.59	0.13	-0.34	-0.31	-0.60	72.12	51.32	48.03	36.43	-1.28	-3.31	-1.82	-2.35	-2.19
SMC1L2	27127	217.69	181.11	174.01	139.98	1.55	1.25	1.35	1.51	62.77	77.52	31.82	39.80	-2.18	-0.35	-3.36	-2.87	-2.19
SOAT1	6646	29.00	26.64	33.50	39.91	-2.04	-2.30	-2.07	-2.47	66.62	66.87	37.26	52.17	-1.48	-1.60	-3.11	-2.57	-2.19
WDTC1	23038	27.57	28.54	27.02	17.72	-3.34	-3.15	-3.70	-4.43	73.04	53.76	38.90	45.80	-1.01	-3.24	-2.83	-1.68	-2.19
LRRC14	9684	82.44	48.07	82.87	53.16	-0.98	-2.14	-1.25	-1.46	70.91	46.94	57.50	42.08	-1.21	-3.65	-1.72	-2.17	-2.19
LOC203522	203522	91.64	104.13	102.10	62.29	-0.65	-0.78	-0.54	-1.03	56.83	56.03	49.01	39.10	-2.01	-3.21	-1.34	-2.20	-2.19
HYPB	29072	43.99	82.45	67.22	58.55	-1.44	-0.58	-1.16	-0.83	69.33	78.28	37.53	34.11	-1.45	-0.66	-2.65	-3.98	-2.19
BCOR	54880	87.59	69.36	88.01	68.82	-0.80	-1.16	-1.02	-0.64	69.05	50.85	52.17	45.62	-1.42	-3.16	-2.41	-1.74	-2.18
INSL5	10022	84.48	87.43	106.52	81.03	-0.31	-0.16	-0.05	0.19	55.27	56.93	38.39	54.04	-1.94	-2.62	-2.66	-1.52	-2.18
SPFH2	11160	87.88	81.71	98.61	66.55	-0.75	-1.48	-0.67	-0.84	56.40	56.28	43.93	44.29	-2.06	-3.17	-1.83	-1.68	-2.18
TUSC4	10641	49.64	33.39	48.19	33.08	-1.63	-2.51	-2.35	-2.20	58.35	70.01	50.10	42.54	-2.57	-1.70	-1.94	-2.51	-2.18
FLJ12748	79929	69.45	34.78	62.68	21.68	-1.15	-3.07	-1.56	-3.29	44.85	72.18	34.02	47.61	-2.76	-1.57	-2.58	-1.81	-2.18
UNQ1912	345757	133.20	100.31	138.09	95.82	0.27	-0.88	0.56	0.22	63.41	48.13	52.05	41.35	-1.33	-4.35	-1.07	-1.96	-2.18
MGC14798	89978	119.24	138.95	125.28	79.41	0.00	0.06	0.21	-0.32	57.81	58.05	49.96	35.32	-1.90	-2.94	-1.25	-2.62	-2.18
RRM2B	50484	37.03	44.43	63.07	25.89	-1.41	-1.23	-0.64	-1.99	61.67	51.72	37.79	40.80	-0.53	-2.65	-3.23	-2.30	-2.18

		Mock								ATRi								
		% of Control				Robust Z-score				% of Control				Robust Z-score				
Gene Symbol	Gene ID	Rep 1	Rep 2	Rep 3	Rep 4	Rep 1	Rep 2	Rep 3	Rep 4	Rep 1	Rep 2	Rep 3	Rep 4	Rep 1	Rep 2	Rep 3	Rep 4	Average
LOC283377	283377	68.47	86.73	80.27	46.01	-1.28	-0.75	-1.18	-1.81	68.98	62.72	44.55	33.08	-0.93	-2.04	-2.50	-3.23	-2.18
LOC51161	51161	144.31	119.55	122.03	89.03	0.48	0.16	0.23	0.13	80.69	86.90		48.07				-2.17	-2.17
KREMEN1	83999	95.71	116.36	104.73	88.69	-0.10	0.17	-0.13	0.00	49.71	68.41	59.78	45.83	-3.79	-1.87	-0.90	-2.13	-2.17
IDH3B	3420	20.13	23.15	14.75	19.65	-2.55	-2.57			66.16	50.08	41.17	63.08	-1.08	-3.27			-2.17
FLJ16237	392636	42.02	32.05	45.80	40.03	-1.19	-1.80	-1.22	-1.10	34.94	78.28	40.31	43.69	-3.64	-0.26	-2.82	-1.97	-2.17
TRAP1	10131	81.37	103.98	78.98	73.85	-0.09	0.07	-0.36	-0.64	55.80	77.76	39.62	51.48	-2.64	-0.62	-2.77	-2.65	-2.17
CNN1	1264	59.92	69.35	69.76	60.85	-1.19	-0.94	-1.30	-0.84	60.51	71.03	51.58	38.61	-2.29	-1.60	-1.77	-3.01	-2.17
CPOX	1371	76.32	71.60	84.89	57.71	-0.30	-0.53	-0.18	-0.42	57.93	60.76	44.55	37.23	-1.97	-2.06	-1.99	-2.66	-2.17
ZC3H3	23144	43.29	32.14	36.62	49.70	-2.02	-2.19	-2.63	-2.04	85.56	44.19	76.38	44.88	0.04	-3.57	-1.63	-3.50	-2.16
PPP2R2B	5521	136.58	126.91	126.45	88.25	0.50	0.56	0.61	0.46	52.83	53.58	39.83	38.29	-1.80	-2.46	-2.22	-2.17	-2.16
MGC35118	145942	94.47	76.01	50.03	59.03	-0.53	-1.04	-2.21	-0.75	55.06	80.24	22.54	46.71	-1.68	-0.75	-4.32	-1.90	-2.16
S100A2	6273	72.43	60.69	67.65	64.22	-1.03	-1.12	-1.24	-0.54	61.12	62.36	40.09	37.98	-2.00	-1.58	-2.66	-2.39	-2.16
NCOA5	57727	41.54	53.95	53.49	49.60	-2.53	-1.47	0.42	0.74	46.82	45.86		45.34	-3.26	-3.61		0.40	-2.16
C14ORF80	283643	23.21	13.21	21.31	27.94			-4.58	-3.24	45.70	97.62	37.05	62.42			-3.87	-0.44	-2.16
OR5R1	219479	41.25	53.22	41.18	29.22	-1.49	-1.20	-1.86	-1.75	48.54	51.08	56.19	40.89	-2.36	-3.22	-0.62	-2.42	-2.15
PYC1	260434	19.76	33.68	50.24	20.79	-5.44	-3.70	-3.10	-4.03	59.52	55.78		40.74	-1.84	-2.48		-2.14	-2.15
KIAA0284	283638	84.64	64.67	102.98	66.93	-0.39	-1.09	-0.18	-0.63	51.40	76.88	41.22	57.80	-3.54	-1.03	-3.09	-0.94	-2.15
TSPAN3	10099	108.22	98.41	109.66	83.42	0.00	-0.21	0.00	0.14	64.05	60.63	60.10	31.74	-1.15	-3.00	-1.38	-3.07	-2.15
LOC126075	126075	42.71	54.93	39.27	14.23	-2.01	-1.57	-3.35	-2.37	53.86	61.85	45.15	49.92	-2.67	-2.38	-2.81	-0.72	-2.15
FLJ90586	135932	125.93	109.05	100.90	76.49	-0.05	0.00	-0.24	-0.07	51.43	72.47	44.91	41.28	-2.48	-1.51	-2.30	-2.31	-2.15
KIF9	64147	53.00	44.32	32.37	47.79	-0.81	-0.98	-1.70	-0.71	76.88	42.97	48.52	40.86	0.14	-4.93	-1.32	-2.47	-2.15
ATG5	9474	62.32	67.44	58.78	53.92	-1.20	-1.79	-1.55	-1.14	46.64	90.67	41.72	35.93	-2.60	-0.48	-2.53	-2.97	-2.15
MBTPS1	8720	119.33	134.84	133.46	97.53	0.30	0.37	0.66	0.41	61.62	57.61	53.98	44.27	-1.69	-2.85	-1.25	-2.79	-2.15
C21ORF66	94104	42.65	36.64	44.71	37.26	-1.89	-2.47	-2.32	-1.91	65.54	61.96	37.37	43.13	-1.88	-2.05	-3.15	-1.49	-2.14
ZNF509	166793	70.51	62.25	66.15	30.54	-0.52	-0.79	-0.67	-1.27	58.62	68.08	36.43	41.79	-1.80	-1.35	-3.13	-2.29	-2.14
NSDHL	50814	41.10	28.58	27.10	33.71	-1.16	-2.14	-2.45	-1.77	59.59	54.00	47.14	46.48	-1.71	-2.95	-1.66	-2.25	-2.14
TMPRSS11B	132724	23.99	29.45	39.80	33.76	-2.14	-1.95	-1.48	-1.45	50.07	47.56	50.74	39.80	-1.67	-3.13	-1.35	-2.42	-2.14
LOC345651	345651	100.47	92.51	99.85	84.52	-0.45	-0.70	-0.46	0.03	65.33	58.08		35.33	-1.32	-2.22		-2.88	-2.14
DHFR	1719	91.95	102.64	100.03	80.66	0.19	0.16	0.00	0.23	55.05	72.60	39.81	44.82	-1.93	-1.24	-2.67	-2.71	-2.14
DAAM1	23002	99.46	109.67	117.31	82.94	-0.25	-0.03	0.16	0.27	61.22	59.48	39.64	45.71	-1.13	-2.72	-2.63	-2.07	-2.14
KCNA4	3739	22.15	60.91	139.39	37.93	-0.94	-0.92	0.03	-1.32	48.46	62.83	36.78	42.05	-1.65	-2.60	-2.85	-1.45	-2.14
PCDHB10	56126	23.93	23.35	16.24	15.75	-2.57	-2.38			58.43	56.70	52.61	50.06	-1.82	-2.45			-2.14
C7ORF27	221927	90.96	80.56	94.06	69.77	-0.32	-0.64	-0.32	-0.38	34.95	71.13	58.40	49.24	-5.81	-1.13	-0.79	-0.82	-2.14
SLC29A4	222962	52.26	41.05	38.10	22.97	-1.68	-2.12	-2.72	-3.01	61.80	68.90	38.00	35.05	-1.81	-1.38	-2.01	-3.35	-2.14
CLN5	1203	38.68	28.54	35.87	13.90	-1.57	-2.36	-2.26	-2.67	64.86	51.72	43.86	47.79	-0.87	-3.04	-2.89	-1.74	-2.14
SYNGR1	9145	22.80	30.77	45.30	15.14	-3.31	-3.42	-3.35	-4.11	58.11	54.05	49.26	44.77	-2.09	-3.30	-1.47	-1.67	-2.13
C1QTNF3	114899	70.93	71.20	63.33	53.15	-1.25	-0.80	-1.68	-1.47	57.21	71.79	40.90	43.81	-2.36	-1.16	-2.55	-2.47	-2.13
CDK5R1	8851	16.74	24.50	17.45	5.70	-2.75	-2.79			63.97	59.71	49.29	55.86	-1.67	-2.60			-2.13
KIF3A	11127	43.08	46.55	46.02	26.01	-1.27	-1.31	-1.53	-1.88	56.38	65.97	37.62	44.31	-2.15	-1.54	-2.96	-1.88	-2.13
DGCR14	8220	15.98	32.67	22.77	21.97	-4.30	-3.54	-4.67	-4.32	67.89	45.51		49.48	-1.16	-3.79		-1.44	-2.13
MGC10992	92922	23.59	23.30	12.10	14.61	-4.18	-3.73			75.85	50.67		36.65	-0.52	-3.74			-2.13
LOC647060	647060	66.00	76.69	68.23	36.43	-1.12	-0.93	-1.33	-1.75	53.86	56.61	37.17	42.60	-1.78	-3.15	-2.14	-1.45	-2.13
MYH7B	57644	90.65	67.99	99.88	58.05	-0.56	-0.96	-0.05	-0.93	66.07	74.41		53.85	-1.30	-0.60		-4.48	-2.13
ABCC5	10057	15.88	20.34	28.06	16.62			-2.70	-3.09	56.14	60.56	38.65	55.79			-2.85	-1.40	-2.13
CIB3	117286	26.30	24.27	17.12	9.90	-2.39	-2.32			54.27	61.28	32.02	33.52	-2.27	-1.98			-2.12
ATP6V1B2	526	21.43	22.72	22.75	23.13	-2.30	-2.56	-2.82	-2.59	66.32	60.70	55.39	32.23	-1.12	-2.17	-0.70	-4.50	-2.12
SIGLEC11	114132	85.27	62.34	81.51	59.36	-0.80	-1.09	-0.74	-1.02	44.18	54.97	67.28	57.14	-4.30	-2.82	-0.47	-0.91	-2.12
SOX8	30812	51.96	54.24	48.80	19.31	-0.85	-0.67	-1.01	-2.31	57.98	63.42	38.98	42.32	-1.48	-2.11	-2.60	-2.30	-2.12
H2AFB2	474381	33.11	14.98	31.70	22.30	-3.15	-4.18	-3.45	-3.91	45.40	67.35	50.03	59.63	-4.10	-1.53	-2.16	-0.68	-2.12
OR13C5	138799	92.77	50.61	90.02	69.72	-0.17	-1.62	-0.57	-0.54	62.87	62.59	46.12	51.42	-2.00	-2.50	-2.43	-1.54	-2.12
OR6C76	390326	94.86	105.93	83.40	69.89	-0.32	-0.12	-0.78	-0.61	58.64	59.04		42.03	-1.93	-2.08		-2.35	-2.12
MX1	4599	90.75	94.35	78.98	61.41	-0.42	-0.79	-0.85	-0.79	53.76	78.76	44.78	33.96	-1.75	-1.30	-2.15	-3.25	-2.11
P29	25949	97.45	77.26	95.93	66.72	-0.48	-1.07	-0.56	-0.74	67.85	60.77	48.70	33.77	-1.03	-2.25	-2.05	-3.13	-2.11
C14ORF43	91748	25.97	36.13	41.39	27.28	-3.14	-2.34	-2.79	-2.63	60.21	51.42	54.79	59.50	-2.33	-3.91	-1.42	-0.80	-2.11
AP2A2	161	34.32	30.28	36.25	31.24	-3.11	-3.01	-3.24	-2.56	74.15	58.96	34.50	42.27	-0.79	-1.84	-4.05	-1.78	-2.11
LRRFIP2	9209	40.62	31.11	58.05	26.46	-2.26	-2.94	-2.04	-2.34	54.18	75.84	39.09	48.22	-2.18	-1.14	-4.06	-1.07	-2.11
KISS1	3814	17.34	24.01	31.27	17.41	-4.22	-3.56	-4.02	-3.24	52.68	71.07	45.30	46.18	-2.35	-1.68	-3.14	-1.28	-2.11
CXCL14	9547	89.45	63.91	72.72	88.90	-0.37	-0.86	-0.85	0.03	66.71	61.64	75.05	45.99	-1.61	-1.75	-1.75	-3.33	-2.11
ALPI	248	34.16	72.09	84.02	64.63	-1.61	-0.42	-0.21	-0.13	48.85	52.20	38.21	47.85	-2.20	-2.61	-2.41	-1.22	-2.11
KIAA0676	23061	108.32	67.93	96.98	52.59	-0.24	-1.43	-0.52	-1.43	70.54	53.03	47.03	40.44	-0.80	-3.18	-2.22	-2.21	-2.11
PDZK11	51248	45.30	64.75	64.32	41.89	-2.21	-1.56	-1.96	-2.08	60.71	57.37	50.36	40.43	-1.68	-2.65	-1.88	-2.22	-2.11
CDC34	997	90.08	99.84	79.15	45.79	-0.45	-0.18	-0.57	-0.73	66.03	55.25	34.92	38.93	-0.76	-2.07	-2.75	-2.84	-2.10
NR1H3	10062	27.88	42.97	39.48	37.69	-1.90	-1.54	-1.62	-1.44	71.89	59.01	39.22	48.01	-0.65	-2.85	-2.59	-2.32	-2.10
CSNK2A1	1457	51.38	78.16	42.25	32.48	-1.07	-0.53	-1.73	-1.61	75.00	53.81	41.71	51.69	-0.60	-3.33	-3.03	-1.46	-2.10
DMTF1	9988	56.87	57.67	53.13	51.83	-1.39	-2.26	-1.79	-1.25	40.06	69.37	57.56	43.17	-3.51	-2.05	-0.81	-2.04	-2.10
EIF4ENIF1	56478	74.19	104.49	65.59	72.09	-0.35	0.15	-0.75	-0.02	47.59	56.07	59.81	40.53	-3.28	-2.56	-0.29	-2.28	-2.10
CAPN7	23473	36.85	123.82	205.74	96.92	-0.28	0.50	0.81	0.67	55.85	67.86	47.19	25.23	-1.09	-2.02	-1.73	-3.56	-2.10
LOC653499	653499	19.61	22.09	13.09	10.51	-4.46	-3.73			53.48	61.23	60.95	54.93	-2.58	-1.61			-2.10
NMNAT3	349565	100.21	84.76	88.08	68.74	0.21	-0.15	-0.01	-0.17	69.36	54.79	39.96	46.30	-1.62	-2.60	-2.11	-2.04	-2.10
CLTC	1213	25.70	40.58	37.56	21.26	-2.20	-1.69	-2.16	-1.93	64.02	55.07	54.97	37.07	-0.94	-2.65	-1.52	-3.28	-2.09
GP2	2813	54.06	33.92	50.21	35.19	-1.14	-2.01	-1.83	-2.15	37.96	97.72	35.63	52.16	-4.20	0.56	-3.04	-1.70	-2.09
MRPL55	128308	42.79	48.06	39.02	33.34	-1.98	-1.73	-2.96	-2.18	62.96	55.93	48.50	57.86	-1.99	-3.31	-2.13	-0.94	-2.09
FLJ30834	132332	94.06	72.47	60.99	51.91	-0.70	-1.74	-2.32	-2.18	64.78	68.61	43.84	47.59	-1.49	-1.89	-2.68	-2.31	-2.09
VGLL4	9686	70.50	64.62	98.89	49.21	-0.65	-0.75	-0.23	-1.21	54.32	64.10	46.86	42.29	-2.05	-1.92	-1.65	-2.76	-2.09
FLJ10901	55765	121.32	137.01	125.38	103.19	-0.04	0.49	0.22	0.45	62.69	69.36	43.83	33.77	-1.21	-1.53	-1.94	-3.69	-2.09
PEX5L	51555	131.86	115.30	125.07	90.02	0.39	0.21	-1.32	-0.91	69.73	61.59		52.58	-0.99	-1.78		-3.50	-2.09
KIAA0663	9877	42.96	44.34	61.58	35.72	-1.96	-2.33	-1.64	-1.80	58.76	54.22	35.03	45.50	-1.31	-3.47	-2.40	-1.18	-2.09
MAGEL2	54551	78.27	62.49	67.49	67.54	-0.67	-0.90	-1.04	-0.95	56.36	66.09	80.79	48.29	-2.73	-1.37	-1.25	-2.99	-2.09
MTIF3	219402	85.48	104.48	109.12	93.62	0.01	0.08	0.28	0.07	77.94	65.40	36.91	49.04	-0.46	-1.75	-3.17	-2.96	-2.08
RASL10B	91608	18.58	17.68	25.56	33.04			-3.42	-2.33	70.14	80.38	37.13	55.99			-2.83	-1.34	-2.08
C10orf62	414157	40.21	72.34	83.14	51.24	-2.06	-1.05	-1.17	-1.12	70.34	57.40	49.69	33.41	-0.90	-2.85	-1.42	-3.16	-2.08
TAS2R41	259287	102.92	114.92	105.74	88.62	-0.24	0.20	-3.16	-4.24	102.65	79.82		62.93	1.20	-0.16		-7.29	-2.08
COQ4	51117	48.14	81.65	74.55	43.26	-1.64	-0.61	-0.94	-1.54	93.16	54.84	34.69	37.37	0.32	-2.87	-3.55	-2.22	-2.08
APOA4	337	94.69	89.44	82.75	66.48	0.01	-0.99	-0.93	-0.73	66.02	60.48	44.63	57.73	-1.06	-3.17	-2.95	-1.13	-2.08
FBXW7	55294	37.45	33.83	45.55	26.87	-1.94	-2.18	-2.08	-2.31	51.73	68.78	35.21	47.57	-1.92	-1.28	-3.74	-1.35	-2.07
LOC90342	90342	80.69	64.61	76.55	38.83	-0.72	-1.36	-0.99	-1.61	47.19	69.25	32.37	43.40	-2.50	-1.66	-2.74	-1.37	-2.07
ZNF529	57711	90.62	71.13	67.17	59.57	-0.56	-0.86	-2.94	-2.64	53.76	41.33		33.57	-2.47	-4.26		0.52	-2.07
IPF1	3651	47.98	32.81	42.11	26.23	-0.89	-1.88	-1.53	-2.31	39.33	66.90	49.64	53.28	-4.00	-1.52	-1.35	-1.41	-2.07
MPP3	4356	38.28	41.80	58.26	55.14	-1.43	-1.36	-0.95	-0.44	53.91	51.45	35.82	48.39	-1.70	-2.70	-2.71	-1.17	-2.07
SPRYD5	84767	114.40	97.03	69.48	70.28	-1.69	-1.70	-2.79	-1.75	59.34	72.08	45.73	63.14	-2.08	-2.39	-2.27	-1.53	-2.07
DDI1	414301	69.50	65.73	43.50	29.30	-1.01	-1.51	-2.73	-3.40	48.75	68.96		42.82	-2.90	-1.06		-2.25	-2.07

		Mock								ATRi								
		% of Control				Robust Z-score				% of Control				Robust Z-score				
Gene Symbol	Gene ID	Rep 1	Rep 2	Rep 3	Rep 4	Rep 1	Rep 2	Rep 3	Rep 4	Rep 1	Rep 2	Rep 3	Rep 4	Rep 1	Rep 2	Rep 3	Rep 4	Average
ARL4A	10124	80.08	105.38	100.60	77.36	-0.11	0.01	0.06	0.02	67.68	50.24	43.82	57.86	-1.01	-4.04	-1.99	-1.23	-2.07
TNPO1	3842	49.91	64.28	72.13	34.41	-1.18	-1.10	-0.98	-2.21	67.77	68.50	35.80	46.43	-1.58	-1.68	-2.90	-2.09	-2.07
EGF	1950	81.76	162.63	146.33	124.08	-0.07	0.77	0.73	0.98	55.89	71.26	32.42	59.99	-2.15	-1.46	-3.64	-1.01	-2.06
SENP6	26054	63.80	80.24	52.35	54.47	-0.86	-0.79	-1.56	-1.07	49.75	69.66	40.35	65.41	-3.05	-1.56	-3.05	-0.59	-2.06
C10ORF95	79946	52.00	49.66	42.62	28.90	-1.66	-2.32	-2.79	-3.44	60.51	64.19		38.16	-1.77	-1.53		-2.89	-2.06
FLJ38281	163051	88.93	69.24	73.58	33.61	-0.65	-1.28	-1.11	-2.18	54.17	67.33	32.34	50.14	-1.77	-2.11	-2.80	-1.56	-2.06
TARSL2	123283	117.16	85.45	109.06	63.07	0.30	-0.06	0.00	-0.25	43.83	63.23	55.66	37.56	-2.85	-1.41	-1.46	-2.50	-2.06
SSBP2	23635	102.78	91.88	83.36	72.41	-0.24	-0.29	0.18	-0.10	68.88	49.54		57.68	-1.06	-3.13		-1.97	-2.06
MGC99813	130612	58.78	103.41	80.86	53.98	-0.74	0.01	-0.57	-0.52	57.37	56.87	39.26	46.10	-1.52	-2.53	-2.33	-1.84	-2.06
IGSF9	57549	23.11	23.72	34.71	26.53	-3.49	-3.19	-2.96	-2.65	58.99	61.85	56.25	33.94	-1.44	-2.32	-0.68	-3.78	-2.05
HSD17B12	51144	47.02	82.84	91.08	49.66	-1.10	-0.19	0.05	-0.93	79.18	57.15	37.96	41.77	-0.88	-2.33	-2.39	-2.61	-2.05
WASF2	10163	139.88	118.64	108.29	81.53	0.55	0.20	0.00	-0.11	59.93	66.13		37.35	-1.82	-1.33		-3.01	-2.05
C9ORF9	11092	115.15	81.01	92.15	74.06	0.10	-0.51	-0.40	-0.44	59.79	68.00	53.08	37.08	-2.06	-1.47	-1.28	-3.40	-2.05
SSA2	6738	40.87	36.77	52.00	24.98	-2.32	-2.82	-2.78	-3.53	53.80	66.85	35.28	52.16	-2.04	-1.81	-3.02	-1.34	-2.05
OR4N5	390437	138.96	145.01	118.76	25.67	0.75	0.69	0.43	-1.43	64.79	67.01	46.70	34.41	-1.42	-1.84	-2.61	-2.34	-2.05
DAPK3	1613	63.37	82.67	68.16	57.94	-0.75	-0.42	-0.76	-0.52	55.28	59.92	57.02	47.41	-2.65	-2.57	-1.06	-1.91	-2.05
PCDHB16	57717	107.10	97.85	105.47	80.60	0.14	-0.23	0.03	0.39	61.81	63.80	46.96	39.75	-1.74	-2.17	-2.57	-1.71	-2.05
ZNF2	7549	49.48	31.33	43.98	38.58	-2.51	-3.29	-3.70	-2.47	59.24	55.01	55.88	53.01	-2.65	-2.68	-1.92	-0.95	-2.05
LOC56964	56964	98.22	32.81	33.36	37.84	-0.44	-2.48	-3.30	-2.35	70.75	52.43	49.33	47.65	-0.97	-3.12	-2.24	-1.86	-2.04
GLP1R	2740	62.53	113.62	68.13	97.39	-0.81	0.12	-1.13	0.46	75.85	65.23	31.11	45.73	-1.15	-1.57	-3.13	-2.32	-2.04
RPP14	11102	20.71	34.68	27.54	28.69	-3.78	-3.52	-4.02	-3.53	49.71	74.73	43.04	63.44	-2.72	-1.69	-2.65	-1.11	-2.04
AP2E	339488	89.06	77.60	79.42	58.25	-0.53	-0.90	-0.88	-0.66	53.32	57.33	36.40	46.94	-1.84	-3.05	-2.23	-1.05	-2.04
ALPL	249	27.92	36.77	25.37	20.70	-1.91	-1.59	-2.62	-2.31	51.15	45.71	53.36	40.33	-1.97	-3.39	-0.87	-1.95	-2.04
GCN1L1	10985	102.62	97.51	90.05	81.39	0.32	-0.03	-0.01	0.14	56.93	59.03	44.69	39.60	-1.52	-2.31	-1.37	-2.97	-2.04
S100A11	6282	52.48	27.37	26.43	35.98	-1.67	-3.09	-3.69	-1.91	43.63	72.03	38.09	52.55	-3.84	-1.07	-2.00	-1.26	-2.04
MTMR6	9107	47.67	29.41	31.81	13.57	-1.10	-1.97	-2.17	-3.12	49.01	45.86	40.94	56.21	-2.18	-3.37	-2.09	-0.52	-2.04
SNX11	29916	42.04	34.58	45.07	34.01	-1.92	-2.61	-2.29	-2.13	77.81	60.41	34.67	42.35	-0.81	-2.22	-3.55	-1.59	-2.04
OR7C1	26664	89.09	61.64	55.23	43.09	-0.69	-1.11	-1.86	-1.96	57.47	76.21	43.51	46.22	-2.44	-0.75	-2.95	-2.02	-2.04
ASB18	401036	34.64	36.15	54.90	31.45	-2.09	-2.06	-1.63	-1.98	47.46	67.85	44.27	42.49	-2.41	-1.37	-2.47	-1.91	-2.04
TRIM62	55223	31.27	19.63	34.05	19.99	-2.28	-3.19	-2.77	-2.94	48.48	78.42	44.39	34.15	-2.29	-0.41	-2.45	-3.01	-2.04
S100A1	6271	28.83	19.38	23.11	8.83	-3.76	-3.79			54.00	69.81	55.70	79.10	-2.76	-1.32			-2.04
PNMA5	114824	109.48	93.93	104.89	92.30	0.09	-0.11	0.11	0.16	49.01	65.64	71.54	63.95	-3.66	-1.41	-2.08	-1.01	-2.04
APEX2	27301	34.11	47.65	29.88	28.59	-1.73	-1.29	-2.30	-3.46	69.16	55.54	34.32	71.61	-1.24	-2.81	-3.57	-0.53	-2.04
KRTAP12-1	353332	24.58	15.62	28.50	17.86	-3.48	-4.44	-3.49	-3.63	54.75	66.07	35.57	48.60	-2.52	-1.67	-2.30	-1.66	-2.04
MGC71999	342538	25.22	30.11	24.82	20.77	-3.34	-3.32	-5.30	-4.05	58.79	55.52	40.49	55.08	-1.56	-3.20	-2.34	-1.05	-2.04
GP5	2814	22.35	14.49	51.56	23.37			-1.95	-2.05	54.57	90.45	44.19	49.72			-2.90	-1.17	-2.03
SHARPIN	81858	46.61	27.20	29.22	29.35	-2.30	-2.88	-3.68	-3.10	60.71	67.75	46.45	46.34	-2.05	-1.50	-2.58	-2.01	-2.03
RNF26	79102	33.42	57.71	53.20	78.18	-5.40	-3.30	-3.79	-1.35	71.68	78.45	45.78	47.55	-0.67	-1.49	-2.26	-3.71	-2.03
OTOR	56914	104.47	90.45	79.96	91.31	-0.29	-0.28	-0.80	0.26	64.82	61.03	48.16	46.33	-1.59	-2.16	-2.37	-2.01	-2.03
UGT2B28	54490	64.73	54.05	49.69	24.89	-0.58	-1.04	-1.36	-1.96	62.54	65.69	43.33	34.92	-1.45	-1.57	-2.15	-2.95	-2.03
LOC201191	201191	103.25	103.48	94.71	84.94	-0.35	-0.24	-0.38	0.17	53.36	62.27	41.08	48.04	-1.84	-2.71	-1.79	-1.76	-2.03
WIT-1	51352	87.25	70.09	83.67	59.36	-0.57	-1.16	-0.73	-0.62	53.59	72.30	27.90	41.51	-1.81	-1.35	-3.39	-1.55	-2.03
LOC152098	152098	87.71	86.36	84.71	67.96	-0.76	-1.32	-1.23	-0.78	62.71	54.78	41.59	49.10	-1.40	-3.38	-2.07	-1.25	-2.03
HNRPUL2	221092	64.75	54.48	89.16	65.42	-1.39	-2.15	-0.95	-0.53	67.15	61.79	29.58	43.19	-1.66	-2.22	-2.52	-1.70	-2.03
INCA1	388324	46.73	51.61	103.81	52.38	-1.35	-0.90	-0.13	-0.59	67.65	58.78	41.83	37.73	-0.49	-1.87	-3.25	-2.48	-2.02
OPLAH	26873	56.66	49.10	55.44	51.42	-0.60	-1.15	-0.96	-0.85	54.76	71.51	46.46	40.53	-2.17	-1.07	-1.74	-3.09	-2.02
T	6862	26.26	25.40	28.73	18.89	-2.02	-1.86	-1.90	-2.35	47.24	52.60	49.83	57.25	-2.65	-3.47	-1.17	-0.79	-2.02
EPS8L2	64787	49.57	52.89	80.77	42.50	-1.19	-1.18	-0.54	-0.72	73.21	60.30	43.59	39.84	-0.22	-2.08	-2.93	-2.84	-2.02
UMPK	7371	40.34	34.11	41.96	30.32	-1.52	-1.93	-1.98	-2.19	58.39	68.81	40.64	41.29	-1.92	-1.30	-2.69	-2.16	-2.02
GRB7	2886	22.88	18.40	22.95	18.64	-3.81	-4.23	-4.14	-4.29	70.50	62.08	45.95	37.71	-1.25	-2.29	-1.95	-2.58	-2.02
ZNF154	7710	45.06	63.05	87.04	51.82	-1.49	-0.80	-0.53	-1.06	60.55	46.32	46.99	57.44	-1.40	-3.83	-1.63	-1.21	-2.02
LOC646424	646424	98.79	99.33	81.66	76.97	-0.61	-0.22	-0.94	-0.05	34.48	70.12	59.27	57.94	-4.93	-1.76	-0.92	-0.45	-2.02
EXOC8	149371	79.42	80.50	75.29	51.97	-0.57	-0.75	-1.52	-1.09	63.32	62.79	37.81	46.04	-1.56	-2.18	-2.79	-1.53	-2.01
CTAG1B	1485	98.00	91.95	113.51	78.08	-0.23	-0.37	0.11	0.00	60.80	68.97	55.73	33.52	-1.47	-1.93	-1.85	-2.81	-2.01
MYO9B	4650	77.77	62.91	77.61	53.02	-0.45	-2.00	-1.12	-1.41	52.74	73.33	52.48	45.56	-2.24	-1.52	-1.71	-2.59	-2.01
MYLIP	29116	82.84	64.43	55.84	45.76	-2.66	-2.96	-3.61	-3.40	67.59	65.74	62.63	53.94	-1.11	-3.38	-0.83	-2.74	-2.01
FLJ22965	63932	83.70	72.79	77.77	58.40	-1.03	-1.72	-1.42	-1.69	59.76	74.82	46.20	46.19	-1.98	-1.20	-2.40	-2.48	-2.01
RYR2	6262	146.83	51.38	51.88	27.01	0.34	-1.45	-1.52	-1.70	67.25	41.69	41.82	46.22	-0.65	-3.55	-1.91	-1.93	-2.01
C20ORF141	128653	33.27	19.34	28.77	22.97	-2.75	-3.93	-3.46	-3.01	52.43	58.11	49.71	46.64	-2.77	-2.55	-0.84	-1.87	-2.01
LOC134492	134492	60.75	81.12	81.87	44.99	-1.65	-1.50	-1.36	-1.99	53.53	61.33	41.88	51.13	-2.38	-2.53	-2.04	-1.08	-2.01
USP11	8237	52.44	138.79	199.98	108.46	0.17	0.73	0.75	0.90	33.70	68.15	39.41	53.99	-3.09	-1.99	-2.54	-0.42	-2.01
ZNF473	25888	115.94	117.67	112.26	66.19	0.71	0.25	0.06	-0.11	56.41	55.82	43.87	44.86	-1.61	-2.65	-1.80	-1.97	-2.01
CLDN5	7122	26.05	50.56	49.16	27.07	-2.71	-1.77	-2.26	-2.14	51.81	70.07	43.00	44.11	-2.00	-1.55	-2.21	-2.27	-2.01
LOC343066	343066	26.88	28.53	19.13	14.53	-3.07	-3.59			52.35	67.74	41.91	40.21	-1.95	-2.06			-2.00
S100A9	6280	45.38	34.66	56.53	38.22	-2.36	-2.36	-1.79	-2.32	71.65	77.84	39.27	38.51	-0.88	-0.62	-3.54	-2.98	-2.00
TCF8	6935	96.48	94.90	106.21	69.34	0.28	0.00	0.13	-0.08	66.53	57.04	43.96	50.05	-0.84	-3.02	-2.09	-2.05	-2.00
ZNF225	7768	131.57	103.19	108.89	90.14	0.47	0.05	0.16	0.17	60.62	53.01	46.89	54.50	-1.97	-2.90	-1.88	-1.25	-2.00
PPM1F	9647	81.58	56.56	67.00	41.69	-0.29	-0.84	-0.67	-0.97	52.76	64.76	37.62	36.78	-1.81	-1.36	-2.48	-2.35	-2.00
C20ORF136	140700	18.75	36.73	19.31	23.94	-5.18	-4.36	-6.60	-5.39	74.02	66.36	49.78	40.60	-0.67	-2.15	-1.99	-3.17	-2.00
FLJ38159	220388	72.85	77.51	77.11	58.51	-1.26	-0.82	-1.00	-1.11	67.88	52.62		49.15	-1.21	-3.45		-1.33	-2.00
SPRY4	81848	28.33	13.47	16.53	11.34	-3.54	-4.41			68.04	55.57	47.97	39.58	-1.24	-2.75			-2.00

APPENDIX B

SECONDARY SCREENS DATA

This appendix includes table B.1 of the siRNAs which validated in the secondary screen with the ATRi. There are three replicates for each drug condition and the average is included in the table. The results for the other drug conditions tested are also listed in the table as an average of the three replicates. The stars indicate genes which still validated after correction for false discovery rate calculated by the Benjamini-Hochberg method. Genes are listed alphabetically. For a gene to validate, as least two of the four siRNAs must have validated.

Plate	Well	Gene Symbol	GENEID	*	ATRi Avg	*	A/C Avg	*	Cis Avg	Arm2 Untreated	*	Low HU Avg	*	High HU Avg	*	CHK1i Avg	Arm1 Untreated
Plate 09	A20	ACP6	51205	*	72.91	*	78.74		76.65	124.66		77.97	*	38.73		81.48	115.42
Plate 09	B20	ACP6	51205	*	62.71		84.50		81.10	56.41	*	59.84		40.20		85.03	60.93
Plate 09	D20	ACP6	51205	*	67.84		90.36		85.67	36.39	*	55.31	*	32.24	*	67.73	38.96
Plate 04	M09	ACSM2B	348158	*	77.85	*	81.95		83.09	105.64		76.19		40.42		72.99	90.51
Plate 04	P09	ACSM2B	348158	*	74.20	*	81.56	*	67.44	91.78		82.10		41.29		72.63	87.40
Plate 09	G10	ADNP2	22850	*	51.86	*	68.67	*	117.94	3.54		105.64	*	81.17		95.24	3.50
Plate 09	H10	ADNP2	22850	*	58.70	*	61.37	*	69.67	29.43	*	63.60	*	33.33	*	51.50	26.38
Plate 06	H03	AIRE	326	*	70.58		98.03	*	100.77	16.72	*	59.75	*	77.43	*	51.49	18.32
Plate 05	A09	AKAP17A	8227	*	69.95		89.77	*	105.65	33.78	*	57.46		49.05	*	44.63	63.76
Plate 01	M04	AKAP8L	26993	*	38.91	*	82.11		141.66	8.18		79.93	*	64.50	*	91.18	10.21
Plate 10	A09	ALG12	79087	*	66.61		82.73		89.81	31.00		76.09	*	55.54		84.68	55.83
Plate 10	E15	ALKBH7	84266	*	76.70	*	101.26	*	104.59	6.94		69.74	*	53.18	*	56.91	9.09
Plate 09	O06	ANAPC10	10393	*	68.53		88.17		91.24	60.15	*	71.07	*	59.44	*	50.21	72.91
Plate 09	P06	ANAPC10	10393	*	67.62	*	73.02	*	70.87	42.36	*	56.46	*	36.10	*	68.04	45.16
Plate 11	E10	ANKRD24	170961	*	40.92		90.45	*	113.47	56.90	*	45.19	*	28.91	*	24.11	85.55
Plate 11	H10	ANKRD24	170961	*	71.73	*	82.26		98.84	5.82	*	54.05	*	54.42	*	55.85	6.78
Plate 03	E06	ANO10	55129	*	73.42		79.98		83.21	22.56		93.51	*	66.13	*	72.49	24.92
Plate 03	G06	ANO10	55129	*	73.80	*	76.68		74.83	91.79		75.09	*	35.81	*	62.12	90.85
Plate 08	M21	AP3B2	8120	*	73.70		97.80		93.28	56.22		85.96		53.10		89.63	50.21
Plate 08	N21	AP3B2	8120	*	77.55		91.40		85.38	59.40		79.30		47.55		86.80	95.96
Plate 08	P21	AP3B2	8120		27.02		33.35	*	4.15	0.17	*	77.53	*	107.64		-93.83	0.02
Plate 06	G18	ARID3B	10620	*	67.87		80.72		80.14	27.08	*	43.26	*	38.02	*	67.97	35.64
Plate 06	H18	ARID3B	10620	*	59.81	*	60.53	*	66.81	32.04	*	41.59	*	22.34	*	59.93	64.98
Plate 11	A18	ASAH2B	653308	*	59.29		96.21	*	63.82	5.44	*	38.74	*	29.06	*	55.57	13.92
Plate 11	P05	ASB9	140462	*	44.58		86.98	*	95.28	13.92	*	42.19		43.81	*	41.93	21.50
Plate 06	C19	ATAD2	29028	*	68.51		93.55		99.52	27.05	*	61.83	*	41.19	*	46.34	15.91
Plate 06	D19	ATAD2	29028	*	70.61		84.98		90.35	86.01	*	61.35	*	39.92	*	54.64	89.19
Plate 11	H20	ATAD2	29028	*	62.28		89.86		87.97	54.03	*	45.09	*	31.21	*	59.21	79.58
Plate 06	B21	ATAD5	79915	*	56.64	*	71.33		82.77	50.90	*	72.91	*	28.91	*	45.71	49.39
Plate 06	C21	ATAD5	79915	*	76.18		87.78		89.26	116.88	*	72.12	*	39.52	*	65.66	111.88
Plate 09	C10	ATF5	22809	*	64.49		89.09	*	103.74	27.57	*	62.16	*	59.18	*	43.57	32.93
Plate 07	F06	ATP6V0D1	9114	*	71.58	*	71.55	*	56.16	2.92		81.33	*	80.09	*	69.90	4.45
Plate 09	I04	ATP6V1G1	9550	*	77.02		110.74		91.18	10.15	*	31.66	*	24.56	*	64.96	62.23
Plate 09	J04	ATP6V1G1	9550	*	72.89		88.25		99.61	13.12	*	34.63	*	49.47	*	50.36	16.57
Plate 09	K04	ATP6V1G1	9550	*	68.28	*	66.41		92.70	28.58	*	62.92	*	21.64	*	40.96	43.08
Plate 09	I20	ATRAID	51374	*	65.95	*	77.48		115.01	4.81	*	33.44		42.95	*	41.43	5.26
Plate 08	G16	ATXN2	6311	*	66.63	*	71.51	*	80.29	70.01	*	63.42	*	23.98	*	56.17	82.21
Plate 10	N18	BAGE4	85317	*	68.97	*	67.34		89.45	1.43		71.55	*	75.03		74.58	1.93
Plate 10	O18	BAGE4	85317	*	34.10	*	43.86	*	64.72	20.78	*	40.11	*	13.90	*	35.58	28.08
Plate 09	A09	BAZ1A	11177	*	-75.89	*	32.94	*	-47.22	3.24	*	14.09	*	15.71	*	54.71	6.54
Plate 09	B09	BAZ1A	11177	*	68.04	*	75.15		89.00	70.68	*	63.51	*	25.10		80.63	66.33
Plate 04	M11	BEND3	57673	*	77.54		96.71		88.77	95.96		76.62		40.77	*	57.28	82.37
Plate 11	M09	BHLHA15	168620	*	54.06		82.37		83.70	63.18	*	42.16	*	34.87	*	46.57	98.72
Plate 08	J03	BIK	638	*	77.65	*	48.83		89.94	0.66		96.69	*	82.75	*	37.35	1.92
Plate 09	M20	BIN2	51411	*	54.25	*	74.83		88.63	44.88	*	43.08	*	21.17	*	41.93	39.22
Plate 09	P20	BIN2	51411	*	38.37	*	70.22		89.47	11.66	*	63.84		42.69	*	27.15	31.71
Plate 08	C03	BIRC2	329	*	71.32		93.75	*	76.03	31.48	*	58.94	*	37.00	*	56.50	43.39
Plate 10	A11	BORA	79866		53.31	*	53.01	*	148.16	0.24	*	58.06	*	70.75	*	65.12	1.57
Plate 09	E12	BRCA2	675	*	74.73	*	70.13	*	58.47	38.94	*	75.45	*	52.02	*	69.74	38.59
Plate 09	F12	BRCA2	675	*	51.46	*	63.43		78.89	15.52	*	56.34	*	33.60	*	48.16	22.81
Plate 08	I21	BRD3	8019	*	74.49	*	81.33		85.19	100.91		83.89		45.49		88.03	112.92
Plate 08	J21	BRD3	8019	*	76.81		88.43		82.70	90.74	*	72.09	*	36.15	*	68.53	79.10
Plate 08	K21	BRD3	8019	*	77.61	*	79.07		87.40	58.07		82.06		53.57		82.19	37.50
Plate 08	L21	BRD3	8019	*	66.79	*	77.58		84.45	97.53		81.62		46.74		86.45	102.27
Plate 10	F03	BSPRY	54836	*	56.92		89.76	*	110.51	19.03	*	53.68	*	29.82	*	66.72	58.51
Plate 10	G03	BSPRY	54836	*	67.97		89.55	*	94.16	100.24		82.98		50.81	*	94.64	128.80
Plate 09	J06	BTN3A3	10384	*	64.54	*	72.71		81.99	76.59	*	55.03	*	29.58	*	72.22	101.15
Plate 09	L06	BTN3A3	10384	*	72.06	*	80.30	*	73.61	18.49	*	68.14	*	27.11	*	54.87	34.00
Plate 08	P03	BYSL	705	*	58.12	*	113.62	*	73.95	1.03		85.81	*	86.56	*	126.70	1.20
Plate 01	B07	C12orf54	121273	*	74.45	*	77.03	*	91.52	6.94	*	69.94	*	31.45	*	57.78	6.85
Plate 01	C07	C12orf54	121273	*	44.56	*	73.60		98.20	62.00		82.17		47.22	*	41.96	68.88
Plate 01	D07	C12orf54	121273	*	64.41		98.22		92.32	21.23	*	52.97		48.87	*	41.66	24.41
Plate 11	D13	C14orf182	283551	*	59.43	*	76.25		87.07	2.36	*	52.30		46.96	*	35.95	4.43
Plate 06	M03	C16orf57	79650	*	71.24	*	114.54	*	106.31	6.22	*	69.61	*	77.21		77.91	10.73
Plate 11	N15	C19orf45	374877	*	-197.06	*	-130.66	*	22.63	0.40		73.49	*	187.38		99.95	0.84
Plate 11	O15	C19orf45	374877	*	73.74		98.92		80.23	66.15	*	48.81	*	36.11	*	59.14	75.93
Plate 11	P15	C19orf45	374877		32.58	*	57.16	*	65.00	-0.05		214.47		63.55	*	13.46	1.77
Plate 01	B09	C19orf57	79173	*	56.73	*	58.68	*	126.77	0.81	*	68.81	*	81.30	*	172.93	1.17
Plate 10	I05	C1orf63	57035	*	71.99	*	101.48	*	97.43	88.09		74.53	*	52.40		75.18	111.58
Plate 10	L05	C1orf63	57035	*	53.46	*	66.22		73.61	3.22		76.01	*	54.73		73.91	11.45
Plate 10	C16	C2orf40	84417	*	49.89	*	58.36		86.15	9.76	*	61.33	*	38.82	*	35.13	8.93

Plate	Well	Gene Symbol	GENEID	*	ATRi Avg	*	A/C Avg	*	Cis Avg	Arm2 Untreated	*	Low HU Avg	*	High HU Avg	*	CHK1i Avg	Arm1 Untreated
Plate 10	D16	C2orf40	84417	*	71.70		87.48		92.30	113.78		82.18	*	60.54	*	89.98	104.78
Plate 11	K18	C5orf24	134553	*	44.92	*	78.12	*	101.73	27.56	*	27.58	*	29.79	*	35.31	42.43
Plate 11	L18	C5orf24	134553	*	75.76		95.25	*	95.39	106.39	*	48.94	*	31.00	*	69.86	129.70
Plate 11	I07	C5orf38	153571	*	42.35		86.71	*	103.70	29.07	*	46.17		46.05	*	28.96	30.44
Plate 11	J16	C5orf48	389320	*	63.09		81.61		80.53	6.31	*	52.52		42.38		90.79	6.18
Plate 11	A08	C6orf165	154313	*	53.36	*	76.01		87.11	0.69	*	46.54	*	69.95	*	31.07	3.72
Plate 02	K20	CABIN1	23523	*	65.80	*	80.03		84.51	47.99	*	72.03	*	27.93	*	63.56	51.02
Plate 03	F17	CACNG6	59285	*	48.78		80.28		81.81	46.65	*	51.72	*	24.41	*	48.96	40.46
Plate 02	A19	CCDC127	133957	*	68.78		96.63		98.93	19.18	*	73.73	*	70.92	*	61.67	31.13
Plate 10	J22	CCDC159	126075	*	60.68		83.56		82.47	48.66	*	38.87	*	18.16	*	52.48	66.49
Plate 10	L22	CCDC159	126075	*	73.38	*	26.13	*	40.38	0.52		82.59		48.90		73.75	1.15
Plate 09	F13	CCDC19	25790	*	73.86		82.05		81.84	82.03	*	67.27	*	34.95	*	73.84	80.28
Plate 09	H13	CCDC19	25790	*	73.14	*	65.72	*	70.47	37.74		91.19	*	75.20		75.53	32.95
Plate 08	A04	CCNA2	890	*	70.81		91.71	*	100.95	44.32	*	58.44		44.00	*	50.91	61.80
Plate 08	C04	CCNA2	890	*	55.48		98.36	*	121.84	2.94		86.10	*	89.50	*	28.93	4.59
Plate 10	K07	CCNB1IP1	57820	*	66.63		85.36	*	94.30	73.98	*	57.97		45.71		75.25	99.73
Plate 10	L07	CCNB1IP1	57820		77.14		94.01		88.91	109.03		77.71		48.06	*	88.67	129.44
Plate 11	A11	CCNY	219771	*	65.60	*	79.63		84.14	24.52	*	40.92	*	31.75	*	72.75	40.96
Plate 05	I17	CCPG1	9236	*	58.59	*	70.74		74.20	43.51	*	63.14		42.53	*	62.69	40.35
Plate 11	J09	CDC20B	166979	*	46.09	*	57.96	*	73.88	9.48	*	38.67	*	20.67	*	26.59	15.81
Plate 11	L09	CDC20B	166979	*	66.34		94.75	*	65.41	64.17	*	25.96	*	15.72	*	68.74	90.29
Plate 10	M19	CDCA5	113130		76.92	*	106.50	*	131.60	4.53		83.16	*	199.29	*	98.40	3.02
Plate 10	K08	CDK15	65061	*	76.10	*	106.49	*	98.70	12.70	*	68.08		48.07		77.72	34.60
Plate 10	L08	CDK15	65061	*	61.14		83.89		84.23	84.52	*	61.34	*	31.98		71.74	101.75
Plate 08	F04	CDKN2B	1030	*	63.83	*	74.48		84.96	8.75	*	75.09		45.22	*	46.33	29.65
Plate 10	C05	CENPQ	55166	*	69.56		95.99		87.28	60.87		75.60	*	53.63		82.15	87.12
Plate 10	D05	CENPQ	55166	*	68.04		97.32	*	97.23	28.10		77.08	*	61.49	*	47.88	40.95
Plate 05	B07	CEP19	84984	*	69.30	*	72.26		87.37	35.02	*	38.10	*	22.64	*	60.47	84.03
Plate 11	P19	CGGBP1	8545	*	-128.05	*	-84.76		-239.02	0.35	*	44.08	*	36.86	*	36.93	2.40
Plate 11	D17	CHCHD10	400916	*	65.28		103.46		91.49	18.03	*	35.11	*	31.08	*	62.01	20.60
Plate 10	A06	CHMP1B	57132	*	63.89		86.11		90.44	98.79		77.17		47.76	*	92.64	112.90
Plate 10	B06	CHMP1B	57132	*	76.15		86.18		110.33	34.94	*	60.40		47.97		78.16	18.42
Plate 10	D06	CHMP1B	57132	*	69.34		96.35		85.64	35.87	*	64.76		48.44	*	58.82	58.50
Plate 09	B18	CHMP4A	29082	*	74.15		91.28		87.03	13.24		87.40	*	85.47		87.65	11.59
Plate 09	C18	CHMP4A	29082	*	63.77	*	77.30		79.66	19.16	*	66.21		46.96	*	70.40	13.00
Plate 09	D18	CHMP4A	29082	*	71.61	*	66.48		90.49	41.96		79.07	*	65.38	*	70.48	29.01
Plate 08	I04	CHRM5	1133	*	74.88		94.79		88.72	44.60		83.63	*	40.70	*	31.79	51.93
Plate 08	L04	CHRM5	1133	*	77.71	*	58.38		82.30	3.29	*	72.61	*	88.31	*	45.47	2.79
Plate 03	I17	CHRNE	1145	*	74.49	*	60.74	*	72.31	84.65		76.17	*	40.36	*	60.53	115.77
Plate 03	J17	CHRNE	1145	*	75.16	*	65.46	*	106.55	28.13	*	52.63	*	33.69	*	74.74	23.07
Plate 03	K17	CHRNE	1145	*	68.06		94.84	*	106.67	3.27	*	61.98	*	71.49	*	70.55	13.18
Plate 10	B19	CHURC1	91612	*	69.40		88.17	*	107.52	52.19	*	55.40	*	38.92	*	69.99	68.16
Plate 11	P03	CIB4	130106		-8.01		-142.73		69.61	0.02		-106.41		-5.59	*	-6.20	0.20
Plate 09	K17	CIDEB	27141	*	49.29		83.86		80.62	16.43	*	49.97		52.03	*	52.34	14.48
Plate 02	M07	CLIC3	9022	*	69.79		90.14		104.84	9.77	*	59.12	*	39.45	*	65.34	21.24
Plate 02	O07	CLIC3	9022	*	59.17		86.85	*	221.44	-11.85		81.99		48.50	*	117.85	1.21
Plate 08	M15	CLIP1	6249	*	69.89		86.12	*	78.90	44.34	*	64.50	*	34.78	*	57.99	18.31
Plate 08	N15	CLIP1	6249	*	77.73	*	69.16	*	65.39	107.78	*	63.57	*	35.55		84.20	84.18
Plate 09	B15	CNTNAP2	26047	*	58.15	*	75.30		88.98	50.19	*	55.08	*	30.33	*	60.13	50.03
Plate 09	A08	COPS6	10980	*	51.27	*	79.04	*	102.40	31.81	*	62.45	*	24.30	*	27.67	54.80
Plate 09	D08	COPS6	10980	*	69.80	*	77.88		95.45	5.62	*	110.38	*	71.69	*	63.77	7.32
Plate 01	I21	CPSF2	53981	*	30.44	*	80.53		102.04	16.32		76.14	*	39.28	*	12.58	23.16
Plate 01	J21	CPSF2	53981	*	56.52	*	56.27		91.37	2.65	*	69.94	*	60.65		75.76	3.36
Plate 01	K21	CPSF2	53981	*	14.11	*	56.78	*	132.26	9.79	*	65.17	*	23.69	*	18.03	15.28
Plate 01	L21	CPSF2	53981	*	41.41	*	78.23		121.46	6.18	*	70.59	*	37.80	*	37.50	8.72
Plate 09	E21	CPSF3	51692	*	74.35		103.42	*	128.65	58.75	*	72.83		46.40	*	25.05	37.50
Plate 09	F21	CPSF3	51692	*	59.45		99.35		94.89	42.98	*	59.39	*	38.37	*	9.97	40.30
Plate 09	G21	CPSF3	51692	*	62.89		96.78		96.45	40.54	*	55.43		44.10	*	19.08	33.83
Plate 09	H21	CPSF3	51692	*	64.98		88.77		76.41	4.25	*	116.87	*	82.78	*	39.42	4.42
Plate 08	B05	CSNK2A1	1457	*	72.90	*	79.38		89.49	136.05		81.78	*	32.26	*	68.00	121.87
Plate 08	F05	CSNK2B	1460	*	71.91	*	80.39	*	78.61	42.92	*	57.24	*	27.26	*	66.56	26.79
Plate 08	H05	CSNK2B	1460	*	73.88	*	82.65		84.33	60.71	*	60.77	*	31.23	*	73.16	59.51
Plate 02	I06	CXCL3	2921	*	64.19		90.79		86.61	65.91		88.33		54.81	*	27.15	102.10
Plate 02	M16	CYP4F2	8529	*	75.61		89.47		91.56	63.14	*	58.04	*	31.17	*	75.55	47.34
Plate 02	N16	CYP4F2	8529	*	71.23		98.21	*	111.48	40.85	*	57.50	*	34.95	*	34.58	58.30
Plate 09	A16	DAZAP1	26528	*	76.82		91.48	*	111.20	7.54	*	73.15	*	36.77	*	71.52	20.09
Plate 09	B16	DAZAP1	26528	*	65.16	*	74.82		89.74	30.55		80.94		38.79	*	62.41	33.67
Plate 10	F21	DBX1	120237	*	52.78	*	64.61		90.98	10.83	*	60.87	*	29.40	*	52.07	16.80
Plate 11	E14	DCAF12L2	340578	*	74.19		99.44		86.01	4.54	*	46.34		40.91	*	51.23	6.21
Plate 11	G14	DCAF12L2	340578	*	76.75		86.72		88.80	46.21	*	51.18		44.41		78.39	62.92
Plate 01	B10	DHCR7	1717	*	71.80	*	48.36	*	114.03	0.47	*	17.18	*	61.74	*	210.80	0.61

Plate	Well	Gene Symbol	GENEID	*	ATRi Avg	*	A/C Avg	*	Cis Avg	Arm2 Untreated	*	Low HU Avg	*	High HU Avg	*	CHK1i Avg	Arm1 Untreated
Plate 05	D21	DHX57	90957	*	72.51		73.38		74.74	1.81	*	17.92		45.72	*	45.91	3.47
Plate 09	O08	DIDO1	11083	*	70.70		84.84		82.52	27.93	*	69.16	*	31.85	*	51.24	45.54
Plate 09	P08	DIDO1	11083	*	16.23	*	-8.55	*	94.23	0.11	*	139.79	*	110.35		80.06	1.18
Plate 09	N12	DMXL2	23312	*	71.19		85.40		87.07	9.01		95.23	*	55.48		80.02	17.72
Plate 09	P12	DMXL2	23312	*	76.96		85.70		77.42	44.63		87.93		45.52	*	73.17	53.19
Plate 11	J05	DOCK11	139818	*	57.01		84.51		81.27	95.87	*	40.69	*	24.67	*	64.06	106.84
Plate 11	K05	DOCK11	139818	*	70.99		90.22	*	101.07	13.10	*	43.26		46.64	*	52.40	7.78
Plate 10	J06	DOLPP1	57171	*	73.80		93.80		89.01	83.48	*	67.14		43.97	*	89.51	96.85
Plate 10	K06	DOLPP1	57171	*	64.28		84.32	*	71.18	34.08	*	49.75	*	14.49	*	50.82	33.15
Plate 03	L05	DPY19L2	283417	*	75.10		95.06	*	111.49	20.16	*	71.44		45.40	*	68.52	31.11
Plate 08	N05	DPYSL3	1809	*	70.24		91.25		86.30	36.18		82.92		42.47	*	65.29	30.54
Plate 11	A14	DUPD1	338599	*	69.97		83.41		87.56	15.94	*	41.13	*	34.25	*	65.90	31.51
Plate 11	C14	DUPD1	338599	*	60.28	*	71.02		107.37	0.65		96.00	*	118.11		80.78	0.67
Plate 09	M03	DYRK1B	9149	*	64.46	*	76.76		97.73	30.33	*	69.83	*	29.89	*	63.86	37.10
Plate 09	N03	DYRK1B	9149	*	47.14		90.04	*	112.12	23.55	*	44.51	*	16.80	*	19.00	48.47
Plate 09	O03	DYRK1B	9149	*	72.48	*	74.51	*	115.48	0.95		81.19	*	32.26	*	47.75	5.37
Plate 09	P03	DYRK1B	9149	*	64.76		88.18		92.71	18.10	*	69.17		48.14	*	59.75	35.93
Plate 04	F19	EED	8726	*	66.98		87.36		98.98	22.38	*	69.19	*	71.91		87.04	22.02
Plate 01	I22	EFEMP2	30008	*	72.33		95.15	*	87.58	59.70	*	64.77	*	28.71	*	72.91	66.83
Plate 01	J22	EFEMP2	30008	*	31.57	*	45.59		99.43	8.01	*	48.50	*	23.70	*	29.45	12.54
Plate 01	L22	EFEMP2	30008	*	47.51		100.19		135.05	1.55	*	71.68	*	34.17	*	67.31	3.48
Plate 11	I04	EGFLAM	133584	*	76.04		90.86		97.55	18.56	*	66.73	*	105.74		86.76	5.64
Plate 11	L04	EGFLAM	133584	*	43.21	*	65.02	*	73.24	17.56	*	55.44	*	34.08	*	51.12	16.65
Plate 08	F06	ERBB3	2065	*	66.47	*	58.36	*	51.36	35.25	*	51.23	*	28.70	*	65.64	25.62
Plate 08	G06	ERBB3	2065	*	72.18		100.36		81.55	22.22	*	53.88	*	27.11	*	46.15	17.06
Plate 04	O03	F8A1	8263	*	69.48	*	113.62		100.17	56.53	*	64.53		43.42	*	66.10	82.40
Plate 04	P03	F8A1	8263	*	73.12		98.75	*	62.16	2.03	*	8.82	*	106.71	*	54.36	1.43
Plate 09	N21	FAM105A	54491	*	54.04	*	59.50	*	71.89	14.87	*	44.99	*	25.78	*	35.08	19.88
Plate 09	E05	FAM115A	9747	*	76.59	*	72.46		99.85	0.99	*	128.19	*	78.84		95.00	1.63
Plate 11	M08	FAM122B	159090	*	74.40		99.15		92.60	3.18	*	46.51	*	66.02	*	50.10	3.02
Plate 11	L13	FAM153A	285596	*	59.79		83.70	*	99.10	9.17	*	27.47	*	17.39	*	32.44	10.18
Plate 11	I08	FAM154A	158297	*	67.33		97.66		81.24	53.86	*	35.63	*	23.54	*	51.21	64.32
Plate 11	K08	FAM154A	158297	*	54.66		87.60		85.92	104.06	*	43.71	*	26.43	*	61.80	126.28
Plate 11	L08	FAM154A	158297	*	67.27		103.90	*	94.40	26.03	*	32.35	*	32.20	*	49.17	24.60
Plate 11	B19	FAM178A	55719	*	52.39	*	68.35		81.07	11.53	*	34.41		48.37	*	37.27	10.26
Plate 11	M07	FAM71B	153745	*	65.94		97.98		83.91	27.60	*	38.59	*	30.61	*	37.53	30.92
Plate 11	O07	FAM71B	153745	*	53.52	*	75.67	*	68.40	22.68	*	36.29	*	38.09		79.89	25.74
Plate 10	J13	FAM83D	81610	*	70.37		88.56	*	113.72	9.96	*	53.86		43.64	*	46.76	16.22
Plate 10	K13	FAM83D	81610	*	61.06		86.80		82.66	8.04		69.95	*	70.07		81.17	18.21
Plate 10	L13	FAM83D	81610	*	68.51		91.65		81.68	10.41	*	49.45	*	25.33	*	43.69	28.90
Plate 11	P17	FAM83G	644815	*	71.75		129.72		133.85	2.76	*	13.79	*	18.42	*	42.48	7.19
Plate 07	P21	FBXO17	115290	*	77.34		110.24		51.17	0.35	*	77.56		41.96		-45.08	-0.03
Plate 10	J20	FCHO2	115548	*	64.37		82.31		77.97	68.55	*	61.33	*	35.99	*	66.46	79.40
Plate 10	K20	FCHO2	115548	*	59.58	*	81.01	*	73.33	12.55	*	59.65	*	29.29	*	38.73	15.71
Plate 10	L20	FCHO2	115548	*	61.26	*	79.16		84.96	92.24	*	64.39	*	26.55		72.44	134.77
Plate 10	N22	FCRLB	127943	*	39.66	*	72.28		86.13	55.87	*	47.94	*	23.93	*	41.63	42.03
Plate 10	O22	FCRLB	127943	*	44.57	*	71.89	*	72.93	21.99	*	38.82	*	17.68	*	43.35	56.23
Plate 10	P22	FCRLB	127943		74.38	*	291.66	*	343.02	-0.07	*	9.42	*	43.20		125.23	0.08
Plate 02	A15	FEM1B	10116	*	64.26	*	78.37	*	113.39	-6.53	*	108.32	*	92.63	*	95.55	6.37
Plate 02	B15	FEM1B	10116	*	72.54		89.85		92.61	100.14	*	75.40		45.96		88.11	91.86
Plate 02	C15	FEM1B	10116	*	68.82		85.42		80.57	84.11	*	64.64	*	43.43		82.42	84.75
Plate 02	E15	FOXD4L1	200350	*	67.62		93.00		100.77	53.83	*	59.66		48.28	*	73.63	67.58
Plate 04	A15	FOXD4L6	653404	*	77.79		86.28		94.12	38.44	*	61.51	*	30.35	*	69.33	49.91
Plate 04	C15	FOXD4L6	653404	*	74.20		97.20		95.84	58.23	*	70.72	*	63.18	*	90.44	71.31
Plate 08	K06	FOXO1	2308	*	75.46	*	83.57		82.29	140.20	*	76.84		43.59	*	98.47	131.16
Plate 10	K21	FRMD6	122786	*	70.02	*	100.52		87.47	86.94	*	59.27		42.31		78.59	93.07
Plate 10	L21	FRMD6	122786	*	49.08		92.54		85.29	2.25	*	56.95		48.68	*	50.94	3.21
Plate 01	N21	FZD4	8322	*	74.96	*	69.96	*	70.73	127.23	*	61.82	*	21.31	*	62.85	127.58
Plate 01	O21	FZD4	8322	*	47.38	*	78.92	*	83.34	103.89	*	56.62	*	21.06	*	43.78	118.68
Plate 09	P09	GABARAPI	11345		-239.78		-275.11		-182.98	-0.09	*	120.80	*	0.01		-72.44	-0.07
Plate 11	K15	GALNT18	374378	*	76.12		100.32	*	98.61	4.24	*	55.95	*	78.30	*	47.86	8.18
Plate 11	L15	GALNT18	374378	*	49.59		87.32		86.67	88.67	*	42.98	*	29.30	*	53.62	96.84
Plate 09	M22	GATAD2A	54815	*	76.64		109.43	*	117.25	4.40	*	68.80	*	54.88	*	43.13	13.22
Plate 09	P22	GATAD2A	54815		29.26		-26.05	*	110.33	0.01	*	160.03	*	202.24		165.82	0.23
Plate 08	A07	GCKR	2646	*	75.14	*	63.40	*	69.57	19.38	*	71.78	*	34.55	*	52.97	35.55
Plate 08	B07	GCKR	2646	*	56.18	*	84.40		88.27	5.55	*	60.10	*	26.99	*	41.55	14.28
Plate 10	B03	GDAP2	54834		77.62		86.02		91.92	2.51	*	36.11	*	25.32	*	24.14	8.58
Plate 10	C03	GDAP2	54834	*	69.10		95.88		79.62	50.39	*	47.34	*	38.70		77.63	67.85
Plate 10	D03	GDAP2	54834	*	67.06	*	61.61		88.90	1.78		85.66	*	36.73	*	64.84	12.28
Plate 03	P19	GLIPR1L2	144321	*	43.75	*	59.68		89.81	23.53		84.76		48.13	*	32.52	28.52
Plate 11	H07	GLIPR2	152007	*	74.11		98.78		88.38	39.53	*	39.39	*	22.61	*	63.08	67.87

Plate	Well	Gene Symbol	GENEID	*	ATRi Avg	*	A/C Avg	*	Cis Avg	Arm2 Untreated	*	Low HU Avg	*	High HU Avg	*	CHK1i Avg	Arm1 Untreated
Plate 08	K07	GLRA1	2741	*	69.46	*	81.09		94.33	108.56	*	68.83	*	33.37		78.53	103.62
Plate 09	A07	GNA13	10672	*	51.43	*	67.49		89.91	79.96		79.30		45.22	*	48.69	87.57
Plate 09	D07	GNA13	10672	*	73.10	*	63.68		85.56	65.04		77.70	*	56.11		81.85	49.04
Plate 03	E22	GPC6	10082	*	70.97	*	77.72		95.93	19.56	*	73.79	*	35.77	*	55.05	38.67
Plate 09	O19	GPN3	51184	*	59.35		93.05	*	98.08	50.38		78.99	*	31.79	*	36.17	54.46
Plate 02	J18	GPR63	81491	*	44.58		83.84		101.63	12.97	*	48.11	*	26.30	*	34.51	58.74
Plate 10	A07	GRAMD1A	57655	*	70.79	*	104.11	*	109.65	37.04	*	66.26	*	40.16	*	93.08	96.42
Plate 11	B10	GSX2	170825	*	50.40		102.98	*	120.92	1.49	*	50.06	*	35.36	*	70.57	4.95
Plate 11	D10	GSX2	170825	*	64.77	*	178.41	*	154.55	0.82		74.82	*	138.20	*	69.90	1.41
Plate 10	B15	HAGHL	84264	*	75.27	*	122.26		93.88	4.28	*	34.81	*	34.02	*	60.26	12.57
Plate 10	C15	HAGHL	84264	*	61.27		95.16		85.84	51.04	*	63.49		45.33	*	59.58	53.90
Plate 10	D15	HAGHL	84264	*	74.24	*	112.84	*	72.32	4.70	*	53.53	*	28.07	*	48.60	8.98
Plate 09	E03	HAP1	9001	*	65.82		87.52	*	108.43	23.77	*	68.56		41.57	*	61.61	50.61
Plate 09	F03	HAP1	9001	*	77.77	*	74.05		81.28	47.92	*	64.18	*	33.46	*	66.58	88.23
Plate 09	G03	HAP1	9001	*	66.34		81.07		86.53	11.39	*	64.49	*	37.78	*	51.83	35.07
Plate 10	D04	HAUS4	54930	*	68.85	*	97.62	*	109.62	20.43	*	90.17	*	100.21		75.63	17.68
Plate 06	B20	HDAC8	55869	*	62.05		89.49	*	110.09	58.04	*	57.83	*	26.22	*	39.53	70.57
Plate 09	K14	HINFP	25988	*	69.13		85.99	*	74.18	32.38	*	47.58	*	33.69	*	71.23	39.40
Plate 09	L14	HINFP	25988	*	70.34		80.52		84.24	66.25	*	64.42	*	32.84	*	67.07	82.79
Plate 08	P19	HIRA	7290	*	61.85	*	81.70		81.32	84.06		89.53		44.76		80.07	102.26
Plate 08	E22	HIST1H2BC	8339	*	76.75		82.54	*	74.32	5.11		80.12		43.15	*	73.81	15.41
Plate 08	F22	HIST1H2BC	8339	*	53.44		89.08		86.21	16.08		83.84	*	56.98	*	57.45	42.33
Plate 08	H22	HIST1H2BC	8339	*	51.42	*	42.49	*	70.88	1.79	*	74.47		42.75	*	32.34	12.23
Plate 03	L10	HMGB3	3149	*	72.53		77.07	*	116.89	57.23	*	69.67		44.16	*	60.57	55.51
Plate 10	M07	INF2	64423	*	64.32	*	98.36		95.18	71.55		70.78		50.07		79.12	106.99
Plate 10	O07	INF2	64423	*	73.50	*	84.45		98.93	0.15	*	50.64	*	79.52	*	92.68	1.07
Plate 10	P07	INF2	64423		76.02	*	42.07	*	160.63	2.87	*	60.72	*	32.75	*	42.73	21.94
Plate 04	A08	INS-IGF2	723961	*	71.23	*	121.67		97.98	3.97	*	48.48		49.58	*	29.03	7.31
Plate 04	B08	INS-IGF2	723961	*	31.14	*	80.88	*	136.15	26.52	*	70.84	*	28.14	*	21.08	59.67
Plate 10	F08	IQCH	64799	*	53.84		97.28		74.48	6.26	*	51.84	*	28.41	*	59.28	13.67
Plate 10	H08	IQCH	64799	*	33.10	*	61.02		79.14	47.53	*	35.52	*	17.00	*	40.09	72.62
Plate 09	N05	IQSEC1	9922	*	76.74	*	72.48	*	118.53	1.30	*	32.68	*	20.45	*	30.10	7.38
Plate 03	D07	IRX2	153572	*	31.86	*	59.25		86.63	57.65	*	60.45	*	40.61	*	15.82	72.69
Plate 10	N21	ISCA2	122961	*	75.28		98.05		85.77	26.73	*	64.84	*	56.02	*	67.45	18.93
Plate 10	P21	ISCA2	122961	*	70.01	*	80.55		85.77	49.84	*	68.44	*	40.01	*	46.68	75.02
Plate 09	M11	KANK1	23189	*	55.90	*	57.76	*	60.98	29.27	*	59.40	*	22.53	*	53.45	53.08
Plate 09	O11	KANK1	23189	*	75.38		81.15	*	69.32	6.46		95.22	*	34.64	*	58.24	10.03
Plate 08	K08	KCNJ2	3759	*	70.61	*	80.25		79.98	76.80	*	76.03	*	40.10	*	63.89	116.12
Plate 10	J14	KCTD10	83892	*	71.98	*	69.63	*	69.04	85.77	*	62.99	*	24.49	*	50.00	107.89
Plate 10	L14	KCTD10	83892	*	56.17	*	79.67		77.98	51.62	*	41.45	*	38.71	*	47.60	56.65
Plate 05	P07	KIAA0195	9772	*	68.48	*	73.97	*	57.11	26.54	*	44.96	*	37.65	*	37.25	20.75
Plate 02	F20	KIAA0317	9870	*	75.37		91.42		89.08	46.04	*	57.31		48.04	*	67.06	38.71
Plate 02	G20	KIAA0317	9870	*	77.92		83.65		89.09	28.19		85.67	*	63.96	*	64.98	50.50
Plate 02	H20	KIAA0317	9870	*	65.20		86.51		86.33	18.81	*	62.73	*	60.47	*	33.79	27.35
Plate 11	O14	KIAA1211L	343990	*	76.88	*	106.30	*	106.13	6.95		83.24	*	70.08	*	49.60	11.45
Plate 11	P14	KIAA1211L	343990	*	63.05	*	80.08	*	71.38	24.27	*	49.07	*	51.03		81.91	41.02
Plate 09	F14	KIAA1429	25962	*	44.88	*	54.04		77.01	50.28	*	15.96	*	17.11	*	34.22	47.77
Plate 09	G14	KIAA1429	25962	*	76.91	*	68.69	*	72.49	182.95	*	57.01	*	21.87	*	75.52	142.65
Plate 09	H14	KIAA1429	25962	*	65.57	*	69.68	*	72.31	69.81	*	55.61	*	37.82	*	61.08	60.80
Plate 10	O14	KIRREL2	84063	*	77.32	*	75.03		76.88	37.14	*	65.34		42.46	*	69.15	82.60
Plate 11	C03	KLF17	128209	*	65.13	*	61.89	*	54.31	2.78	*	31.96	*	24.78	*	45.54	5.38
Plate 10	C20	KLHDC7B	113730	*	64.36	*	69.19	*	71.52	78.44	*	63.78	*	40.31	*	67.79	106.77
Plate 01	G07	KLHL30	377007	*	70.99	*	109.90	*	119.82	13.46		92.45	*	69.10	*	55.60	29.44
Plate 09	G19	KLHL5	51088	*	68.01	*	69.15	*	73.34	122.13	*	55.92	*	28.70		76.80	103.51
Plate 09	H19	KLHL5	51088	*	44.59	*	53.06	*	55.86	4.97	*	64.43	*	74.57	*	56.32	3.00
Plate 10	E13	LBH	81606	*	61.37	*	65.67	*	51.21	16.73	*	57.87	*	35.63		75.57	6.96
Plate 10	G13	LBH	81606	*	70.21		103.95		85.27	2.82		85.33	*	64.96	*	102.76	4.61
Plate 10	H13	LBH	81606	*	59.32	*	75.16	*	73.06	62.05	*	61.05	*	21.09	*	64.47	50.08
Plate 01	K15	LEO1	123169	*	75.03	*	90.06	*	107.62	8.12		74.22	*	72.17	*	43.10	10.44
Plate 01	L15	LEO1	123169	*	60.42	*	80.34	*	88.79	17.40		76.07	*	58.88	*	32.61	23.32
Plate 11	J06	LRRC71	149499	*	69.58		83.61	*	73.84	31.20	*	33.25	*	16.77	*	48.62	62.14
Plate 11	L06	LRRC71	149499	*	60.78	*	103.05		91.98	23.86	*	47.55	*	54.33	*	69.96	31.66
Plate 03	C06	LRRC8D	55144	*	77.03		99.93	*	99.93	108.75	*	62.46		52.21	*	99.12	112.30
Plate 10	F18	LSM10	84967	*	64.22		89.11	*	97.43	95.31		77.07		43.04	*	32.59	107.20
Plate 10	G18	LSM10	84967	*	62.28	*	74.83	*	67.58	19.20		71.15	*	53.03	*	56.47	11.66
Plate 10	H18	LSM10	84967	*	24.93	*	61.12		96.18	81.47	*	51.65	*	21.69	*	9.07	88.13
Plate 11	E04	LSMEM2	132228	*	73.91	*	109.43		94.81	25.55	*	55.71		50.89	*	66.27	48.22
Plate 11	G04	LSMEM2	132228	*	29.47	*	54.87		80.50	66.90	*	33.24	*	24.97	*	11.49	83.93
Plate 11	H04	LSMEM2	132228	*	65.74	*	103.25	*	104.44	10.93		71.20	*	85.15	*	64.91	12.91
Plate 01	B12	LZTS2	84445	*	63.60	*	49.02		87.74	1.34	*	62.49	*	65.98	*	99.23	2.21
Plate 01	D12	LZTS2	84445	*	67.01	*	85.71	*	107.83	31.24		87.80	*	37.81	*	60.68	43.97

Plate	Well	Gene Symbol	GENEID	*	ATRi Avg	*	A/C Avg	*	Cis Avg	Arm2 Untreated	*	Low HU Avg	*	High HU Avg	*	CHK1i Avg	Arm1 Untreated
Plate 01	L07	MAB21L2	10586	*	69.75	*	122.78	*	108.99	14.10		84.09	*	68.54	*	74.47	22.83
Plate 10	A18	MAEL	84944	*	32.56	*	63.73		81.53	15.14		70.00	*	33.91		70.88	41.80
Plate 10	B18	MAEL	84944	*	67.10	*	65.39		89.18	1.35	*	65.45	*	62.89	*	60.56	3.18
Plate 10	D18	MAEL	84944	*	69.32		83.31		93.59	48.50	*	45.12	*	27.69	*	50.19	53.55
Plate 01	B13	MANF	7873	*	46.24	*	88.44	*	131.38	3.41	*	103.94	*	76.33	*	104.97	5.10
Plate 08	I14	MAP2K3	5606	*	76.21	*	79.37		83.03	60.35		88.27	*	55.48	*	51.72	59.59
Plate 08	J14	MAP2K3	5606	*	59.51	*	75.09	*	80.34	61.31	*	58.92		41.16	*	34.04	42.38
Plate 10	I11	MAP3K19	80122	*	73.10		88.84		86.62	129.96		76.01	*	34.68	*	89.77	134.01
Plate 10	K11	MAP3K19	80122	*	44.93	*	51.02		89.38	7.40	*	44.88	*	61.15	*	38.57	11.82
Plate 10	L11	MAP3K19	80122	*	63.62	*	74.95		76.96	7.34	*	50.66	*	35.89	*	53.76	18.50
Plate 09	A04	MAP4K4	9448	*	62.10		82.00		97.48	41.93	*	65.01	*	31.65	*	59.31	69.93
Plate 09	B04	MAP4K4	9448	*	36.41	*	73.64		77.65	35.64	*	43.48	*	21.94	*	39.74	43.98
Plate 09	C04	MAP4K4	9448	*	76.02	*	69.47		85.58	23.70	*	77.42		46.92	*	69.71	30.17
Plate 09	D04	MAP4K4	9448	*	70.53		87.81		93.06	41.04	*	50.28	*	34.67	*	72.18	72.62
Plate 07	N15	MAP4K4	9448	*	63.27	*	79.39		71.42	59.87	*	48.01	*	28.51	*	59.24	64.95
Plate 07	P15	MAP4K4	9448	*	72.89		89.14		81.96	50.81		78.17		48.33	*	64.69	68.75
Plate 08	L22	MAPKAPK5	8550	*	63.95	*	82.87		84.91	87.65	*	72.55	*	36.36		82.32	93.19
Plate 08	C09	MDM4	4194	*	65.79		89.88		93.62	70.48	*	65.02	*	39.68	*	60.06	73.17
Plate 11	E06	MIPOL1	145282	*	73.96		95.88		79.32	29.00	*	47.73	*	52.67	*	74.26	34.43
Plate 11	G06	MIPOL1	145282	*	68.73		87.61		78.52	115.90	*	56.85	*	36.84	*	53.59	117.10
Plate 01	O15	MLANA	2315	*	57.86		97.15	*	151.89	3.31	*	96.99	*	61.02		75.86	5.75
Plate 09	P16	MLH3	27030	*	61.54		84.65		79.28	19.60	*	64.89	*	31.42	*	51.18	31.55
Plate 09	F20	MRPL35	51318	*	50.29	*	69.55		77.26	85.11	*	67.56	*	31.53	*	62.93	80.38
Plate 09	G20	MRPL35	51318	*	69.37	*	76.77		88.06	35.19	*	67.50		46.35	*	48.62	29.86
Plate 09	H20	MRPL35	51318	*	58.30	*	69.26		80.70	11.38	*	67.26	*	52.07	*	45.45	13.51
Plate 09	N17	MRPS18B	28973	*	77.05		90.65		89.37	92.09	*	62.61		44.41	*	69.29	90.97
Plate 09	O17	MRPS18B	28973	*	73.86	*	72.91		81.73	54.65		83.05		49.37	*	61.89	67.49
Plate 10	F22	MSI2	124540	*	56.62	*	65.34	*	67.40	0.97	*	69.31	*	74.51	*	91.37	0.69
Plate 10	H22	MSI2	124540	*	65.00		97.65	*	110.66	58.39	*	60.15	*	37.06	*	54.44	73.69
Plate 09	G17	MTBP	27085	*	76.29		86.81	*	138.01	3.07		76.94	*	110.65	*	65.77	4.85
Plate 09	H17	MTBP	27085	*	66.09		85.87		95.66	9.35		87.78	*	86.80	*	67.18	9.88
Plate 11	B05	MUM1L1	139221	*	76.92	*	105.68	*	94.87	41.32	*	58.62		46.45		85.25	47.20
Plate 10	A17	NAA11	84779	*	69.57	*	79.32	*	71.51	38.41	*	35.87	*	29.24		74.21	50.25
Plate 10	C17	NAA11	84779	*	44.65	*	75.51	*	65.10	3.61	*	47.07	*	66.31		77.94	3.72
Plate 10	D17	NAA11	84779	*	65.83	*	67.53		75.28	9.66	*	43.33	*	36.02	*	54.37	6.07
Plate 07	J10	NAA50	80218	*	75.23		86.93		94.25	13.03	*	110.48	*	100.13		77.12	13.35
Plate 08	I09	NAP1L4	4676	*	71.53	*	77.18		90.27	82.17	*	60.55	*	30.96	*	66.98	114.10
Plate 10	A08	NARFL	64428	*	75.89	*	114.12	*	106.23	9.27	*	52.72	*	57.03	*	50.34	25.08
Plate 10	C08	NARFL	64428	*	74.37		94.25	*	95.26	20.81	*	58.95		50.30		78.65	42.81
Plate 11	M20	NCBP1	4686	*	64.24	*	127.27		99.26	1.60	*	57.40	*	69.64	*	64.18	1.62
Plate 05	N10	NCBP1	4686	*	72.22		92.84	*	65.16	9.57	*	68.78	*	79.11	*	57.41	5.66
Plate 11	N20	NCBP1	4686	*	75.84		108.55		93.54	1.76	*	54.47	*	85.28	*	65.80	2.52
Plate 05	P10	NCBP1	4686	*	74.03		97.35	*	22.82	0.76	*	33.17	*	105.07	*	66.55	0.94
Plate 08	M09	NDUFV3	4731	*	75.83		82.47		80.90	61.89		83.29		53.22	*	73.31	67.48
Plate 08	O09	NDUFV3	4731	*	59.78	*	43.30		78.58	1.79		85.79		56.16	*	41.19	4.26
Plate 10	F19	NEK9	91754	*	74.96		89.17		89.08	41.68		80.71		47.51		79.44	44.84
Plate 08	A10	NEU2	4759	*	75.06		87.62	*	101.05	25.50	*	56.90	*	31.82	*	37.03	62.03
Plate 10	N17	NFATC2IP	84901	*	50.04	*	114.61	*	126.75	11.51	*	61.85	*	55.59	*	62.92	14.75
Plate 10	O17	NFATC2IP	84901	*	75.96	*	78.19	*	64.98	84.69	*	53.96	*	32.27	*	64.67	96.28
Plate 10	P17	NFATC2IP	84901	*	69.83	*	68.08	*	71.61	20.12	*	56.24	*	21.61	*	62.07	28.40
Plate 02	A20	NFYB	4801	*	42.31		93.18		97.95	10.57	*	57.14	*	73.61	*	23.90	19.95
Plate 02	B20	NFYB	4801	*	69.34		94.45		135.40	-10.24	*	55.94		63.20	*	72.02	2.45
Plate 02	D20	NFYB	4801	*	75.13		97.15	*	121.87	55.04	*	47.09	*	43.24	*	24.45	39.70
Plate 07	A09	NIN	51199	*	73.71	*	77.98		84.84	88.87	*	58.76	*	26.48	*	63.26	84.88
Plate 07	B09	NIN	51199	*	72.78		92.24		82.79	5.48	*	71.65	*	64.90	*	72.67	11.62
Plate 11	J03	NMS	129521	*	61.88	*	127.63	*	104.67	6.24	*	37.10	*	21.25	*	57.23	17.71
Plate 05	G13	NOD1	10392	*	74.75	*	75.62		73.94	112.28	*	45.32	*	25.74	*	69.60	130.87
Plate 11	G13	NOMO2	283820	*	67.15		82.31	*	93.42	60.47	*	41.56	*	17.96	*	57.20	76.24
Plate 11	H13	NOMO2	283820	*	77.47		81.99		82.20	24.08	*	52.49		46.63	*	42.22	23.41
Plate 08	J10	NPAT	4863	*	48.90		92.55	*	127.05	8.25	*	114.23	*	100.74	*	26.65	11.80
Plate 10	A13	NPL	80896	*	27.51	*	67.95		79.36	8.20	*	42.82	*	16.48	*	31.04	42.24
Plate 10	B13	NPL	80896	*	42.84		84.78		85.70	17.21	*	48.52	*	37.12		75.37	45.07
Plate 10	C13	NPL	80896	*	76.57	*	106.66		77.58	9.33	*	46.28	*	38.65	*	34.75	26.88
Plate 10	D13	NPL	80896	*	69.32	*	57.86		79.04	1.38	*	99.07		48.28	*	90.97	3.28
Plate 08	B19	NR2C2	7182	*	73.89		89.41	*	102.15	64.59	*	62.89	*	27.74	*	57.61	81.27
Plate 08	C19	NR2C2	7182	*	70.87		91.85	*	100.40	38.48	*	60.77	*	31.50	*	55.85	58.59
Plate 08	D19	NR2C2	7182	*	60.03		93.43		107.84	53.08	*	69.19		42.87	*	46.47	23.28
Plate 09	J22	NSMCE4A	54780	*	34.19	*	59.84		80.13	13.75	*	62.24	*	23.74	*	67.19	17.61
Plate 09	K22	NSMCE4A	54780	*	62.41		81.81		96.74	34.55	*	50.21		43.55	*	56.79	36.33
Plate 01	M09	NTNG2	84628	*	71.98	*	81.81	*	133.88	1.97		75.92	*	68.06	*	113.95	3.18
Plate 11	E18	NUCKS1	64710	*	63.20	*	102.97	*	107.68	43.00	*	53.20		46.24	*	59.71	46.20

Plate	Well	Gene Symbol	GENEID	*	ATRi Avg	*	A/C Avg	*	Cis Avg	Arm2 Untreated	*	Low HU Avg	*	High HU Avg	*	CHK1i Avg	Arm1 Untreated
Plate 11	H18	NUCKS1	64710	*	76.88	*	109.36		80.27	11.55	*	61.19	*	59.35	*	62.09	18.16
Plate 10	E05	NUP133	55746		77.97	*	66.41		86.35	0.80	*	96.17	*	96.23	*	116.02	1.09
Plate 10	G05	NUP133	55746	*	69.17		84.27	*	98.90	2.29		87.68	*	122.23		75.78	3.83
Plate 10	H05	NUP133	55746	*	47.32	*	79.53	*	140.83	4.66	*	157.20	*	231.25	*	59.16	4.52
Plate 01	I06	OBP2A	29991	*	61.88		96.72		119.53	9.01	*	37.33	*	21.73	*	59.11	24.70
Plate 01	J06	OBP2A	29991	*	62.43	*	57.54	*	81.57	1.80		74.50	*	82.42	*	119.86	2.38
Plate 01	K06	OBP2A	29991	*	60.81	*	76.27		96.91	45.88	*	99.60	*	67.63	*	65.53	56.91
Plate 01	L06	OBP2A	29991	*	47.03	*	90.27	*	82.47	13.15	*	50.30	*	26.38	*	98.51	15.23
Plate 11	P16	ONECUT3	390874		-86.00		42.18		-79.66	-0.10		16675.89	*	22.33	*	-9310.76	0.49
Plate 09	L16	OR7C1	26664	*	72.82		88.46	*	72.76	33.03	*	44.81	*	28.69		90.68	35.57
Plate 08	A11	ORC1	4998	*	72.02		95.85	*	104.86	44.20		81.68		51.42	*	55.99	58.81
Plate 08	C11	ORC1	4998	*	69.09	*	85.47	*	131.63	8.79	*	72.06	*	58.27	*	74.71	9.46
Plate 08	D11	ORC1	4998	*	47.35	*	73.36	*	112.27	21.33		82.15	*	93.80	*	51.90	20.08
Plate 08	F11	OSBP	5007	*	72.94	*	84.98	*	79.26	97.09	*	74.40	*	31.87		78.45	109.77
Plate 08	L11	P2RY1	5028	*	70.43	*	83.05	*	79.85	90.74	*	61.37	*	29.91	*	69.18	82.11
Plate 09	I18	PADI1	29943	*	77.83		84.20		81.88	23.08	*	72.58		42.16		82.76	21.99
Plate 09	L18	PADI1	29943	*	47.98	*	73.68		78.43	17.29	*	48.88	*	19.90	*	43.46	18.49
Plate 09	F04	PAGE4	9506	*	60.46		96.81	*	166.76	0.63	*	66.90	*	165.12		104.95	1.03
Plate 09	H04	PAGE4	9506	*	69.42		95.30		106.03	12.37	*	41.28		39.29	*	57.88	26.60
Plate 08	P11	PAK1	5058	*	77.39		99.50	*	76.39	22.99		79.63	*	38.97	*	95.26	61.43
Plate 10	G17	PARP10	84875	*	70.62	*	78.57		103.90	5.37		71.42	*	40.08	*	61.95	6.72
Plate 09	H22	PARP14	54625	*	77.55		80.72		89.42	34.72	*	74.58	*	64.14		78.75	27.28
Plate 05	P03	PATE3	100169851	*	27.82	*	71.92	*	61.81	7.25	*	47.40	*	40.24	*	42.58	22.91
Plate 08	A12	PCBD1	5092	*	-451.83	*	15.29		-96.92	0.38	*	40.84	*	26.62	*	29.28	2.87
Plate 08	C12	PCBD1	5092	*	51.97	*	71.72	*	69.49	13.89	*	56.70	*	29.68	*	53.32	26.35
Plate 08	D12	PCBD1	5092	*	77.28		99.68		97.33	11.58	*	61.68		55.55	*	57.91	22.58
Plate 09	G06	PDCD6IP	10015	*	67.42		92.71		92.25	1.39	*	62.25	*	63.69		94.75	5.35
Plate 05	E22	PDS5B	23047	*	74.76		89.84	*	97.69	20.87	*	75.41	*	54.04	*	60.94	24.95
Plate 11	H17	PEF1	553115	*	59.95	*	71.67		85.43	29.88	*	35.36	*	30.13	*	52.76	24.81
Plate 01	L04	PHF23	79142	*	37.52	*	64.22		104.81	1.09		101.86	*	91.53	*	141.58	1.81
Plate 07	K05	PIAS1	8554	*	65.85	*	76.46		82.70	111.95	*	68.13	*	28.49	*	53.31	100.20
Plate 09	A19	PIK3R4	30849	*	70.36		93.83	*	120.08	4.44	*	59.93	*	55.99		79.59	18.69
Plate 09	B19	PIK3R4	30849	*	60.18	*	77.28		80.97	51.12	*	67.85	*	28.48	*	68.64	62.81
Plate 09	C19	PIK3R4	30849	*	59.38	*	79.25	*	102.49	7.63	*	67.73	*	72.67	*	45.52	7.30
Plate 09	D19	PIK3R4	30849	*	61.32	*	68.35	*	73.12	43.91	*	69.11	*	38.38	*	68.39	44.23
Plate 08	B13	PLAGL2	5326	*	59.78	*	108.35	*	109.39	1.38	*	158.11	*	187.89	*	123.79	0.91
Plate 10	G04	PLEKHB2	55041	*	74.21		90.04		87.73	50.60	*	61.03	*	37.18		82.53	91.45
Plate 08	E13	POU6F1	5463	*	70.02		89.50		86.84	27.49		86.99		42.14	*	61.13	27.54
Plate 08	H13	POU6F1	5463	*	59.69	*	62.81	*	73.33	12.23		85.09		47.38	*	48.38	19.67
Plate 09	M07	PPP1R13L	10848	*	70.35	*	69.01		77.62	90.10	*	67.36	*	31.76		79.92	109.64
Plate 09	O07	PPP1R13L	10848	*	77.62		94.35		90.38	82.13		80.18	*	58.17		84.46	101.26
Plate 09	A13	PPP1R15A	23645	*	75.82		92.25		88.64	55.69	*	51.71	*	31.76	*	72.23	70.97
Plate 09	B13	PPP1R15A	23645	*	68.20		81.38		83.41	51.82	*	66.43	*	32.73		85.65	29.20
Plate 09	C13	PPP1R15A	23645	*	59.68	*	70.53		80.57	25.49	*	32.61	*	16.70	*	41.60	23.53
Plate 08	I13	PPP2R1B	5519	*	68.45	*	84.15	*	78.42	127.48	*	74.97	*	38.60	*	62.88	117.85
Plate 08	N13	PPP2R5A	5525	*	70.15	*	80.40	*	78.30	49.63	*	60.71	*	23.90		79.65	40.65
Plate 09	M04	PPP6R2	9701	*	64.41	*	117.30	*	156.03	5.93		86.59		47.42	*	65.01	15.27
Plate 09	O04	PPP6R2	9701	*	75.94		83.00		81.00	24.23		78.89	*	58.96	*	61.23	35.86
Plate 09	P04	PPP6R2	9701	*	57.94	*	77.55		87.40	17.26	*	60.46	*	56.51	*	35.83	22.14
Plate 09	I03	PRC1	9055	*	59.40	*	135.24	*	153.25	0.79		87.41	*	71.79	*	111.47	2.39
Plate 09	J03	PRC1	9055	*	61.55		89.00	*	125.84	1.07	*	69.85		42.98		90.10	4.78
Plate 09	K03	PRC1	9055	*	14.13		98.47	*	196.85	0.48	*	64.69	*	74.16	*	40.56	2.36
Plate 09	L03	PRC1	9055	*	60.00		85.12	*	99.95	106.20	*	73.22		44.31		85.58	121.17
Plate 08	M12	PRIM2	5558	*	64.80	*	71.03	*	78.08	43.51	*	27.63	*	24.75	*	20.39	13.28
Plate 08	N12	PRIM2	5558	*	45.37	*	45.19	*	70.41	9.95	*	74.36		41.86	*	14.56	7.54
Plate 08	A14	PRKAR2A	5576	*	55.46		86.13		86.40	4.00	*	43.40	*	22.20	*	39.07	21.52
Plate 08	C14	PRKAR2A	5576	*	53.68	*	66.03	*	73.62	12.18	*	55.23	*	27.97	*	33.65	28.31
Plate 08	D14	PRKAR2A	5576	*	65.07	*	77.33		88.61	43.84	*	48.31	*	30.40	*	75.24	53.91
Plate 11	N13	PRR18	285800	*	58.18		91.62	*	73.50	39.39	*	59.36	*	38.47	*	62.93	41.60
Plate 01	N22	PRTN3	5657	*	76.41		-20.30		166.24	0.23	*	31.88	*	35.73	*	165.31	0.45
Plate 01	O22	PRTN3	5657	*	33.36	*	87.12	*	94.04	14.01	*	59.12	*	36.39	*	44.46	15.32
Plate 08	B21	PTP4A1	7803	*	64.14	*	72.05	*	79.91	70.58	*	68.33	*	30.11	*	50.90	76.97
Plate 03	D19	RAB4B	53916	*	44.38		79.63	*	114.99	2.78	*	47.16	*	63.45	*	40.53	5.39
Plate 08	P14	RABGGTA	5875	*	77.12	*	-50.57		-392.04	0.45	*	26.57	*	40.55	*	2.07	0.65
Plate 10	F12	RAD1	5810	*	15.60	*	38.26	*	72.97	108.04	*	31.03	*	11.31	*	15.57	109.10
Plate 10	G12	RAD1	5810	*	60.98	*	51.04	*	58.00	5.54		69.61	*	39.13		70.71	9.87
Plate 10	H12	RAD1	5810	*	42.67		77.06		81.64	42.68	*	42.23	*	33.97	*	38.98	34.09
Plate 08	A15	RAG1	5896	*	37.80		96.53		88.07	14.27	*	31.33	*	12.18	*	41.96	55.19
Plate 08	B15	RAG1	5896	*	69.14		86.33		88.69	24.97	*	62.95	*	20.95	*	65.83	35.36
Plate 09	K10	RALY	22913	*	72.17		81.63		91.28	66.82	*	72.66	*	32.90		76.64	88.91
Plate 02	G16	RAP2C	57826	*	75.20		88.23	*	106.19	90.76		79.47	*	32.75	*	28.98	79.10

Plate	Well	Gene Symbol	GENEID	*	ATRi Avg	*	A/C Avg	*	Cis Avg	Arm2 Untreated	*	Low HU Avg	*	High HU Avg	*	CHK1i Avg	Arm1 Untreated
Plate 11	M11	RASGEF1C	255426	*	74.99	*	142.51		84.30	3.75	*	27.78		47.42	*	50.48	7.67
Plate 11	N11	RASGEF1C	255426	*	53.22	*	62.86		70.42	12.45	*	51.79	*	37.58	*	44.16	12.00
Plate 11	O11	RASGEF1C	255426	*	68.42		94.03		85.00	8.57		71.95	*	92.06		90.82	13.30
Plate 11	P11	RASGEF1C	255426	*	72.51	*	110.76		86.57	4.36	*	47.20		41.22	*	62.96	19.50
Plate 08	E15	RBBP4	5928	*	71.21		85.58	*	74.51	52.04	*	70.83	*	29.52	*	42.10	45.42
Plate 08	G15	RBBP4	5928	*	73.18		88.42	*	75.03	48.55	*	54.87	*	25.71	*	53.24	28.22
Plate 09	B22	RHOF	54509	*	73.18		88.76	*	104.45	12.21	*	68.66		49.86	*	64.66	18.50
Plate 06	I05	RNF186	54546	*	74.41		86.68		88.18	70.06	*	45.40	*	25.24	*	44.01	63.44
Plate 06	L05	RNF186	54546	*	70.58		92.87	*	117.25	12.75	*	44.01	*	38.06	*	32.08	21.01
Plate 05	I19	RNF208	727800	*	69.45		97.02	*	113.52	4.37	*	38.26		46.36	*	55.77	10.17
Plate 05	J19	RNF208	727800	*	61.99		86.86	*	105.45	48.37	*	39.05	*	29.57	*	31.51	45.92
Plate 10	M03	RNF43	54894	*	48.18		88.91		91.82	3.09	*	61.92	*	53.97	*	68.44	15.28
Plate 10	O03	RNF43	54894	*	63.64		91.45	*	100.70	25.65	*	65.98	*	39.90		73.72	40.87
Plate 10	K15	RPAIN	84268	*	66.88	*	71.26		81.08	24.61	*	40.66		41.70	*	38.86	13.83
Plate 10	L15	RPAIN	84268	*	67.12		84.86		97.38	2.34	*	64.73	*	83.32	*	68.55	3.45
Plate 09	M14	RPAP1	26015	*	70.19		103.32	*	113.41	3.79		83.00	*	73.66	*	63.62	7.29
Plate 09	P14	RPAP1	26015	*	-4323.65		-1106.53	*	545.06	2.85		86.25	*	52.75	*	65.94	4.40
Plate 10	A10	RPAP3	79657		76.35	*	40.15		54.44	0.33	*	52.36	*	61.62		79.72	2.67
Plate 10	B10	RPAP3	79657	*	73.55		82.12		96.91	16.25	*	66.41		43.76	*	43.12	33.32
Plate 10	C10	RPAP3	79657	*	72.39		93.51	*	100.25	4.25	*	97.54	*	93.03		78.45	4.58
Plate 10	M05	RPGRIP1	57096	*	65.91		87.90	*	107.94	39.28		69.79		48.53	*	50.91	52.92
Plate 10	N05	RPGRIP1	57096	*	64.12	*	19.63	*	18.90	0.25		89.26	*	72.28	*	48.01	1.28
Plate 10	P05	RPGRIP1	57096		-197.76		6445.04		8487.50	0.06	*	0.01	*	0.01	*	55.24	0.25
Plate 08	K15	RPS6KA3	6197	*	48.10	*	74.39		86.89	90.93	*	50.48	*	25.29	*	35.25	84.83
Plate 08	L15	RPS6KA3	6197	*	73.56		94.23		90.81	16.83		81.12	*	61.36	*	67.11	18.43
Plate 09	K19	RRNAD1	51093	*	59.26	*	62.38	*	61.19	47.16	*	57.48	*	36.74	*	48.28	43.48
Plate 09	L19	RRNAD1	51093	*	43.01	*	62.56		87.88	18.63	*	39.71	*	19.37	*	50.48	31.16
Plate 09	L21	RSF1	51773	*	68.68	*	79.72	*	72.11	27.50		92.03		42.95	*	71.68	17.44
Plate 09	I05	RUSC2	9853	*	61.65	*	57.52		91.52	18.80	*	48.57	*	24.17	*	63.62	36.12
Plate 09	L05	RUSC2	9853	*	68.28		96.96	*	99.82	2.76		86.62	*	91.84		96.35	4.31
Plate 10	L09	SAP130	79595	*	73.06		101.18		98.24	1.71	*	57.75		48.31	*	64.16	7.65
Plate 08	O22	SAP30	8819	*	73.88	*	84.93		84.87	53.23	*	68.49		42.78	*	73.79	69.53
Plate 08	P22	SAP30	8819	*	69.10		95.00	*	100.95	12.05		85.85	*	65.08	*	57.09	17.97
Plate 08	A16	SARS	6301	*	73.50		86.15		94.82	90.62		78.37	*	39.15	*	69.26	89.07
Plate 10	E06	SCYL3	57147	*	59.34	*	110.88	*	101.30	20.15	*	65.59		46.08	*	47.11	48.10
Plate 09	F15	SENP6	26054	*	58.67		82.28		78.43	30.33	*	62.52	*	57.20	*	40.72	32.43
Plate 09	H15	SENP6	26054	*	76.43		85.09		90.55	27.97	*	58.14		49.72	*	41.76	37.28
Plate 09	M10	SEPHS1	22929	*	77.86		88.38		80.79	63.06	*	74.58		46.22	*	53.83	87.35
Plate 04	A09	SERPINA11	256394	*	74.56		94.96	*	117.50	26.92	*	75.28	*	57.70	*	66.18	42.08
Plate 03	M14	SERPINA6	866	*	68.94		79.55	*	106.52	9.30	*	93.46	*	58.70		93.55	14.85
Plate 03	N14	SERPINA6	866	*	66.22		88.69	*	134.40	38.44		107.97	*	75.16		85.92	35.99
Plate 09	M18	SERTAD1	29950	*	60.95		82.15		93.67	1.32	*	115.38	*	81.94	*	70.09	3.15
Plate 09	A05	SETD1A	9739	*	60.42	*	57.21	*	67.51	54.20	*	61.88	*	22.02	*	32.47	44.54
Plate 09	C05	SETD1A	9739	*	75.47	*	79.71		86.77	109.70	*	70.32		41.55	*	71.28	89.94
Plate 04	J13	SEZ6	124925	*	72.86		100.27		90.75	49.22	*	65.47	*	32.91	*	67.79	57.27
Plate 04	L13	SEZ6	124925	*	65.57	*	70.72	*	63.82	45.21	*	28.91	*	28.45	*	49.26	16.75
Plate 11	P06	SGOL1	151648	*	55.43		135.42	*	168.24	0.86	*	58.21	*	32.11	*	48.29	1.37
Plate 01	I05	SHMT1	6470	*	8.52	*	44.39		91.58	80.35		79.78	*	39.61	*	14.48	107.16
Plate 11	H16	SIMC1	375484	*	74.80		89.35		81.36	63.17	*	54.93	*	52.24	*	68.81	44.10
Plate 08	J16	SLC15A2	6565	*	58.11	*	77.59		81.57	99.01	*	75.17	*	40.52	*	65.31	98.34
Plate 08	K16	SLC15A2	6565	*	76.32	*	78.10	*	72.41	123.68	*	65.84	*	32.25		84.46	112.05
Plate 08	L16	SLC15A2	6565	*	70.99		85.77		99.07	49.75	*	66.31	*	40.02	*	56.74	36.40
Plate 04	J05	SLC17A1	6568	*	68.16		101.56		89.98	7.93	*	75.10	*	63.51		72.00	6.19
Plate 04	L05	SLC17A1	6568	*	70.28	*	81.20		82.85	115.92	*	66.44		40.77		78.20	117.00
Plate 10	G20	SLC26A7	115111	*	65.91		96.08		91.01	43.27	*	57.96	*	33.50	*	56.94	39.74
Plate 10	H20	SLC26A7	115111	*	42.58	*	65.76		84.08	44.46	*	42.62	*	19.87	*	32.62	50.28
Plate 10	B22	SLC51B	123264	*	57.22	*	77.78		78.01	9.36	*	46.59	*	30.10	*	56.51	24.41
Plate 10	C22	SLC51B	123264	*	76.05		85.06		80.91	75.36		75.97		50.12		82.08	96.86
Plate 10	N08	SLX1B	79008	*	56.82		80.86		88.46	37.09		71.41	*	36.52	*	49.22	52.36
Plate 08	M16	SMARCD2	6603	*	65.77		89.02		82.45	39.12	*	70.58		46.68	*	44.03	38.62
Plate 11	J19	SMCHD1	23347	*	67.02		85.86	*	62.06	2.50	*	43.64		49.13	*	65.99	3.29
Plate 01	L17	SNTB2	6645	*	77.38		102.24		100.43	10.66	*	58.87	*	31.20	*	55.89	11.88
Plate 08	A17	SOD1	6647	*	76.84	*	70.03	*	73.83	12.32	*	61.60	*	30.73	*	60.48	24.22
Plate 08	D17	SOD1	6647	*	55.17	*	70.89		84.61	32.90		77.49		45.13	*	70.34	6.59
Plate 08	A08	SP110	3431	*	70.11	*	82.12		101.51	4.64	*	58.24	*	39.76	*	54.55	7.25
Plate 08	F17	SPAG1	6674	*	77.73		94.46		90.82	62.67	*	74.01		49.19		86.73	66.85
Plate 10	M04	SRBD1	55133	*	70.34		96.36		77.95	0.91	*	56.86	*	72.00	*	89.28	2.67
Plate 11	B06	SREK1	140890	*	52.79		86.97	*	98.21	18.47	*	68.71		50.40	*	60.36	33.54
Plate 08	M17	SSRP1	6749	*	55.87		86.88		94.49	42.53	*	76.20	*	30.18	*	34.23	22.66
Plate 08	N17	SSRP1	6749	*	67.85		90.50		87.76	30.94		83.78	*	36.62	*	36.80	18.75
Plate 09	E18	SSU72	29101	*	45.87	*	56.77	*	66.99	45.97	*	39.76		44.91	*	40.29	14.87

Plate	Well	Gene Symbol	GENEID	*	ATRi Avg	*	A/C Avg	*	Cis Avg	Arm2 Untreated	*	Low HU Avg	*	High HU Avg	*	CHK1i Avg	Arm1 Untreated
Plate 09	G18	SSU72	29101	*	70.23		91.98		94.98	22.57	*	49.43	*	25.27	*	45.07	17.65
Plate 09	H18	SSU72	29101	*	59.26	*	77.31	*	75.03	71.32	*	44.59	*	16.01	*	57.99	74.22
Plate 08	E21	ST7	7982	*	71.88	*	79.51	*	79.72	111.27		81.40		44.99		86.19	88.61
Plate 08	F21	ST7	7982	*	73.55		86.64	*	108.94	5.53	*	74.87	*	84.10	*	55.57	3.82
Plate 08	H21	ST7	7982	*	74.13	*	72.68	*	76.72	26.75	*	103.76		51.24		81.60	16.93
Plate 10	I03	ST7L	54879	*	48.93		90.40		88.96	10.21	*	66.72	*	30.06	*	43.71	30.22
Plate 10	K03	ST7L	54879	*	69.84		90.91	*	108.36	45.32	*	68.44		49.08	*	35.43	92.71
Plate 10	L03	ST7L	54879	*	42.01		-1.91	*	59.62	0.19	*	20.53	*	25.99	*	48.40	3.54
Plate 11	P10	STOX1	219736	*	47.12	*	69.04		77.44	10.07	*	37.71	*	25.35	*	49.20	22.49
Plate 09	B21	STYXL1	51657	*	52.49	*	53.96	*	59.35	22.07	*	53.16	*	19.81	*	58.01	12.71
Plate 09	D21	STYXL1	51657	*	73.33		85.37		92.50	29.97	*	53.59		47.89	*	74.54	28.59
Plate 04	M19	SYCP2	10388	*	55.20		106.69	*	108.64	46.26	*	64.38		41.18	*	56.78	34.32
Plate 04	N19	SYCP2	10388	*	72.23		92.91		89.33	80.20	*	65.02		40.63	*	58.35	84.27
Plate 08	A22	SYMPK	8189	*	-126.64	*	45.59	*	-223.63	0.10	*	122.31	*	85.23		-152.83	-0.02
Plate 08	B22	SYMPK	8189	*	60.28		87.60	*	102.50	55.87	*	53.52	*	29.30	*	24.76	68.96
Plate 08	D22	SYMPK	8189	*	29.41	*	71.46	*	113.92	17.00	*	47.46	*	39.81	*	12.93	18.41
Plate 05	F04	SYNPO	11346	*	67.36		97.69		99.84	6.50	*	39.05	*	69.44	*	64.87	8.25
Plate 11	C15	TBC1D26	353149	*	47.28	*	71.25		91.09	8.98	*	54.58		41.13	*	62.25	8.88
Plate 01	L20	TBC1D4	9882	*	74.62		90.86	*	180.86	0.66		73.73	*	83.64	*	163.34	1.30
Plate 09	E16	TBL2	26608	*	74.55	*	77.13		77.31	99.16		87.27	*	50.11		87.21	80.96
Plate 09	F16	TBL2	26608	*	74.81		100.27		97.21	34.79	*	55.69	*	36.03	*	60.65	21.81
Plate 09	H16	TBL2	26608	*	68.49	*	64.54	*	67.20	84.27	*	64.35	*	31.79	*	63.21	78.14
Plate 04	K21	TCTE1	202500	*	67.49	*	78.88		85.93	66.71	*	39.91	*	17.84	*	41.90	68.63
Plate 02	C03	TEAD1	7003	*	53.70		83.55	*	75.48	8.55	*	57.86	*	29.76	*	67.07	28.03
Plate 09	A06	THOC1	9984	*	77.72		94.57		93.88	63.41	*	55.74	*	35.41		76.78	49.88
Plate 09	B06	THOC1	9984	*	60.55	*	76.43		90.54	12.52		78.89	*	36.36	*	51.70	14.47
Plate 09	C06	THOC1	9984	*	47.91		94.21		100.12	13.34	*	75.66	*	54.40	*	31.04	15.20
Plate 11	H11	TIGD3	220359	*	63.88	*	49.13	*	59.01	6.38	*	49.00	*	39.41		79.59	6.48
Plate 01	I14	TIMP3	7078	*	68.73	*	116.41		103.85	25.75		73.70	*	59.59		76.33	33.66
Plate 01	L14	TIMP3	7078	*	68.00	*	92.63		97.05	111.84		74.67	*	30.25	*	60.15	129.10
Plate 09	E08	TLK2	11011	*	46.70	*	59.41		85.26	88.68	*	62.65	*	23.27	*	39.52	98.98
Plate 09	F08	TLK2	11011	*	65.55	*	76.08		92.18	40.24		83.12		42.05	*	57.44	48.91
Plate 09	G08	TLK2	11011	*	71.34		81.13		78.63	12.22		79.25		46.86	*	66.15	24.51
Plate 04	L19	TMCO6	55374	*	67.95		87.04	*	67.42	38.98	*	53.56	*	33.49	*	67.83	21.26
Plate 11	C16	TMEM110	375346	*	65.03	*	100.88		88.04	24.35	*	47.18		48.42	*	68.70	23.58
Plate 11	K10	TMEM154	201799	*	62.93		90.97	*	74.47	17.89	*	40.39	*	28.78	*	29.33	20.96
Plate 11	L10	TMEM154	201799	*	49.37	*	74.04		79.15	6.37	*	19.19	*	30.45	*	50.29	6.54
Plate 10	I17	TMTC4	84899	*	72.88		87.86		85.50	145.94	*	59.80	*	38.42	*	69.45	155.95
Plate 09	K15	TOR1AIP1	26092	*	67.77	*	71.00	*	73.31	120.43	*	59.70	*	24.68	*	69.00	103.43
Plate 09	L15	TOR1AIP1	26092	*	29.05	*	55.62		86.98	92.85	*	62.88	*	35.11	*	18.39	81.49
Plate 08	J18	TP53	7157	*	76.32	*	115.91		104.83	8.21	*	60.97		51.54		90.46	15.24
Plate 01	N08	TP53	7157	*	59.60	*	81.62		101.64	14.67	*	70.36	*	54.72		84.86	16.32
Plate 01	O08	TP53	7157	*	49.46		118.07	*	142.96	0.86	*	60.79		48.20	*	101.23	2.28
Plate 08	F19	TRAF5	7188	*	67.38	*	79.99		96.33	15.01		79.40		47.21	*	68.29	9.89
Plate 02	I05	TRAF7	84231	*	56.58		83.70	*	115.81	-4.64		81.52		61.40	*	111.60	25.57
Plate 02	K05	TRAF7	84231	*	50.06		91.20		96.53	38.18	*	67.86	*	19.08	*	30.63	52.84
Plate 09	J08	TRIM31	11074	*	63.08		85.38		98.75	5.27		78.24	*	70.56	*	47.44	12.71
Plate 09	L08	TRIM31	11074	*	66.07	*	75.25	*	74.86	139.86	*	58.91	*	30.39	*	73.31	146.22
Plate 02	A13	TRIM62	55223	*	69.37		87.48		99.14	2.82		82.37		49.03	*	44.61	12.78
Plate 02	B13	TRIM62	55223	*	66.10		84.19		104.74	4.19	*	68.78	*	41.33	*	68.12	13.76
Plate 02	D13	TRIM62	55223	*	76.89		96.40		89.80	59.12		77.44	*	57.70	*	74.94	71.80
Plate 08	K17	TROVE2	6738	*	74.16		87.95	*	78.59	72.39	*	61.52	*	34.06	*	69.36	70.73
Plate 08	I19	TSN	7247	*	76.75	*	72.88	*	76.89	69.86	*	68.44	*	29.59	*	65.63	71.57
Plate 08	L19	TSN	7247	*	71.46	*	76.43	*	68.20	104.23	*	63.95	*	32.08		79.03	90.88
Plate 09	B17	TSPAN13	27075	*	68.90	*	72.42		73.30	18.76	*	69.92	*	56.01		82.21	17.85
Plate 09	D17	TSPAN13	27075	*	63.11		106.20		76.57	22.91		90.00	*	72.44		85.81	12.45
Plate 09	J11	TTLL5	23093	*	76.23	*	76.12		79.43	111.91	*	62.26		42.52	*	97.81	119.90
Plate 09	K11	TTLL5	23093	*	65.85		85.89		82.76	14.70	*	37.91	*	33.35	*	64.80	20.26
Plate 08	B20	TXN	7295	*	60.79		91.38	*	132.72	9.76	*	138.75	*	76.34	*	36.40	4.92
Plate 08	C20	TXN	7295	*	61.49	*	74.28	*	78.46	73.03	*	65.05		42.45	*	46.82	72.69
Plate 08	D20	TXN	7295	*	60.40	*	106.85	*	107.28	32.38	*	151.16	*	119.74	*	58.14	5.27
Plate 06	I16	UBE2I	7329	*	75.07		94.55		91.02	4.75	*	35.10	*	77.65		75.76	6.89
Plate 05	A15	UBE2M	9040	*	42.70	*	64.86		81.37	8.82	*	50.05	*	18.99	*	25.44	31.15
Plate 05	B15	UBE2M	9040	*	59.42		78.11		87.87	52.44	*	39.51	*	28.56	*	44.29	67.31
Plate 08	E20	UBE2N	7334	*	66.23	*	68.55	*	68.14	137.15		90.58		51.61		80.82	114.37
Plate 11	D04	UBR3	130507	*	71.61		89.07		87.09	50.28	*	33.41	*	19.53	*	39.94	58.10
Plate 08	I20	UCP2	7351	*	62.13		95.81	*	76.30	45.56	*	76.34	*	58.54		88.44	54.63
Plate 08	J20	UCP2	7351	*	69.50		96.23	*	80.03	75.32	*	75.04		45.61	*	62.58	82.29
Plate 02	C05	UGT2B4	7363	*	73.05		91.54	*	107.24	93.27	*	66.88	*	40.62	*	72.97	104.45
Plate 06	A05	UHRF1	29128	*	51.15	*	59.69		79.76	46.09	*	60.88	*	23.38	*	43.17	51.72
Plate 06	I19	UHRF1	29128	*	43.12	*	60.12	*	69.88	46.76	*	44.37	*	15.48	*	37.43	62.34

Plate	Well	Gene Symbol	GENEID	*	ATRi Avg	*	A/C Avg	*	Cis Avg	Arm2 Untreated	*	Low HU Avg	*	High HU Avg	*	CHK1i Avg	Arm1 Untreated
Plate 02	C22	USP38	84640	*	74.05	*	73.86		96.76	9.14		75.06		49.87	*	70.97	18.99
Plate 11	E15	USP50	373509	*	59.71	*	65.77	*	70.67	21.12	*	31.06	*	35.01	*	40.77	8.39
Plate 11	F15	USP50	373509	*	73.12	*	116.42	*	107.65	71.52	*	29.03	*	14.41	*	68.18	78.32
Plate 08	A18	VPS72	6944	*	64.38	*	70.76		88.87	53.66		77.69	*	27.98	*	63.36	71.41
Plate 08	B18	VPS72	6944	*	69.47	*	79.16		97.54	47.95	*	57.73	*	16.65	*	33.10	45.51
Plate 09	A03	WASF1	8936	*	32.18	*	65.53	*	100.28	21.56	*	66.23		40.34	*	20.32	35.48
Plate 09	B03	WASF1	8936	*	77.13	*	71.97		74.99	41.67		81.95		45.93		75.67	25.77
Plate 09	D03	WASF1	8936	*	65.83	*	79.86		88.04	29.87	*	67.29	*	36.32	*	57.80	47.49
Plate 05	F03	WDR33	55339	*	38.27		78.88		76.49	4.43	*	11.22	*	37.08	*	18.76	8.89
Plate 10	M06	WDR48	57599		77.02	*	108.47	*	101.84	24.90		80.55	*	72.26		74.23	29.52
Plate 10	O06	WDR48	57599	*	73.37	*	105.53	*	121.41	1.38		81.50	*	64.44	*	68.76	3.12
Plate 11	B07	WDR49	151790	*	58.70	*	76.74	*	95.97	34.37	*	50.19	*	36.21	*	34.88	22.21
Plate 10	J12	WDR61	80349	*	59.07		84.93		79.20	5.02	*	48.50	*	33.55	*	51.53	8.90
Plate 10	A12	WDR82	80335	*	41.74		84.19		90.93	21.37	*	47.10	*	17.43	*	15.08	24.91
Plate 10	B12	WDR82	80335	*	28.89	*	67.85		85.35	18.40	*	39.33	*	20.90	*	6.92	49.16
Plate 10	C12	WDR82	80335	*	58.68		95.21	*	100.16	14.60	*	38.87	*	27.39	*	42.93	25.48
Plate 10	D12	WDR82	80335	*	58.30		90.39		88.11	83.44		74.59		45.69	*	38.05	108.70
Plate 09	H11	WDTC1	23038	*	75.08		82.99		80.26	42.77	*	61.09	*	37.51		82.63	52.23
Plate 11	P12	WFDC10B	280664	*	15.71	*	35.79	*	47.16	-0.02	*	25.84	*	18.07	*	18.55	0.94
Plate 09	N15	WIPI2	26100	*	61.02		80.72		80.42	32.03		84.32	*	38.16	*	71.27	37.92
Plate 09	P15	WIPI2	26100	*	62.16		81.46		79.58	54.37	*	57.49	*	31.46	*	57.35	70.94
Plate 08	O20	WNT8B	7479	*	76.78	*	67.07	*	72.47	26.74		106.45	*	80.75		90.74	2.09
Plate 08	P20	WNT8B	7479	*	60.16		86.59	*	58.48	46.72	*	68.57		44.21	*	70.41	39.62
Plate 04	B21	XKRX	402415	*	76.45		87.11	*	100.51	68.61	*	67.42		41.01	*	50.05	61.49
Plate 04	C21	XKRX	402415	*	62.79	*	80.53		75.76	119.05	*	59.06	*	23.60		74.26	104.01
Plate 10	E14	YPEL3	83719	*	71.72		83.88		92.61	66.68	*	61.35	*	33.88	*	56.60	91.23
Plate 10	F14	YPEL3	83719	*	71.12		87.40		90.66	45.21		78.63		48.87		76.54	46.45
Plate 11	K11	ZBTB38	253461	*	44.33	*	77.34		83.21	24.00	*	23.61	*	17.03	*	38.87	26.43
Plate 11	L11	ZBTB38	253461	*	72.12		82.97		88.19	62.97	*	40.57	*	39.04	*	56.31	74.49
Plate 09	A12	ZC3H4	23211		-655.12		466.79		-26.03	-0.08		93.94	*	88.30		76.38	0.40
Plate 09	D12	ZC3H4	23211	*	58.85		102.24	*	101.45	2.71	*	74.90	*	33.74	*	32.09	3.15
Plate 10	A14	ZMIZ2	83637	*	49.93	*	80.33	*	94.74	19.21	*	51.97	*	30.29	*	35.69	44.78
Plate 10	B14	ZMIZ2	83637	*	53.56	*	74.26		85.68	36.02	*	57.86	*	39.10	*	51.12	62.16
Plate 11	H09	ZNF100	163227	*	77.24		106.07		81.64	15.29	*	39.00	*	27.05	*	41.67	18.08
Plate 11	E19	ZNF24	7572	*	63.62	*	65.40		73.23	17.72	*	51.48		40.95	*	55.90	13.71
Plate 11	F19	ZNF24	7572	*	48.37		84.65		88.23	23.47	*	24.09	*	20.82	*	37.54	32.83
Plate 09	F09	ZNF277	11179	*	77.73		91.50		86.92	38.59	*	49.40	*	28.68		82.66	32.38
Plate 11	I20	ZNF280C	55609	*	73.06		95.85		75.58	88.39	*	39.57	*	19.13	*	64.88	105.30
Plate 11	L20	ZNF280C	55609	*	72.11		89.61		89.75	115.04	*	55.32	*	20.95	*	49.25	135.43
Plate 11	A09	ZNF383	163087	*	77.17		100.08		83.75	28.13	*	48.23	*	54.45		83.91	45.58
Plate 11	B09	ZNF383	163087	*	66.65		96.74	*	115.56	6.36	*	49.02	*	50.76	*	59.29	10.05
Plate 11	D09	ZNF383	163087	*	64.70		96.27		88.38	5.19	*	64.08	*	57.70	*	49.39	5.33
Plate 10	I16	ZNF528	84436	*	57.63	*	77.84		80.42	65.51	*	61.83	*	31.65	*	63.33	88.83
Plate 10	K16	ZNF528	84436		77.26	*	81.02	*	74.63	36.36		71.43		56.40	*	87.80	22.75
Plate 10	L16	ZNF528	84436	*	65.97		86.81		92.69	18.01	*	59.22	*	68.06	*	46.02	14.23
Plate 11	M18	ZNF644	84146	*	76.43	*	110.50		89.50	42.30	*	35.58	*	27.48	*	66.94	42.81
Plate 11	O18	ZNF644	84146	*	71.76	*	104.86		91.91	10.77		72.15	*	52.00	*	58.54	11.43
Plate 03	D22	ZNF674	641339	*	72.21	*	102.29	*	103.53	6.08	*	67.23		51.26	*	67.67	12.98
Plate 11	I17	ZNF704	619279	*	70.99	*	81.12	*	68.21	11.79	*	48.24		44.50	*	68.53	13.60
Plate 11	J17	ZNF704	619279	*	50.68	*	74.97		83.54	37.86	*	46.42	*	30.77	*	50.16	47.31
Plate 11	K17	ZNF704	619279	*	76.30		94.98		86.25	38.02	*	46.73	*	50.49	*	67.36	53.62
Plate 03	M08	ZNF709	163051	*	74.32		81.90	*	145.77	2.55	*	129.83	*	126.58	*	177.93	1.94
Plate 10	I10	ZNF768	79724	*	74.66	*	120.55	*	97.65	88.06		74.90		41.52	*	100.88	117.06
Plate 10	J10	ZNF768	79724	*	70.90		80.69	*	100.66	14.10	*	64.69		41.51	*	47.01	26.85
Plate 10	L10	ZNF768	79724	*	40.00		84.95	*	112.73	5.72	*	38.99	*	18.10	*	54.63	24.46

APPENDIX C

ETAA1 IS A NOVEL ATR ACTIVATOR

ETAA1 was identified in two proteomic screens in the lab. It was identified as an RPA interactor and as being enriched at stalled replication forks by IPOND [103]. ETAA1 has no previously described function. A graduate student in the lab, Thomas Bass, identified ETAA1 as not only interacting with RPA but also ATR and ATRIP. Knockdown of ETAA1 in the presence of DNA damage results in reduced phosphorylation of RPA, an ATR substrate. Thomas wanted to know if ETAA1 can activate ATR. I used the *in vitro* kinase assays with ATR and ETAA1 to test if ETAA1 can activate ATR. I found that ETAA1 can activate ATR to similar levels as TOPBP1, this activation is inhibited in the presence of the ATRi, and mutation of a conserved tryptophan within ETAA1 prevents activation of ATR. The ETAA1 ATR activation domain (AAD) is located between amino acids 75-250 (Figure AC.1). We next wanted to know if ETAA1 binds ATR on the same surface as TOPBP1. Previous work in the lab by Dan Mordes, discovered mutation of K2587/2589E on ATR prevents TOPBP1 activation of ATR [51]. Similarly, when I conducted the *in vitro* kinase assays with K2587/2589E-ATR, ETAA1 could not activate ATR (Figure AC.2). ETAA1 is in a pathway parallel to TOPBP1 and is only a minor activator of ATR in cells. This work will be published soon in Nature Cell Biology.

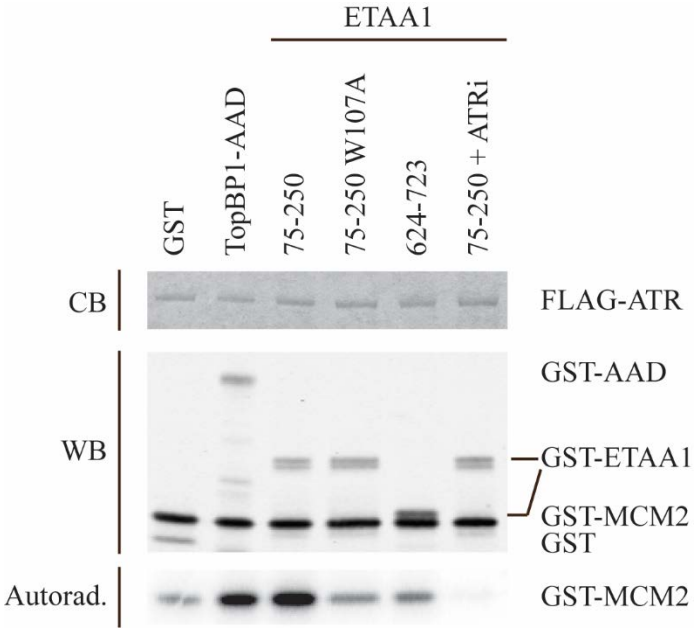

Figure AC.1. ETAA1 contains an ATR activating domain within amino acids 75-250. The ATR/ATRIP complex was purified from HEK293T cells and incubated with [γ^{32}P]-ATP, substrate GST-MCM2, and GST-TOPBP1-AAD, GST-ETAA1-75-250, GST-ETAA1-75-250W107A, GST-ETAA1-624-723, or GST. Lane 6 includes the ATRi. Kinase reactions were separated by SDS-PAGE and [^{32}P]-MCM2 was measured by autoradiography. ATR levels were measured by coomasie blue and GST-tagged components of the kinase reaction were measured by western blot. n=3

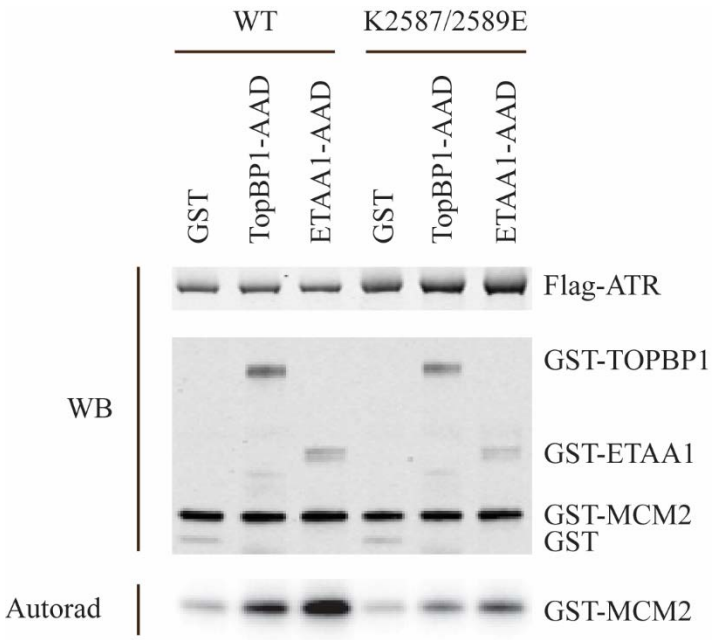

Figure AC.2. ETAA1 activates ATR using the same binding surface on ATR as TOPBP1. The wild-type ATR/ATRIP complex or mutant ATR (K2587/2589E)/ATRIP was purified from HEK293T cells and incubated with [γ^{32}P]-ATP, substrate GST-MCM2, and GST-TOPBP1-AAD, GST-ETAA1-AAD, or GST. Kinase reactions were separated by SDS-PAGE and [^{32}P]-MCM2 was measured by autoradiography. ATR and GST-tagged components of the kinase reaction levels were measured by western blot. n=3

REFERENCES

1. Luzwick JW, Nam EA, Zhao R, Cortez D (2014) Mutation of Serine 1333 in the ATR HEAT Repeats Creates a Hyperactive Kinase. PLoS ONE 9: e99397.

2. Brown EJ, Baltimore D (2000) ATR disruption leads to chromosomal fragmentation and early embryonic lethality. Genes & Development 14: 397-402.

3. Cortez D, Guntuku S, Qin J, Elledge SJ (2001) ATR and ATRIP: Partners in Checkpoint Signaling. Science 294: 1713-1716.

4. de Klein A, Muijtjens M, van Os R, Verhoeven Y, Smit B, et al. (2000) Targeted disruption of the cell-cycle checkpoint gene ATR leads to early embryonic lethality in mice. Current Biology 10: 479-482.

5. Morgan DO (2007) The Cell Cycle: Principles of Control: New Science Press.

6. Sclafani RA, Holzen TM (2007) Cell Cycle Regulation of DNA Replication. Annual Review of Genetics 41: 237-280.

7. Bielinsky AK, Gerbi SA (2001) Where it all starts: eukaryotic origins of DNA replication. Journal of Cell Science 114: 643-651.

8. Bell SP, Dutta A (2002) DNA Replication in Eukaryotic Cells. Annual Review of Biochemistry 71: 333-374.

9. Masai H, Matsumoto S, You Z, Yoshizawa-Sugata N, Oda M (2010) Eukaryotic Chromosome DNA Replication: Where, When, and How? Annual Review of Biochemistry 79: 89-130.

10. Stillman B (2005) Origin recognition and the chromosome cycle. FEBS Letters 579: 877-884.

11. Sun J, Kawakami H, Zech J, Speck C, Stillman B, et al. (2012) Cdc6-Induced Conformational Changes in ORC Bound to Origin DNA Revealed by Cryo-Electron Microscopy. Structure 20: 534-544.

12. Evrin C, Clarke P, Zech J, Lurz R, Sun J, et al. (2009) A double-hexameric MCM2-7 complex is loaded onto origin DNA during licensing of eukaryotic DNA replication. Proceedings of the National Academy of Sciences 106: 20240-20245.

13. Remus D, Beuron F, Tolun G, Griffith JD, Morris EP, et al. (2009) Concerted Loading of Mcm2–7 Double Hexamers around DNA during DNA Replication Origin Licensing. Cell 139: 719-730.

14. Gambus A, Khoudoli GA, Jones RC, Blow JJ (2011) MCM2-7 Form Double Hexamers at Licensed Origins in Xenopus Egg Extract. The Journal of Biological Chemistry 286: 11855-11864.

15. Chang F, Riera A, Evrin C, Sun J, Li H, et al. (2015) Cdc6 ATPase activity disengages Cdc6 from the pre-replicative complex to promote DNA replication. eLife 4: e05795.

16. Gambus A, Jones RC, Sanchez-Diaz A, Kanemaki M, van Deursen F, et al. (2006) GINS maintains association of Cdc45 with MCM in replisome progression complexes at eukaryotic DNA replication forks. Nat Cell Biol 8: 358-366.

17. Ilves I, Petojevic T, Pesavento JJ, Botchan MR (2010) Activation of the MCM2-7 Helicase by Association with Cdc45 and GINS Proteins. Molecular Cell 37: 247-258.

18. Moyer SE, Lewis PW, Botchan MR (2006) Isolation of the Cdc45/Mcm2–7/GINS (CMG) complex, a candidate for the eukaryotic DNA replication fork helicase. Proceedings of the National Academy of Sciences 103: 10236-10241.

19. Fu Yu V, Yardimci H, Long David T, Guainazzi A, Bermudez Vladimir P, et al. (2011) Selective Bypass of a Lagging Strand Roadblock by the Eukaryotic Replicative DNA Helicase. Cell 146: 931-941.

20. Hills Stephanie A, Diffley John FX (2014) DNA Replication and Oncogene-Induced Replicative Stress. Current Biology 24: R435-R444.

21. Douglas Max E, Diffley John FX (2012) Replication Timing: The Early Bird Catches the Worm. Current Biology 22: R81-R82.

22. Pope BD, Gilbert DM (2013) The Replication Domain Model: Regulating Replicon Firing in the Context of Large-Scale Chromosome Architecture. Journal of Molecular Biology 425: 4690-4695.

23. Garg P, Burgers PMJ (2005) DNA Polymerases that Propagate the Eukaryotic DNA Replication Fork. Critical Reviews in Biochemistry and Molecular Biology 40: 115-128.

24. O'Donnell M, Langston L, Stillman B (2013) Principles and Concepts of DNA Replication in Bacteria, Archaea, and Eukarya. Cold Spring Harbor Perspectives in Biology 5.

25. Langston LD, Indiani C, O'Donnell M (2009) Whither the replisome: Emerging perspectives on the dynamic nature of the DNA replication machinery. Cell Cycle 8: 2686-2691.

26. Zeman MK, Cimprich KA (2014) Causes and consequences of replication stress. Nat Cell Biol 16: 2-9.

27. Matsuoka S, Ballif BA, Smogorzewska A, McDonald ER, Hurov KE, et al. (2007) ATM and ATR Substrate Analysis Reveals Extensive Protein Networks Responsive to DNA Damage. Science 316: 1160-1166.

28. Cimprich KA, Cortez D (2008) ATR: an essential regulator of genome integrity. Nature Reviews Molecular Cell Biology 9: 616-627.

29. O'Driscoll M, Ruiz-Perez VL, Woods CG, Jeggo PA, Goodship JA (2003) A splicing mutation affecting expression of ataxia-telangiectasia and Rad3-related protein (ATR) results in Seckel syndrome. Nat Genet 33: 497-501.

30. Nam EA, Zhao R, Cortez D (2011) Analysis of Mutations That Dissociate G2 and Essential S Phase Functions of Human Ataxia Telangiectasia-mutated and Rad3-related (ATR) Protein Kinase. Journal of Biological Chemistry 286: 37320-37327.

31. Byun TS, Pacek M, Yee M-c, Walter JC, Cimprich KA (2005) Functional uncoupling of MCM helicase and DNA polymerase activities activates the ATR-dependent checkpoint. Genes & Development 19: 1040-1052.

32. Willis J, Patel Y, Lentz BL, Yan S (2013) APE2 is required for ATR-Chk1 checkpoint activation in response to oxidative stress. Proceedings of the National Academy of Sciences 110: 10592-10597.

33. Symington LS, Gautier J (2011) Double-Strand Break End Resection and Repair Pathway Choice. Annual Review of Genetics 45: 247-271.

34. Huang M, Kim JM, Shiotani B, Yang K, Zou L, et al. (2010) The FANCM/FAAP24 Complex Is Required for the DNA Interstrand Crosslink-Induced Checkpoint Response. Molecular Cell 39: 259-268.

35. Collis SJ, Ciccia A, Deans AJ, Hořejší Z, Martin JS, et al. (2008) FANCM and FAAP24 Function in ATR-Mediated Checkpoint Signaling Independently of the Fanconi Anemia Core Complex. Molecular Cell 32: 313-324.

36. Ball HL, Ehrhardt MR, Mordes DA, Glick GG, Chazin WJ, et al. (2007) Function of a Conserved Checkpoint Recruitment Domain in ATRIP Proteins. Molecular and Cellular Biology 27: 3367-3377.

37. Ball HL, Cortez D (2005) ATRIP Oligomerization Is Required for ATR-dependent Checkpoint Signaling. Journal of Biological Chemistry 280: 31390-31396.

38. Ball HL, Myers JS, Cortez D (2005) ATRIP Binding to Replication Protein A-Single-stranded DNA Promotes ATR–ATRIP Localization but Is Dispensable for Chk1 Phosphorylation. Molecular Biology of the Cell 16: 2372-2381.

39. Ünsal-Kaçmaz K, Makhov AM, Griffith JD, Sancar A (2002) Preferential binding of ATR protein to UV-damaged DNA. Proceedings of the National Academy of Sciences 99: 6673-6678.

40. Choi J-H, Lindsey-Boltz LA, Sancar A (2009) Cooperative activation of the ATR checkpoint kinase by TopBP1 and damaged DNA. Nucleic Acids Research 37: 1501-1509.

41. Kondo T, Wakayama T, Naiki T, Matsumoto K, Sugimoto K (2001) Recruitment of Mec1 and Ddc1 Checkpoint Proteins to Double-Strand Breaks Through Distinct Mechanisms. Science 294: 867-870.

42. Melo JA, Cohen J, Toczyski DP (2001) Two checkpoint complexes are independently recruited to sites of DNA damage in vivo. Genes & Development 15: 2809-2821.

43. Ellison V, Stillman B (2003) Biochemical Characterization of DNA Damage Checkpoint Complexes: Clamp Loader and Clamp Complexes with Specificity for 5′ Recessed DNA. PLoS Biol 1: e33.

44. Bermudez VP, Lindsey-Boltz LA, Cesare AJ, Maniwa Y, Griffith JD, et al. (2003) Loading of the human 9-1-1 checkpoint complex onto DNA by the checkpoint clamp loader hRad17-replication factor C complex in vitro. Proceedings of the National Academy of Sciences 100: 1633-1638.

45. Zou L, Liu D, Elledge SJ (2003) Replication protein A-mediated recruitment and activation of Rad17 complexes. Proceedings of the National Academy of Sciences 100: 13827-13832.

46. Xu X, Vaithiyalingam S, Glick GG, Mordes DA, Chazin WJ, et al. (2008) The Basic Cleft of RPA70N Binds Multiple Checkpoint Proteins, Including RAD9, To Regulate ATR Signaling. Molecular and Cellular Biology 28: 7345-7353.

47. Furuya K, Poitelea M, Guo L, Caspari T, Carr AM (2004) Chk1 activation requires Rad9 S/TQ-site phosphorylation to promote association with C-terminal BRCT domains of Rad4TOPBP1. Genes & Development 18: 1154-1164.

48. Yan S, Michael WM (2009) TopBP1 and DNA polymerase-α directly recruit the 9-1-1 complex to stalled DNA replication forks. The Journal of Cell Biology 184: 793-804.

49. Acevedo J, Yan S, Michael WM (2016) Direct Binding to Replication Protein A (RPA)-coated Single-stranded DNA Allows Recruitment of the ATR Activator TopBP1 to Sites of DNA Damage. J Biol Chem 291: 13124-13131.

50. Yoo HY, Shevchenko A, Shevchenko A, Dunphy WG (2004) Mcm2 Is a Direct Substrate of ATM and ATR during DNA Damage and DNA Replication Checkpoint Responses. Journal of Biological Chemistry 279: 53353-53364.

51. Mordes DA, Glick GG, Zhao R, Cortez D (2008) TopBP1 activates ATR through ATRIP and a PIKK regulatory domain. Genes & Development 22: 1478-1489.

52. Delacroix S, Wagner JM, Kobayashi M, Yamamoto K-i, Karnitz LM (2007) The Rad9–Hus1–Rad1 (9–1–1) clamp activates checkpoint signaling via TopBP1. Genes & Development 21: 1472-1477.

53. Kumagai A, Lee J, Yoo HY, Dunphy WG (2006) TopBP1 Activates the ATR-ATRIP Complex. Cell 124: 943-955.

54. Lee J, Kumagai A, Dunphy WG (2007) The Rad9-Hus1-Rad1 Checkpoint Clamp Regulates Interaction of TopBP1 with ATR. Journal of Biological Chemistry 282: 28036-28044.

55. Wang J, Chen J, Gong Z (2013) TopBP1 Controls BLM Protein Level to Maintain Genome Stability. Molecular Cell 52: 667-678.

56. Tanaka S, Komeda Y, Umemori T, Kubota Y, Takisawa H, et al. (2013) Efficient Initiation of DNA Replication in Eukaryotes Requires Dpb11/TopBP1-GINS Interaction. Molecular and Cellular Biology 33: 2614-2622.

57. Jeon Y, Lee KY, Ko MJ, Lee YS, Kang S, et al. (2007) Human TopBP1 Participates in Cyclin E/CDK2 Activation and Preinitiation Complex Assembly during G1/S Transition. Journal of Biological Chemistry 282: 14882-14890.

58. Schmidt U, Wollmann Y, Franke C, Grosse F, Saluz H-P, et al. (2008) Characterization of the interaction between the human DNA topoisomerase IIβ-binding protein 1 (TopBP1) and the cell division cycle 45 (Cdc45) protein. Biochemical Journal 409: 169-177.

59. Liu T, Lin Y-H, Leng W, Jung Sung Y, Zhang H, et al. (2014) A Divergent Role of the SIRT1-TopBP1 Axis in Regulating Metabolic Checkpoint and DNA Damage Checkpoint. Molecular Cell 56: 681-695.

60. Chapman JR, Jackson SP (2008) Phospho-dependent interactions between NBS1 and MDC1 mediate chromatin retention of the MRN complex at sites of DNA damage. EMBO reports 9: 795-801.

61. Melander F, Bekker-Jensen S, Falck J, Bartek J, Mailand N, et al. (2008) Phosphorylation of SDT repeats in the MDC1 N terminus triggers retention of NBS1 at the DNA damage–modified chromatin. The Journal of cell biology 181: 213-226.

62. Spycher C, Miller ES, Townsend K, Pavic L, Morrice NA, et al. (2008) Constitutive phosphorylation of MDC1 physically links the MRE11–RAD50–NBS1 complex to damaged chromatin. The Journal of cell biology 181: 227-240.

63. Wu L, Luo K, Lou Z, Chen J (2008) MDC1 regulates intra-S-phase checkpoint by targeting NBS1 to DNA double-strand breaks. Proceedings of the National Academy of Sciences 105: 11200-11205.

64. Wang J, Gong Z, Chen J (2011) MDC1 collaborates with TopBP1 in DNA replication checkpoint control. The Journal of Cell Biology 193: 267-273.

65. Zhang B, Wang E, Dai H, Shen J, Hsieh H-J, et al. (2014) Phosphorylation of the BRCA1 C Terminus (BRCT) Repeat Inhibitor of hTERT (BRIT1) Protein Coordinates TopBP1 Protein Recruitment and Amplifies Ataxia Telangiectasia-mutated and Rad3-related (ATR) Signaling. Journal of Biological Chemistry 289: 34284-34295.

66. Hassan BH, Lindsey-Boltz LA, Kemp MG, Sancar A (2013) Direct Role for the Replication Protein Treslin (Ticrr) in the ATR Kinase-mediated Checkpoint Response. Journal of Biological Chemistry 288: 18903-18910.

67. Cotta-Ramusino C, McDonald ER, Hurov K, Sowa ME, Harper JW, et al. (2011) A DNA Damage Response Screen Identifies RHINO, a 9-1-1 and TopBP1 Interacting Protein Required for ATR Signaling. Science 332: 1313-1317.

68. Lindsey-Boltz LA, Kemp MG, Capp C, Sancar A (2015) RHINO forms a stoichiometric complex with the 9-1-1 checkpoint clamp and mediates ATR-Chk1 signaling. Cell Cycle 14: 99-108.

69. Gong Z, Kim J-E, Leung CCY, Glover JNM, Chen J (2010) BACH1/FANCJ Acts with TopBP1 and Participates Early in DNA Replication Checkpoint Control. Molecular Cell 37: 438-446.

70. Kemp MG, Akan Z, Yilmaz S, Grillo M, Smith-Roe SL, et al. (2010) Tipin-replication protein A interaction mediates Chk1 phosphorylation by ATR in response to genotoxic stress. Journal of Biological Chemistry 285: 16562-16571.

71. Liu Y, Bertram CC, Shi Q, Zinkel SS (2011) Proapoptotic Bid mediates the Atr-directed DNA damage response to replicative stress. Cell Death & Differentiation 18: 841-852.

72. Liu Y, Vaithiyalingam S, Shi Q, Chazin WJ, Zinkel SS (2011) BID binds to replication protein A and stimulates ATR function following replicative stress. Molecular and cellular biology 31: 4298-4309.

73. Maréchal A, Li J-M, Ji Xiao Y, Wu C-S, Yazinski Stephanie A, et al. (2014) PRP19 Transforms into a Sensor of RPA-ssDNA after DNA Damage and Drives ATR Activation via a Ubiquitin-Mediated Circuitry. Molecular Cell 53: 235-246.

74. Zhang N, Kaur R, Akhter S, Legerski RJ (2009) Cdc5L interacts with ATR and is required for the S-phase cell-cycle checkpoint. EMBO reports 10: 1029-1035.

75. Lovejoy CA, Xu X, Bansbach CE, Glick GG, Zhao R, et al. (2009) Functional genomic screens identify CINP as a genome maintenance protein. Proceedings of the National Academy of Sciences 106: 19304-19309.

76. Yu DS, Zhao R, Hsu EL, Cayer J, Ye F, et al. (2010) Cyclin-dependent kinase 9–cyclin K functions in the replication stress response. EMBO reports 11: 876-882.

77. Navadgi-Patil VM, Burgers PM (2008) Yeast DNA replication protein Dpb11 activates the Mec1/ATR checkpoint kinase. Journal of Biological Chemistry 283: 35853-35859.

78. Mordes DA, Nam EA, Cortez D (2008) Dpb11 activates the Mec1–Ddc2 complex. Proceedings of the National Academy of Sciences 105: 18730-18734.

79. Navadgi-Patil VM, Burgers PM (2009) The unstructured C-terminal tail of the 9-1-1 clamp subunit Ddc1 activates Mec1/ATR via two distinct mechanisms. Molecular cell 36: 743-753.

80. Kumar S, Burgers PM (2013) Lagging strand maturation factor Dna2 is a component of the replication checkpoint initiation machinery. Genes & Development 27: 313-321.

81. Myers JS, Cortez D (2006) Rapid Activation of ATR by Ionizing Radiation Requires ATM and Mre11. Journal of Biological Chemistry 281: 9346-9350.

82. Jazayeri A, Falck J, Lukas C, Bartek J, Smith GCM, et al. (2006) ATM- and cell cycle-dependent regulation of ATR in response to DNA double-strand breaks. Nat Cell Biol 8: 37-45.

83. Lee J, Dunphy WG (2013) The Mre11-Rad50-Nbs1 (MRN) complex has a specific role in the activation of Chk1 in response to stalled replication forks. Molecular Biology of the Cell 24: 1343-1353.

84. Duursma Anja M, Driscoll R, Elias Josh E, Cimprich Karlene A (2013) A Role for the MRN Complex in ATR Activation via TOPBP1 Recruitment. Molecular Cell 50: 116-122.

85. Shiotani B, Nguyen HD, Håkansson P, Maréchal A, Tse A, et al. (2013) Two Distinct Modes of ATR Activation Orchestrated by Rad17 and Nbs1. Cell reports 3: 1651-1662.

86. Stojic L, Mojas N, Cejka P, di Pietro M, Ferrari S, et al. (2004) Mismatch repair-dependent G2 checkpoint induced by low doses of SN1 type methylating agents requires the ATR kinase. Genes & Development 18: 1331-1344.

87. Yoshioka K-i, Yoshioka Y, Hsieh P (2006) ATR Kinase Activation Mediated by MutSα and MutLα in Response to Cytotoxic O6-Methylguanine Adducts. Molecular Cell 22: 501-510.

88. Liu Y, Fang Y, Shao H, Lindsey-Boltz L, Sancar A, et al. (2010) Interactions of Human Mismatch Repair Proteins MutSα and MutLα with Proteins of the ATR-Chk1 Pathway. Journal of Biological Chemistry 285: 5974-5982.

89. Pabla N, Ma Z, McIlhatton MA, Fishel R, Dong Z (2011) hMSH2 Recruits ATR to DNA Damage Sites for Activation during DNA Damage-induced Apoptosis. Journal of Biological Chemistry 286: 10411-10418.

90. Tomida J, Itaya A, Shigechi T, Unno J, Uchida E, et al. (2013) A novel interplay between the Fanconi anemia core complex and ATR-ATRIP kinase during DNA cross-link repair. Nucleic Acids Research 41: 6930-6941.

91. Sørensen CS, Syljuåsen RG (2012) Safeguarding genome integrity: the checkpoint kinases ATR, CHK1 and WEE1 restrain CDK activity during normal DNA replication. Nucleic Acids Research 40: 477-486.

92. Guo C, Kumagai A, Schlacher K, Shevchenko A, Shevchenko A, et al. (2015) Interaction of Chk1 with Treslin Negatively Regulates the Initiation of Chromosomal DNA Replication. Molecular Cell 57: 492-505.

93. Trenz K, Errico A, Costanzo V (2008) Plx1 is required for chromosomal DNA replication under stressful conditions. The EMBO Journal 27: 876-885.

94. Toledo Luis I, Altmeyer M, Rask M-B, Lukas C, Larsen Dorthe H, et al. (2013) ATR Prohibits Replication Catastrophe by Preventing Global Exhaustion of RPA. Cell 155: 1088-1103.

95. Petermann E, Woodcock M, Helleday T (2010) Chk1 promotes replication fork progression by controlling replication initiation. Proceedings of the National Academy of Sciences 107: 16090-16095.

96. Couch FB, Bansbach CE, Driscoll R, Luzwick JW, Glick GG, et al. (2013) ATR phosphorylates SMARCAL1 to prevent replication fork collapse. Genes & Development 27: 1610-1623.

97. Syljuåsen RG, Sørensen CS, Hansen LT, Fugger K, Lundin C, et al. (2005) Inhibition of Human Chk1 Causes Increased Initiation of DNA Replication, Phosphorylation of ATR Targets, and DNA Breakage. Molecular and Cellular Biology 25: 3553-3562.

98. Petermann E, Maya-Mendoza A, Zachos G, Gillespie DA, Jackson DA, et al. (2006) Chk1 requirement for high global rates of replication fork progression during normal vertebrate S phase. Molecular and cellular biology 26: 3319-3326.

99. Cobb JA, Bjergbaek L, Shimada K, Frei C, Gasser SM (2003) DNA polymerase stabilization at stalled replication forks requires Mec1 and the RecQ helicase Sgs1. The EMBO Journal 22: 4325-4336.

100. Cobb JA, Schleker T, Rojas V, Bjergbaek L, Tercero JA, et al. (2005) Replisome instability, fork collapse, and gross chromosomal rearrangements arise synergistically from Mec1 kinase and RecQ helicase mutations. Genes & development 19: 3055-3069.

101. Lucca C, Vanoli F, Cotta-Ramusino C, Pellicioli A, Liberi G, et al. (2004) Checkpoint-mediated control of replisome–fork association and signalling in response to replication pausing. Oncogene 23: 1206-1213.

102. De Piccoli G, Katou Y, Itoh T, Nakato R, Shirahige K, et al. (2012) Replisome Stability at Defective DNA Replication Forks Is Independent of S Phase Checkpoint Kinases. Molecular Cell 45: 696-704.

103. Dungrawala H, Rose Kristie L, Bhat Kamakoti P, Mohni Kareem N, Glick Gloria G, et al. (2015) The Replication Checkpoint Prevents Two Types of Fork Collapse without Regulating Replisome Stability. Molecular Cell 59: 998-1010.

104. Bansbach CE, Bétous R, Lovejoy CA, Glick GG, Cortez D (2009) The annealing helicase SMARCAL1 maintains genome integrity at stalled replication forks. Genes & Development 23: 2405-2414.

105. Bétous R, Mason AC, Rambo RP, Bansbach CE, Badu-Nkansah A, et al. (2012) SMARCAL1 catalyzes fork regression and Holliday junction migration to maintain genome stability during DNA replication. Genes & Development 26: 151-162.

106. Ammazzalorso F, Pirzio LM, Bignami M, Franchitto A, Pichierri P (2010) ATR and ATM differently regulate WRN to prevent DSBs at stalled replication forks and promote replication fork recovery. The EMBO Journal 29: 3156-3169.

107. Lavin MF (2008) Ataxia-telangiectasia: from a rare disorder to a paradigm for cell signalling and cancer. Nat Rev Mol Cell Biol 9: 759-769.

108. Shechter D, Costanzo V, Gautier J (2004) Regulation of DNA replication by ATR: signaling in response to DNA intermediates. DNA Repair 3: 901-908.

109. Nghiem P, Park PK, Kim Y-s, Vaziri C, Schreiber SL (2001) ATR inhibition selectively sensitizes G1 checkpoint-deficient cells to lethal premature chromatin condensation. Proceedings of the National Academy of Sciences 98: 9092-9097.

110. Brown EJ, Baltimore D (2003) Essential and dispensable roles of ATR in cell cycle arrest and genome maintenance. Genes & Development 17: 615-628.

111. Gubanova E, Issaeva N, Gokturk C, Djureinovic T, Helleday T (2013) SMG-1 suppresses CDK2 and tumor growth by regulating both the p53 and Cdc25A signaling pathways. Cell Cycle 12: 3770-3780.

112. Gehen SC, Staversky RJ, Bambara RA, Keng PC, O'Reilly MA (2008) hSMG-1 and ATM sequentially and independently regulate the G1 checkpoint during oxidative stress. Oncogene 27: 4065-4074.

113. Gewandter JS, Bambara RA, O'Reilly MA (2011) The RNA surveillance protein SMG1 activates p53 in response to DNA double-strand breaks but not exogenously oxidized mRNA. Cell Cycle 10: 2561-2567.

114. Perry J, Kleckner N (2003) The ATRs, ATMs, and TORs Are Giant HEAT Repeat Proteins. Cell 112: 151-155.

115. Sibanda BL, Chirgadze DY, Blundell TL (2010) Crystal structure of DNA-PKcs reveals a large open-ring cradle comprised of HEAT repeats. Nature 463: 118-121.

116. Rubinson EH, Gowda ASP, Spratt TE, Gold B, Eichman BF (2010) An unprecedented nucleic acid capture mechanism for excision of DNA damage. Nature 468: 406-411.

117. Sawicka M, Wanrooij PH, Darbari VC, Tannous E, Hailemariam S, et al. (2016) The dimeric architecture of checkpoint kinases Mec1ATR and Tel1ATM reveal a common structural organisation. Journal of Biological Chemistry.

118. Chen X, Zhao R, Glick GG, Cortez D (2007) Function of the ATR N-terminal domain revealed by an ATM/ATR chimera. Experimental Cell Research 313: 1667-1674.

119. Bakkenist CJ, Kastan MB (2003) DNA damage activates ATM through intermolecular autophosphorylation and dimer dissociation. Nature 421: 499-506.

120. Bosotti R, Isacchi A, Sonnhammer ELL (2000) FAT: a novel domain in PIK-related kinases. Trends in Biochemical Sciences 25: 225-227.

121. Sun Y, Jiang X, Chen S, Fernandes N, Price BD (2005) A role for the Tip60 histone acetyltransferase in the acetylation and activation of ATM. Proceedings of the

National Academy of Sciences of the United States of America 102: 13182-13187.

122. Sun Y, Xu Y, Roy K, Price BD (2007) DNA Damage-Induced Acetylation of Lysine 3016 of ATM Activates ATM Kinase Activity. Molecular and Cellular Biology 27: 8502-8509.

123. Spagnolo L, Rivera-Calzada A, Pearl LH, Llorca O (2006) Three-Dimensional Structure of the Human DNA-PKcs/Ku70/Ku80 Complex Assembled on DNA and Its Implications for DNA DSB Repair. Molecular Cell 22: 511-519.

124. Sekulić A, Hudson CC, Homme JL, Yin P, Otterness DM, et al. (2000) A Direct Linkage between the Phosphoinositide 3-Kinase-AKT Signaling Pathway and the Mammalian Target of Rapamycin in Mitogen-stimulated and Transformed Cells. Cancer Research 60: 3504-3513.

125. Long X, Ortiz-Vega S, Lin Y, Avruch J (2005) Rheb Binding to Mammalian Target of Rapamycin (mTOR) Is Regulated by Amino Acid Sufficiency. Journal of Biological Chemistry 280: 23433-23436.

126. Gottlieb TM, Jackson SP (1993) The DNA-dependent protein kinase: Requirement for DNA ends and association with Ku antigen. Cell 72: 131-142.

127. Dvir A, Peterson SR, Knuth MW, Lu H, Dynan WS (1992) Ku autoantigen is the regulatory component of a template-associated protein kinase that phosphorylates RNA polymerase II. Proceedings of the National Academy of Sciences of the United States of America 89: 11920-11924.

128. Falck J, Coates J, Jackson SP (2005) Conserved modes of recruitment of ATM, ATR and DNA-PKcs to sites of DNA damage. Nature 434: 605-611.

129. Guo Z, Kozlov S, Lavin MF, Person MD, Paull TT (2010) ATM Activation by Oxidative Stress. Science 330: 517-521.

130. Hara K, Maruki Y, Long X, Yoshino K-i, Oshiro N, et al. (2002) Raptor, a Binding Partner of Target of Rapamycin (TOR), Mediates TOR Action. Cell 110: 177-189.

131. Kim D-H, Sarbassov DD, Ali SM, King JE, Latek RR, et al. (2002) mTOR Interacts with Raptor to Form a Nutrient-Sensitive Complex that Signals to the Cell Growth Machinery. Cell 110: 163-175.

132. Dos DS, Ali SM, Kim D-H, Guertin DA, Latek RR, et al. (2004) Rictor, a Novel Binding Partner of mTOR, Defines a Rapamycin-Insensitive and Raptor-Independent Pathway that Regulates the Cytoskeleton. Current Biology 14: 1296-1302.

133. Stocker H, Radimerski T, Schindelholz B, Wittwer F, Belawat P, et al. (2003) Rheb is an essential regulator of S6K in controlling cell growth in Drosophila. Nature cell biology 5: 559-566.

134. Saucedo LJ, Gao X, Chiarelli DA, Li L, Pan D, et al. (2003) Rheb promotes cell growth as a component of the insulin/TOR signalling network. Nature cell biology 5: 566-571.

135. Yamashita A, Kashima I, Ohno S (2005) The role of SMG-1 in nonsense-mediated mRNA decay. Biochimica et Biophysica Acta (BBA) - Proteins and Proteomics 1754: 305-315.

136. Mordes DA, Cortez D (2008) Activation of ATR and related PIKKs. Cell Cycle 7: 2809-2812.

137. Lee J-H, Paull TT (2005) ATM activation by DNA double-strand breaks through the Mre11-Rad50-Nbs1 complex. Science 308: 551-554.

138. Sato T, Nakashima A, Guo L, Tamanoi F (2009) Specific Activation of mTORC1 by Rheb G-protein in Vitro Involves Enhanced Recruitment of Its Substrate Protein. Journal of Biological Chemistry 284: 12783-12791.

139. Sancak Y, Thoreen CC, Peterson TR, Lindquist RA, Kang SA, et al. (2007) PRAS40 Is an Insulin-Regulated Inhibitor of the mTORC1 Protein Kinase. Molecular Cell 25: 903-915.

140. Long X, Lin Y, Ortiz-Vega S, Yonezawa K, Avruch J (2005) Rheb Binds and Regulates the mTOR Kinase. Current Biology 15: 702-713.

141. Acosta-Jaquez HA, Keller JA, Foster KG, Ekim B, Soliman GA, et al. (2009) Site-Specific mTOR Phosphorylation Promotes mTORC1-Mediated Signaling and Cell Growth. Molecular and Cellular Biology 29: 4308-4324.

142. Soliman GA, Acosta-Jaquez HA, Dunlop EA, Ekim B, Maj NE, et al. (2010) mTOR Ser-2481 Autophosphorylation Monitors mTORC-specific Catalytic Activity and Clarifies Rapamycin Mechanism of Action. Journal of Biological Chemistry 285: 7866-7879.

143. Rosner M, Siegel N, Valli A, Fuchs C, Hengstschläger M (2009) mTOR phosphorylated at S2448 binds to raptor and rictor. Amino Acids 38: 223-228.

144. Kozlov SV, Graham ME, Jakob B, Tobias F, Kijas AW, et al. (2011) Autophosphorylation and ATM Activation: ADDITIONAL SITES ADD TO THE COMPLEXITY. Journal of Biological Chemistry 286: 9107-9119.

145. Kozlov SV, Graham ME, Peng C, Chen P, Robinson PJ, et al. (2006) Involvement of novel autophosphorylation sites in ATM activation. The EMBO journal 25: 3504-3514.

146. Pellegrini M, Celeste A, Difilippantonio S, Guo R, Wang W, et al. (2006) Autophosphorylation at serine 1987 is dispensable for murine Atm activation in vivo. Nature 443: 222-225.

147. Daniel JA, Pellegrini M, Lee J-H, Paull TT, Feigenbaum L, et al. (2008) Multiple autophosphorylation sites are dispensable for murine ATM activation in vivo. The Journal of Cell Biology 183: 777-783.

148. Dobbs TA, Tainer JA, Lees-Miller SP (2010) A structural model for regulation of NHEJ by DNA-PKcs autophosphorylation. DNA Repair 9: 1307-1314.

149. Chan DW, Chen BP-C, Prithivirajsingh S, Kurimasa A, Story MD, et al. (2002) Autophosphorylation of the DNA-dependent protein kinase catalytic subunit is required for rejoining of DNA double-strand breaks. Genes & Development 16: 2333-2338.

150. Chen BP, Chan DW, Kobayashi J, Burma S, Asaithamby A, et al. (2005) Cell cycle dependence of DNA-dependent protein kinase phosphorylation in response to DNA double strand breaks. Journal of Biological Chemistry 280: 14709-14715.

151. Ding Q, Reddy YVR, Wang W, Woods T, Douglas P, et al. (2003) Autophosphorylation of the Catalytic Subunit of the DNA-Dependent Protein Kinase Is Required for Efficient End Processing during DNA Double-Strand Break Repair. Molecular and Cellular Biology 23: 5836-5848.

152. Yajima H, Lee K-J, Chen BPC (2006) ATR-Dependent Phosphorylation of DNA-Dependent Protein Kinase Catalytic Subunit in Response to UV-Induced Replication Stress. Molecular and Cellular Biology 26: 7520-7528.

153. Chen BP, Uematsu N, Kobayashi J, Lerenthal Y, Krempler A, et al. (2007) Ataxia telangiectasia mutated (ATM) is essential for DNA-PKcs phosphorylations at the Thr-2609 cluster upon DNA double strand break. Journal of Biological Chemistry 282: 6582-6587.

154. Reddy YVR, Ding Q, Lees-Miller SP, Meek K, Ramsden DA (2004) Non-homologous End Joining Requires That the DNA-PK Complex Undergo an Autophosphorylation-dependent Rearrangement at DNA Ends. Journal of Biological Chemistry 279: 39408-39413.

155. Nagasawa H, Little JB, Lin Y-F, So S, Kurimasa A, et al. (2010) Differential Role of DNA-PKcs Phosphorylations and Kinase Activity in Radiosensitivity and Chromosomal Instability. Radiation Research 175: 83-89.

156. Zhang S, Yajima H, Huynh H, Zheng J, Callen E, et al. (2011) Congenital bone marrow failure in DNA-PKcs mutant mice associated with deficiencies in DNA repair. The Journal of Cell Biology 193: 295-305.

157. Uematsu N, Weterings E, Yano K-i, Morotomi-Yano K, Jakob B, et al. (2007) Autophosphorylation of DNA-PKCS regulates its dynamics at DNA double-strand breaks. The Journal of cell biology 177: 219-229.

158. Hammel M, Yu Y, Mahaney BL, Cai B, Ye R, et al. (2010) Ku and DNA-dependent protein kinase dynamic conformations and assembly regulate DNA binding and the initial non-homologous end joining complex. Journal of Biological Chemistry 285: 1414-1423.

159. Cui X, Yu Y, Gupta S, Cho Y-M, Lees-Miller SP, et al. (2005) Autophosphorylation of DNA-dependent protein kinase regulates DNA end processing and may also

alter double-strand break repair pathway choice. Molecular and cellular biology 25: 10842-10852.

160. Meek K, Douglas P, Cui X, Ding Q, Lees-Miller SP (2007) trans Autophosphorylation at DNA-dependent protein kinase's two major autophosphorylation site clusters facilitates end processing but not end joining. Molecular and cellular biology 27: 3881-3890.

161. Myers JS, Zhao R, Xu X, Ham A-JL, Cortez D (2007) Cyclin-Dependent Kinase 2–Dependent Phosphorylation of ATRIP Regulates the G2-M Checkpoint Response to DNA Damage. Cancer Research 67: 6685-6690.

162. Wu C-S, Ouyang J, Mori E, Nguyen HD, Maréchal A, et al. (2014) SUMOylation of ATRIP potentiates DNA damage signaling by boosting multiple protein interactions in the ATR pathway. Genes & Development 28: 1472-1484.

163. Jarrett Stuart G, Horrell Erin MW, Christian Perry A, Vanover Jillian C, Boulanger Mary C, et al. (2014) PKA-Mediated Phosphorylation of ATR Promotes Recruitment of XPA to UV-Induced DNA Damage. Molecular Cell 54: 999-1011.

164. Nam EA, Zhao R, Glick GG, Bansbach CE, Friedman DB, et al. (2011) Thr-1989 Phosphorylation Is a Marker of Active Ataxia Telangiectasia-mutated and Rad3-related (ATR) Kinase. Journal of Biological Chemistry 286: 28707-28714.

165. Liu S, Shiotani B, Lahiri M, Maréchal A, Tse A, et al. (2011) ATR Autophosphorylation as a Molecular Switch for Checkpoint Activation. Molecular Cell 43: 192-202.

166. Bartkova J, Horejsi Z, Koed K, Kramer A, Tort F, et al. (2005) DNA damage response as a candidate anti-cancer barrier in early human tumorigenesis. Nature 434: 864-870.

167. Gorgoulis VG, Vassiliou L-VF, Karakaidos P, Zacharatos P, Kotsinas A, et al. (2005) Activation of the DNA damage checkpoint and genomic instability in human precancerous lesions. Nature 434: 907-913.

168. Halazonetis TD, Gorgoulis VG, Bartek J (2008) An Oncogene-Induced DNA Damage Model for Cancer Development. Science 319: 1352-1355.

169. Bester Assaf C, Roniger M, Oren Yifat S, Im Michael M, Sarni D, et al. (2011) Nucleotide Deficiency Promotes Genomic Instability in Early Stages of Cancer Development. Cell 145: 435-446.

170. Bermejo R, Lai Mong S, Foiani M (2012) Preventing Replication Stress to Maintain Genome Stability: Resolving Conflicts between Replication and Transcription. Molecular Cell 45: 710-718.

171. Jones RM, Mortusewicz O, Afzal I, Lorvellec M, Garcia P, et al. (2013) Increased replication initiation and conflicts with transcription underlie Cyclin E-induced replication stress. Oncogene 32: 3744-3753.

172. Curtin NJ (2012) DNA repair dysregulation from cancer driver to therapeutic target. Nat Rev Cancer 12: 801-817.

173. Leijen S, Van Geel R, Sonke GS, de Jong D, Rosenberg EH, et al. Phase II study with Wee1 inhibitor AZD1775 plus carboplatin in patients with p53 mutated ovarian cancer refractory or resistant (< 3 months) to standard first line therapy; 2015. pp. 2507.

174. Tentori L, Ricci-Vitiani L, Muzi A, Ciccarone F, Pelacchi F, et al. (2014) Pharmacological inhibition of poly(ADP-ribose) polymerase-1 modulates resistance of human glioblastoma stem cells to temozolomide. BMC Cancer 14: 1-12.

175. Curtin NJ, Wang L-Z, Yiakouvaki A, Kyle S, Arris CA, et al. (2004) Novel Poly(ADP-ribose) Polymerase-1 Inhibitor, AG14361, Restores Sensitivity to Temozolomide in Mismatch Repair-Deficient Cells. Clinical Cancer Research 10: 881-889.

176. Erice O, Smith MP, White R, Goicoechea I, Barriuso J, et al. (2015) MGMT Expression Predicts PARP-Mediated Resistance to Temozolomide. Molecular Cancer Therapeutics 14: 1236-1246.

177. McLornan DP, List A, Mufti GJ (2014) Applying Synthetic Lethality for the Selective Targeting of Cancer. New England Journal of Medicine 371: 1725-1735.

178. Lord CJ, Ashworth A (2008) Targeted therapy for cancer using PARP inhibitors. Current Opinion in Pharmacology 8: 363-369.

179. Bryant HE, Schultz N, Thomas HD, Parker KM, Flower D, et al. (2005) Specific killing of BRCA2-deficient tumours with inhibitors of poly(ADP-ribose) polymerase. Nature 434: 913-917.

180. Farmer H, McCabe N, Lord CJ, Tutt ANJ, Johnson DA, et al. (2005) Targeting the DNA repair defect in BRCA mutant cells as a therapeutic strategy. Nature 434: 917-921.

181. Foote KM, Blades K, Cronin A, Fillery S, Guichard SS, et al. (2013) Discovery of 4-{4-[(3R)-3-Methylmorpholin-4-yl]-6-[1-(methylsulfonyl)cyclopropyl]pyrimidin-2-yl}-1H-indole (AZ20): A Potent and Selective Inhibitor of ATR Protein Kinase with Monotherapy in Vivo Antitumor Activity. Journal of Medicinal Chemistry 56: 2125-2138.

182. Charrier J-D, Durrant SJ, Golec JMC, Kay DP, Knegtel RMA, et al. (2011) Discovery of Potent and Selective Inhibitors of Ataxia Telangiectasia Mutated and Rad3 Related (ATR) Protein Kinase as Potential Anticancer Agents. Journal of Medicinal Chemistry 54: 2320-2330.

183. Mohni KN, Thompson PS, Luzwick JW, Glick GG, Pendleton CS, et al. (2015) A Synthetic Lethal Screen Identifies DNA Repair Pathways that Sensitize Cancer

Cells to Combined ATR Inhibition and Cisplatin Treatments. PLoS ONE 10: e0125482.

184. Hall AB, Newsome D, Wang Y, Boucher DM, Eustace B, et al. (2014) Potentiation of tumor responses to DNA damaging therapy by the selective ATR inhibitor VX-970.

185. Lima M, Bouzid H, Soares DG, Selle F, Morel C, et al. (2016) Dual inhibition of ATR and ATM potentiates the activity of trabectedin and lurbinectedin by perturbing the DNA damage response and homologous recombination repair.

186. Fokas E, Prevo R, Pollard JR, Reaper PM, Charlton PA, et al. (2012) Targeting ATR in vivo using the novel inhibitor VE-822 results in selective sensitization of pancreatic tumors to radiation. Cell Death Dis 3: e441.

187. Huntoon CJ, Flatten KS, Wahner Hendrickson AE, Huehls AM, Sutor SL, et al. (2013) ATR Inhibition Broadly Sensitizes Ovarian Cancer Cells to Chemotherapy Independent of BRCA Status. Cancer Research 73: 3683-3691.

188. Peasland A, Wang LZ, Rowling E, Kyle S, Chen T, et al. (2011) Identification and evaluation of a potent novel ATR inhibitor, NU6027, in breast and ovarian cancer cell lines. Br J Cancer 105: 372-381.

189. Luong KV, Wang L, Roberts BJ, Wahl III JK, Peng A (2016) Cell fate determination in cisplatin resistance and chemosensitization.

190. Muralidharan SV, Bhadury J, Nilsson LM, Green LC, McLure KG, et al. (2016) BET bromodomain inhibitors synergize with ATR inhibitors to induce DNA damage, apoptosis, senescence-associated secretory pathway and ER stress in Myc-induced lymphoma cells. Oncogene.

191. Mohni KN, Kavanaugh GM, Cortez D (2014) ATR Pathway Inhibition Is Synthetically Lethal in Cancer Cells with ERCC1 Deficiency. Cancer Research 74: 2835-2845.

192. Sanjiv K, Hagenkort A, Calderón-Montaño José M, Koolmeister T, Reaper Philip M, et al. (2016) Cancer-Specific Synthetic Lethality between ATR and CHK1 Kinase Activities. Cell Reports 14: 298-309.

193. Middleton FK, Patterson MJ, Elstob CJ, Fordham S, Herriott A, et al. (2015) Common cancer-associated imbalances in the DNA damage response confer sensitivity to single agent ATR inhibition.

194. Reaper PM, Griffiths MR, Long JM, Charrier J-D, MacCormick S, et al. (2011) Selective killing of ATM- or p53-deficient cancer cells through inhibition of ATR. Nat Chem Biol 7: 428-430.

195. Vendetti FP, Lau A, Schamus S, Conrads TP, O'Connor MJ, et al. (2015) The orally active and bioavailable ATR kinase inhibitor AZD6738 potentiates the anti-tumor effects of cisplatin to resolve ATM-deficient non-small cell lung cancer in vivo.

196. Sultana R, Abdel-Fatah T, Perry C, Moseley P, Albarakti N, et al. (2013) Ataxia Telangiectasia Mutated and Rad3 Related (ATR) Protein Kinase Inhibition Is Synthetically Lethal in XRCC1 Deficient Ovarian Cancer Cells. PLoS ONE 8: e57098.

197. Toledo LI, Murga M, Zur R, Soria R, Rodriguez A, et al. (2011) A cell-based screen identifies ATR inhibitors with synthetic lethal properties for cancer-associated mutations. Nat Struct Mol Biol 18: 721-727.

198. Hocke S, Guo Y, Job A, Orth M, Ziesch A, et al. (2016) A synthetic lethal screen identifies ATR-inhibition as a novel therapeutic approach for POLD1-deficient cancers.

199. Krajewska M, Fehrmann RSN, Schoonen PM, Labib S, de Vries EGE, et al. (2015) ATR inhibition preferentially targets homologous recombination-deficient tumor cells. Oncogene 34: 3474-3481.

200. Flynn RL, Cox KE, Jeitany M, Wakimoto H, Bryll AR, et al. (2015) Alternative lengthening of telomeres renders cancer cells hypersensitive to ATR inhibitors. Science 347: 273-277.

201. Méndez J, Stillman B (2000) Chromatin Association of Human Origin Recognition Complex, Cdc6, and Minichromosome Maintenance Proteins during the Cell Cycle: Assembly of Prereplication Complexes in Late Mitosis. Molecular and Cellular Biology 20: 8602-8612.

202. Lee K-y, Yang K, Cohn MA, Sikdar N, D'Andrea AD, et al. (2010) Human ELG1 Regulates the Level of Ubiquitinated Proliferating Cell Nuclear Antigen (PCNA) through Its Interactions with PCNA and USP1. Journal of Biological Chemistry 285: 10362-10369.

203. Benjamini Y, Hochberg Y (1995) Controlling the False Discovery Rate: A Practical and Powerful Approach to Multiple Testing. Journal of the Royal Statistical Society Series B (Methodological) 57: 289-300.

204. Keith CT, Schreiber SL (1995) PIK-related kinases: DNA repair, recombination, and cell cycle checkpoints. Science 270: 50-51.

205. Sirbu BM, Cortez D (2013) DNA Damage Response: Three Levels of DNA Repair Regulation. Cold Spring Harbor Perspectives in Biology 5.

206. Nyberg KA, Michelson RJ, Putnam CW, Weinert TA (2002) TOWARD MAINTAINING THE GENOME: DNA Damage and Replication Checkpoints. Annual Review of Genetics 36: 617-656.

207. Schoppy DW, Ragland RL, Gilad O, Shastri N, Peters AA, et al. (2012) Oncogenic stress sensitizes murine cancers to hypomorphic suppression of ATR. The Journal of Clinical Investigation 122: 241-252.

208. Nam EA, Cortez D (2011) ATR signalling: more than meeting at the fork. Biochemical Journal 436: 527-536.

209. Zou L, Elledge SJ (2003) Sensing DNA Damage Through ATRIP Recognition of RPA-ssDNA Complexes. Science 300: 1542-1548.

210. Lord CJ, Ashworth A (2012) The DNA damage response and cancer therapy. Nature 481: 287-294.

211. Kamal A, Shaik TB, Malik MS (2015) Embracing synthetic lethality of novel anticancer therapies. Expert Opinion on Drug Discovery 10: 1119-1132.

212. Lord CJ, Tutt ANJ, Ashworth A (2015) Synthetic Lethality and Cancer Therapy: Lessons Learned from the Development of PARP Inhibitors. Annual Review of Medicine 66: 455-470.

213. McCabe N, Turner NC, Lord CJ, Kluzek K, Białkowska A, et al. (2006) Deficiency in the repair of DNA damage by homologous recombination and sensitivity to poly (ADP-ribose) polymerase inhibition. Cancer research 66: 8109-8115.

214. Kim G, Ison G, McKee AE, Zhang H, Tang S, et al. (2015) FDA Approval Summary: Olaparib Monotherapy in Patients with Deleterious Germline BRCA-Mutated Advanced Ovarian Cancer Treated with Three or More Lines of Chemotherapy. Clinical Cancer Research 21: 4257-4261.

215. Birmingham A, Selfors LM, Forster T, Wrobel D, Kennedy CJ, et al. (2009) Statistical methods for analysis of high-throughput RNA interference screens. Nat Meth 6: 569-575.

216. Zabludoff SD, Deng C, Grondine MR, Sheehy AM, Ashwell S, et al. (2008) AZD7762, a novel checkpoint kinase inhibitor, drives checkpoint abrogation and potentiates DNA-targeted therapies. Molecular Cancer Therapeutics 7: 2955-2966.

217. Chen J, Bardes EE, Aronow BJ, Jegga AG (2009) ToppGene Suite for gene list enrichment analysis and candidate gene prioritization. Nucleic Acids Research 37: W305-W311.

218. Dimova DK, Dyson NJ (0000) The E2F transcriptional network: old acquaintances with new faces. 24: 2810-2826.

219. Smith E, Dejsuphong D, Balestrini A, Hampel M, Lenz C, et al. (2009) An ATM- and ATR-dependent checkpoint inactivates spindle assembly by targeting CEP63. Nat Cell Biol 11: 278-285.

220. Zhang S, Hemmerich P, Grosse F (2007) Centrosomal localization of DNA damage checkpoint proteins. Journal of Cellular Biochemistry 101: 451-465.

221. Kramer A, Mailand N, Lukas C, Syljuasen RG, Wilkinson CJ, et al. (2004) Centrosome-associated Chk1 prevents premature activation of cyclin-B-Cdk1 kinase. Nat Cell Biol 6: 884-891.

222. Al-Dosari MS, Shaheen R, Colak D, Alkuraya FS (2010) Novel CENPJ mutation causes Seckel syndrome. Journal of Medical Genetics 47: 411-414.

223. Griffith E, Walker S, Martin C-A, Vagnarelli P, Stiff T, et al. (2008) Mutations in pericentrin cause Seckel syndrome with defective ATR-dependent DNA damage signaling. Nat Genet 40: 232-236.

224. Kalay E, Yigit G, Aslan Y, Brown KE, Pohl E, et al. (2011) CEP152 is a genome maintenance protein disrupted in Seckel syndrome. Nature genetics 43: 23-26.

225. Yigit G, Brown KE, Kayserili H, Pohl E, Caliebe A, et al. (2015) Mutations in CDK5RAP2 cause Seckel syndrome. Molecular Genetics & Genomic Medicine 3: 467-480.

226. FINBOW ME, HARRISON MA (1997) The vacuolar H+-ATPase: a universal proton pump of eukaryotes. Biochemical Journal 324: 697-712.

227. Sautin YY, Lu M, Gaugler A, Zhang L, Gluck SL (2005) Phosphatidylinositol 3-Kinase-Mediated Effects of Glucose on Vacuolar H+-ATPase Assembly, Translocation, and Acidification of Intracellular Compartments in Renal Epithelial Cells. Molecular and Cellular Biology 25: 575-589.

228. Liao C, Hu B, Arno MJ, Panaretou B (2007) Genomic Screening in Vivo Reveals the Role Played by Vacuolar H+ ATPase and Cytosolic Acidification in Sensitivity to DNA-Damaging Agents Such as Cisplatin. Molecular Pharmacology 71: 416-425.

229. Oliveros JC (2007-2015) Venny, An interactive tool for comparing lists with Venn's diagrams. .

230. Park J, Long DT, Lee KY, Abbas T, Shibata E, et al. (2013) The MCM8-MCM9 Complex Promotes RAD51 Recruitment at DNA Damage Sites To Facilitate Homologous Recombination. Molecular and Cellular Biology 33: 1632-1644.

231. Nishimura K, Ishiai M, Horikawa K, Fukagawa T, Takata M, et al. (2012) Mcm8 and Mcm9 Form a Complex that Functions in Homologous Recombination Repair Induced by DNA Interstrand Crosslinks. Molecular Cell 47: 511-522.

232. Gottesman MM (2002) Mechanisms of Cancer Drug Resistance. Annual Review of Medicine 53: 615-627.

233. Cong L, Ran FA, Cox D, Lin S, Barretto R, et al. (2013) Multiplex Genome Engineering Using CRISPR/Cas Systems. Science 339: 819-823.

234. Mali P, Yang L, Esvelt KM, Aach J, Guell M, et al. (2013) RNA-Guided Human Genome Engineering via Cas9. Science 339: 823-826.

235. Jinek M, Chylinski K, Fonfara I, Hauer M, Doudna JA, et al. (2012) A Programmable Dual-RNA–Guided DNA Endonuclease in Adaptive Bacterial Immunity. Science 337: 816-821.

236. Cerami E, Gao J, Dogrusoz U, Gross BE, Sumer SO, et al. (2012) The cBio Cancer Genomics Portal: An Open Platform for Exploring Multidimensional Cancer Genomics Data. Cancer Discovery 2: 401-404.

237. Gao J, Aksoy BA, Dogrusoz U, Dresdner G, Gross B, et al. (2013) Integrative Analysis of Complex Cancer Genomics and Clinical Profiles Using the cBioPortal. Science Signaling 6: pl1-pl1.

238. Lewis KA, Mullany S, Thomas B, Chien J, Loewen R, et al. (2005) Heterozygous ATR Mutations in Mismatch Repair–Deficient Cancer Cells Have Functional Significance. Cancer Research 65: 7091-7095.

239. Kim CJ, Lee JH, Song JW, Cho YG, Kim SY, et al. (2007) Chk1 frameshift mutation in sporadic and hereditary non-polyposis colorectal cancers with microsatellite instability. European Journal of Surgical Oncology (EJSO) 33: 580-585.

240. Menoyo A, Alazzouzi H, Espín E, Armengol M, Yamamoto H, et al. (2001) Somatic Mutations in the DNA Damage-Response Genes ATR and CHK1 in Sporadic Stomach Tumors with Microsatellite Instability. Cancer Research 61: 7727-7730.

241. Barretina J, Caponigro G, Stransky N, Venkatesan K, Margolin AA, et al. (2012) The Cancer Cell Line Encyclopedia enables predictive modelling of anticancer drug sensitivity. Nature 483: 603-307.

242. Alimov A, Kost-Alimova M, Liu J, Li C, Bergerheim U, et al. (2000) Combined LOH/CGH analysis proves the existence of interstitial 3p deletions in renal cell carcinoma. Oncogene 19: 1392-1399.

243. Marsit CJ, Hasegawa M, Hirao T, Kim D-H, Aldape K, et al. (2004) Loss of Heterozygosity of Chromosome 3p21 Is Associated with Mutant TP53 and Better Patient Survival in Non–Small-Cell Lung Cancer. Cancer Research 64: 8702-8707.

244. Martinez A, Walker RA, Shaw JA, Dearing SJ, Maher ER, et al. (2001) Chromosome 3p allele loss in early invasive breast cancer: detailed mapping and association with clinicopathological features. Molecular Pathology 54: 300-306.

245. Gatto F, Nookaew I, Nielsen J (2014) Chromosome 3p loss of heterozygosity is associated with a unique metabolic network in clear cell renal carcinoma. Proceedings of the National Academy of Sciences of the United States of America 111: E866-E875.

246. Fang Y, Tsao CC, Goodman BK, Furumai R, Tirado CA, et al. (2004) ATR functions as a gene dosage-dependent tumor suppressor on a mismatch repair-deficient background. The EMBO Journal 23: 3164-3174.

247. Zighelboim I, Ali S, Lankes HA, Backes F, Moore K, et al. (2015) Assessing the prognostic role of ATR mutation in endometrioid endometrial cancer: An NRG Oncology/Gynecologic Oncology Group study. Gynecologic Oncology 138: 614-619.

248. Sakurikar N, Eastman A (2015) Will Targeting Chk1 Have a Role in the Future of Cancer Therapy? Journal of Clinical Oncology.

249. Barnard D, Diaz HB, Burke T, Donoho G, Beckmann R, et al. (2016) LY2603618, a selective CHK1 inhibitor, enhances the anti-tumor effect of gemcitabine in xenograft tumor models. Investigational new drugs 34: 49-60.

250. Flohr T, Dai J-C, Büttner J, Popanda O, Hagmüller E, et al. (1999) Detection of mutations in the DNA polymerase δ gene of human sporadic colorectal cancers and colon cancer cell lines. International Journal of Cancer 80: 919-929.

251. Church DN, Briggs SEW, Palles C, Domingo E, Kearsey SJ, et al. (2013) DNA polymerase ε and δ exonuclease domain mutations in endometrial cancer. Human Molecular Genetics 22: 2820-2828.

252. Lane AN, Fan TW-M (2015) Regulation of mammalian nucleotide metabolism and biosynthesis. Nucleic Acids Research.

253. Kavanaugh G, Ye F, Mohni KN, Luzwick JW, Glick G, et al. (2015) A whole genome RNAi screen identifies replication stress response genes. DNA Repair 35: 55-62.

254. Sigoillot FD, Lyman S, Huckins JF, Adamson B, Chung E, et al. (2012) A bioinformatics method identifies prominent off-targeted transcripts in RNAi screens. Nat Meth 9: 363-366.

255. Yilmazel B, Hu Y, Sigoillot F, Smith JA, Shamu CE, et al. (2014) Online GESS: prediction of miRNA-like off-target effects in large-scale RNAi screen data by seed region analysis. BMC Bioinformatics 15: 192-192.

256. Joazeiro CAP, Weissman AM (2000) RING Finger Proteins: Mediators of Ubiquitin Ligase Activity. Cell 102: 549-552.

257. Wilsker D, Patsialou A, Dallas PB, Moran E (2002) ARID Proteins: A Diverse Family of DNA Binding Proteins Implicated in the Control of Cell Growth, Differentiation, and Development. Cell Growth Differ 13: 95-106.

258. Kortschak RD, Tucker PW, Saint R (2000) ARID proteins come in from the desert. Trends in Biochemical Sciences 25: 294-299.

259. Kim D, Probst L, Das C, Tucker PW (2007) REKLES Is an ARID3-restricted Multifunctional Domain. Journal of Biological Chemistry 282: 15768-15777.

260. Peeper DS, Shvarts A, Brummelkamp T, Douma S, Koh EY, et al. (2002) A functional screen identifies hDRIL1 as an oncogene that rescues RAS-induced senescence. Nat Cell Biol 4: 148-153.

261. Numata S-i, Claudio PP, Dean C, Giordano A, Croce CM (1999) Bdp, a New Member of a Family of DNA-binding Proteins, Associates with the Retinoblastoma Gene Product. Cancer Research 59: 3741-3747.

262. Kobayashi K, Era T, Takebe A, Jakt LM, Nishikawa S-I (2006) ARID3B Induces Malignant Transformation of Mouse Embryonic Fibroblasts and Is Strongly Associated with Malignant Neuroblastoma. Cancer Research 66: 8331-8336.

263. Florence B, Faller DV (2001) You bet-cha: a novel family of transcriptional regulators. Front Biosci 6: D1008-1018.

264. LeRoy G, Rickards B, Flint SJ (2008) The Double Bromodomain Proteins Brd2 and Brd3 Couple Histone Acetylation to Transcription. Molecular Cell 30: 51-60.

265. Gamsjaeger R, Webb SR, Lamonica JM, Billin A, Blobel GA, et al. (2011) Structural Basis and Specificity of Acetylated Transcription Factor GATA1 Recognition by BET Family Bromodomain Protein Brd3. Molecular and Cellular Biology 31: 2632-2640.

266. Sirbu BM, Couch FB, Feigerle JT, Bhaskara S, Hiebert SW, et al. (2011) Analysis of protein dynamics at active, stalled, and collapsed replication forks. Genes & Development 25: 1320-1327.

267. Sobel RE, Cook RG, Perry CA, Annunziato AT, Allis CD (1995) Conservation of deposition-related acetylation sites in newly synthesized histones H3 and H4. Proceedings of the National Academy of Sciences of the United States of America 92: 1237-1241.

268. Taddei A, Roche D, Sibarita J-B, Turner BM, Almouzni G (1999) Duplication and Maintenance of Heterochromatin Domains. The Journal of Cell Biology 147: 1153-1166.

269. Singer RA, Johnston GC (2004) The FACT chromatin modulator: genetic and structure/function relationships. Biochemistry and Cell Biology 82: 419-427.

270. Heo K, Kim H, Choi SH, Choi J, Kim K, et al. (2008) FACT-Mediated Exchange of Histone Variant H2AX Regulated by Phosphorylation of H2AX and ADP-Ribosylation of Spt16. Molecular Cell 30: 86-97.

271. Wei D, Sun Y (2010) Small RING Finger Proteins RBX1 and RBX2 of SCF E3 Ubiquitin Ligases: The Role in Cancer and as Cancer Targets. Genes & Cancer 1: 700-707.

272. Shirakawa R, Fukai S, Kawato M, Higashi T, Kondo H, et al. (2009) Tuberous Sclerosis Tumor Suppressor Complex-like Complexes Act as GTPase-activating Proteins for Ral GTPases. Journal of Biological Chemistry 284: 21580-21588.

273. Personnic N, Lakisic G, Gouin E, Rousseau A, Gautreau A, et al. (2014) A role for Ral GTPase-activating protein subunit β in mitotic regulation. FEBS Journal 281: 2977-2989.

274. Shiomi Y, Nishitani H (2013) Alternative replication factor C protein, Elg1, maintains chromosome stability by regulating PCNA levels on chromatin. Genes to Cells 18: 946-959.

275. Lee K-y, Fu H, Aladjem MI, Myung K (2013) ATAD5 regulates the lifespan of DNA replication factories by modulating PCNA level on the chromatin. The Journal of Cell Biology 200: 31-44.

276. Maruyama T, Farina A, Dey A, Cheong J, Bermudez VP, et al. (2002) A Mammalian Bromodomain Protein, Brd4, Interacts with Replication Factor C and Inhibits Progression to S Phase. Molecular and Cellular Biology 22: 6509-6520.

277. Rahman S, Sowa ME, Ottinger M, Smith JA, Shi Y, et al. (2011) The Brd4 Extraterminal Domain Confers Transcription Activation Independent of pTEFb by Recruiting Multiple Proteins, Including NSD3. Molecular and Cellular Biology 31: 2641-2652.

278. Dawson MA, Prinjha RK, Dittman A, Giotopoulos G, Bantscheff M, et al. (2011) Inhibition of BET recruitment to chromatin as an effective treatment for MLL-fusion leukaemia. Nature 478: 529-533.

279. Filippakopoulos P, Qi J, Picaud S, Shen Y, Smith WB, et al. (2010) Selective inhibition of BET bromodomains. Nature 468: 1067-1073.

280. Delmore Jake E, Issa Ghayas C, Lemieux Madeleine E, Rahl Peter B, Shi J, et al. (2011) BET Bromodomain Inhibition as a Therapeutic Strategy to Target c-Myc. Cell 146: 904-917.

281. Vassileva I, Yanakieva I, Peycheva M, Gospodinov A, Anachkova B (2014) The mammalian INO80 chromatin remodeling complex is required for replication stress recovery. Nucleic Acids Research 42: 9074-9086.

282. Lovejoy CA, Cortez D (2009) Common mechanisms of PIKK regulation. DNA Repair 8: 1004-1008.

283. Canman CE, Lim D-S, Cimprich KA, Taya Y, Tamai K, et al. (1998) Activation of the ATM Kinase by Ionizing Radiation and Phosphorylation of p53. Science 281: 1677-1679.

284. Banin S, Moyal L, Shieh S-Y, Taya Y, Anderson CW, et al. (1998) Enhanced Phosphorylation of p53 by ATM in Response to DNA Damage. Science 281: 1674-1677.

285. Nam EA (2011) Phospho-regulation of the DNA Damage Response Kinase ATR: Vanderbilt University.

286. Daub H, Olsen JV, Bairlein M, Gnad F, Oppermann FS, et al. (2008) Kinase-selective enrichment enables quantitative phosphoproteomics of the kinome across the cell cycle. Molecular cell 31: 438-448.

287. Jarrett SG, Wolf Horrell EM, Boulanger MC, D'Orazio JA (2015) Defining the Contribution of MC1R Physiological Ligands to ATR Phosphorylation at Ser435, a Predictor of DNA Repair in Melanocytes. Journal of Investigative Dermatology 135: 3086-3095.

288. Zhou Z-W, Liu C, Li T-L, Bruhn C, Krueger A, et al. (2013) An Essential Function for the ATR-Activation-Domain (AAD) of TopBP1 in Mouse Development and Cellular Senescence. PLoS Genet 9: e1003702.

289. Belotserkovskaya R, Oh S, Bondarenko VA, Orphanides G, Studitsky VM, et al. (2003) FACT facilitates transcription-dependent nucleosome alteration. Science 301: 1090-1093.

290. Tan BCM, Chien CT, Hirose S, Lee SC (2006) Functional cooperation between FACT and MCM helicase facilitates initiation of chromatin DNA replication. The EMBO journal 25: 3975-3985.

291. Cascone I, Selimoglu R, Ozdemir C, Del Nery E, Yeaman C, et al. (2008) Distinct roles of RalA and RalB in the progression of cytokinesis are supported by distinct RalGEFs. The EMBO Journal 27: 2375-2387.

292. Alderton GK, Joenje H, Varon R, Børglum AD, Jeggo PA, et al. (2004) Seckel syndrome exhibits cellular features demonstrating defects in the ATR-signalling pathway. Human Molecular Genetics 13: 3127-3138.

293. Tibelius A, Marhold J, Zentgraf H, Heilig CE, Neitzel H, et al. (2009) Microcephalin and pericentrin regulate mitotic entry via centrosome-associated Chk1. The Journal of Cell Biology 185: 1149-1157.

294. Bensimon A, Schmidt A, Ziv Y, Elkon R, Wang S-Y, et al. (2010) ATM-Dependent and -Independent Dynamics of the Nuclear Phosphoproteome After DNA Damage. Science Signaling 3: rs3-rs3.

295. Stokes MP, Rush J, MacNeill J, Ren JM, Sprott K, et al. (2007) Profiling of UV-induced ATM/ATR signaling pathways. Proceedings of the National Academy of Sciences 104: 19855-19860.

296. Bajrami I, Frankum JR, Konde A, Miller RE, Rehman FL, et al. (2014) Genome-wide Profiling of Genetic Synthetic Lethality Identifies CDK12 as a Novel Determinant of PARP1/2 Inhibitor Sensitivity. Cancer Research 74: 287-297.

297. Verlinden L, Vanden Bempt I, Eelen G, Drijkoningen M, Verlinden I, et al. (2007) The E2F-Regulated Gene Chk1 Is Highly Expressed in Triple-Negative Estrogen Receptor−/Progesterone Receptor−/HER-2− Breast Carcinomas. Cancer Research 67: 6574-6581.

298. Harris LA, Frick PL, Garbett SP, Hardeman KN, Paudel BB, et al. (2016) An unbiased metric of antiproliferative drug effect in vitro. Nat Meth advance online publication.

299. Hafner M, Niepel M, Chung M, Sorger PK (2016) Growth rate inhibition metrics correct for confounders in measuring sensitivity to cancer drugs. Nat Meth advance online publication.

300. Wang T, Wei JJ, Sabatini DM, Lander ES (2014) Genetic Screens in Human Cells Using the CRISPR-Cas9 System. Science 343: 80-84.

301. Slaymaker IM, Gao L, Zetsche B, Scott DA, Yan WX, et al. (2016) Rationally engineered Cas9 nucleases with improved specificity. Science 351: 84-88.